A Stochastic Approach to Measurement-Driven Damage Detection And Prognosis in Structural Health Monitoring

by

Guru Prakash

A thesis
presented to the University of Waterloo
in fulfillment of the
thesis requirement for the degree of
Doctor of Philosophy
in
Civil Engineering

Waterloo, Ontario, Canada, 2017

Examining Committee Membership:

The following served on the Examining Committee for this thesis. The decision of the Examining Committee is by majority vote.

External Examiner:	Wilson Q. Wang Professor Dept. of Mechanical Engg., Lakehead University
Supervisor:	Sriram Narasimhan Associate professor, Dept. of Civil and Environmental Engg., University of Waterloo
Internal Member:	Mahesh D. Pandey Professor, Dept. of Civil and Environmental Engg., University of Waterloo
Internal-external Member:	Kumaraswamy Ponnambalam Professor, Dept. of Systems and Design Engg., University of Waterloo
Other Member(s):	Giovanni Cascante Professor, Dept. of Civil and Environmental Engg., University of Waterloo
	Scott Walbridge Associate professor, Dept. of Civil and Environmental Engg., University of Waterloo

I hereby declare that I am the sole author of this thesis. This is a true copy of the thesis, including any required final revisions, as accepted by my examiners.

I understand that my thesis may be made electronically available to the public.

Abstract

Damage detection and prognosis are integral to asset management of critical mechanical and civil engineering infrastructure. In practice, these two aspects are often decoupled, where the former is carried out independently using sensor data (e.g., vibrations), while the latter is undertaken based on reliability principles using life time failure data of the system or the component of interest. Only in a few studies damage detection results are extended to remaining useful life estimation, which is achieved by modeling the underlying degradation process using a surrogate measure of degradation. However, an integrated framework which undertakes damage detection, prognosis, and maintenance planning in a systematic way is lacking in the literature. Furthermore, the parameters of degradation model which are utilized for prognosis are often solely estimated using the degradation data obtained from the monitored unit, which represents the degradation of a specific unit, but ignores the general population trend.

The main objectives of this thesis are three-fold: first, a mathematical framework using surrogate measure of degradation is developed to undertake the damage detection and prognosis in a single framework; next, the prior knowledge obtained from the historical failed units are integrated in model parameter estimation and residual useful life (RUL) updating of a monitored unit using a Bayesian approach; finally, the proposed degradation modeling framework is applied for maintenance planning of civil and industrial systems, specifically, for reinforced concrete beams and rolling element bearings. The initiation of a fault in these applications is often followed by a sudden change in the degradation path. The location of a change-point can be associated with a sudden loss of stiffness in the case of structural members, or fault initiation in the case of bearings. Hence, in this thesis, the task of change point location identification is thought of as being synonymous with damage or fault detection in the context of structural health monitoring. Furthermore, the change point results are used for two-phase degradation modeling, future degradation level prediction and subsequent RUL estimation. The model parameters are updated using a Bayesian approach, which systematically integrates the prior knowledge obtained from historical failure-time data with monitored data obtained from an in-situ unit. Once such a model is established, it is projected to a failure threshold, thereby allowing for RUL estimation and maintenance planning.

Results from the numerical as well as actual field data shows that the proposed degradation modeling framework is good in performing these two tasks. It was also found that as more degradation data is utilized from the monitoring unit, the progressing fault is detected in a timely manner and the model parameters estimates and the end life predictions become more accurate.

Acknowledgements

I would like to express my deepest gratitude to my supervisor, Prof. Sriram Narasimhan, for his guidance, enlightening discussions, refreshing encouragement and financial support throughout the doctorate program. Without his help, the thesis could not have been completed. I would also like to thank Prof. Mahesh D. Pandey, for many useful discussions and encouragement during various stages of this work. I would like to express my sincere gratitude towards my thesis committee members, Prof. Kumaraswamy Ponnambalam, Prof. Mahesh D. Pandey, Prof. Giovanni Cascante and Prof. Scott Walbridge. I am grateful to Prof. Wilson Q. Wang from Lakehead University, for agreeing to serve on my thesis committee in the capacity of an external examiner.

I would also like to offer my thanks to Mr. Mike Riseborough, Greater Toronto Airport Authority for providing industry support which enabled matching grants through the NSERC-CRD program. I would like to thank Dr. Budhaditya Hazra, Dr. Ayan Sadhu, Dr. Rania Al-Hammoud, Dr. Xianxun Yuan and Dr. Ali Ashasi Sorkhabi for their valuable input. I would like to thank my office-mate Kevin Joseph Goorts, who always helped and encouraged me during difficult situations. I would also like to thank my research group members; Dr. Pampa Dey, Shilpa Reddy Pantula, Ann Sychterz, Dr. José de Jesús Nuño Ayón, Stan Fong, Rajdip Nayek, Roya Cody, Marshal Deep Kafle, Dylan Dowling, Nicholas Charron, Stephen Phillips, Nina Feng, Dr. Jinane Harmouche and Murad Ilomame for their outstanding support. I would also like to thank Richard Morrison, Rob Sluban, Kevin Rampersad and Paul Thompson for their assistance in the laboratory.

Finally, I thank my wife Parvati, sisters Niwedita, Sujata & Nutan, daughters Nandini & Sristi, my parents and uncle & Late aunty for their support, patience and motivation during my study. Without their love and support, this work could not have been possible.

Dedication

To my wife Parvati, daugthers Nandini & Sristi, my parents, uncle & late aunty.

Table of Contents

List of Tables

List of Figures

List of symbols

C_p	Preventive maintenance cost
C_f	Failure maintenance cost
f_s	Sampling frequency
$F(L_k)$	RUL CDF
$G(a, b)$	Gamma distribution
$I(\cdot)$	Indicator function
L_k	RUL at time t_k
$N(\mu, \sigma^2)$	Normal distribution
t_p	Replacement time
W(t)	Standard Weiner process
$\bar{X}$	Sample mean
y_t or Y_t	degradation measure at time
y_t^*	Predicted degradation level at future time t
Z	Standard random variable
η_D	Failure threshold
λ	Change point location
$\eta(\cdot)$	Functional form
ρ	Correlation coefficient

List of abbreviations

ABR	Age based replacement
ACF	Auto-correlation function
AIC	Akaike information criterion
ARMA	Auto-regressive moving-average
BIC	Bayesian information criterion
BPFO	Ball pass frequency outer race
BPFI	Ball pass frequency inner race
BHS	Baggage handling system
BSF	Ball spin frequency
CP	Change point
CBM	Condition based maintenance
CM	Condition monitoring
DSF	Damage sensitive feature
ECR	Expected cost rate
EM	Expectation maximization
FHT	First hitting time
FFT	Fast Fourier transform
GMM	Gaussian mixture model

GP	Gamma process
HPD	Highest probability density
HMM	Hidden Markov model
HSMM	Hidden semi Markov model
IG	Inverse gamma
MAP	Maximum a posteriori
MCMC	Markov chain Monte Carlo
MED	Minimum entropy deconvolution
ML	Maximum likelihood
MLE	Maximum likelihood estimate
MTTF	Mean time to failure
PDF	Probability density function
PHM	Proportional hazard model
PCA	Principal component analysis
RPM	Revolution per minute
RMS	Root mean square
RUL	Remaining useful life
RV	Random variable
SK	Spectral kurtosis
SNR	Signal to noise ratio
SHM	Structural health monitoring
SPC	Statistical process control
WP	Weiner process

Chapter 1

Introduction

1.1 Background

Civil and mechanical systems such as buildings, bridges, and machinery are an integral part of a modern society. Many of these systems operate under harsh operating and loading conditions, a significant portion nearing their end of design life. This combination of factors often leads to a decrease in their overall reliability. Capital and other resource constraints means that replacement at the end of their design life is often not feasible, and a more proactive maintenance technique based on the monitored health of system has been argued to increase performance and reliability for expensive equipment (preventative maintenance make more economic sense for cheap components), while reducing the overall capital and maintenance costs.

An effective framework which allows measurements to be formally integrated into maintenance planning is condition based maintenance (CBM). CBM entails judgmental maintenance, repair, and replacement on the basis of the actual condition of the system, rather

than being reactive or on pre-set schedules. The basic argument for making the case of monitoring is that for expensive components, there is still some useful life left if the component is removed preventively from service. A well-implemented CBM could make use of nearly the entire life of a system or a component and prolong a components' (or a system, for this thesis this distinction is not as important) maintenance action, while avoiding catastrophic failures.

Diagnostics and prognostics are two main components in a CBM program. Diagnostics tries to answer questions such as: is there something wrong in the monitored system (i.e., fault detection)? If yes, then which component is faulty (fault isolation)? What is the nature of the fault (fault identification)? On the other hand, prognostics deals with fault prediction prior to its occurrence. It addresses questions like: what is the speed of a progressing fault? When and with what probability is a progressing fault likely cross a predefined failure threshold? When should one plan for a maintenance action? Diagnostics involves posterior event analysis, while prognostics is a prior event analysis. A CBM program can be used to perform diagnostics or prognostics, or both.

This thesis mainly deals with the problem of how best to undertake diagnostics and prognostic tasks when the underlying damage mechanisms remain hidden, and indirect measurements are the only feasible means of inferring their condition. This is best explained using an example of a rolling element bearing. Figure 1.1 shows a typical bearing, in which faults could manifest in the inner race, outer race, or on the rolling element. Bearings are typically sealed and hence a direct inspection of the fault is generally not possible. An extensively studied problem in the literature is how to diagnose the progress of the three types of faults using indirect monitoring means such as vibrations, oil monitoring or temperature. Amongst these, vibration monitoring is by far the most commonly used method. The underlying principle is that faults manifest themselves as modulations

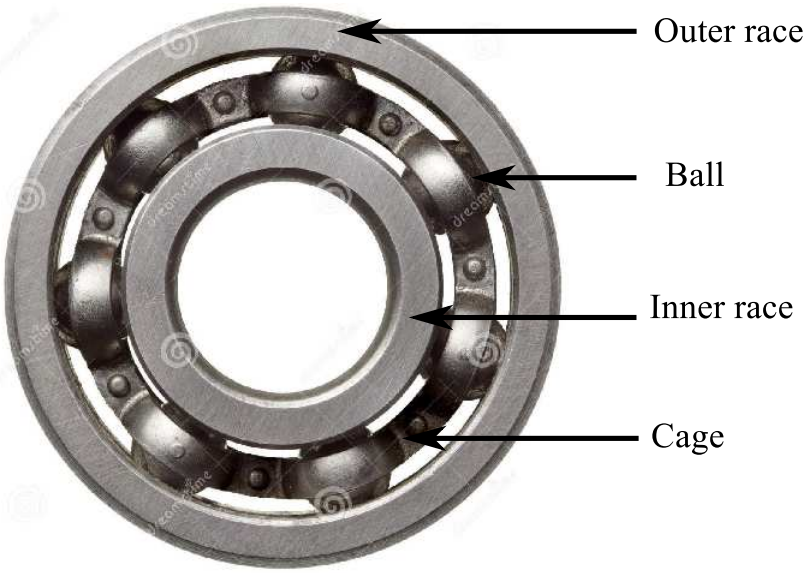

Figure 1.1: Typical rolling element bearing [1]

in the vibration signatures and hence monitoring such changes provide insight into the underlying degradation mechanisms. One of the questions relevant to this thesis is how best to interrogate such indirect vibration measurements for fault detection and to estimate the remaining useful life of a bearing, given that both the occurrence of the fault and the failure time are random in nature, even for bearings of similar type.

Such problems are of great practical importance in civil infrastructure applications as well. Fatigue in metal connections found in buildings and bridges, loss of bondage in embedded steel inside reinforced concrete members (see Figure 1.2), erosion in structural foundations, to name a few examples. In many of these cases, the underlying damage mechanism may not be directly observable, but it may be possible to indirectly measure its effects. For example, loss of stiffness in a metal connection due to fatigue could manifest itself in the strain or acceleration measurements, or a loss of bonding of steel reinforcement bars within a reinforced concrete member may manifest itself in changes in the deflection.

Figure 1.2: Loss of bonding between concrete and the embedded steel bars, resulting in slip [2]

This thesis attempts to develop a mathematical framework to undertake diagnosis (detection, which is of primary interest in this thesis, can be thought of the first level in diagnosis) and prognosis in such situations by using surrogates of the underlying damage/degradation mechanism.

Damage or fault detection by itself may be useful in cases where such a damage may render a component useless and a replacement may be necessary, but often there is residual useful life left in components after damage initiation, which can be used to schedule maintenance. In such cases, the process of damage detection and residual useful life predictions have largely been addressed in silos. While the issue of damage detection (the reference here is to vibration based methods) has been dealt with extensively in the realm of signal processing or statistical classification, the end of life predictions have been dealt with based on reliability principles using historical failure data. The issue of integrating the process

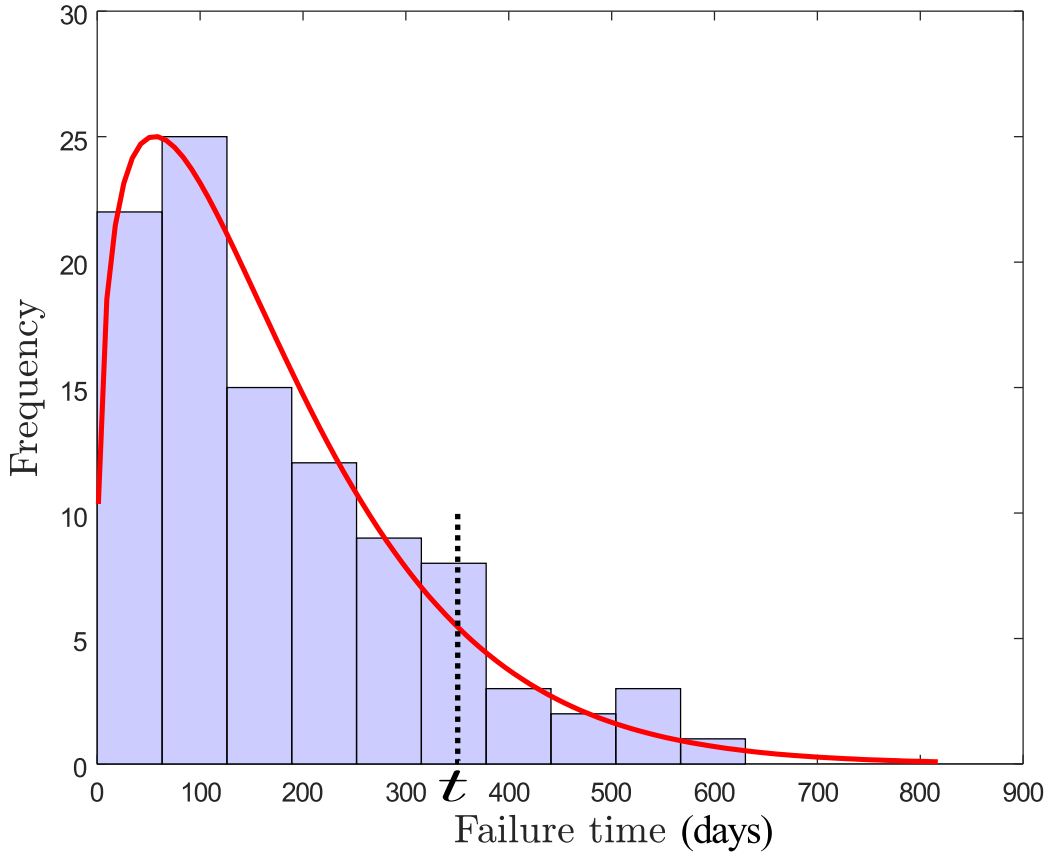

Figure 1.3: Reliability based approach for end of life prediction

of damage diagnosis and prognosis is of central importance in this thesis and will be dealt with extensively later.

In the reliability approach to end of life prediction, an appropriate distribution is fitted to the historical life-time data and reliability is assessed at any given time in the future. One such example distribution based on simulated failure-time data for a bearing is shown in Figure 1.3. The probability of failure at time t for an in-situ unit (from the same population) is given by the area under curve until the time, t. This approach is good for the components that are relatively cheap, where the failure cost is not high and maintenance

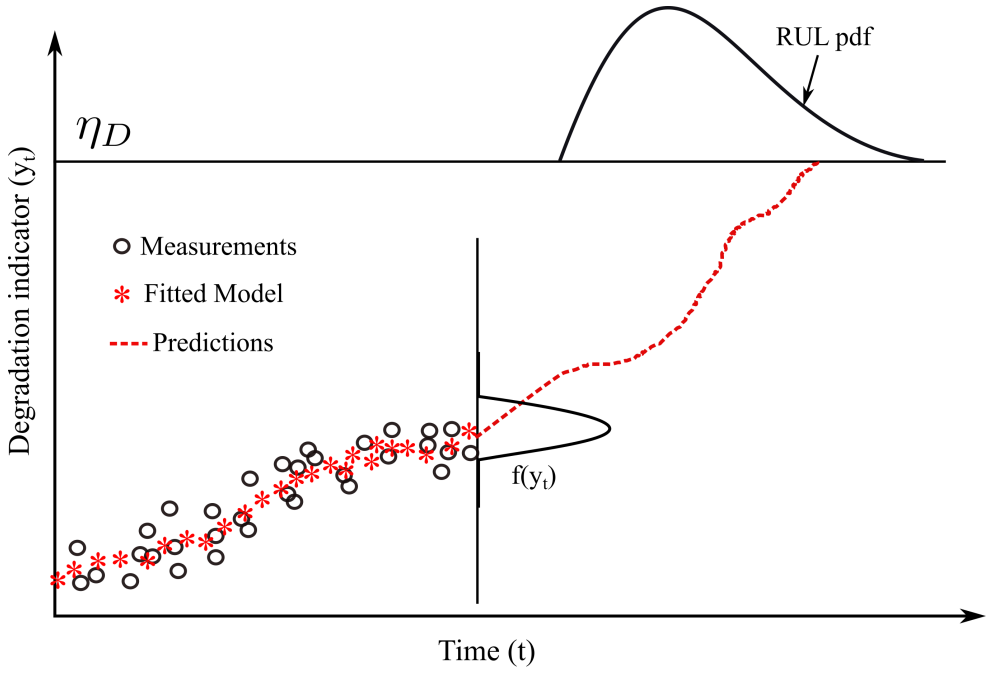

Figure 1.4: Condition based approach for end life predictions

decisions are conducted on a large scale (e.g., replacement of street lamps). However, for expensive and highly reliable systems with significant failure consequences, it is better to integrate condition monitoring information into maintenance interval planning. Such a strategy would allow one to extend a component's operational life, while providing continuous information regarding the health of the component and the ability to adapt inspection intervals based on such information.

Figure 1.4 illustrates the condition monitoring approach for the end of life prediction in the context of condition monitoring pursued in this thesis. Let $y_1, y_2, \cdots, y_t$ denote the degradation measurements, stochastic in nature, from the monitored unit until time t. The first step is to describe these measurements in terms of a degradation model. The choice of degradation model depends upon the application type and can be chosen based on domain knowledge and/or engineering judgment.

Much of the work in the literature involving degradation models assume that the damage mechanism is directly observable (e.g., wall thinning due to corrosion, loss of material due to friction). This thesis deals with those cases when such degradation may not directly be observable. Specifically, two cases, one involving rolling element bearings and the other involving loss of bond in embedded steel bars within concrete, will be studied. In both cases, the degradation modeling approach using indirect measures (surrogates) will be explored. A versatile model which can address such problems will be presented along with the necessary parameter estimation algorithms. Once such a model is established, it will be projected to a failure threshold (η_D), thereby allowing for RUL estimation and maintenance planning. The model parameter estimation will be based on a Bayesian approach, which can systematically integrate prior knowledge obtained from historical failure-time data with monitored data from an in-situ unit.

Amongst various degradation models, one of the models explored extensively in this thesis is a model containing an abrupt change (change-point), called a two-phase degradation model. Such a model is capable of modeling sudden changes in the rate of degradation, such as those found in bearings and in civil structures. Abrupt changes in the overall stiffness, and hence rate of degradation, is commonly associated with bearing faults and structural damage and hence a two-phase degradation model is naturally suited for such problems. One of main aspects which will be studied in this thesis is to model indirect measures of degradation using such a two-phase model. Figure 1.5 shows a few examples where the degradation path contains a change point. As seen form this figure, a two-phase degradation model can be used not only for bearings, but also for modeling deterioration of capacitance, decrease in luminosity of plasma display panels (PDPs) or light emitting diodes (LEDs), and sudden decrease in the number of accidents in coal mines.

In dealing with two-phase degradation, it is important to identify or locate the change

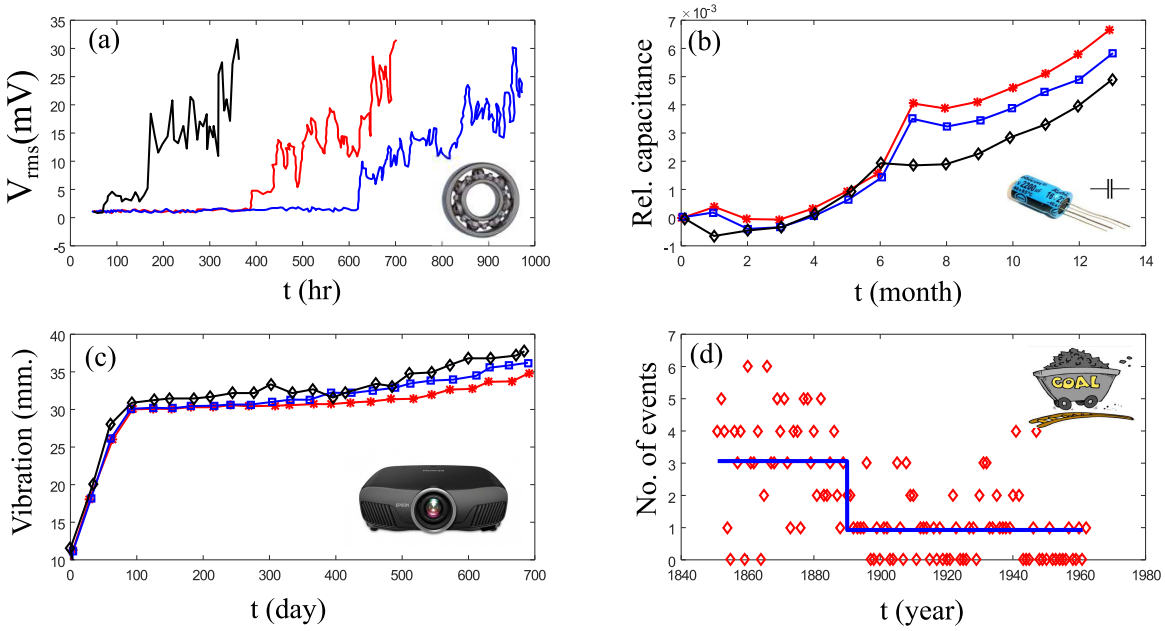

Figure 1.5: Degradation paths containing a change point: (a) rolling element bearing [74] (b) a capacitor; [61] (c) an LCD, and [238] (d) coal mine accidents [177]

point first, and then project the degradation path to the the failure threshold for RUL estimation. The location of change-point can be associated with a sudden loss of stiffness in the case of structural members, or fault initiation in the case of bearings. Both these phenomena are associated with a change in the degradation path, or the rate of deterioration. Hence, the task of change point location identification can be thought of as being synonymous with damage or fault detection in the context of structural health monitoring. This is illustrated in Figure 1.6 for a sample degradation path containing one change point, i.e., a two-phase degradation model. A closer look of figure reveals that, there is a discontinuity in the degradation indicator value around $t = t_1$. Figure 1.6 also depicts the estimated RUL distribution for two specific times, $t = t_1$ and $t = t_2$. Note that the RUL estimate corresponding to $t = t_1$ has a larger uncertainty associated with it than for $t = t_2$, which is the consequence of smaller degradation rate during the first phase. In the

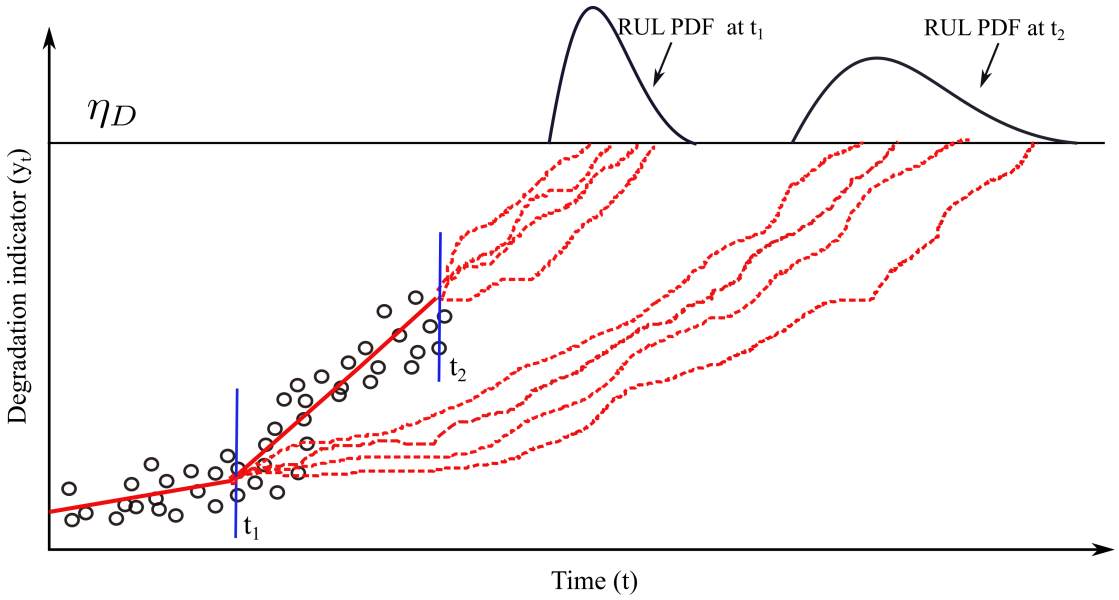

Figure 1.6: condition based approach in case of a change point

context of Bayesian estimation, this under-scores the importance of prior selection, which will be dealt with in detail in this thesis.

1.2 Objectives

Given the above context and background, the overarching objectives of this thesis are as follows:

- Develop an integrated mathematical framework for damage (or, fault) detection and prognosis incorporating measured condition information and prior knowledge about similar units obtained from historical data.
- Demonstrate the applicability of this approach along with a systematic evaluation of the results when combined with surrogate degradation measures for applications where the degradation process is not directly observable.

- Apply the proposed framework to two case studies involving rolling element bearings and structural components.

1.3 Overall Methodology

The overall methodology of the methodology presented in this thesis is illustrated in Figure 1.7. First, a surrogate measure of degradation (often called a degradation indicator or

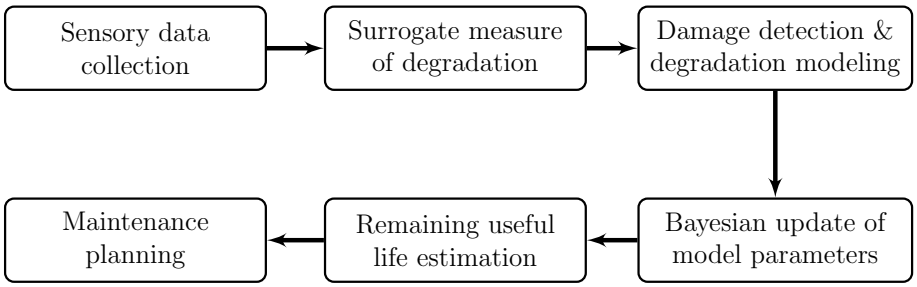

Figure 1.7: Overall methodology

a damage sensitive feature) is extracted from the sensory measurements. In both cases, these measures are surrogates for the underlying hidden degradation mechanism. Next, a suitable degradation model such as random variable (e.g., regression type) or stochastic (e.g., Gamma, Weiner process) is selected for degradation modeling. The degradation model parameters are updated in a Bayesian framework, where the prior knowledge obtained from historical data is integrated with the sensory measurements of a monitored component. For the cases where historical run-to-failure degradation signals are not available, a diffuse prior is used with the philosophy "*let the data speak for itself.*" Next, the degradation model in conjunction with a pre-set threshold is used for reliability assessment and RUL predictions. The task of RUL prediction is straight forward where a closed form

solution for the failure time distribution can be derived (e.g., Weiner process). However, if an analytical solution is difficult to derive, the RUL distribution can be found using sampling techniques such as Markov chain Monte Carlo (MCMC). Finally, the predicted RUL distribution is used for maintenance planning, where the optimum replacement time is obtained by minimizing the expected cost rate. The above described maintenance cycle is updated time-to-time with available degradation data.

1.4 Organization of the thesis

A flow chart showing the thesis organization is given in Figure 1.8, which contains six chapters and organized as follows:

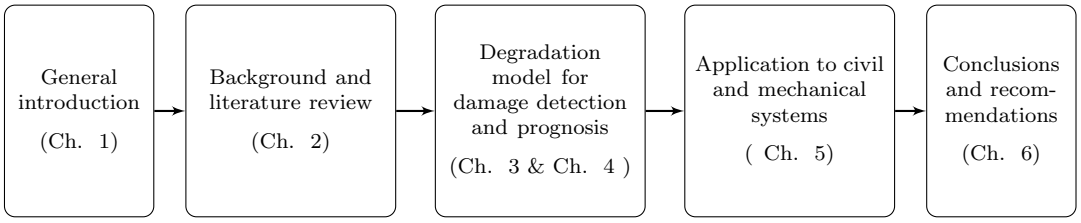

Figure 1.8: Thesis organization

1. **Chapter 1** provides a brief introduction to the problem of damage detection and prognosis for critical infrastructure and a summary of overarching research objectives.

2. A detailed background and literature review on damage detection and prognosis methods for civil and industrial application is presented in **Chapter 2**. Damage detection methods using condition information are reviewed first, followed by the prognosis models. Next, literature on different degradation models (e.g., random variable and stochastic model) applied to damage prognosis are reviewed. Finally, change

point based degradation models and various maintenance models are reviewed. During the course of relevant literature review, the basic demerits of these methods are highlighted to underscore the importance of the proposed research. More specific objectives of this thesis are described following the identified gaps in the literature.

3. **Chapters 3 & Chapter 4** present the theoretical development of integrated degradation modeling framework for damage detection, prognosis and maintenance planning. In Chapter 3, two degradation models namely, linear and exponential models are considered. For these two models, the analytical expression for posterior distribution of model parameters and remaining useful life distribution are derived. More advanced two-phase degradation models are presented in Chapter 4. First, the motivation for two-phase degradation modeling is presented followed by problem formulation for three different cases: random variable, Gamma and Weiner process. Next, the mathematical details for parameter estimation, RUL predictions and maintenance planning are provided for the two-phase models. The overall methodology is illustrated with a numerical example.

4. **Chapter 5** summarizes the results of application of the proposed methodology for damage detection and prognosis of civil and industrial systems. The two example applications investigated are for the deterioration of a reinforced concrete member and the degradation of a rolling element bearing. The degradation of reinforced concrete is modeled using a stochastic gamma process with mid-span beam deflection and slip of steel bars, separately as a measure of degradation. The degradation of the rolling element bearing is undertaken using a random variable model. For both applications, the model parameters and RUL of a monitored unit are updated with available condition data.

5. Finally, a number of conclusions resulting from the presented work are discussed in **Chapter 6**. Several recommendations for future study are also discussed, followed by a summary of the significant contributions of the current work. A list of publications resulting from this work are included in Appendix E.

Chapter 2

Literature review and background

In this chapter, a review of relevant literature on damage detection and prognosis methods for civil and industrial applications is presented. It is important to recognize that the volume of literature, especially in the general areas of fault detection of bearings and damage detection of structures, is extensive. However, most of the literature on these subjects (especially so in the case of bearings) tend to focus on the signal processing aspects; while important, this aspect is not central to this thesis. Hence, a balanced review of the same is presented in this context. Secondly, for the purposes of this thesis, only fault detection is dealt with. This is because for the two applications considered herein, of primary importance is to establish whether a fault or damage exists; knowing the type of damage (diagnosis) is not as critical. Hence damage detection and diagnosis are sometimes used interchangeably throughout this thesis. In this chapter, first, a background on damage detection methods including data-driven methods, time domain methods and frequency domain techniques are presented. Following this, a background on damage prognosis is presented where the literature on various degradation models are reviewed in the context of present research. Finally, a summary of various maintenance models and gap areas in

existing literature are given, followed by the specific objectives of this thesis in the context of this literature review.

2.1 Background on fault detection using condition information

In this section, the relationship between measurable quantities and damage (or, faults) is described from a literature review standpoint, in the context of civil engineering and industrial engineering applications. Along-side this, a brief description of the methods used to process measured information to extract the underlying damage information is also reviewed. This review will provide a segue into the following section on prognostics, which deals with using such measured information to make predictions on RUL and maintenance planning.

2.1.1 Damage detection in civil engineering applications

Damage detection in civil infrastructure such as buildings, bridges and dams has witnessed significant activity during the last two decades [60]. A wide range of non-destructive techniques such as acoustic emission, eddy current, thermal field, radio-graphs, strain measurements, magnetic field methods and ambient vibration response monitoring have all been studied and have been shown to be effective for undertaking damage detection [201, 191, 212, 140]. The basic premise of most of these methods is that structural damage manifests itself indirectly through changes in measurable quantities, even though the mechanism may not directly be measurable in most cases. For example, changes in physical properties such as stiffness, damping or mass of the system, will result in changes in the

vibration data and also in the modal properties: frequencies, mode shape and modal damping, and an extensive review can be found in these papers [41, 26, 57]. Hence, tracking the evolution of parameters obtained using indirect measurements enables damage detection.

Damage detection methods in civil engineering literature can be classified into physics based and data-driven methods. Physics based methods model the governing equations (say, equilibrium) in order to construct a mathematical abstraction of the physical problem, parametrized by variables which have direct physical meaning, followed by a comparison between predicted and measured vibration outputs to quantitatively assess damage e.g., [159, 194]. While these models have shown to work well, they are often accompanied by finite element models which are computationally expensive to build and run for large systems. On the other hand, data-driven approaches do not rely on physical models and use statistical principles in conjunction with monitored data to construct models (input-output models such as auto-regressive (AR) family of time-series models) representing observations. In addition to being able to apply directly to a range of measurement types, the computational complexity in such models is significantly less than physics based models, and hence have been extensively adopted by the researchers [124, 204, 250, 63]. However, the main drawback in these methods is that the quantity being measured and used for decision-making is often indirectly related to the underlying mechanism of interest, and hence can sometimes obfuscate the presence of damage.

Auto-regressive moving-average (ARMA) time series models [204, 142, 154], support vector machines (SVM) [250, 24], neural networks (NNs) [126, 59], self-organizing maps (SOMs) [215], principle component analysis (PCA) [124] and statistical process control [203, 243, 139, 244, 245, 138] are all examples of powerful data driven tools to undertake damage detection tasks. Sohn et al. [204] presented an auto-regressive time series modeling approach for damage localization using acceleration data obtained from an eight degree-of-

freedom lumped parameter structural dynamic system. A more general time series model including AR as well as moving-average (MA) parameters for damage detection and localization was proposed by Nair et al. [142], where the first three AR coefficients were used to derive a damage sensitive feature. Time series models (e.g., AR, MA) combined with SVM [24], hidden Markov model (HMM) [134], and Gaussian mixture model [141] have all been used successfully for feature extraction, damage diagnosis and damage classification. In all these cases, surrogate measures such as Mahalanobis distance, residual error, features extracted from ARMA coefficients have been used in lieu of the physical damage mechanism.

When used in conjunction with time-series models, statistical process control (SPC) charts [135] are powerful on-line monitoring tools for anomaly detection in structural health monitoring (SHM) applications. Sohn et al. [203] used an univariate Shewhart $\bar{X}$ control chart for damage detection, where the control limits are constructed based on features constituted from AR coefficients obtained from an undamaged structure. The use of multivariate Hotelling's T^2 control chart to monitor progressive damage in a reinforced concrete (RC) frame was presented by Wang et al. [243]. Other studies based on SPC charts include Wang et al. [244, 245] who proposed an exponentially weighted moving average control chart, Yao et al. [254] who utilized Mahalanobis distance and spectral distance measures for damage detection, and Mujica et al. [138] who used principal component based Q-statistic and T^2-statistic for damage detection. Ubertini et al. [220] presented multivariate T^2 control charts to track the time evolution of five natural frequencies of structure and successfully applied these charts to condition monitoring of a bell tower in Italy. Comanducci et al. [36] proposed the use of such techniques for damage detection in a long-span arch bridge and applied to Infante D. Henrique bridge, which is the second-largest arch bridge in Europe. Here, it should be pointed out that most of the literature

based on data driven techniques only focuses on the damage detection, and not on damage prognosis, which is an important focus of the present thesis.

Prognosis in civil engineering applications

Unlike damage detection, the volume of literature related to damage prognosis for civil infrastructure is relatively small. The common prognosis problems addressed in civil engineering include fatigue cracking in steel structures, steel rebar corrosion in reinforced concrete structures and age related loss of structural stiffness. Prognosis is the task of assessing the future performances of a structure, given its present health condition. This is often done by projecting the condition information acquired from the system to a predefined threshold. The end result of prognosis is given in terms of RUL, health index, or the probability of failure at a given time in the future.

RUL of riveted aluminum alloy lap joints with multiple cracks subject to fatigue loading was undertaken by Singh et al. [199]. A structural damage prognosis procedure for large structural systems was presented by Haldar et al. [7]. In their study, the health of the structure is assessed through system identification by tracking the stiffness parameter using a ian unscented Kalman filter (UKF) algorithm. Wang et al. [232] proposed an expectation-maximization (EM) algorithm embedded statistical damage prognosis algorithm for in-service civil structures against natural hazards. An extreme value theory (EVT) based Bayesian approach for prognosis of cover plate in a highway steel girder bridge, and pitting corrosion of steel rebars in RC structures, was undertaken by [113]. One advantage of the EVT-based prognosis method is that only a small set of full sensor data is used in Bayesian updating and RUL prediction. This is very important for real time implementation because Bayesian updating tasks are computationally computation-

ally expensive and time consuming. Li et al. [114] presented a framework for sensor-driven structural health prognosis and its application to probabilistic maintenance scheduling and applied this to prototype steel girder bridges.

A probabilistic approach for reliability predictions of nuclear piping system [160, 258], oil and gas pipelines [162], highway bridges [64], deteriorating structure [65] and reinforced concrete bridge beams under corrosion [55] have previously been undertaken in a reliability framework. In [258] Yuan et al. modeled the wall thinning of nuclear feeder pipes in CANDU reactors using a stochastic gamma process and predicted their end of life characteristics. A probabilistic model for condition assessment and determination of optimum replacement interval for oil and gas pipelines was undertaken by Pandey et al. [162]. Frangopol and his colleagues have extensively studied the life-cycle management of highway bridges [64, 65, 66] and concluded that current bridge management system based on condition states has several limitations, which can be overcome using a reliability based approach. To better predict the future states of a bridge, inclusion of monitoring data was deemed necessary. They demonstrated the use of monitored data for reliability assessment of an existing highway bridge (the Lehigh River Bridge SR-33) located in Pennsylvania [66].

The aforementioned studies using degradation modeling or the reliability-based approach do not consider the existence of a change point in the degradation path. However, in the case of shock events, a change point(s) is often found in the degradation path and needs to be considered for accurate RUL predictions. Moreover, integration of damage detection results for prognosis has not been studied comprehensively in the civil engineering literature.

2.1.2 Industrial applications

Much of industrial applications of relevance in this thesis is related to gearbox and bearing diagnostics. The volume of literature on these topics is vast and a comprehensive literature review is not attempted. Numerous methods using indirect measurements have been developed for damage detection of rolling element bearings. Indirect fault sensitive features have been extracted from acoustic measurements [84], temperature [83], electrical motor current [192], wear debris analysis [50] and vibrations [181, 236]. Amongst these, vibration analysis has shown to have several advantages [181]. First, it is easy to implement and reliable [181]. Secondly, it has been shown that various defect types in gears and bearings produce different vibration patterns; hence, vibration signatures can be related to a specific type of defect [182] (see Appendix A for background). However, it can sometimes be expensive compared to methods such as current monitoring and furthermore direct access to the rotating component is required to install the sensors.

The ensuing discussion relates to the literature which relies on vibration measurements for bearing fault detection, as this is the mode employed in this thesis. Furthermore, to limit the scope of the review, the focus will be on literature on bearing faults. One of the first steps in the detection of bearing faults is to acquire vibration measurements using accelerometers from the bearings, bearing support housing, or other structural parts that respond to the impulsive forces resulting from these faults. The acquired signal is then analyzed using various signal processing techniques to ascertain the presence of faults and if possible to diagnose them. In general, these techniques can be summarized as belonging to the class of: i) time domain methods ii) frequency domain methods, and (iii) time-frequency methods. In the following section, pertinent literature belonging to these classes are reviewed. A brief background on bearing faults and the resulting vibration

characteristics is given in Appendix A.

Time domain methods

In time-domain analysis, a bearing fault is detected by monitoring the variation of statistical moments (often called condition indicators) such as the mean, variance, skewness, peak value, root mean square (RMS) value, the crest factor, or the kurtosis [226]. Mathematical expressions for these condition indicators are given in Appendix A. A bearing is assumed to be damaged when a condition indicator value exceeds a pre-defined threshold; however, it is usually difficult to determine the appropriate thresholds because they may vary in different applications and depends upon operating and loading conditions.

RMS value of a signal represents the signal energy and has been applied for the detection of localized defects by Miyachi et al [133]. It was shown that the RMS value with defects is always higher than without defects, which makes RMS a good indicator to monitor the damage progression. The fourth moment, normalized with respect to the fourth power of standard deviation called kurtosis has proven to be another good indicator of fault. It has good sensitivity to shocks and impulses. Kurtosis is also widely used to detect non-periodic shocks. For a healthy bearing, kurtosis value should be very close to three, which is a Gaussian distribution [249]. In the initial stages, when the bearing deteriorates, this value initially increases, but later decreases. This happens because severely damaged bearings produce frequent impulses, which makes vibration signals nearly Gaussian [156]. However, if the signal is filtered to accentuate these impulses (e.g., using minimum entropy deconvolution (MED) filter), the kurtosis value is found to increase with the progression of the fault, as shown in [190]. Another indicator, crest factor, which is defined as the ratio of the maximum peak of the signal to its RMS value is often used for fault detection. It is very

sensitive to the shape of the signal and detects the impulsive nature in the signal better than many indicators. Crest factor greater than six is generally considered as a reliable sign for fault [40] and has been used for bearing fault detection in [186]. In all these studies, the primary aim is to extract various damage sensitive features from raw vibration measurements are use it for diagnosis. A link between such indicators for prognosis has not been pursued extensively in the literature. Another important point worth mentioning here is that compared to pure time-domain methods, there is a disproportionately large volume of methods and studies on bearing diagnostics based on time-frequency methods, which will be described later.

Frequency domain analysis

Frequency domain analysis (also called spectral analysis) is based on the spectral content of a vibration signal. In this method, the time domain signal is transformed from the time domain to the frequency domain using Fourier transform (its fast version, FFT) and power spectrum [56]. The FFT permits to: (1) recognize and separate harmonic or side-band patterns and (2) identify the different types of bearing faults by monitoring the increasing amplitude of the characteristic fault frequencies. A detailed presentation of the fundamentals of frequency analysis can be found in the book by Randall [180] and a brief review of the same is presented in Appendix A. Chao et al. [30] classify frequency domain methods into two categories: direct spectrum analysis and processed spectrum methods. The processed spectrum methods such as envelope spectrum [129], cepstrum analysis [183], time synchronous averaging [130] and Hilbert transform [169, 155] is generally used when the signal to noise ratio is low. Recently, Wang and Osman [155] developed a novel normalized HHT technique for bearing fault detection. Envelope analysis (see Appendix A) is a fault detection technique that is widely used in the industry. It consists of a sequence of op-

erations where the raw vibration signal is band-pass filtered,enveloped (or rectified), and then the spectrum of the enveloped signal is calculated. An adaptive envelope spectrum technique for bearing fault detection was proposed by [210].

Time-frequency analysis

Time as well as frequency domain analysis are based on the assumption that statistical characteristics such as mean and variance of signals do not vary over time. Such signals are known as stationary signals, but when signals are non-stationary, the above methods are unable to capture the variations. Deterioration is inherently a non-stationary event and since time frequency domain transforms retain both the time and frequency information, it provides the requisite tools to deal with non-stationary signals. A number of time-frequency domain techniques have been used bearing fault detection, including the Short Time Frequency Transform (STFT), the Wigner-Ville Distribution (WVD), the empirical mode decomposition (EMD) [107], the spectral kurtosis [14] and the Wavelet Transform (WT) [185, 172, 119]. STFT and WVD have many limitations (for example constant window size for STFT and spectrum aliasing in the case of WVD) that prevent their effective use. These limitations were discussed in detail in the following reference [170]. As mentioned previously, the field of bearing fault diagnostics—even pertaining to just time-frequency analysis—is quite vast. Only a brief background on the underlying methodology and some relevant references are included here.

Wavelet transform based techniques

Wavelet transform (WT) is one of the most widely used tools in time-frequency domain analysis [185, 146, 170]. It is defined in terms of an inner product between the signal and

the wavelet basis, which unlike the sine and cosine bases used in the Fourier transform, provides a richer variety of orthogonal and non-orthogonal bases to capture a variety of vibration signals. The Wavelet basis function is obtained by a dilation and translation from the mother wavelet or wavelet prototype ψ(t) given by [173]:

$$\psi_{a,b}(t) = \frac{1}{\sqrt{a}}\psi\left(\frac{t-b}{a}\right) \tag{2.1}$$

where a is the scale factor and b is the time location. The factor $\frac{1}{\sqrt{a}}$ takes care of energy preservation of the signal. The wavelet transform of signal $x(t)$ is the inner product in the Hilbert space of the L^2 norm

$$W(a,b) = <\psi_{a,b}(t), x(t)> = \frac{1}{\sqrt{a}}\int x(t)\psi^*_{a,b}dt \tag{2.2}$$

where the asterisk denotes the complex conjugate.

Leducq et al. [103] first used WTs to analyze the hydraulic noise of the centrifugal pump, which is possibly the first paper on the use of wavelets in diagnostics. Later, Wang and McFadden [234] applied wavelets to analyze gear vibration signals and they found that wavelets are able to detect different types of faults simultaneously. Denoising and extraction of weak signals are very important aspects for bearing fault diagnostics, especially for early fault detection where features are often very weak and masked by noise from other components, especially from gear meshing. The powerful de-noising capability of wavelets makes them suitable for bearing fault detection and has been used extensively by many researchers [117, 90, 76, 206]. Yang and Liao [253] proposed a wavelet-based de-noising approach, in which the noise thresholds are adjusted adaptively according to the background noise. Altmann and Mathew [10] used discrete wavelet packet analysis-based

multiple band-pass filtering to deal with the vibration signals from a low speed rolling-element bearing and they presented results which were significantly improved compared to their high-pass counterpart in terms of SNR. Wang et al. [233] proposed an energy kurtosis demodulation (EKD) technique that uses WT and maximum kurtosis deconvolution (MKD) filter for bearing fault detection. Wavelets have proved to be useful for detection of non-stationary and irregular signals, such as transient signals for the reason that it could eliminate background noise. Lin [117] applied a wavelet-based method to remove the noise from the machine sound, and, furthermore to extract the fault features for diagnostics.

The principle of wavelets for denoising is different from that of traditional filter-based methods. In brief, in the filter-based methods, the frequency components outside a certain range are generally set to zero, which may cause some useful fault information to be lost. This is because some burst faults often appear as impulses in signals and these impulses cover a wide frequency range; filter-based denoising methods will smooth such impulses. On the other hand, wavelet-based methods set some wavelet transform coefficients to zero, which can retain such impulses in signals. Examples include edge cracks in cantilever beams [213], crack in rotors [264], cracks in beam structures [176], damage in structures [231, 38], cracks in composite plates [39], etc. Staszewski [205] presented an extensive review on structural and mechanical damage detection using wavelets, which covers a wide range of techniques and applications involving WT.

Spectral Kurtosis

Spectral kurtosis (SK) is a statistical parameter which measures the impulsive nature of a signal as a function of the frequency present in the signal [14, 48, 190]. SK was first applied by Dwyer et al. [48] to detect impulsive events in sonar signals. Kurtosis has long been

used as a measure of severity of machine faults, since it was first proposed by Stewart et al. [49] in the 1970s. The application of SK to bearing faults was clearly explained by Antoni et al. [14], who developed the methods for calculation of SK. Recently, it has been applied for bearing fault detection by Sawalhi et al. [190], Zhang et al. [262] and Randall et al. [182]; for gear fault detection by Barszcz et al. [19] and Combet et al. [37]; gear-bearing interactions by Sawalhi et al. [188, 189].

Figure 2.1 illustrates the procedure for the calculation of SK as described by Randall and Antoni [14, 182]. To calculate SK, first the STFT of a non-stationary signal is obtained by translating a window along the signal and evaluating the frequency spectra for each window [190]. The square of resulting time-frequency envelope $H(t, f)$ represents the power spectrum values as a function of time. The average of all these short-time power spectra is the power spectrum of the whole record. The kurtosis $K(f)$ for each frequency f can be calculated by taking the fourth power of $H(t, f)$ at each time and averaging its value along the record, then normalizing it by the square of the mean square value. It has been shown that subtracting 2 from this ratio results in a zero value for, $K(f)$ a Gaussian signal [227]:

$$K(f) = \frac{\langle H^4(t, f)\rangle}{\langle H^2(t, f)\rangle^2} - 2 \tag{2.3}$$

The numerator in Eq. 2.3 depends on the window length. To maximize kurtosis, the window length must be shorter than the spacing between the pulses, but longer than the individual pulses.

To maximize the SK value in a given frequency band, different window lengths are considered. This can be visualized using a "*kurtogram*" [15], which is a two dimensional color map indicating the optimum center frequency and range for the bandpass filter which

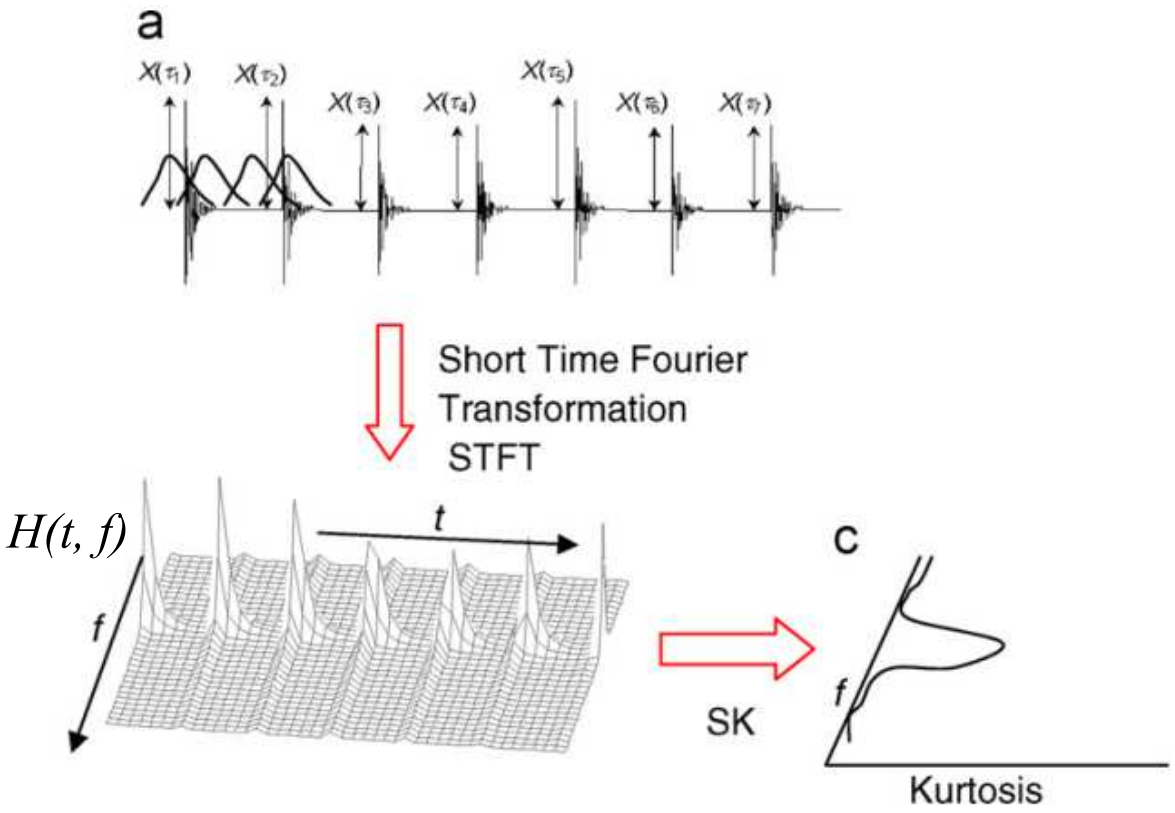

Figure 2.1: Calculation of SK from the STFT for a simulated bearing fault signal adopted from [14] (a) simulated time signal (b) STFT (c) SK as function of frequency

maximizes the kurtosis. An example kurtogram is shown in Figure 2.2. In this case, the optimum center frequency is 10.68 kHz and the bandwidth 50 Hz. This means that if the signal is band-passed with a central frequency of 10.68 KHz with a spectral band of 50 Hz, the impulsiveness can be captured well. In this range, the maximum kurtosis is found to be 27.2 as shown in Figure 2.2, indicating the presence of a fault. Many researchers have combined SK with other signal de-noising techniques for effective bearing fault detection. For example, SK with MED [190], SK with AR modeling [187], SK with envelop analysis [22] and SK with EMD [209] have all been studied in the literature.

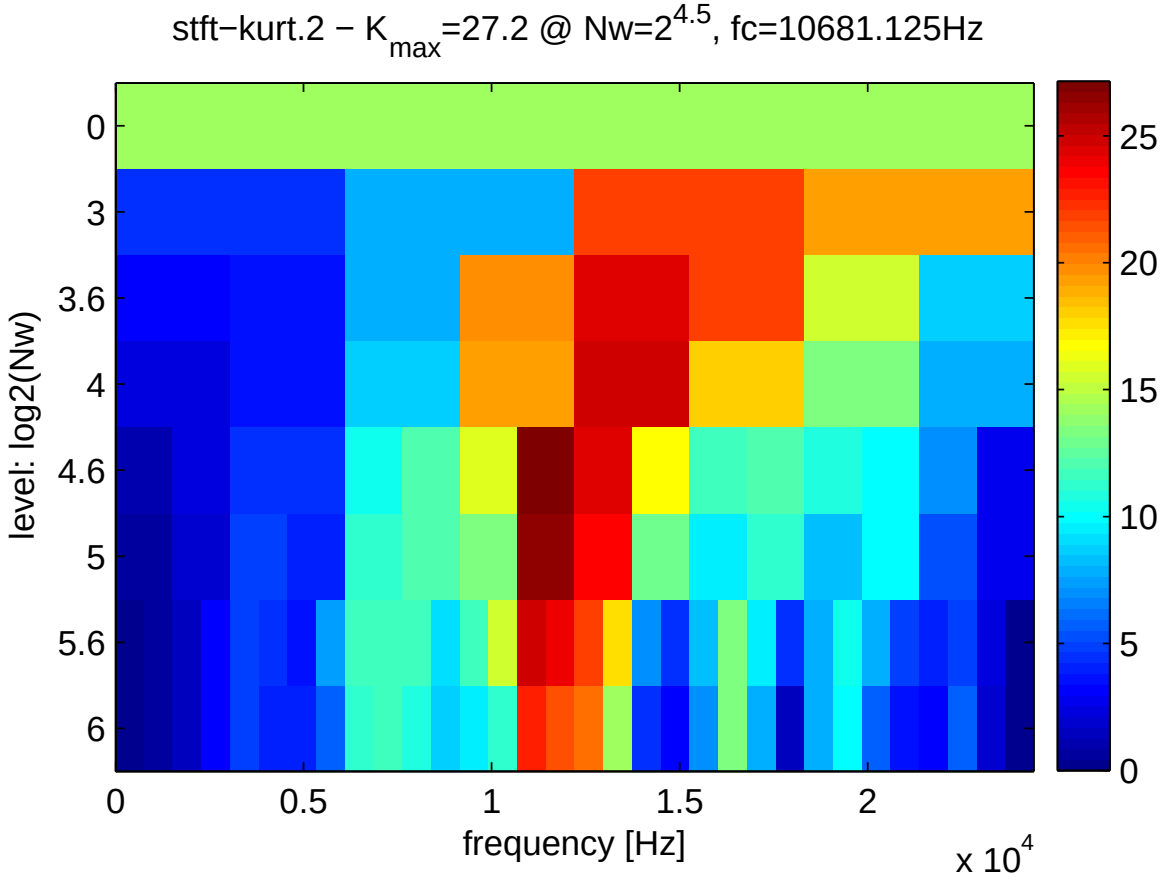

Figure 2.2: Kurtogram

Empirical mode decomposition

Empirical mode decomposition [86] is one of the most powerful time-frequency analysis techniques. It is based on the local characteristic time scales of a signal and can decompose a signal into a set of complete and almost orthogonal components called intrinsic mode function (IMF). The IMFs indicate the natural oscillatory mode embedded in the signal and serves as the basis functions, which are determined by the signal itself, rather than pre-determined kernels. Thus, it is a self-adaptive signal processing technique that is suitable for nonlinear and non-stationary processes. EMD has been extensively applied

to detect and diagnose faults in rolling element bearings. Xu et al. [251] used EMD to analyze vibration signals obtained from accelerated life tests of bearings and investigated the evolving trend of a bearing life cycle. Cheng et al. [95] proposed the energy operator demodulation approach based on EMD for bearing fault diagnosis. Fan and Zuo [58] utilized the amplitude acceleration energy of IMFs to represent fault characteristics for both bearings and gears. Yan and Gao [252] detected the deterioration in a test bearing through instantaneous frequencies identified by EMD. Li et al. [108] utilized the marginal spectrum based on EMD to identify different patterns of bearing faults.

In recent years, many researchers have integrated EMD with other techniques such as: independent component analysis [132], Teager-Kaiser energy operator [110], Fourier transform of IMFs [179], Wigner–Ville distribution [111], order tracking [109] and wavelet packet transform [106] for effective bearing fault detection. The use of EMD continues to see significant activity and adoption in bearing fault diagnostics community.

2.2 Background on damage prognosis

In the previous section, the literature on damage detection was reviewed, which is only one component of a CBM program. If a progressing damage is detected early on, then the condition information acquired from the monitored unit can be utilized for damage prognosis. RUL prediction and maintenance planning are two major components of prognosis. The task of RUL estimation is achieved by modeling the underlying degradation process using a surrogate measure of degradation and projecting it to the failure threshold. The estimated RUL distribution can then serve as input to the maintenance model and an optimum replacement interval can be sought. These aspects are briefly discussed along with the relevant literature, next.

2.2.1 Degradation modeling

Failure in most of the engineered systems result from a gradual and irreversible accumulation of damage, which occurs during its operation. The evolution of underlying degradation processes can be monitored directly (e.g., crack length) or indirectly (e.g., vibration, acoustic or ultrasonic, magnetic field, radiography, thermal and eddy-current signal) using sensor technology. These periodically acquired signals are collectively known as degradation signals and can serve as a basis for degradation modeling. Degradation modeling focuses on mathematical modeling of degradation signals and estimation of remaining useful life distribution based on pre-defined failure thresholds [143]. Degradation modeling using direct measurements have been studied in a variety of applications such as crack growth in metals [122], nuclear piping system [160], oil and gas pipelines [162] and wall thinning due to flow-accelerated corrosion [258]. Where degradation is not directly observable, surrogate measures such as those extracted from vibration measurements [226, 9, 260, 27, 147, 77], strain measurements [127, 69, 70, 171] and current measurements [225], have been employed in the literature. It is important to mention here that the use of surrogate measures of degradation for modeling of civil and mechanical infrastructure is still in the initial stages of research.

Generally speaking, existing probabilistic degradation models can be classified into broad two categories: (i) parametric models with random/mixed coefficient and (ii) stochastic process models [122, 75, 221, 52]. The former implies a mean degradation path that varies from unit to unit, which is suitable for unit-to-unit variation. The second approach describes the variation in degradation data by a time-dependent stochastic process such as Markov, Gamma or a Wiener process. These two types of degradation models are illustrated in Figure 2.3 and their mathematical details are given in Appendix B.

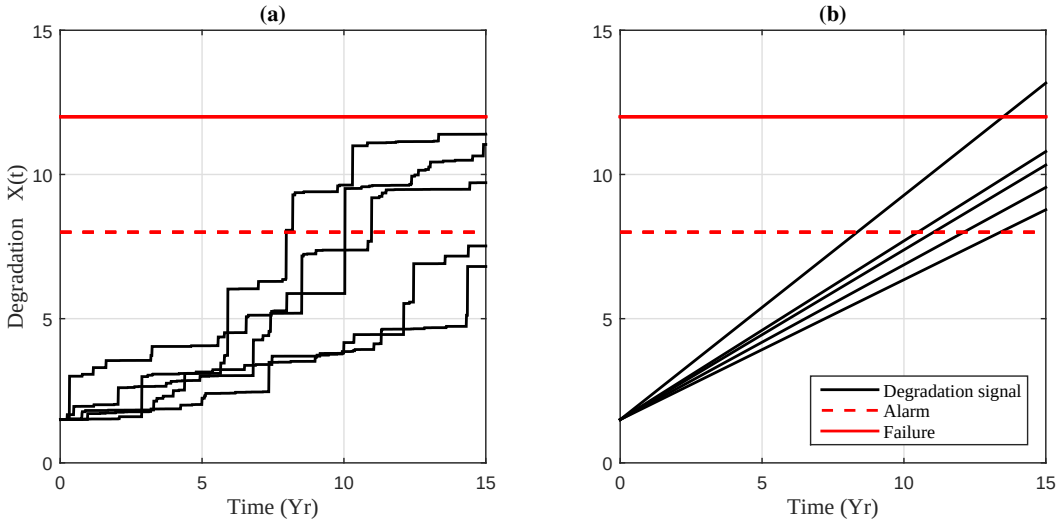

Figure 2.3: Degradation models (a) Stochastic Gamma process and (b) Linear random coefficient

A detailed classification of various degradation models is presented in Figure 2.4 and a summary of their applications including issues addressed are presented in Table 2.1. In the following subsections, literature on random variable models, stochastic process models and two-phase models, which is the focus of this study, are reviewed.

Table 2.1: Summary of degradation models for reliability assessment

Model	References	Issue addressed	Application
Random Variable	[122]	Time to failure distribution	Fatigue-crack-growth
	[75, 71, 72]	Remaining useful life	Rolling element bearing
	[257]	Nonlinear mixed-effects model	Flow-accelerated corrosion
	[67, 68]	Model parameters estimation	Train wheel degradation
	[118]	Parametric Bayesian models	Locomotive wheels
	[81]	Life-time vs degradation data	Laser degradation
	[94]	Graphical representation data	Numerical example
	[211]	Dynamic maintenance threshold	Numerical study
	[265]	Mixture model	Valve recession data

Table 2.1: Summary of degradation models for reliability assessment

Model	References	Issue addressed	Application
	[224]	Bayesian approach	Resistance heating cables
Gamma Process	[221]	Theoretical aspects	Inspection and maintenance
	[87, 51, 163]	Time-dependent reliability	Deteriorating structures
	[100]	Covariates and random effects	Fatigue-crack-growth
	[123, 259, 223]	Parameters and RUL estimation	Corrosion of nuclear pipes
	[35]	Calculation of confidence limits	Creep of concrete
	[157]	Bivariate degradation	Fatigue crack
	[218]	With random effects	Laser degradation
	[78, 115, 34]	Condition based maintenance	Numerical example
	[207]	Integration of SHM data	Creep deformations of bridges
	[88]	Temporal variability and uncertainties	Concrete sewer pipes
	[89]	Aging and shock events	Bilinear structural systems
Weiner Process	[246]	Time scale transformation	Heating cable
	[256]	With measurement error	Wear of magnetic heads
	[237]	With random effects	bridge beam degradation
	[197]	RUL using recursive filter	Gyros used for navigation
	[247]	Bivariate Weiner process	Aluminum reduction cells
	[112]	Time correlated structure	Resistors and sliding metal
	[241]	Real-time reliability evaluation	Capacitance loss over time
Inverse Gaussian	[32]	With random-drift	Optimal CBM policy
	[242]	Maximum likelihood estimation	Laser devices
	[255]	Random effects, explanatory variables	Laser devices
	[174]	Bayesian method using inspection data	Corrosion growth modeling
	[167]	A Bayesian perspective	GaAs laser degradation data
Change point	[31]	Two-phase, Bayesian approach	RUL prediction of bearings
	[17]	Piecewise linear model	Light display units
	[239]	Gamma and Wiener process	Liquid coupling devices
	[151]	Structural damage diagnosis	Four-story steel frame
	[79, 80]	Poisson process	Earthquake occurrence data

Table 2.1: Summary of degradation models for reliability assessment

Model	References	Issue addressed	Application
	[62]	Multi-phase Weiner	Storage life of capacitor
	[13]	Two-phase Weiner	Liquid coupling devices
	[99]	Abrupt jump at change point	Numerical Example
	[43]	Weiner and Inverse Gaussian	Variable-stress testing
	[145]	Localized damage detection	A steel tube frame testbed
Markov processes	[20]	Hidden Markov model	Diagnosis and prognosis
	[216, 217]	Mixture of Gaussian HMM	RUL estimation
	[44, 168, 46]	Hidden semi-Markov model	Diagnosis & prognosis of pumps
	[153, 172, 261]	Hidden Markov model	Bearing fault diagnosis
	[136, 137, 96]	Markov model	Bridge deck systems
	[144]	Semi-Markov model	Bridge deterioration modeling

2.2.2 Random variable degradation model

One of earliest studies based on a random coefficient model (also referred to as the general path or a random variable model) was undertaken by Lu and Meeker [122]. Let Y_{ij} be the observed degradation for the ith unit at the jth time t_{ij}. Then, the random coefficient model is given by:

$$Y_{ij} = \eta(t_{ij}, \boldsymbol{\theta}_i, \boldsymbol{\phi}) + \epsilon_{ij} \tag{2.4}$$

where $\eta(\cdot)$ is some function, $\boldsymbol{\theta}_i$ is a vector of random effects and $\boldsymbol{\phi}$ is a vector of parameters common to all units. Previously, linear, exponential, power law, logistic and Gompertz functional forms $\eta(\cdot)$ have been used [202] in Eq. 2.4. Typically, measurement errors ϵ_{ij} are assumed to be additive, conditionally independent and normally distributed with mean 0

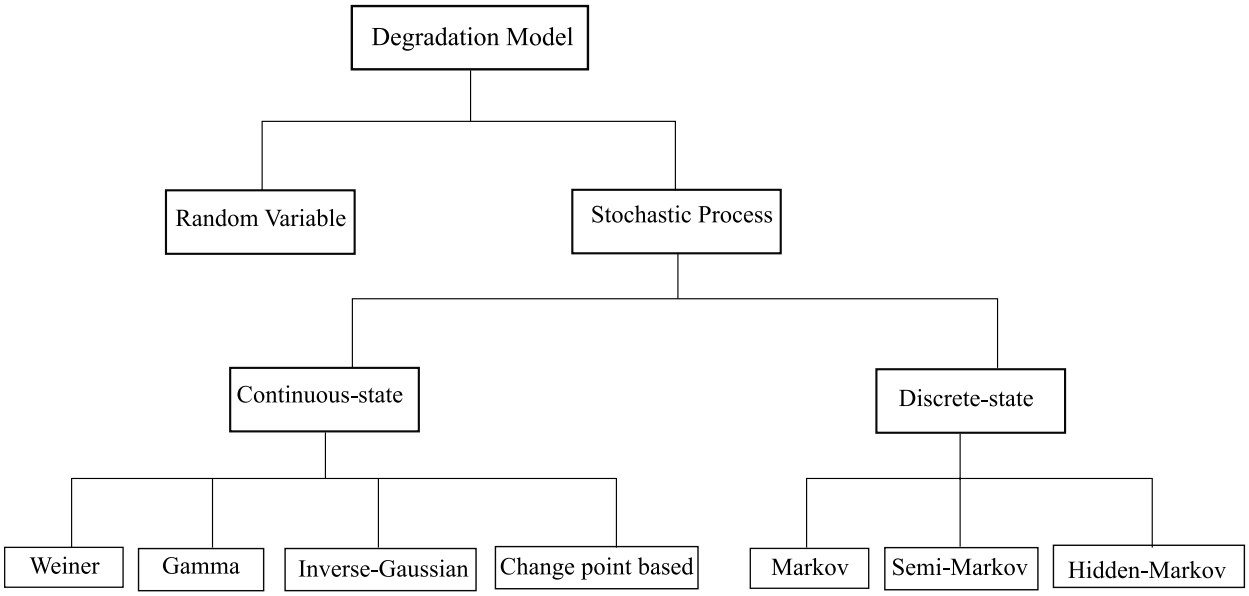

Figure 2.4: Degradation models

and variance σ_ϵ^2 [122]. But it need not have to be normally distributed and additive always. For example, a multiplicative measurement error model has the form $Y_{ij} = \eta(t_{ij}, \boldsymbol{\theta}_i, \boldsymbol{\phi})\epsilon_{ij}$, and the ϵ_{ij} might have a log-normal distribution [82], or can follow a Brownian motion [75]. Failure of a unit is declared when the degradation level first reaches a predefined failure threshold, η_D i.e.,

$$T_i = \inf\{t_j : Y_{ij} \geq \eta_D\} \tag{2.5}$$

where T_i is failure time of ith unit.

Lu and Meeker [122] used a random coefficient model to analyze and assess the reliability of fatigue crack growth data. They also derived closed form analytical solutions for the cumulative failure time distribution for the special functional forms $\eta(\cdot)$ of exponential and linear. Gebraeel and his colleagues [75, 71, 52, 72] used an exponential functional form for bearing degradation modeling using vibration measurements and derived a closed

form expression for residual life distribution. Other works using this approach include a non-linear random coefficients model with a non-parametric degradation path to capture the burn-in characteristics of vacuum fluorescent displays by Bae et al. [16], a random coefficient degradation model with random sample size by Su et al. [208] and lifetime distribution based degradation analysis by Chen et al. [33].

The random coefficient model is a simple model to study, and it is directly related to statistical analysis of deterioration data. However, a fixed functional form $\eta(\cdot)$ may not be conducive under variations in the environmental and operational loading conditions. Another problem is that this model does not account for temporal uncertainty, i.e., uncertainty associated with the evolution or progression of deterioration over time [161].

2.2.3 Stochastic degradation model

A special category of stochastic processes that have been used extensively in degradation modeling is the process with stationary and independent increments (called Lévy process) [147]. A stochastic process $Y(t)$ is said to have stationary and independent increments if it has the following two properties:

1. For any $0 \leq t_1 \leq \cdots \leq t_n$, random variables $Y(t_1) - Y(0)$, $Y(t_2) - Y(t_1)$, $\cdots$, $Y(t_n) - Y(t_{n-1})$ are independent.

2. For any $t \geq 0$ and $s > 0$, the distribution of increments $Y(t+s) - Y(t)$ depends on the time difference s.

When the random increments $Y(t_n) - Y(t_{n-1})$ between two consecutive time periods is normally distributed, it is called a Wiener process [97]. Doksum et al. [42] modeled the

variable-stress accelerated life testing fatigue failure data using a Wiener process. In their study, the accumulated fatigue decay was modeled using two separate Wiener processes which change from one to another at a certain stress change point, t. Wang [237] applied a Wiener process with random effects to analyze bridge beam degradation data. In their model, the unit-to-unit variability was incorporated through random effects and the uncertainties in the model parameters were estimated using a bootstrap method. In another study, Wang and his colleagues [197] used a Wiener-process-based degradation model with a recursive filter for RUL estimation of gyros in an inertial navigation system. They were able to update the drift coefficient in the Wiener process using a recursive filter and other parameters using an EM algorithm. In this way the updating was done in real-time upon the availability of online degradation data.

Time scale transformation of a Wiener diffusion process was considered by Whitmore et al. [246] and applied towards degradation modeling of a self-regulating heating cable. The problem of measurement noise in the degradation signal, which gives inaccurate Wiener process parameter estimates was undertaken by Ye et al. [256]. They modeled a traditional Wiener process with positive drifts compounded with identically and independently distributed Gaussian noises and improved its estimation efficiency compared to existing inference procedures. The developed methodologies that are applicable to the wear problem of hard disk drive magnetic heads and the light intensity degradation problem of LED lights. Wiener process is good for modeling the stochastic nature of degradation, which can increase or decrease between two consecutive times. However, in many cases, degradation is monotonically increasing, where this cannot be applied.

Another Lévy process that has been widely used for degradation modeling is the Gamma process, which assumes Gamma distributed random increments. The monotonically increasing property of the Gamma process makes it ideal for modeling gradual damage that

accumulates over time. It is also well suited for modelling the temporal variability of deterioration and proven to be useful in determining optimal inspection and maintenance decisions. Noortwijk [221] first introduced the application of Gamma process to the civil engineering community for degradation modelling and the aforementioned paper presents an exhaustive survey for maintenance applications. Huang et al. [87] used a Gamma process to develop a time-dependent reliability model for deteriorating structures. A stochastic Gamma process model was used for building deterioration by Edirisinghe et al. [51], for creep of concrete by Cinlar et al. [35], for fatigue crack growth by Lawless et al. [100], and for thinning caused by corrosion by Noortwijk et al. [222]. Grall et al. [78] used a Gamma process to analytically model the deterioration of a continuously deteriorating single-unit system and proposed an optimum preventive replacement policy structure. Liao et al. [115] presented a condition-based maintenance model for continuously degrading systems under continuous monitoring. The use of Gamma process for modeling degradation of products involving multiple performance characteristics was undertaken by Pan et al. [158]. Recently, the probability distribution of maintenance cost of a system affected by the Gamma process of degradation was undertaken by Cheng et al. [34].

Both random coefficient and stochastic models can be used for RUL estimation of a monitored unit once the corresponding parameters are estimated. However, such a degradation model may not be able detect fault localized in time; for example, as a change point in the degradation signal. Such models incorporating change points are effective for damage detection and damage prognosis within a single framework. This aspect is discussed next in the context of a two-phase model.

2.2.4 Two-phase degradation model

Most of the existing literature for degradation modeling (either random variable or stochastic process) assume that the deterioration of the system is governed by a single stochastic process. However, in many situations, the degradation signal often contains a change point, which occurs due to a sudden change in the operating or in the environmental condition, impurities in the material, or damage initiation. For example, empirical results have shown that bearing degradation generally consists of two phases: in the first phase, the deterioration is slow until a spall or a defect is formed in the bearing raceways. Once a defect is formed, the degradation process grows rapidly in the second phase [75]. Figure 2.5 shows

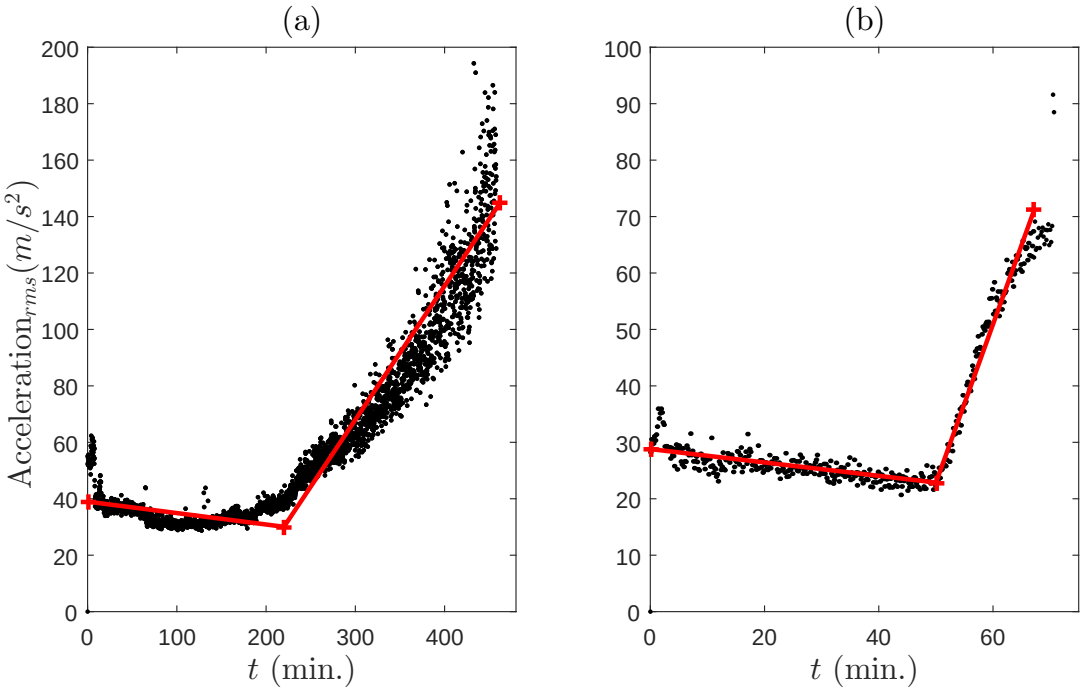

Figure 2.5: Example run-to-failure bearing degradation signal ([166])

an example for one run-to-failure bearing degradation (RMS value of vibration with time) where a two-phase degradation rate with a change point can be clearly observed.

A two-phase degradation modelling approach was used for rolling elements bearings by Gebraeel et al. [75, 71, 73]. In the aforementioned work, the authors developed a two-phase degradation model using the RMS value of acceleration and they integrated real time condition data in a Bayesian framework. In their model, the first phase consists of a relatively constant signal representing the period before damage initiation, followed by a second phase—monotonically increasing—representing damage progression. Using this approach, they arrived at a closed form solution to predict and update the RUL. Their study underscores the use of change point detection as a proxy for bearing fault detection. Change point detection along with RUL estimation was studied by Chen et al. ([31]). The authors in this study proposed a Bayesian change point detection approach for two-phase degradation modeling and RUL predictions, assuming that the location of the change point does not have a significant effect on other degradation parameters such as the degradation rate. This approach reduces the Bayesian computations significantly, since the estimation process for the parameters of the two phases can be decoupled. Furthermore, this approach is limited to those cases where the posterior distribution of the change point is narrow enough to be assumed to be concentrated at a point. Moreover, experimental data on bearing degradation has shown [31] that the degradation rate and the change point are often correlated, which is undertaken in the thesis. In an another study [98] a two-phase Weiner process was used to model bearing degradation, where change detection and failure prediction were undertaken using a Kalman filter. However, these studies do not update the model parameters and the reliability with the availability of monitored data. Recently, Wang et al. [228] proposed a two-phase mixed effects model to analytically model the bearing degradation process. In their model, two cases for the error term namely, multiplicative normal random error and multiplicative Brownian motion error, are considered and two different closed-form distributions for bearing remaining useful life are

derived. It was found that the model with a multiplicative Brownian motion error results in lower prediction errors than the model with multiplicative normal random error for bearing RUL prediction.

The Bayesian change point approach is not limited to rolling element bearings only. Bae et al. ([17]) used this approach to model the degradation of light display units (plasma display panels) and derived a prediction for the failure time distribution of a randomly selected unit, while Vanli ([225]) utilized a Bayesian approach to model the degradation of a heating cable. Recently, Yan et al. [13] applied change point based two-phase Weiner degradation process for real-time reliability evaluation of liquid coupling devices (LCDs). In their method, change point detection was undertaken using the Akaike information criterion and a bootstrap method wass used to obtain the confidence interval of reliability. The application of two-phase degradation model is relatively new in the civil engineering discipline, compared to either the mechanical or computer engineering disciplines. Recently, Noh et al. [150] applied the change point detection method for sequential structural damage detection of a four-story steel special moment-resisting frame and Gupta et al., [79] for change detection in seismic rates. In the latter, a Bayesian change point model was implemented to find when the number of earthquakes events suddenly increased in Oklahoma city.

Two-phase degradation modeling with two different functional forms in the two phases has been undertaken by Wang et al. [240] for real time reliability evaluation of LCDs, in which the initial sharply increasing phase was modeled using a Gamma process, while the latter using a Weiner process. The approach used for two-phase degradation modeling can be extended to model the processes which shows multi-phase degradation. Feng et al. [62] used a multi-phase Weiner degradation model for storage life prediction for a high-performance capacitor. It was found in this study that ignoring change points which exist

in the degradation path could lead to significant prediction uncertainty in the storage life of a capacitor.

2.3 Maintenance models

Maintenance decision models focus on establishing economical policies for inspection, repair, replacement and spare parts inventory, and they have been studied extensively in the literature [4, 229, 23, 52, 78]. In general, maintenance policies can be divided into two categories: preventive maintenance and corrective maintenance (also known as run-to-failure or reactive maintenance). Preventive maintenance is carried out at predetermined intervals, while corrective maintenance is undertaken when a break-down occurs in the system. Preventive maintenance can be further divided into two categories: (i) time (age) based maintenance (TBM) and (ii) condition based maintenance. Ahmad et al., [4] presented an overview of various maintenance strategies for industrial applications. Under TBM policy—which is generally applied to non-repairable systems—a unit is replaced after a time t_p, or at failure, whichever occurs first. The mathematical formulation for this model was developed by Barlow et al. [18], which was based on minimization of expected cost rate (ECR), details of which are discussed in Appendix C.

In recent years, CBM has emerged as an effective maintenance program that utilizes condition information for maintenance planning. CBM attempts to avoid unnecessary maintenance tasks by taking maintenance actions only when there is evidence of abnormal behaviour of a physical asset. A CBM program, if properly established and effectively implemented, can significantly reduce maintenance cost by reducing the number of unnecessary scheduled preventive maintenance operations [91]. The concept of CBM was first introduced by the Rio Grande railway company in late 1940s and initially it was called

predictive maintenance [195]. Ever since, CBM has been widely applied in rotating machinery applications [45, 53, 229, 92], wind turbines [214], bridges [66] and various other deteriorating systems [3]. The performance measures widely used for CBM models are cost minimization and reliability or availability maximization. Wang et al. [235] developed a model which can be used to determine the optimum critical level (also called the threshold or the control limit) and monitoring interval in CBM by minimizing the long-term expected cost per unit time. The model was established on the basis of a random variable model, where the coefficients of the regression model were assumed to follow known distribution functions. The minimization of the ECR was further investigated by Grall et al. [78], where both the replacement threshold and the inspection schedule are considered as decision variables for the maintenance optimization problem.

Castanier et al. [29] assumed a multi-level control-limit rule repair/replacement policy and obtained optimal inspection scheduling based on a cost criterion and an availability criterion. Amari and McLaughlin [11] utilized a Markov chain to describe the CBM model for a deteriorating system subject to periodic inspection. The optimal monitoring interval frequency and failure threshold were found to maximize the system availability. Elwany et al. [53] formulated the single-unit replacement problem as a Markov decision process to determine the optimal replacement policy and successfully applied this to rotating machinery. Abdel-Hameed [3] studied CBM of a system subject to stochastic deterioration. A recent review on condition-based maintenance optimization models for stochastically deteriorating systems was presented by Alaswad et al. [8].

Even though the theory of CBM is well developed, its on-line implementation is limited due to integration of a variety of software and hardware components. A guide for implementing CBM in manufacturing industry considering the technical constituents and organizational aspects (during execution of CBM) are given by Rastegari et al. [184]. Niu

et al. [149] presented a CBM system that uses reliability-centered maintenance mechanism to optimize maintenance cost, and employs data fusion strategy for improving condition monitoring, health assessment, and prognostics. One of the most important steps for CBM implementation was undertaken by the Machinery Information Management Open System Alliance (MIMOSA^{TM}) for next generation of machinery diagnosis and prognosis [102]. This framework employs an open system architecture for CBM that uses a distributed software model approach to facilitate the integration and interchangeability between a variety of hardware and software components.

2.4 Gaps in the research literature

For the damage detection and prognosis of highly reliable systems, a large amount of research, as discussed in the previous sections, has been published in recent years, which broadly focuses on damage detection, degradation modeling, change detection and maintenance planning. However, several important issues such as an integrated framework for damage detection and prognosis, use of historical failure data for maintenance planning of a monitored unit, updating the model parameters and RUL with available condition information, remain at best only partially addressed in the literature. A summary of the gap areas in the existing research on damage detection and prognosis is described below, which forms the motivation for the current thesis.

1. **Integration of damage detection and prognosis:** The literature review showed that most of the work is focused on damage detection. Research using condition information for damage prognosis of civil and mechanical infrastructure is lacking and needs to be expanded upon. Only in a few studies, damage detection results are

extended to RUL estimation. An integrated framework which undertakes damage detection, prognosis, and maintenance planning in a systematic way is lacking in the literature.

2. **Use of historical data for better reliability assessment:** Although many degradation models have been developed, their parameters are solely estimated using the degradation data obtained from the monitored unit. In other words, the established model may represents the degradation of a specific unit, but ignores the general population trend. If the prior knowledge obtained from the historical degradation data are integrated in the parameter estimation of an in-situ monitored unit, then more accurate failure predictions can be made possible.

3. **Consideration of correlation amongst model parameters:** Most of the existing research using two-phase degradation models do not consider the correlation amongst model parameters. However, run-to-failure experiments on bearing degradation have shown that the degradation rate in the second phase depends upon the change point location. Hence, it is imperative to consider the correlation between change point and other model parameters, especially the second phase degradation rate.

4. **Application to civil and industrial disciplines:** Finally, most of the studies using degradation modeling are applied in the computer and electrical engineering disciplines such as: light emitting diodes, hard disks, liquid coupling devices, capacitor and laser devices. Few studies exist for industrial components such as bearings and gyros, however, very little for civil infrastructure. Hence, there is an immediate need for the transfer of technology from other disciplines to civil and industrial applications.

2.5 Specific objectives

Based on the identified gaps in the literature, the specific objectives of this thesis are as follows:

1. develop a degradation modeling framework using surrogate measures of degradation to integrate damage detection and prognosis for highly reliable components, with particular emphasis on models enabling change point detection;

2. develop a systematic methodology which combines prior knowledge obtained from the historical failed units with degradation model parameter estimation and RUL prediction for a monitored unit;

3. account for the correlation between different degradation model parameters in the methodology, in particular the second phase degradation rate and change point location; and,

4. evaluate the performance of the proposed degradation modeling framework for maintenance planning of civil and industrial engineering systems with focus on deterioration of reinforced concrete beams and rolling element bearings, respectively.

Chapter 3

Degradation modeling and RUL estimation

In this chapter, the basics of degradation modeling and the basic concepts of parameter estimation and RUL estimation employing Bayesian principles are presented. A justification for using surrogates to model the underlying degradation process is presented, followed by a general approach to degradation modeling and end life predictions for a component. Next, the methodology is illustrated for use through linear and exponential degradation models, where the parameters and RUL estimation are updated in a Bayesian framework. The primary focus of this chapter will be for those cases where analytical solutions are possible. Finally, a numerical example is presented to illustrate this approach.

3.1 Degradation modeling

Degradation modeling is a way to mathematically quantify the underlying degradation mechanism and subsequently predict incipient faults. In general, deterioration-related failures can be classified into two categories: i) hard failures and ii) soft failures. A hard failure (also called shock failure) occurs when a system experiences sudden shock (e.g., earthquake, tsunami, tornado, sudden load increase etc), irrespective of the current health state of the system. On the other hand, a soft failure is directly related to the continuous deterioration process, and occurs when the degradation level first reaches a preset failure threshold. Degradation modeling of soft failures is the major concern of this thesis.

For some degradation processes such as wear, corrosion and crack-growth, it is possible to measure a physical quantity that is directly related to the underlying degradation mechanism or failure. However, for many degradation processes such as bearing degradation and deterioration of reinforced concrete structures, the degradation process can only be modeled through some indirect measure of degradation (called a surrogate) derived from the sensory measurements. Let X_t be the underlying degradation process, Y_t the surrogate measure at time t and $\mathcal{F}$ denote the mapping from the original degradation space to the surrogate space. This is depicted in Figure 3.1. The mapping function $\mathcal{F}$ in some cases can be derived from the physics of the process (e.g., equilibrium, deflection). However, in general, $\mathcal{F}$ is unknown. In the absence of such knowledge, the mapping $\mathcal{F}$ is assumed to preserve the monotonic trend of the actual degradation process into the surrogate space. In other words, the increasing degradation level is reflected in the magnitude of the surrogate Y_t. Furthermore, the functional forms describing X_t and Y_t may or may not be the same in the two spaces. For example, if the actual degradation X_t follows a quadratic form, it can be mapped to a linear form in Y_t. As long as the thresholds are set in the surrogate

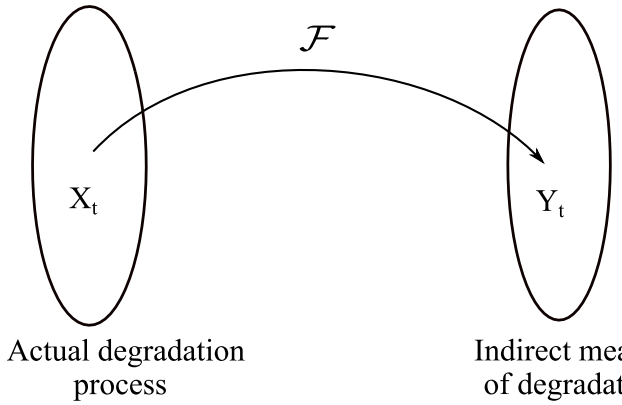

Figure 3.1: Actual degradation process and indirect measure

space to predict the end of useful life, it is not mandatory to preserve the functional form in the two spaces.

Given this context, let the surrogate measure Y_j of an unit at time t_j be given by:

$$Y_j = \eta(t_j, \boldsymbol{\theta}, \boldsymbol{\phi}) + \epsilon_j, \qquad j = 1, 2, \cdots, m \tag{3.1}$$

where $\eta(\cdot)$ is some function (e.g., linear, exponential, power law, gamma process, Weiner process, logistic and Gompertz forms), ϵ_j is the measurement error at time t_j, $\boldsymbol{\theta}$ is a vector of random parameters which vary from unit to unit and $\boldsymbol{\phi}$ is a vector of fixed-parameters, which is identical for all units. Let, L_k be a random variable representing the RUL at time t_k, given the observation history $Y_1, Y_2, \cdots Y_{t_k}$. The distribution of L_k is obtained by evaluating the distribution of time left until the surrogate reaches a predefined threshold η_D, as given below:

$$F_{L_k} = P\{L_k < t | Y_1, \cdots Y_k\} = P\{\eta(t + t_k, \boldsymbol{\theta}, \phi) + \epsilon_{t+t_k} > \eta_D | Y_1, \cdots Y_k\} \tag{3.2}$$

As discussed above the actual degradation process is complex and degradation models

as in Eq. 3.1 is only a simplified representation of the underlying degradation process. In other words, there is always an uncertainty associated with model predictions, which may or may not be reduced depending upon its origin.

3.2 Uncertainties in degradation modeling

In general, the uncertainties can be classified into two categories: aleatory uncertainty and epistemic uncertainty. The word aleatory derives from the Latin *alea*, which means the rolling of dice. Thus, aleatoric uncertainty appears in the model due to the intrinsic randomness of the degradation process. Such a randomness can either be parameterized by discrete probability values or by a PDF, depending upon the nature of variable. Aleatory uncertainty can further be classified into unit-varying uncertainty (or random effect across units) and time-varying uncertainty (or temporal uncertainty). In this thesis, a random variable model is employed to address the unit-varying uncertainty; and a stochastic degradation model (e.g., Gamma and Weiner process) has been considered to model the temporal uncertainty. Aleatory uncertainty is inherent property of a degrading system, hence, cannot be reduced.

On the other hand, epistemic uncertainty arises due to the lack of knowledge. The word epistemic derives from the Greek *episteme*, which means knowledge. This lack of knowledge can come from many sources such as, partial understanding of underlying degradation mechanism, uncertainty in model structure and parameters, or measurement error, etc. The epistemic uncertainty can be reduced by acquiring more knowledge about the degrading system, e.g., by taking more measurements, by conducting more tests, and by selecting a proper model structure etc. According to the origin of the epistemic uncertainty, different theories such as, probability theory, possibility theory, fuzzy logic, expert

judgment and convex modeling has been applied in the literature [263].

In this thesis a Bayesian framework has been employed to address the parameter uncertainty [47]. Let $M = (S, \boldsymbol{\theta})$ denotes the model, where S is the model structure (e.g., deterministic or stochastic) and $\boldsymbol{\theta}$ is the model parameters. In Bayesian approach, to solve the problem of structural uncertainty model $M = (S, \boldsymbol{\theta})$ is considered as nuisance parameter, and the conditional predictive distribution of future degradation level Y_t is obtained by marginalizing with respect to model M. Mathematically, it can be written as:

$$p(Y_t|t) = \int_M p(Y_t|t, M)p(M|t)dM \tag{3.3}$$

$$= \int\int p(Y_t|t, S, \boldsymbol{\theta})p(S, \boldsymbol{\theta}|t)dSd\boldsymbol{\theta} \tag{3.4}$$

$$= \int\int p(Y_t|t, S, \boldsymbol{\theta})p(S, |t, \boldsymbol{\theta})p(\boldsymbol{\theta}|t, S)dSd\boldsymbol{\theta} \tag{3.5}$$

Note that in Eq. 3.3, the first term, i.e., $p(Y_t|t, M)$ incorporates the aleatory uncertainty, and the second term, i.e., $p(M|t)$ incorporates the epistemic part. In the special case, when $p(S, |t, \boldsymbol{\theta})$ is concentrated on S^*, i.e., a specific model is chosen, Eq. 3.5 reduces to:

$$p(Y_t|t) = \int p(Y_t|t, S^*, \boldsymbol{\theta})p(\boldsymbol{\theta}|t, S^*)d\boldsymbol{\theta} \tag{3.6}$$

where $p(\boldsymbol{\theta}|t, S^*)$ is the parameter uncertainty. In this thesis, the model structure S is kept fixed (e.g., single phase degradation model or two-phase degradation model) and the parameter uncertainty is assessed using MCMC sampling.

In the following section, two types of degradation models are considered—linear and exponential models—to illustrate the parameter estimation process and RUL predictions for a monitored unit in a Bayesian framework. The first model is used to characterize degradation signals that follow a linear path, whereas the second considers signals that

grow exponentially. It is important to note that for these two degradation models, an analytical solution for the posterior distribution of parameters and RUL can be derived, which provides valuable insights into the Bayesian mathematics. Other degradation models which require Markov chain Monte Carlo simulations for Bayesian inference are described in the next chapter.

3.3 Linear degradation model

The linear degradation model is typically used for modeling degradation processes where the rate of degradation remains constant throughout the system's life. For example, wear of brake pads follows linear degradation, where the decrease in the thickness in any given time interval remains the same irrespective of the age of the brake pad. For a given unit, the linear degradation model is expressed as:

$$Y_j = \phi + \theta t_j + \epsilon_j \tag{3.7}$$

where, θ is a random coefficient which can vary from unit to unit, ϕ is a deterministic parameter, which remains constant for all the units. The error ϵ_j is assumed to be normally distributed with mean 0 and variance σ^2. The model parameters are (θ, σ^2) can be estimated using standard Bayesian approach. According to the Baye's rule, the posterior distribution of the parameters, $p(\theta, \sigma^2|\boldsymbol{Y})$ is given by:

$$p(\theta, \sigma^2|\boldsymbol{Y}) \propto \pi(\theta, \sigma^2) L(\boldsymbol{Y}|\theta, \sigma^2) \tag{3.8}$$

where, $\boldsymbol{Y}$ is the vector of surrogates, $L(\boldsymbol{Y}|\theta, \sigma^2)$ is the likelihood of the vector, given the parameters, and $\pi(\theta, \sigma^2)$ is the prior distribution of the parameters. For this model, a conjugate prior exists, which is a normal-inverse Gamma distribution. Using the total probability rule, the joint prior $\pi(\theta, \sigma^2)$ can be written as product to two separate priors: $\pi(\theta|\sigma^2)$ and $\pi(\sigma^2)$, where $\pi(\theta|\sigma^2)$ follows a normal distribution and $\pi(\sigma^2)$ follows an inverse-gamma distribution.

For degradation model in Eq. 3.7, residual error ϵ_j, which consists of model error (error in model structure) and measurement error, is an example of aleatory uncertainty. The uncertainty associated with the parameter (θ, σ^2) is the epistemic uncertainty. Once the marginal posterior distribution of θ and σ^2 is estimated, the epistemic uncertainty is quantified by using the estimated distribution. In this case, $p(\theta|\sigma^2)$ follows normal distribution and $P(\sigma^2)$ follows inverse gamma distribution. For other degradation models, such as, nonlinear and stochastic, MCMC techniques can be used to estimate the posterior distribution and subsequently uncertainty quantification.

The future degradation level Y_{t+t_k} at any time t from the current time t_k can be predicted using:

$$p(Y_{t+t_k}|Y_1, \cdots Y_k) = \int \int p(Y_{t+t_k}|\theta, \sigma^2) p(\theta, \sigma^2|Y_1, \cdots Y_k) d\theta d\sigma^2 \tag{3.9}$$

which can be evaluated numerically using sampling techniques such as MCMC. Through the use of modern computing hardware and software tools, e.g., like WinBUGS [152], evaluating the above integral is relatively straight-forward. The RUL distribution can be estimated by comparing the predicted future degradation level with a failure threshold.

The MCMC based approach is generally applicable to any degradation model. However, it does not provide insights into the details of Bayesian mathematics. If one of the

parameters of the linear degradation model (say, σ^2) was to be known independently, then a closed-form expression for the posterior distribution and RUL can be derived, which helps us understand the updating procedure for a monitored unit. Let the prior distribution $\pi(\theta)$ be normally distributed with mean μ_θ and variance σ_θ^2 and $(Y_1, Y_2, \cdots Y_k)$ represent the measurements monitored at times $(t_1, t_2, \cdots t_k)$. The prior distribution and likelihood function for this model are given by:

$$\pi(\theta) = \frac{1}{(2\pi\sigma_\theta^2)^{1/2}} \exp\left(-\frac{(\theta - \mu_\theta)^2}{2\sigma_\theta^2}\right) \tag{3.10}$$

$$L(\boldsymbol{Y}|\theta) = \frac{1}{(2\pi\sigma^2)^{k/2}} \exp\left(-\sum_{j=1}^{k} \frac{(Y_j - \theta t_j - \phi)^2}{2\sigma^2}\right) \tag{3.11}$$

The posterior distribution $p(\theta|\boldsymbol{Y}, \sigma)$ is obtained by multiplying Eq. 3.10 and Eq. 3.11, which is found to be a normal distribution with mean $\tilde{\mu}_\theta$ and variance $\tilde{\sigma}_\theta^2$:

$$\tilde{\mu}_\theta = \frac{\sigma_\theta^2 \sum_{j=1}^{k} (Y_j - \phi) t_j + \mu_\theta \sigma^2}{\sigma_\theta^2 \sum_{j=1}^{k} t_j^2 + \sigma^2} \tag{3.12}$$

$$\tilde{\sigma}_\theta^2 = \frac{\sigma^2 \sigma_\theta^2}{\sigma_\theta^2 \sum_{j=1}^{k} t_j^2 + \sigma^2} \tag{3.13}$$

Once the model parameters are updated, the updated values can be used to predict the future degradation level. Let the random variable Y_{t_k+t} denote the value at a time t in the future, given that the current time is t_k. The mean and variance of the predictive distribution of Y_{t+t_k} are given by:

$$\mu_{Y_{t+t_k}} = E(Y_{t_k+t}) = E(\phi + \theta'(t_k + t) + \epsilon_{t_k+t}) = \phi + \tilde{\mu}_\theta(t_k + t) \tag{3.14}$$

$$\sigma^2_{Y_{t_k+t}} = Var(Y_{t_k+t}) = Var(\phi + \theta'(t_k + t) + \epsilon_{t_k+t}) = \tilde{\sigma}_\theta^2 (t_k + t)^2 + \sigma^2 \tag{3.15}$$

Thus, each time the monitored data is available, the parameters $\tilde{\mu}_\theta$, $\tilde{\sigma}_\theta^2$ are updated and subsequently used to modify the trajectory of the degradation signal.

The predictive distribution estimated above is used to compute the distribution of RUL, L_k. The definition for RUL is given in Eq. 3.2 and used to derive the expression for RUL. Mathematically, it can be written as:

$$F_{L_k} = P(L_k < t | Y_1, \cdots Y_k) \tag{3.16}$$

$$= P(Y_{t+t_k} > \eta_D | Y_1, \cdots Y_k) \tag{3.17}$$

$$= 1 - P(Z \leq \frac{\eta_D - \mu_{Y_{t+t_k}}}{\sigma_{Y_{t+t_k}}}) \tag{3.18}$$

$$= \Phi\left(\frac{\mu_{Y_{t+t_k}} - \eta_D}{\sigma_{Y_{t+t_k}}}\right) \tag{3.19}$$

where $\Phi(Z)$ is the cumulative density function (CDF) of standard normal random variable Z.

3.4 Exponential degradation model

The exponential model performs well in those applications where the rate of degradation depends upon the cumulative degradation level. Corrosion, crack-growth, deterioration of civil structures, and bearing degradation are some examples of such cases. Gebraeel et al. [72] described the following form for an exponential degradation model:

$$Y_j = \phi + \theta_1 \exp\left(\theta_2 t_j + \epsilon_j - \frac{\sigma^2}{2}\right) \tag{3.20}$$

where, Y_j is an appropriate surrogate measure of degradation at time t_j, ϕ is a constant, θ_1 is a log-normal random variable, where $\ln\theta_1$ has mean μ_{θ_1} and variance $\sigma^2_{\theta_1}$, θ_2 is a normal random variable with mean μ_{θ_2} and variance $\sigma^2_{\theta_2}$ and ϵ_j is the random error with mean 0 and variance σ^2, which is assumed to be known. It is assumed that the θ_1, θ_2 and ϵ_j are mutually independent, and that $\epsilon_1, \cdots \epsilon_k$ are independent and identically distributed random variables. For this model it can be shown that the expectation $E[\exp(\epsilon_j - \sigma^2/2)] = 1$ and hence $E[Y_j|\theta_1, \theta_2] = \phi + \theta_1 \exp(\theta_2 t_j)$.

Proof : Let $z = \epsilon_j$, then

$$\begin{aligned} E\left[e^{\left(z-\frac{\sigma^2}{2}\right)}\right] &= \int_{-\infty}^{\infty} e^{\left(z-\frac{\sigma^2}{2}\right)} f(z)dz \\ &= \int_{-\infty}^{\infty} e^{\left(z-\frac{\sigma^2}{2}\right)} e^{-\frac{z^2}{2\sigma^2}} dz \\ &= \int_{-\infty}^{\infty} e^{-\frac{1}{2}\left(\frac{z^2}{\sigma^2}-2z+\sigma^2\right)} dz \\ &= \int_{-\infty}^{\infty} e^{-\frac{(z-\sigma^2)^2}{2\sigma^2}} dz = 1 \end{aligned} \tag{3.21}$$

and

$$\begin{aligned} E[Y_j|\theta_1, \theta_2] =& E\left[\phi + \theta_1 \exp\left(\theta_2 t_j + \epsilon_j - \frac{\sigma^2}{2}\right)\right] \\ =& \phi + \theta_1 e^{\theta_2 t_j} E\left[e^{\left(\epsilon_j - \frac{\sigma^2}{2}\right)}\right] \\ =& \phi + \theta_1 e^{\theta_2 t_j} \end{aligned} \tag{3.22}$$

For the exponential model given in Eq. 3.20, it will be convenient to work with the logarithm of the signal. Moreover, the logarithm is a monotonic function and hence retains the monotonic nature of the degradation. By taking logarithm on both sides of Eq. 3.20:

$$\log(Y_j - \phi) = \log\theta_1 + \theta_2 t_j + \epsilon_j - \frac{\sigma^2}{2} \tag{3.23}$$

$$\mathcal{L}_j = \theta_1' + \theta_2 t_j + \epsilon_j \tag{3.24}$$

where $\mathcal{L}_j = \log(Y_j - \phi)$ and $\theta_1' = \log\theta_1 - \sigma^2/2$, θ_1' is normally distributed with mean $\mu_{\theta_1'} = \mu_{\theta_1} - \sigma^2/2$ and variance $\sigma^2_{\theta_1'} = \sigma^2_{\theta_1}$. Note that in the log-transformed domain, the exponential degradation model (i.e., Eq. 3.24) is very similar to the linear degradation model, with the key difference that the exponential model has more number of parameters.

Let the logged surrogates $\mathcal{L}_1, \mathcal{L}_2, \cdots, \mathcal{L}_k$ constitute measurements at times $(t_1, t_2, \cdots t_k)$, respectively. Assuming that θ_1' and θ_2 are independent, the joint prior distribution $\pi(\theta_1', \theta_2)$ can be written as the product:

$$\pi(\theta_1', \theta_2) = \pi(\theta_1')\pi(\theta_2) \tag{3.25}$$

$$= \frac{1}{(2\pi\sigma^2_{\theta_1'})^{1/2}} \exp\left(\frac{-(\theta_1' - \mu_{\theta_1'})^2}{2\sigma^2_{\theta_1'}}\right) \frac{1}{(2\pi\sigma^2_{\theta_2})^{1/2}} \exp\left(\frac{-(\theta_2 - \mu_{\theta_2})^2}{2\sigma^2_{\theta_2}}\right) \tag{3.26}$$

$$\propto \exp\left(\frac{-(\theta_1' - \mu_{\theta_1'})^2}{2\sigma^2_{\theta_1'}}\right) \exp\left(\frac{-(\theta_2 - \mu_{\theta_2})^2}{2\sigma^2_{\theta_2}}\right) \tag{3.27}$$

Similarly, the likelihood of the data given the parameters can be written as:

$$L(\boldsymbol{\mathcal{L}}|\theta_1', \theta_2) = \frac{1}{(2\pi\sigma^2)^{k/2}} \exp\left(-\sum_{j=1}^{k} \frac{(\mathcal{L}_j - \theta_1' - \theta_2 t_j)^2}{2\sigma^2}\right) \tag{3.28}$$

where $\boldsymbol{\mathcal{L}}$ is a vector of logged values of the surrogate measurements. Note that in Eq. 3.27, $\mu_{\theta_1'}, \sigma^2_{\theta_1'}, \mu_{\theta_2}$ and $\sigma^2_{\theta_2}$ are the hyper-parameters which are estimated from historical failure data. Estimation of hyper-parameters from historical failure data is discussed in the next chapter. Given the prior and the likelihood of the data, an expression for the joint posterior

distribution of parameters (θ_1', θ_2) can be derived as follows:

$$p(\theta_1', \theta_2|\boldsymbol{\mathcal{L}}) \propto \pi(\theta_1', \theta_2) L(\boldsymbol{\mathcal{L}}|\theta_1', \theta_2) \tag{3.29}$$

$$\begin{aligned}
&\propto \exp\left(\frac{-(\theta_1' - \mu_{\theta_1'})^2}{2\sigma_{\theta_1'}^2}\right) \exp\left(\frac{-(\theta_2 - \mu_{\theta_2})^2}{2\sigma_{\theta_2}^2}\right) \frac{1}{(2\pi\sigma^2)^{k/2}} \exp\left(-\sum_{j=1}^{k} \frac{(\mathcal{L}_j - \theta_1' - \theta_2 t_j)^2}{2\sigma^2}\right) \\
&\propto \exp\Bigg\{-\frac{1}{2}\Bigg[\frac{1}{\sigma^2}\left(k{\theta_1'}^2 + \theta_2^2 \sum_{j=1}^{k} t_j^2 - 2\theta_1' \sum_{j=1}^{k} \mathcal{L}_j - 2\theta_2 \sum_{j=1}^{k} \mathcal{L}_j t_j + 2\theta_1'\theta_2 \sum_{j=1}^{k} t_j\right) \\
&\quad + \frac{1}{\sigma_{\theta_1'}^2}({\theta_1'}^2 - 2\mu_{\theta_1'}\theta_1' + \frac{1}{\sigma_{\theta_2}^2}({\theta_2}^2 - 2\mu_{\theta_2}\theta_2)\Bigg]\Bigg\} \\
&\propto \exp\Bigg\{-\frac{1}{2}\Bigg[{\theta_1'}^2\left(\frac{k}{\sigma^2} + \frac{1}{\sigma_{\theta_1'}^2}\right) + \theta_2^2\left(\frac{\sum_{j=1}^{k} t_j^2}{\sigma^2} + \frac{1}{\sigma_{\theta_2}^2}\right) - 2\theta_1'\left(\frac{\sum_{j=1}^{k} \mathcal{L}_j}{\sigma^2} + \frac{\mu_{\theta_1'}}{\sigma_{\theta_1'}^2}\right) \\
&\quad - 2\theta_2\left(\frac{\sum_{j=1}^{k} \mathcal{L}_j t_j}{\sigma^2} + \frac{\mu_{\theta_2}}{\sigma_{\theta_2}^2}\right) + 2\theta_1'\theta_2\left(\frac{\sum_{j=1}^{k} t_j}{\sigma^2}\right)\Bigg]\Bigg\} \\
&\propto \exp\Bigg\{-\frac{1}{2}\Bigg[{\theta_1'}^2\left(\frac{1}{\tilde{\sigma}_{\theta_1'}^2(1-\rho^2)}\right) + \theta_2^2\left(\frac{1}{\tilde{\sigma}_{\theta_2}^2(1-\rho^2)}\right) - 2\theta_1'\left(\frac{\tilde{\mu}_{\theta_1'}}{\tilde{\sigma}_{\theta_1'}^2(1-\rho^2)} - \frac{\tilde{\mu}_{\theta_2}}{\tilde{\sigma}_{\theta_1'}\tilde{\sigma}_{\theta_2}(1-\rho^2)}\right) \\
&\quad - 2\theta_2\left(\frac{\tilde{\mu}_{\theta_2}}{\tilde{\sigma}_{\theta_2}^2(1-\rho^2)} - \frac{\tilde{\mu}_{\theta_1'}\rho}{\tilde{\sigma}_{\theta_1'}\tilde{\sigma}_{\theta_2}(1-\rho^2)}\right) - 2\theta_1'\theta_2\left(\frac{\rho}{\tilde{\sigma}_{\theta_1'}\tilde{\sigma}_{\theta_2}(1-\rho^2)}\right)\Bigg]\Bigg\} \\
&\propto \frac{1}{2\pi\tilde{\sigma}_{\theta_1'}\tilde{\sigma}_{\theta_2}\sqrt{(1-\rho^2)}} \exp\Bigg\{-\left[\frac{\sigma_{\theta_2}^2(\theta_1' - \mu_{\theta_1'})^2 + 2\sigma_{\theta_1'}\sigma_{\theta_2}\rho(\theta_1' - \mu_{\theta_1'})(\theta_2 - \mu_{\theta_2}) + \sigma_{\theta_1'}^2(\theta_2 - \mu_{\theta_2})^2)}{2\sigma_{\theta_1'}^2\sigma_{\theta_2}^2(1-\rho^2)}\right]\Bigg\}
\end{aligned} \tag{3.30}$$

Eq. 3.30 reveals that the joint posterior distribution of (θ_1', θ_2) follows a bi-variate normal distribution with mean $(\tilde{\mu}_{\theta_1'}, \tilde{\mu}_{\theta_2})$, variance $(\tilde{\sigma}_{\theta_1'}^2, \tilde{\sigma}_{\theta_2}^2)$ and the correlation coefficient ρ given

by:

$$\tilde{\mu}_{\theta_1'} = \frac{\left(\sum_{j=1}^{k} \mathcal{L}_j \sigma_{\theta_1'}^2 + \mu_{\theta_1'}\sigma^2\right)\left(\sum_{j=1}^{k} t_j^2\sigma_{\theta_2}^2 + \sigma^2\right) - \left(\sum_{j=1}^{k} t_j\sigma_{\theta_1'}^2\right)\left(\sum_{j=1}^{k} \mathcal{L}_j t_j\sigma_{\theta_2}^2 + \mu_{\theta_2}\sigma^2\right)}{\left(k\sigma_{\theta_1'}^2 + \sigma^2\right)\left(\sum_{j=1}^{k} t_j^2\sigma_{\theta_2}^2 + \sigma^2\right) - \left(\sum_{j=1}^{k} t_j\sigma_{\theta_2}^2\right)\left(\sum_{j=1}^{k} t_j\sigma_{\theta_1'}^2\right)}$$

$$\tilde{\mu}_{\theta_2} = \frac{\left(k\sigma_{\theta_1'}^2 + \sigma^2\right)\left(\sum_{j=1}^{k} \mathcal{L}_j t_j\sigma_{\theta_2}^2 + \mu_{\theta_2}\sigma^2\right) - \left(\sum_{j=1}^{k} t_j\sigma_{\theta_2}^2\right)\left(\sum_{j=1}^{k} \mathcal{L}_j\sigma_{\theta_1'}^2 + \mu_{\theta_1'}\sigma^2\right)}{\left(k\sigma_{\theta_1'}^2 + \sigma^2\right)\left(\sum_{j=1}^{k} t_j^2\sigma_{\theta_2}^2 + \sigma^2\right) - \left(\sum_{j=1}^{k} t_j\sigma_{\theta_2}^2\right)\left(\sum_{j=1}^{k} t_j\sigma_{\theta_1'}^2\right)}$$

$$\tilde{\sigma}_{\theta_1'}^2 = \frac{\bar{\sigma}^2}{\sigma_{\theta_2}^2} \times \frac{\sum_{j=1}^{k} t_j^2\sigma_{\theta_2}^2 + \sigma^2}{\left(k\sigma_{\theta_1'}^2 + \sigma^2\right)\left(\sum_{j=1}^{k} t_j^2\sigma_{\theta_2}^2 + \sigma^2\right) - \left(\sum_{j=1}^{k} t_j\right)^2\sigma_{\theta_1'}^2\sigma_{\theta_2}^2}$$

$$\tilde{\sigma}_{\theta_2}^2 = \frac{\bar{\sigma}^2}{\sigma_{\theta_1'}^2} \times \frac{k\sigma_{\theta_1'}^2 + \sigma^2}{\left(k\sigma_{\theta_1'}^2 + \sigma^2\right)\left(\sum_{j=1}^{k} t_j^2\sigma_{\theta_2}^2 + \sigma^2\right) - \left(\sum_{j=1}^{k} t_j\right)^2\sigma_{\theta_1'}^2\sigma_{\theta_2}^2}$$

$$\rho = \frac{-\sigma_{\theta_1'}\sigma_{\theta_2}\sum_{j=1}^{k} t_j}{\sqrt{k\sigma_{\theta_1'}^2 + \sigma^2}\sqrt{\sigma_{\theta_2}^2\sum_{j=1}^{k} t_j^2 + \sigma^2}}; \qquad \bar{\sigma}^2 = \sigma^2\sigma_{\theta_1'}^2\sigma_{\theta_2}^2 \tag{3.31}$$

Note that while the priors of the model parameters (θ_1', θ_2) are assumed to be independent, their posterior distribution is correlated with a correlation coefficient ρ. This correlation will influence the future degradation level predictions, as shown later in Eq. 3.33. Moreover, posterior means $(\tilde{\mu}_{\theta_1},\ \tilde{\mu}_{\theta_2})$ and posterior variances $(\tilde{\sigma}_{\theta_1'}^2, \tilde{\sigma}_{\theta_2'}^2)$ depends upon the available degradation data. In other words, with increasing value of k the mean of posterior distribution will shift and spread of distribution will change.

The updated posterior distribution of (θ_1', θ_2) can be used to predict the RUL of a monitored unit. The key idea for RUL prediction is the same as that for a linear degradation model given earlier in Eq. 3.16. A failure happens when the logged value of the measurement reaches a failure threshold, η_D. Let, after time t from the current time t_k,

the surrogate value first cross the threshold. Thus, the RUL t can be found by substituting $\mathcal{L}_j = \eta_D$ in Eq. 3.24 (i.e., $\eta_D = \theta_1' + \theta_2 t_j + \epsilon_j$) and solving for t. However, the parameters (θ_1', θ_2) are random variables and will result in multiple values of t. Alternatively, the RUL distribution can be estimated by finding the mean and variance of the surrogate at time $t + t_k$, which is given by:

$$\tilde{\mu}_{\mathcal{L}_{t+t_k}} = \tilde{\mu}_{\theta_1'} + \tilde{\mu}_{\theta_2}(t + t_k) - \sigma^2/2 \tag{3.32}$$

$$\tilde{\sigma}^2_{\mathcal{L}_{t+t_k}} = \tilde{\sigma}^2_{\theta_1'} + \tilde{\sigma}^2_{\theta_2}(t + t_k)^2 + \sigma^2 + 2\rho(t + t_k)\tilde{\sigma}_{\theta_1'}\tilde{\sigma}_{\theta_2} \tag{3.33}$$

With known $\tilde{\mu}_{\mathcal{L}_{t+t_k}}$ and $\tilde{\sigma}^2_{\mathcal{L}_{t+t_k}}$, the CDF of the RUL is given by:

$$F_{L_k} = P(L_k < t|\mathcal{L}_1, \cdots, \mathcal{L}_k) = P(\mathcal{L}_{t+t_k} > \eta_D|\mathcal{L}_1, \cdots, \mathcal{L}_k) \tag{3.34}$$

$$= 1 - P(Z \leq \frac{\eta_D - \tilde{\mu}_{\mathcal{L}_{t+t_k}}}{\tilde{\sigma}_{\mathcal{L}_{t+t_k}}}) \tag{3.35}$$

$$= \Phi\left(\frac{\tilde{\mu}_{\mathcal{L}_{t+t_k}} - \eta_D}{\tilde{\sigma}_{\mathcal{L}_{t+t_k}}}\right) \tag{3.36}$$

where, $\phi(\cdot)$ is the CDF of the standard normal random variable Z.

The model parameters and RUL distribution can be updated each time a new observation is acquired from a monitored unit. In other words, each time a new measurement is acquired, the posterior distribution for (θ_1', θ_2) can be calculated and used to obtain new estimates for $\tilde{\mu}_{\theta_1'}, \tilde{\mu}_{\theta_2}, \tilde{\sigma}^2_{\theta_1'}, \tilde{\sigma}^2_{\theta_2}$ and ρ. Then, given the updated value of the parameters, the RUL distribution can be updated using $\tilde{\mu}_{\mathcal{L}_{t+t_k}}$ and $\tilde{\sigma}^2_{\mathcal{L}_{t+t_k}}$. Since this procedure only requires the computation of CDF for a standard normal random variable, the procedure can be implemented online.

In the above sections, the procedure for estimating the model parameters and RUL up-

dating for two degradation models namely, linear and exponential has been discussed. The basic framework remains same for more complex degradation models such as, exponential degradation model with a Brownian error term, Gamma process model, or a two-phase degradation model. The case of a two-phase degradation model is taken up in detail in the next chapter. Next, to illustrate the overall approach, a numerical example is presented.

3.5 Numerical Example

The following values for parameters $\phi = 2, \theta_1 = 0.1, \theta_2 = 0.3, \sigma = 0.2$ are used in Eq. 3.20 to simulate an exponential degradation path. The simulated degradation path is shown in Figure 3.2, where the y-axis represents the a degradation measure and the x-axis is the monitoring time. The log-transformed signal is shown in Figure 3.3, where the linear trend in the degradation path is observed following the assumptions in Eq.3.24.

Next, the prior information obtained from historical data can be used to update the model parameters and RUL distribution of this unit. Assume that the following prior distributions are obtained using historical degradation signals:

$$\theta_1' \sim N(-2, 0.5^2), \theta_1' \sim N(0.4, 0.3^2). \tag{3.37}$$

The mean and variance of the model parameters (θ_1', θ_2) are updated according to Eq. 3.31 with the availability of monitored data. Two such updates, say, $t_k = 2.5$ and $t_k = 9$, which correspond to 25 and 90 percent of degradation respectively, are presented in Figure 3.4. Note that the posterior distributions for θ_1', θ_2 are correlated as illustrated earlier in Eq. 3.31. Moreover, as more data is utilized, the densities of the parameters concentrate and converge to their true values.

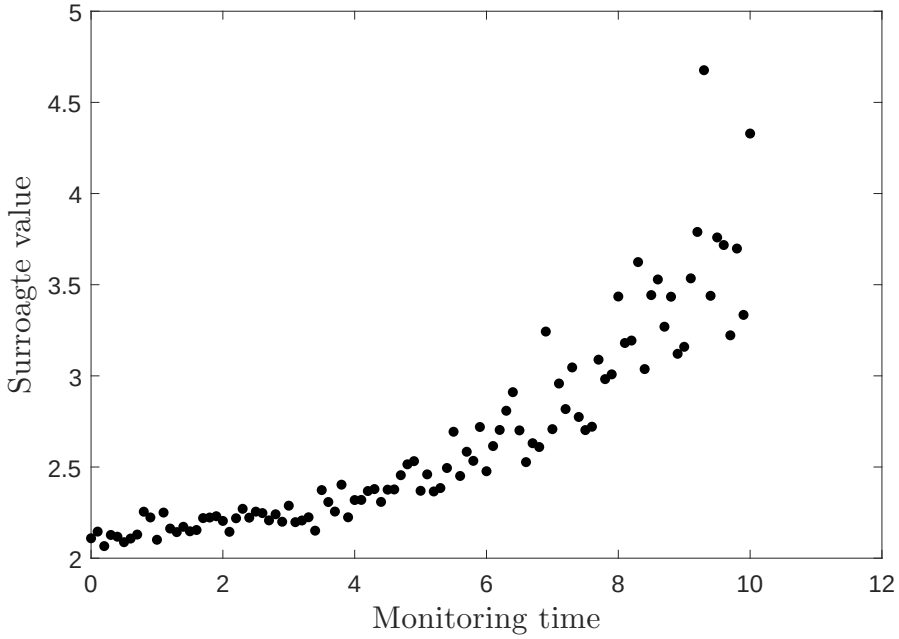

Figure 3.2: Simulated exponential degradation paths

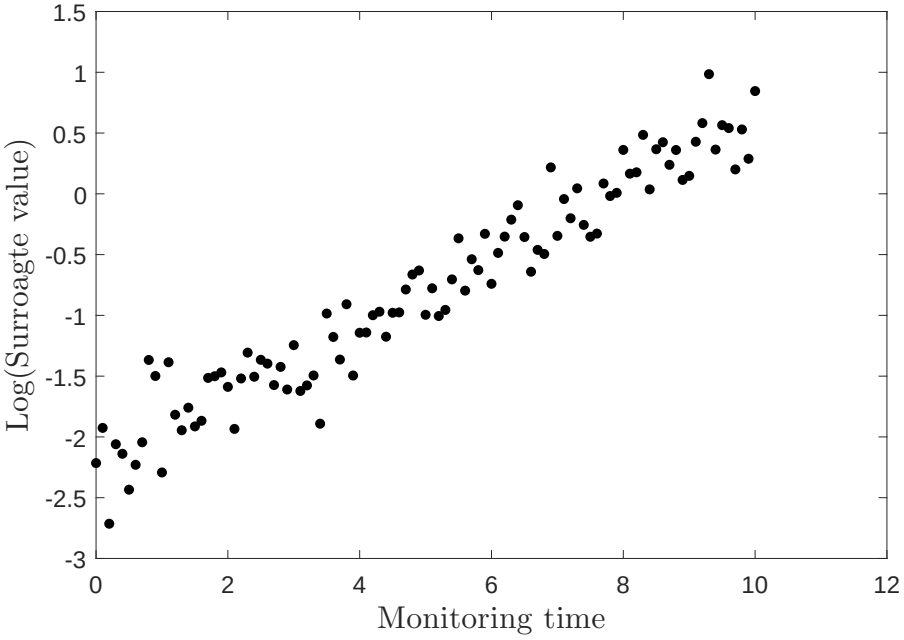

Figure 3.3: Log-transformed degradation paths

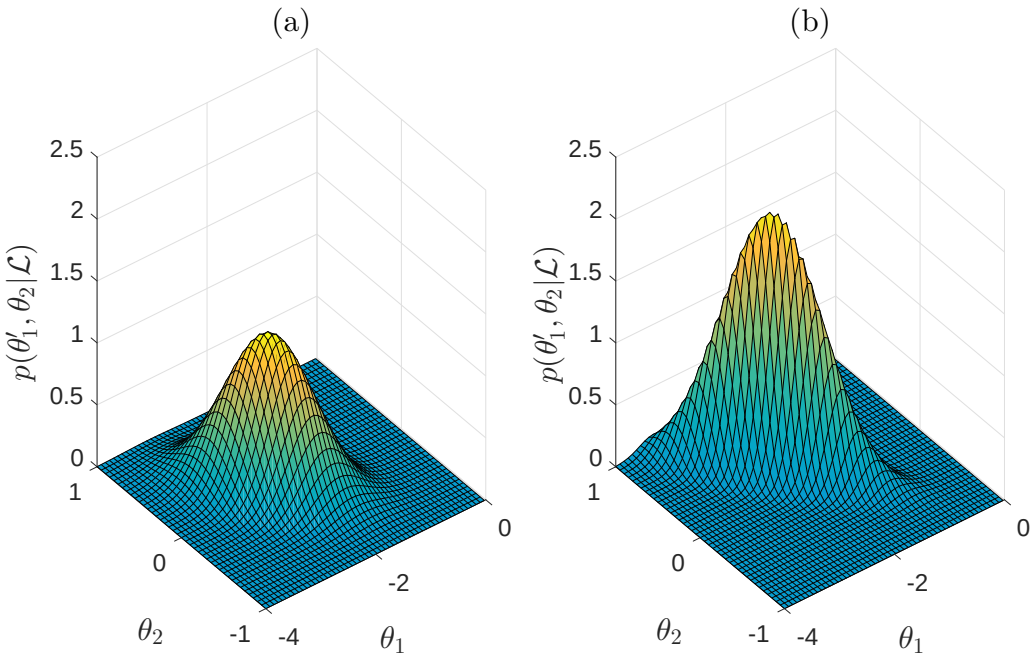

Figure 3.4: Updated degradation model parameters (a) at $t_k = 2.4$ (b) $t_k = 9$

The mean and variance of the future degradation level at any time $t + t_k$ is predicted using Eq. 3.32 and Eq. 3.33, respectively. Furthermore, the estimated mean and variance along with Eq. 3.36 are used to predict the RUL distribution, where the failure threshold η_D is set equal to 1. For two specific times, $t_k = 2.5$ and $t_k = 9$, the updated RUL CDF are shown in Figure 3.5. Note that the RUL estimates tend towards their actual end of life values over time.

3.6 Summary

In this chapter, a brief background on Bayesian degradation modeling and RUL estimation are presented. In those cases where direct degradation measurements are impractical to obtain, a surrogate measure obtained from the sensory data can be used for degradation

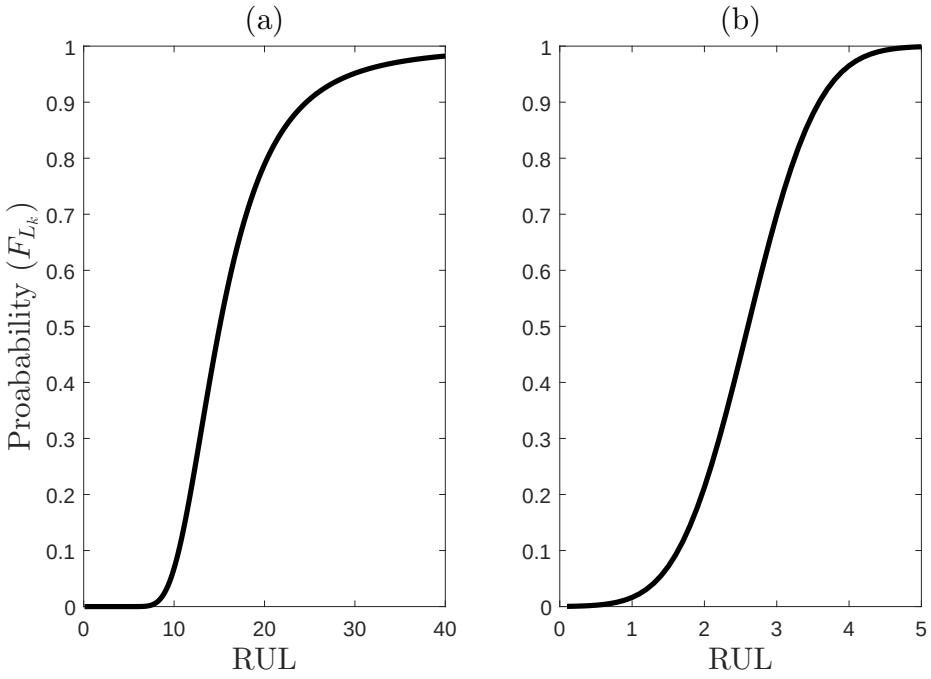

Figure 3.5: RUL CDF estimated at (a) $t_k = 2.5$ (b) $t_k = 9$

modeling. It was shown that for simple degradation models such as linear and exponential, a closed form expression for the posterior distribution of parameters and RUL is possible to derive. This makes computations relatively easy, even conducive to online implementation. The numerical example shows that the model parameters and RUL predictions of a monitoring unit becomes more accurate with the availability of monitored data over time. This framework is further explored for more advanced degradation models such as the two-phase degradation model, in the next chapter.

Chapter 4

An integrated approach to detection and prognosis using a two-phase degradation model

4.1 Introduction

In the previous chapter, the basics of degradation modeling and RUL estimation for the simple cases of linear and exponential degradation was discussed. In both of these cases, under simplifying assumptions, the mathematics of parameter estimation and RUL calculations within the Bayesian framework are greatly simplified. Such simplifications, while helps us understand the basic procedures of importance in this thesis, does not adequately address the complexity associated with real-world applications. This chapter extends the previous concepts to cases where the degradation occurs in distinct phases (see Figure 4.1(a)), which is typical of those cases where an incipient fault or damage changes the

rate of degradation. Of primary importance in such cases is to not only estimate when such changes occur, but also to estimate the parameters associated with such changes and the RUL. This chapter presents an integrated framework for damage detection and maintenance planning which can systematically integrate sensor measurements with prior information, for the case of models exhibiting such changes in the rate of degradation.

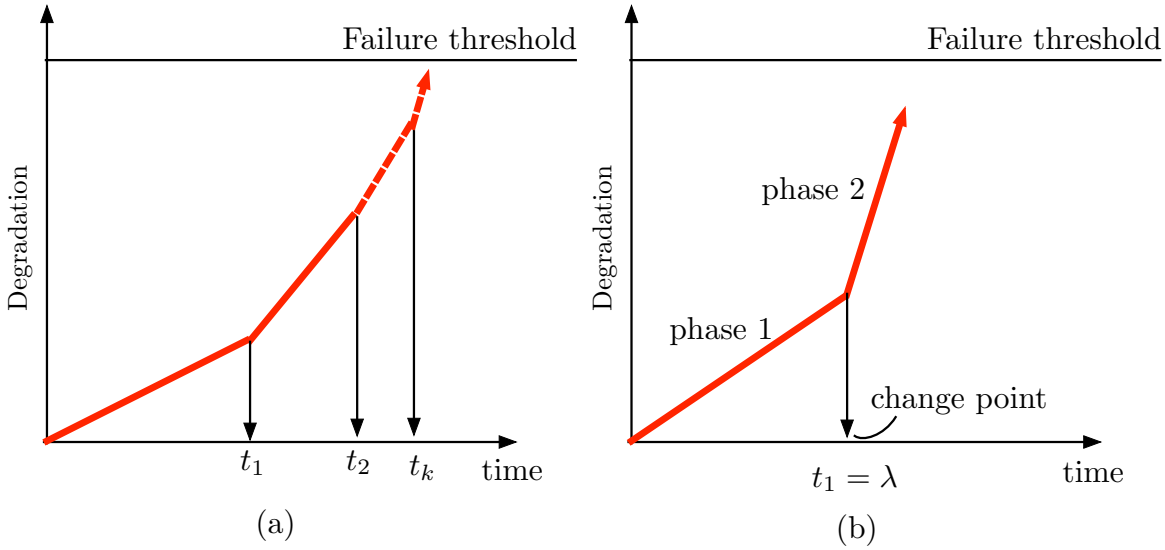

Figure 4.1: Schematic of a: (a) multi-phase degradation model; (b) two-phase model with a change-point

As discussed in the previous chapter, one of the main issues in dealing with degradation of many engineering components is that the underlying degradation mechanism is unobservable and can only be inferred through appropriate surrogate measures obtained from the sensor measurements. Moreover, the stochastic nature of the degradation path renders fault detection and estimating the end of life characteristics from such data extremely challenging. Furthermore, in many cases damage or incipient faults can cause a change in the rate of degradation, which manifests as jump or slope discontinuities.

The main objective in this chapter is to present the details of a two-phase degradation

model (see Figure 4.1(b)) utilizing surrogate measures of degradation. This model is the simplest extension of a single phase model described in the previous chapter. A Bayesian approach is employed to estimate the model parameters. Within the framework of this two-phase model, the problem of fault detection is posed as a change point location problem and the prognosis task is undertaken using the estimated parameters of the degradation model.

The chapter is organized as follows: first, the two-phase degradation model problem is formulated in the context of random variable (RV), gamma process (GP) and Weiner process (WP). Next, the mathematical details for parameter estimation, RUL predictions and maintenance planning are given. The effect of correlation between the degradation rate and change point location is discussed next. Finally, the proposed methodology is validated using a numerical example, which mainly serves to illustrate various steps in the approach.

4.2 Probabilistic degradation modeling

Modeling degradation is the first step towards fault detection and RUL estimation. Two classes of degradation models, namely: (i)RV model and (ii) stochastic model have been widely studied in the literature. RV model, also called a general path model, consists of a functional form $\eta(\cdot)$—which depends upon the nature of the degradation process—with deterministic and stochastic coefficients. Stochastic models such as GP and WP models can include temporal uncertainty i.e., uncertainty associated with the evolution or progression of deterioration over time. The monotonically increasing property of a GP makes it ideal for modeling the gradual damage that accumulates over time. However, in many engineering applications, sensory data are often contaminated with measurement noise or

environmental conditions change, which makes the degradation signal non-monotonic. In such cases, a WP has proven to be a good choice.

Going from a single phase to two-phase is not that straight forward due to mathematical challenges associated with the two-phase degradation modeling. First, the likelihood expression for the two-phase model is more complicated due to the discontinuity introduced by the change-point location. Hence, the likelihood expression cannot be directly maximized to obtain the estimate of model parameters. Secondly, in contrast to the single phase model, a two-step procedure is required for prior specification for a two-phase model. Specifically, in the first step, all possible change points are considered and an optimum change point location is selected which results in maximum likelihood. In the second step, with the known change point location, the degradation path is divided into two regions and the associated model parameters are estimated. Finally, in contrast to a single-phase, an analytical expression for posterior distribution of model parameters and RUL distribution is not generally possible to derive for a two-phase model.

The overall methodology followed in this chapter consists of following three key steps: (i) probabilistic degradation modeling; (ii) parameters estimation and update; and, (iii) RUL prediction and maintenance planning of a monitored unit. A flow chart showing the summary of the proposed methodology is given in Fig. 4.2 and details of each step are described next.

Let y_t denote a surrogate measure of degradation at time t, which can be modeled using a $n-$phase degradation model. In general, the degradation occuring within a phase can be described by a stochastic (e.g., GP or WP) or a random co-efficient (e.g., regression type) model. Let $\lambda_1, \lambda_2, \cdots, \lambda_{(n-1)}$ denote the change point locations and $y_0, y_{\lambda_1}, y_{\lambda_2}, \cdots, y_{\lambda_{(n-1)}}$ be the degradation at the beginning of the $1st, 2nd, 3rd, \cdots nth$ phases, respectively. With

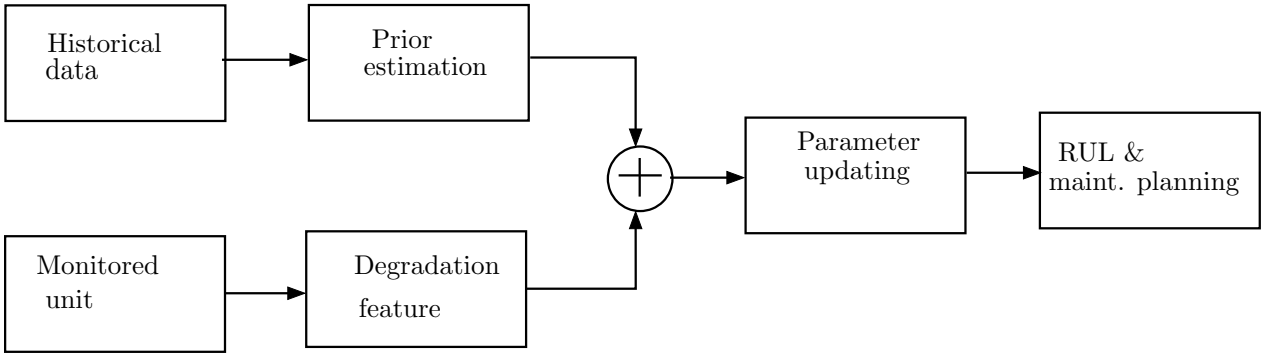

Figure 4.2: Flow chart of the proposed methodology

these notations, a general multi-phase degradation model can be written as:

$$y_t = [y_0 + y_1(t)]I_{(0,\lambda_1)}(t) + [y_{\lambda_1} + y_2(t-\lambda_1)]I_{(\lambda_1,\lambda_2)}(t) + [y_{\lambda_{(n-1)}} + y_n(t-\lambda_{(n-1)})]I_{\lambda_{(n-1,\infty)})}(t) \tag{4.1}$$

where $I_{(a,b)}(t)$ is the indicator function, which is unity in interval $[a, b]$ and zero elsewhere. For the simplest case of a two-phase degradation model:

$$y_t = [y_0 + y_1(t)]I_{(0,\lambda)}(t) + [y_\lambda + y_2(t-\lambda)]I_{(\lambda,\infty)}(t) \tag{4.2}$$

It is important to recognize that even for this simple model, many permutations are possible. For example, the degradation in both the phases can have the same functional form; gamma-gamma, Weiner-Weiner or exponential-exponential etc., or it can be mixed functions such as, linear-Gamma, Gamma-Weiner, linear-Weiner etc. The ensuing discussion is restricted to the same functional form in both the phases. In the following section, the mathematical formulation for the two phase degradation model employing various functional forms is presented.

4.2.1 Linear random variable model

Let the degradation rate in the first and second phases be given by θ_2 and β_2, respectively; then, the two-phase RV model can be written as:

$$y_t = \begin{cases} \theta_1 + \theta_2 t + \epsilon_1 & \text{if} \quad t \leq \lambda \\ \beta_1 + \beta_2 t + \epsilon_2 & \text{if} \quad t > \lambda \end{cases} \tag{4.3}$$

where, θ_1, θ_2 are constants, ϵ_1, ϵ_2 are the additive errors, which are assumed to be $i.i.d$ and normally distributed with mean 0 and variances σ^2 and τ^2, respectively. Here, it should be mentioned that many degradation mechanisms such as in rolling element bearings, follow an exponential behaviour, which can be made linear by taking logarithms of the surrogate measures of degradation. It is implicitly assumed here that these surrogate measures are linear mappings from the underlying degradation mechanisms, which means that the exponential degradation form is preserved in this transformation. Figure 4.3 shows a few sample paths for two-phase linear RV model.

This model can be used to detect faults by locating the discontinuity (change-point) caused by a jump in time and the rate of degradation by estimating the intercept and slope after the occurrence of such a discontinuity. The parameters of this model are contained in $\boldsymbol{\Theta} = \{\theta_1, \theta_2, \beta_1, \beta_2, \lambda, \sigma^2, \tau^2\}$, where λ is change point location, $(\theta_1, \theta_2, \sigma^2)$ and $(\beta_1, \beta_2, \tau^2)$ are the parameters corresponding to the first and second phases, respectively. The steps for undertaking this estimation are outlined later in the chapter.

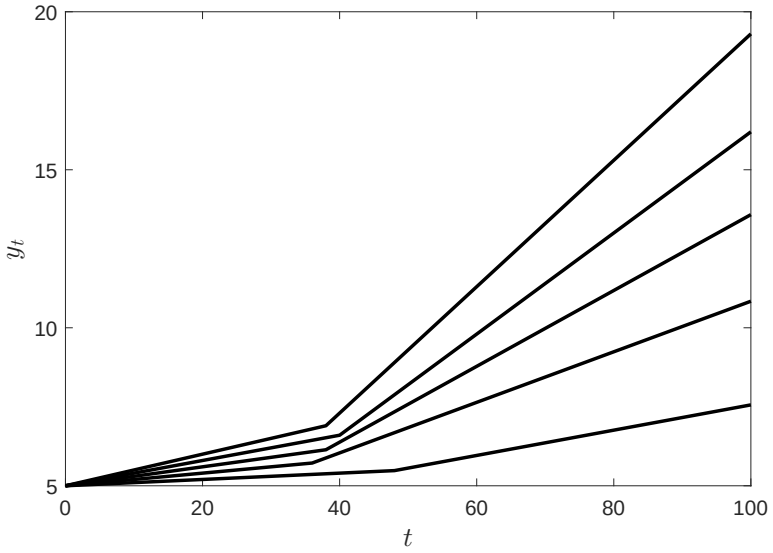

Figure 4.3: Simulated sample paths for two-phase linear RV model

4.2.2 Gamma process model

In this model, the degradation in each phase can be represented using a separate GP, given by:

$$y_t \sim \begin{cases} y_{01} + \Gamma(a_1 t, b_1) & \text{if} \quad t \leq \lambda \\ y_{02} + \Gamma(a_2 t, b_2) & \text{if} \quad t > \lambda \end{cases} \tag{4.4}$$

where y_{01}, y_{02} initial degradation in phase-1 and phase-2, respectively, $\Gamma(at, b)$ is the GP with the shape parameter, at and the scale parameter, b $(a, b \geq 0)$. A GP model $\{Y(t); t \geq 0\}$ is defined as a continuous time stochastic process in the sample space $[0, \infty)$, if it has the following properties [200]:

- Let $\triangle Y_k = Y(t_k) - Y(t_{k-1})$ be the increment in $Y(t)$ in the time interval $[t_k - t_{k-1}]$; then, the random variables $\triangle Y_1, \triangle Y_2, ...\triangle Y_k$ are independent for any $t_0 \leq t_1 \leq ... \leq t_k$.

- For $0 \leq s < t$, the random variable $Y(t) - Y(s)$ is Gamma distributed, $\Gamma(a(t-s), b)$, as in Eq. (4.5):

$$Y(t) - Y(s) \sim \Gamma(a(t-s), b) = f_{(a(t-s),b)}(y) = \frac{b^{a(t-s)} y^{a(t-s)-1} e^{-by}}{\Gamma(a(t-s))} \tag{4.5}$$

Using moment generating functions, it can be shown that the expectation and the variance of the process $Y(t)$ are given by [221]:

$$E(Y(t)) = \frac{a}{b}t, \quad \text{Var}(Y(t)) = \frac{a}{b^2}t \tag{4.6}$$

The monotonically increasing property of the GP makes it suitable for modeling gradually increasing damage, which accumulates over time. According to the additivity property of the gamma distribution, process $Y(t)$ also follows the gamma distribution, $\Gamma(at, b)$ [230]. Using this property, the two-phase model in Eq. 4.4 can be written as:

$$\begin{aligned} \triangle y_t = y_{(t+t_0)} - y_t &\sim \Gamma(a_1 t_0, b_1); \qquad t_0 < t \leq \lambda + 1 \\ \triangle y_t = y_{(t+t_0)} - y_t &\sim \Gamma(a_2 t_2, b_2); \qquad \lambda + 1 < t \leq T \end{aligned} \tag{4.7}$$

where $\triangle y_t$ is the increment in y_t from time t to $t + t_0$, t_0 is the time interval between two successive measurements and T is the time when the last measurement was obtained. This formulation is later used to develop the likelihood expression and subsequently for parameter estimation. The parameters of this model are $\boldsymbol{\Theta} = \{a_1, b_1, a_2, b_2, \lambda\}$. Figure 4.4 shows a few sample paths for two-phase gamma process model.

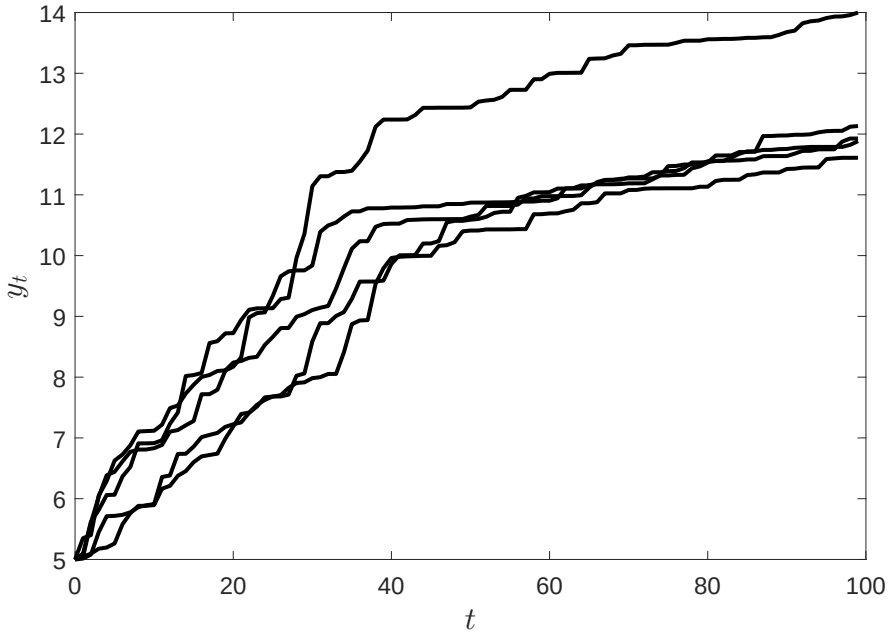

Figure 4.4: Simulated sample paths for two-phase gamma process model

4.2.3 Weiner process model

In this model, the cumulative degradation is given by two separate WPs (also called generalized WP) in two different phases. Mathematically, it can be written as:

$$y_t = \begin{cases} y_{01} + \nu_1 t + \sigma_1 W(t) & \text{if} \quad t \leq \lambda \\ y_{02} + \nu_2 t + \sigma_2 W(t) & \text{if} \quad t > \lambda \end{cases} \tag{4.8}$$

where $(y_{01}, \nu_1, \sigma_1)$ and $(y_{02}, \nu_2, \sigma_2)$ are the constants, drift and diffusion parameters in the $1st$ and $2nd$ phases, respectively. $W(t)$ is the standard Brownian motion term. A standard WP (often called Brownian motion) in the interval $[0, T]$ is a random variable $W(t)$ that depends continuously on $t \in [0, T]$ and has the following properties [219]:

- $W(0) = W_0$.
- For $0 \leq s < t \leq T$; $\quad \triangle W_t = W(t) - W(s) \sim \epsilon\sqrt{t-s} = \epsilon\sqrt{\triangle t}$. Where ϵ is a standard normal random variable $N(0,1)$ and $\triangle t = t - s$. In other words, $\triangle W_t$ is normally distributed with mean zero and variance $\triangle t$ i.e., $\triangle W_t \sim N(0, \triangle t)$.
- For $0 \leq s < t < u < v \leq T$; $\quad W(t) - W(s)$ and $W(v) - W(u)$ are independent. In other words, $\triangle W_t$ is independent of $\triangle W_v$ for all $v \leq t$

In fact, the generalized WP is a special type of a diffusion process. Let the diffusion processes $\mathbf{Y}(t)$ be given by the following stochastic differential equation (SDE):

$$d\mathbf{Y}(t) = \mathbf{a}[\mathbf{Y}, t]dt + \mathbf{b}[\mathbf{Y}, t]d\mathbf{W}(t) \tag{4.9}$$

where $\mathbf{a}[\mathbf{Y}, t]$ is the drift vector function, $\mathbf{b}[\mathbf{Y}, t]$ is the diffusion matrix and $\mathbf{W}(t)$ is a vector function of a standard Weiner process. By taking $\mathbf{a}[\mathbf{Y}, t] = \nu$, $\mathbf{b}[\mathbf{Y}, t] = \sigma$, $\mathbf{W}(t) = W(t)$, $\mathbf{Y}(t) = Y(t)$ in Eq. 4.9, the SDE for a generalized WP can be written as:

$$dY(t) = \nu dt + \sigma dW(t) \tag{4.10}$$

With the initial conditions, $Y(0) = y_0$ and $W(0) = 0$, the integral form is given by:

$$\begin{aligned} Y_t - y_0 &= \int_0^t \nu dt + \int_0^t \sigma dW(t) \\ Y_t &= y_0 + \nu t + \sigma[W(t) - W(0)] \\ &= y_0 + \nu t + \sigma W(t) \end{aligned} \tag{4.11}$$

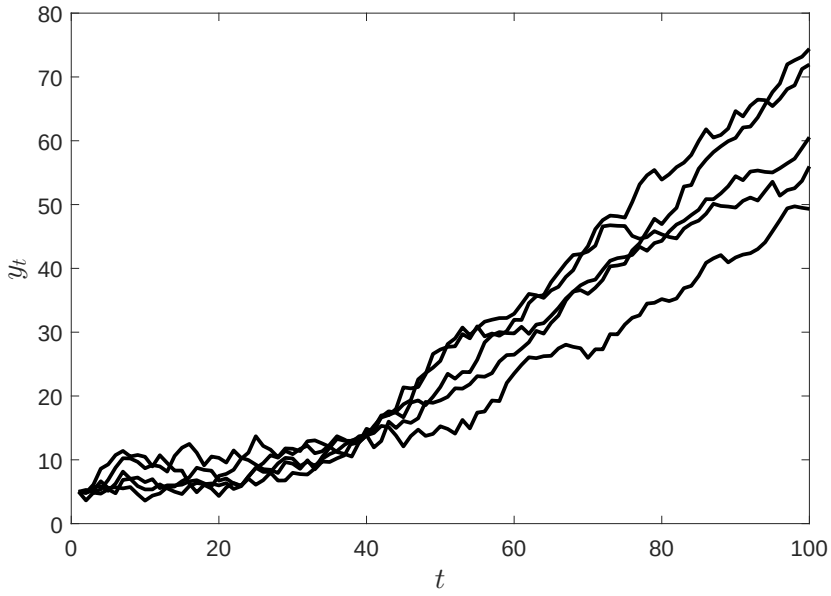

Figure 4.5: Simulated sample paths for two-phase Weiner process model

where $E[W_t] = 0$ and $Var[W_t] = t$. The mean and variance of Y_t is therefore $E[Y_t] = y_0 + \nu t$ and $Var[Y_t] = \sigma^2 t$, i.e., $Y_t \sim N(y_0 + \nu t, \sigma^2 t)$.

This property will be used for parameter estimation subsequently. The parameters of a two-phase Weiner process model are given by $\mathbf{\Theta} = \{\nu_1, \sigma_1, \nu_2, \sigma_2, \lambda\}$. The advantage of using a Weiner process for degradation modeling is two fold: first, the degradation path need not be strictly monotonic, which often occurs when noise is present in the measurements, or the degradation measure fluctuates; secondly, a closed form expression for failure time distribution can be derived which simplifies the Bayesian computations significantly. Figure 4.5 shows a few sample paths for two-phase Weiner process model.

4.3 Estimation of parameters

A Bayesian approach is employed for parameter estimation, which allows us to combine prior knowledge of the parameters $\boldsymbol{\Theta} = \{\boldsymbol{\theta}_1, \boldsymbol{\theta}_2, \lambda\}$ i.e., $\pi(\boldsymbol{\Theta})$, and their likelihood $L(\boldsymbol{y}|\boldsymbol{\Theta})$ obtained from the data $\boldsymbol{y} = \{y_1, y_2, \cdots, y_t\}$, to obtain the posterior distribution for the parameters, $p(\boldsymbol{\Theta}|\boldsymbol{y})$ according to:

$$p(\boldsymbol{\Theta}|\boldsymbol{y}) = \frac{\pi(\boldsymbol{\Theta})L(\boldsymbol{y}|\boldsymbol{\Theta})}{\int p(\boldsymbol{\Theta})L(\boldsymbol{y}|\boldsymbol{\Theta})d\boldsymbol{\Theta}} \propto \pi(\boldsymbol{\Theta})L(\boldsymbol{y}|\boldsymbol{\Theta}) \tag{4.12}$$

where $\boldsymbol{\theta}_1$, $\boldsymbol{\theta}_2$ are the parameters in the two phases. The prior distribution $\pi(\boldsymbol{\Theta})$ can be expressed as a parametric model $\pi(\boldsymbol{\Theta}|\boldsymbol{\xi})$ with hyper-parameters $\boldsymbol{\xi}$. These hyper-parameters can be estimated by maximizing the marginal likelihood of data:

$$\hat{\boldsymbol{\xi}} = \underset{\boldsymbol{\xi}}{\operatorname{argmax}} \prod_{i=1}^{n} \int L(\boldsymbol{y}_i|\boldsymbol{\Theta}_i)\pi(\boldsymbol{\Theta}_i|\boldsymbol{\xi}_i)d\boldsymbol{\Theta}_i \tag{4.13}$$

where $\boldsymbol{y_i} = [y_{i1}, y_{i2}, \cdots, y_{im_i}]^T$ is the historical degradation signal of unit i, m_i is the number of observations and $\boldsymbol{\Theta}_i$ contain the parameters of the degradation model of unit i. Unfortunately, the parametric form of Eq. 4.13 is complex, which makes integration and optimization tasks difficult to conduct.

In this thesis, an alternative approach is employed to estimate the prior distribution and hyper-parameters. Instead of maximizing the marginal distribution of historical data, the maximum likelihood estimates of their model parameters $\boldsymbol{\Theta}_i$ of each unit $i = 1, 2 \cdots, n$ are considered as samples from the prior distribution, i.e.,

$$\boldsymbol{\Theta} = \{\boldsymbol{\Theta}_1, \boldsymbol{\Theta}_2, \cdots, \boldsymbol{\Theta}_n\} \tag{4.14}$$

Subsequently, the hyper-parameters are estimated by fitting the appropriate distribution. Once the prior distribution $\pi(\boldsymbol{\Theta})$ is estimated, this can be integrated with the likelihood of the degradation data available from a monitored unit to update its model parameters (see Eq. 4.12) and subsequently the RUL. Next, the parameter estimation procedure for the three degradation models is discussed.

4.3.1 Linear RV model

Given the degradation measure y_t at time t, the likelihood function can be written as:

$$L(\boldsymbol{y}|\boldsymbol{\Theta}) = \prod_{t\leq\lambda} \phi(y_t; \theta_1 + \theta_2 t, \sigma^2) \prod_{t>\lambda} \phi(y_t; \beta_1 + \beta_2 t, \tau^2) \tag{4.15}$$

$$= \frac{1}{(\sqrt{2\Pi\sigma^2})^{\lambda}} \exp\left[-\sum_{t=1}^{\lambda} (y_t - \theta_1 - \theta_2 t)^2/2\sigma^2\right] \cdots$$

$$\frac{1}{(\sqrt{2\Pi\tau^2})^{(t-\lambda)}} \exp\left[-\sum_{t=\lambda+1}^{t} (y_t - \beta_1 - \beta_2 t)^2/2\tau^2\right] \tag{4.16}$$

where $\phi(y_t; \theta_1 + \theta_2 t, \sigma^2)$ denotes a normal probability density function with mean $\theta_1 + \theta_2 t$, variance σ^2 and evaluated at y_t. In addition to the likelihood function, a joint prior distribution of all parameters $(\theta_1, \theta_2, \beta_1, \beta_2, \sigma^2, \tau^2, \lambda)$, i.e.,

$$\pi(\boldsymbol{\Theta}) = \pi(\theta_1, \theta_2, \beta_1, \beta_2, \sigma^2, \tau^2, \lambda) \tag{4.17}$$

is required to calculate the posterior distribution. To estimate such a multi-dimensional prior distribution, a very large number of degradation paths are required. However, in practice, only a few historical run-to-failure degradation signals may be available; hence, the prior distribution is simplified by assuming most of the parameters to be independent.

By using the law of total probability and independence of $\theta_1, \theta_2, \beta_1, \sigma^2, \tau^2$, the prior $\pi(\boldsymbol{\Theta})$ is given by:

$$\begin{aligned}\pi(\boldsymbol{\Theta}) &= \pi(\theta_1, \theta_2, \beta_1, \sigma^2, \tau^2, \beta_2, \lambda) \\ &= \pi(\theta_1)\pi(\theta_2)\pi(\beta_1)\pi(\sigma^2)\pi(\tau^2)\pi(\beta_2)\pi(\lambda) \end{aligned} \tag{4.18}$$

Moreover, the following prior distributions in terms of hyper-parameter $\boldsymbol{\xi} = (\mu_{\theta_1}, \sigma^2_{\theta_1}, \mu_{\theta_2}, \sigma^2_{\theta_2}, \mu_{\beta_1}, \sigma^2_{\beta_1}, \mu_{\beta_2}, \sigma^2_{\beta_2}, a_{\sigma^2}, b_{\sigma^2}, a_{\tau^2}, b_{\tau^2})$ are assumed:

$$\pi(\theta_1) \sim N(\mu_{\theta_1}, \sigma^2_{\theta_1}); \pi(\theta_2) \sim N(\mu_{\theta_2}; \sigma^2_{\theta_2}); \tag{4.19}$$

$$\pi(\beta_1) \sim N(\mu_{\beta_1}, \sigma^2_{\beta_1}); \pi(\beta_2) \sim N(\mu_{\beta_2}, \sigma^2_{\beta_2})$$

$$\lambda \sim U(0, T); \pi(\sigma^2) \sim IG(a_{\sigma^2}, b_{\sigma^2}); \pi(\tau^2 \sim IG(a_{\tau^2}, b_{\tau^2}) \tag{4.20}$$

Where N, IG and U denotes normal, inverse Gaussian and uniform distribution, respectively. The joint posterior distribution for $\boldsymbol{\Theta}$ can then be obtained by substituting Eq. 4.18 and Eq. 4.16 into Eq. 4.12:

$$\begin{aligned} p(\boldsymbol{\Theta}|\boldsymbol{y}) = \; & \pi(\theta_1)\pi(\theta_2)\pi(\beta_1)\pi(\beta_2)\pi(\sigma^2)\pi(\tau^2)\pi(\lambda) \times \tfrac{1}{(\sqrt{2\Pi\sigma^2})^{\lambda}} \exp\Big[-\textstyle\sum_{t=1}^{\lambda}(y_t - \theta_1 - \theta_2 t)^2/2\sigma^2\Big] \\ & \times \tfrac{1}{(\sqrt{2\Pi\tau^2})^{(t-\lambda)}} \exp\big[-\textstyle\sum_{t=\lambda+1}^{t}(y_t - \beta_1 - \beta_2 t)^2/2\tau^2\big] \end{aligned} \tag{4.21}$$

Clearly, the functional form of $p(\boldsymbol{\Theta}|\boldsymbol{y})$ as given in Eq. 4.21 does not correspond to any recognizable joint distribution function. As a consequence, the marginal posterior density functions are estimated by taking random samples from the joint posterior distribution using MCMC algorithm.

The hyper-parameters $\boldsymbol{\xi} = (\mu_{\theta_1}, \sigma^2_{\theta_1}, \mu_{\theta_2}, \sigma^2_{\theta_2}, \mu_{\beta_1}, \sigma^2_{\beta_1}, \mu_{\beta_2}, \sigma^2_{\beta_2}, a_{\sigma^2}, b_{\sigma^2}, a_{\tau^2}, b_{\tau^2})$ are ob-

tained by fitting the appropriate distribution to the model parameters estimated from the historical units. The following steps are performed to achieve this:

- Step-I: For a given change point location λ of unit i, divide the degradation data into two regimes and fit linear models to each regime, separately. The model parameters $\boldsymbol{\theta}_i, \boldsymbol{\beta}_i, \boldsymbol{\sigma}_i^2, \boldsymbol{\tau}_i^2$ can be found using standard linear regression results [193] :

$$\hat{\boldsymbol{\theta}}_i = (\boldsymbol{X}_{i\theta}^T \boldsymbol{X}_{i\theta})^{-1} \boldsymbol{X}_{i\theta}^T \boldsymbol{y}_{i\theta} \tag{4.22}$$

$$\hat{\boldsymbol{\beta}}_i = (\boldsymbol{X}_{i\beta}^T \boldsymbol{X}_{i\beta})^{-1} \boldsymbol{X}_{i\beta}^T \boldsymbol{y}_{i\beta} \tag{4.23}$$

$$\sigma_i^2 = \frac{1}{n_{i\theta}} (\boldsymbol{y}_{i\theta} - \boldsymbol{X}_{i\theta}\hat{\boldsymbol{\theta}}_i)^T (\boldsymbol{y}_{i\theta} - \boldsymbol{X}_{i\theta}\hat{\boldsymbol{\theta}}_i) \tag{4.24}$$

$$\tau_i^2 = \frac{1}{n_{i\beta}} (\boldsymbol{y}_{i\beta} - \boldsymbol{X}_{i\beta}\hat{\boldsymbol{\beta}}_i)^T (\boldsymbol{y}_{i\beta} - \boldsymbol{X}_{i\beta}\hat{\boldsymbol{\beta}}_i) \tag{4.25}$$

where

$$\boldsymbol{y}_{i\theta} = \begin{bmatrix} y_{i1} & y_{i2} & \cdots & y_{i\lambda} \end{bmatrix}^T ; \tag{4.26}$$

$$\boldsymbol{y}_{i\beta} = \begin{bmatrix} y_{i(\lambda+1)} & y_{i(\lambda+2)} & \cdots & y_{im_i} \end{bmatrix}^T \tag{4.27}$$

$$\boldsymbol{X}_{i\theta} = \begin{bmatrix} 1 & 1 & \cdots & 1 \\ t_{i1} & t_{i2} & \cdots & t_{i\lambda} \end{bmatrix}^T \tag{4.28}$$

$$\boldsymbol{X}_{i\beta} = \begin{bmatrix} 1 & 1 & \cdots & 1 \\ t_{i(\lambda+1)} & t_{i(\lambda+2)} & \cdots & t_{im_i} \end{bmatrix}^T \tag{4.29}$$

At this point, it should be pointed out that this approach is similar to the Bayesian approach of change detection with a diffuse/uniform prior and the change point

distribution assumed to be concentrated at a point [31]. Mathematically, MLE and Bayesian maximum a posteriori (MAP) estimate for parameters $\boldsymbol{\Theta}$ can be given by:

$$\Theta_{MLE} = \underset{\boldsymbol{\Theta}}{\operatorname{argmax}}\, p(\boldsymbol{y}|\boldsymbol{\Theta}) \tag{4.30}$$

$$= \underset{\boldsymbol{\Theta}}{\operatorname{argmax}} \prod_i p(y_i|\boldsymbol{\Theta}) \tag{4.31}$$

$$\Theta_{MAP} = \underset{\boldsymbol{\Theta}}{\operatorname{argmax}}\, p(\boldsymbol{y}|\boldsymbol{\Theta})p(\boldsymbol{\Theta}) \tag{4.32}$$

$$= \underset{\boldsymbol{\Theta}}{\operatorname{argmax}} \prod_i p(y_i|\boldsymbol{\Theta}) \times const. \tag{4.33}$$

Note that, if prior is diffuse, i.e., $p(\boldsymbol{\Theta}) = constant$, then the two estimates become same. In other words, MLE is a special case of MAP, where the prior is uniform or relatively diffuse.

- Step-II: With the estimated parameters in step-I calculate the likelihood of degradation data for unit i using Eq. 4.16 .

- Step-III: Repeat Step-I and Step-II, by varying the change point location $\lambda = 1, 2, \cdots, m_i$. The most likely change point λ_i for unit i is the one that results in the maximum likelihood. Perform this step for all the n historical units and collect the model parameters corresponding to the optimum change point locations.

- Step-IV: Fit the distributions (as described in Eq. 4.20) to the parameters collected in Step-III and obtain the hyper-parameters.

4.3.2 GP model

Let, for the undamaged case, the GP process be parameterized by the shape parameter a_0 and a scale parameter, b_0. At a certain time instant, say $\lambda + 1$, a shock causes the process parameter to change from b_0 to b_1, while a_0 remains the same. In other words, the degradation during the first phase is given by $\Gamma(a_0 t_0, b_0)$ and in the second phase by $\Gamma(a_0 t_0, b_1)$. This choice (i.e., the shape parameter kept fixed) is made to simplify the calculations and to obtain a closed form expression for the posterior distribution of the model parameters by using a conjugate prior. With known damage increments, $\triangle y_1, \triangle y_2, \cdots \triangle y_{(T-1)}$, the likelihood function of the parameters b_1 and λ can be obtained using Eq. 4.5, and written as:

$$\begin{aligned} L(b_1, \lambda) =& \prod_{t=1}^{\lambda} \left[\frac{b_0^{a_0 t_0}}{\Gamma(a_0 t_0)} \triangle y_t^{a_0 t_0 - 1} \exp\left(-\triangle y_t b_0\right) \right] \times \prod_{t=\lambda+1}^{T-1} \left[\frac{b_1^{a_0 t_0}}{\Gamma(a_0 t_0)} \triangle y_t^{a_0 t_0 - 1} \exp\left(-\triangle y_t b_1\right) \right] \\ =& \Gamma(a_0 t_0)^{-(T-1)} b_0^{\lambda a_0 t_0} \times b_1^{(T-\lambda) a_0 t_0} \times \prod_{t=1}^{T-1} \triangle y_t^{a_0 t_0 - 1} \times \exp\left[-\sum_{t=1}^{\lambda} \triangle y_t b_0 - \sum_{t=\lambda+1}^{T-1} \triangle y_t b_1 \right] \end{aligned} \tag{4.34}$$

and the log-likelihood is given by:

$$\begin{aligned} \mathcal{L}(b_1, \lambda) = \ln L(b_1, \lambda) =& -(T-1) \ln \Gamma(a_0 t_0) + \lambda a_0 t_0 \ln b_0 + (T-\lambda) a_0 t_0 \ln b_1 \\ &+ (a_0 t_0 - 1) \sum_{t=1}^{T-1} \ln \triangle y_t - \sum_{t=1}^{\lambda} \triangle y_t b_0 - \sum_{t=\lambda+1}^{T-1} \triangle y_t b_1 \end{aligned} \tag{4.35}$$

The maximum likelihood estimate of b_1 is obtained by partially differentiating Eq. 4.35 with respect to b_1 and setting the equation equal to zero, which is given by:

$$\frac{\partial \mathcal{L}(b_1, \lambda)}{\partial b_1} = -\frac{(T-\lambda)a_0 t_0}{b_1} + \sum_{t=\lambda+1}^{T-1} \triangle y_t = 0 \Rightarrow \hat{b}_1 = \frac{(T-\lambda)a_0 t_0}{\sum_{t=\lambda+1}^{T-1} \triangle y_t} \tag{4.36}$$

Once $\hat{b}_1$ is estimated, this is substituted into equation (4.35) to calculate the profile log-likelihood value $\mathcal{L}(\hat{b}_1, t)$ for any time t. This process is repeated for all t $(1 < t < T)$ and the profile log-likelihoods $\mathcal{L}(\hat{b}_1, t)$ and the corresponding times t are stored in an array. Finally, the value of t that maximizes $\mathcal{L}(\hat{b}_1, t)$ is selected as the most likely change point location $\hat{\lambda}$. Mathematically, it can be written as:

$$\hat{\lambda} = \arg\max_{t} \ \mathcal{L}(\hat{b}_1, t) \tag{4.37}$$

The above procedure is repeated for all the historical units, separately. The estimated parameters $(\hat{\lambda}, \hat{b}_1)$ are collected. The hyper-parameters (α_0, β_0) for the scale parameter b_1 are estimated by distribution fitting, which is a Gamma distribution in this case. Note that for a Gamma distribution with a known shape parameter and an unknown scale parameter, the conjugate prior for b_1 is a Gamma distribution and is given by:

$$p(b_1; \alpha_0, \beta_0) = \frac{\beta_0^{\alpha_0 t_0} b_1^{\alpha_0 t_0 - 1} e^{-\beta_0 b_1}}{\Gamma(\alpha_0 t_0)} \tag{4.38}$$

Next, the estimated prior information is used to obtain the posterior distribution of b_1

of a monitored unit. The likelihood of the available data $\boldsymbol{y}$ is given by:

$$\begin{aligned} L(\boldsymbol{y}|a_0, b_1) &= \prod_{t=1}^{n} \Gamma(\triangle y_t; |a_0 t_0, b_1) = \prod_{t=1}^{n} \frac{b_1^{a_0 t_0} \triangle y_t^{a_0 t_0 - 1} e^{-b_1 \triangle y_t}}{\Gamma(a_0 t_0)} \\ &= \frac{b_1^{a_0 t_0} \triangle y_1^{a_0 t_0 - 1} e^{-b_1 \triangle y_1}}{\Gamma(a_0 t_0)} \times \frac{b_1^{a_0 t_0} \triangle y_2^{a_0 t_0 - 1} e^{-b_1 \triangle y_2}}{\Gamma(a_0 t_0)} \times \ldots \frac{b_1^{a_0 t_0} \triangle y_n^{a_0 t_0 - 1} e^{-b_1 \triangle y_n}}{\Gamma(a_0 t_0)} \end{aligned} \tag{4.39}$$

where $t_0 = t_i - t_{i-1}$ for all i. Using Eqs. 4.38 and 4.39, the posterior distribution for b_1 is given by:

$$\begin{aligned} p(b_1|\boldsymbol{y}) &\propto \frac{b_1^{a_0 n t_0} e^{-b_1 \sum_{t=1}^{n} \triangle y_t} \prod_{t=1}^{n} \triangle y_t^{a_0 t_0 - 1}}{\Gamma(n a_0 t_0)} \times \frac{\beta_0^{\alpha_0 t_0} b_1^{\alpha_0 t_0 - 1} e^{-\beta_0 b_1}}{\Gamma(\alpha_0 t_0)} \\ &\propto \frac{b_1^{n a_0 t_0 + \alpha_0 t_0 - 1} \beta_0^{\alpha_0 t_0} \prod_{t=1}^{n} \triangle y_t^{a_0 t_0 - 1} e^{-b_1 (\sum_{t=1}^{n} \triangle y_t + \beta_0)}}{\Gamma(n a_0 t_0) \Gamma(\alpha_0 t_0)} \end{aligned} \tag{4.40}$$

The posterior of b_1 follows a Gamma distribution, as expected, for the conjugate prior. The posterior hyper-parameters α_0', β_0' and the posterior distribution $p(b_1|\boldsymbol{y})$ in terms of α_0', β_0' are given by:

$$\begin{aligned} \alpha_0' &= n a_0 + \alpha_0; \qquad \beta_0' = \beta_0 + \sum_{t=1}^{n} \triangle y_t \\ p(b_1|\boldsymbol{y}) &\propto \frac{\beta_0^{\alpha_0 t_0} b_1^{\alpha_0' t_0 - 1} \prod_{t=1}^{n} \triangle y_t^{a_0 t_0 - 1} e^{-(\beta_0' b_1)}}{\Gamma(\alpha_0 t_0) \Gamma(n a_0 t_0)} \end{aligned} \tag{4.41}$$

Eq. 4.41 can now be updated as new condition data becomes available. The continual update of b_1 provides a refined degradation model that can be utilized for RUL prediction and maintenance planning.

4.3.3 WP model

Here, again, a maximum likelihood approach is used for change point detection and parameter estimation for the historical degradation paths. To formulate the likelihood expression the differential damage $\triangle y_j = y_j - y_{j-1}$ in the time interval $\triangle t_j = t_j - t_{(j-1)}$ for a WP is assumed to be normally distributed with mean $\nu_1 \triangle t_j$ and variance $\sigma_1^2 \triangle t_j$ i.e., $\triangle y_j \sim N(\nu_1 \triangle t_j, \sigma_1^2 \triangle t_j)$ if $t_j < \lambda$. Similarly, when $t_j > \lambda$, i.e., in the second phase of degradation, $\triangle y_j$ follows $N(\nu_2 \triangle t_j, \sigma_2^2 \triangle t_j)$. The four steps as described for the case of a RV model (see Section 4.3.1) will also be followed here for optimum change point detection and parameter estimation.

In step-I, for a given change point location t, the parameters (ν_1, σ_1) and (ν_2, σ_2) are estimated using the maximum likelihood principle. Then, in step-II, the estimated parameters $\hat{\nu}_1, \hat{\sigma}_1, \hat{\nu}_2, \hat{\sigma}_2$ are used to estimate the joint profile likelihood. Mathematically, this can be written as:

$$
\begin{aligned}
L(\triangle y_t | \hat{\nu}_1, \hat{\sigma}_1, \hat{\nu}_2, \hat{\sigma}_2, t) &= \prod_{j=1}^{t} \phi(\triangle y_j;\ \hat{\nu}_1 \triangle t_j, \hat{\sigma}_1^2 \triangle t_j) \prod_{j=t+1}^{m} \phi(\triangle y_j;\ \hat{\nu}_2 \triangle t_j, \hat{\sigma}_2^2 \triangle t_j) \\
&= \prod_{j=1}^{t} \frac{1}{\sqrt{2\Pi \hat{\sigma}_1^2 \triangle t_j}} \exp\left[-\frac{(\triangle y_j - \hat{\nu}_1 \triangle t_j)^2}{2\hat{\sigma}_1^2 \triangle t_j} \right] \prod_{j=t+1}^{m} \frac{1}{\sqrt{2\Pi \hat{\sigma}_2^2 \triangle t_j}} \exp\left[-\frac{(\triangle X_j - \hat{\nu}_2 \triangle t_j)^2}{2\hat{\sigma}_2^2 \triangle t_j} \right]
\end{aligned}
\tag{4.42}
$$

where $\phi(x; \mu, \sigma^2)$ denotes a normal probability density function (PDF) with mean μ, variance σ^2 and evaluated at x, and m is the number of measurements. In step-III, the process is repeated for all t $(1 < t < m)$ and the profile likelihoods $L(\triangle y_t | \hat{\nu}_1, \hat{\sigma}_1, \hat{\nu}_2, \hat{\sigma}_2, t)$ and the corresponding times t are stored in an array. Finally, the value of t that maximizes $L(\triangle y_t | \hat{\nu}_1, \hat{\sigma}_1, \hat{\nu}_2, \hat{\sigma}_2, t)$ is selected as the optimum change point location $\hat{\lambda}$. Since the loga-

rithm is an increasing function, the log-likelihood (LL) can be maximized according to:

$$\hat{\lambda} = \arg\max_{t} \; LL(\triangle y_t | \hat{\nu}_1, \hat{\sigma}_1, \hat{\nu}_2, \hat{\sigma}_2, t) \tag{4.43}$$

This step is repeated for all the historical units, the model parameters are collected and the hyper-parameters are estimated through distribution fitting.

The following form of prior distributions $\sigma_1^2 \sim IG(a_1, b_1)$, $\sigma_2^2 \sim IG(a_2, b_2)$, $\nu_1 \sim N(c_1, d_1^2)$ and $\nu_2 \sim N(c_2, d_2^2)$ are considered for the model parameters. The posterior distribution of the model parameters for a monitored unit is given by:

$$\begin{aligned} p(\boldsymbol{\Theta}|\boldsymbol{y}) =& \pi(\nu_1, \sigma_1^2)\pi(\nu_2, \sigma_2^2) \prod_{j=1}^{t} \phi(\triangle y_j;\ \hat{\nu}_1 \triangle t_j, \hat{\sigma}_1^2 \triangle t_j) \prod_{j=t+1}^{m} \phi(\triangle y_j;\ \hat{\nu}_2 \triangle t_j, \hat{\sigma}_2^2 \triangle t_j) \\ =& G(a_1, b_1)N(c_1, d_1)G(a_2, b_2)N(c_2, d_2) \prod_{j=1}^{t} \frac{1}{\sqrt{2\Pi\hat{\sigma}_1^2 \triangle t_j}} \exp\left[-\frac{(\triangle y_j - \hat{\nu}_1 \triangle t_j)^2}{2\hat{\sigma}_1^2 \triangle t_j}\right] \\ & \times \prod_{j=t+1}^{m} \frac{1}{\sqrt{2\Pi\hat{\sigma}_2^2 \triangle t_j}} \exp\left[-\frac{(\triangle X_j - \hat{\nu}_2 \triangle t_j)^2}{2\hat{\sigma}_2^2 \triangle t_j}\right] \end{aligned} \tag{4.44}$$

The Bayesian inference of parameters is undertaken using MCMC sampling (see Appendix D). At this point, having discussed the parameter estimation steps using a Bayesian approach, the RUL estimation and maintenance planning steps are explained next.

4.4 RUL predictions and maintenance planning

The RUL of an asset or a system is defined as the length from the current time to the end of its useful life [198]. However, what constitutes the end of useful life depends upon the context and/or application and the operation characteristics. For example, in accounting,

RUL is defined in relation to the productivity of a depreciating asset [198], whereas in mechanical systems this could be a critical flaw size or breakdown [122]. In this thesis, RUL is defined as the time remaining from the last measurement when the degradation parameter y_t first reaches a pre-defined threshold level, η_D. This definition of RUL is commonly used in the literature [122, 196, 101]. Figure 4.6(a) illustrates the concept of RUL using a stochastic (WP) process and the variation in RUL caused by the uncertainty in the model parameters $\boldsymbol{\Theta}$ is shown in Figure 4.6(b). Clearly, RUL of an asset is a RV and depends on the current age, operational environment and the observed condition monitoring information.

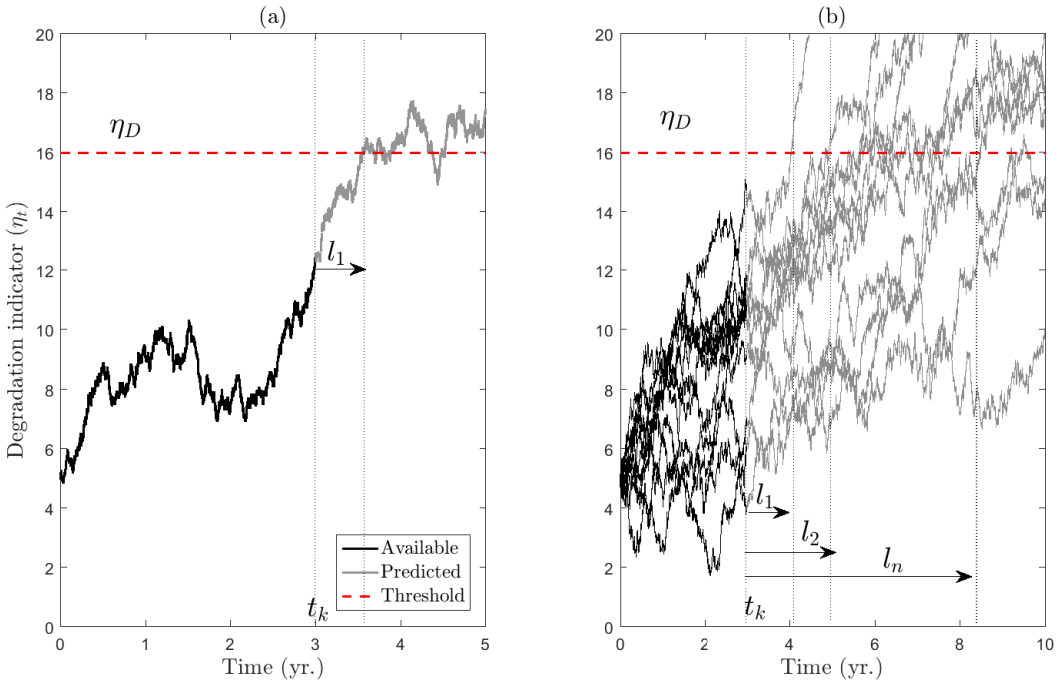

Figure 4.6: (a) Illustration of RUL; (b) effect of unit heterogeneity on RUL

Mathematically, RUL L_k at time t_k given the observation history $y_1, y_2, \cdots y_{t_k}$ is defined

as [198]:

$$L_k = \inf\{l_k : y_{(t_k+l_k)} > \eta_D | y_{1:k} < \eta_D\} \tag{4.45}$$

with the the associated PDF and CDF $f(L_k|y_{1:k})$ and $F(L_k|y_{1:k})$, respectively.

It can be seen from Eq. 4.45 that the RUL is degradation path (characterized by $\boldsymbol{\Theta}$) dependent, whose PDF and CDF are updated with the availability of new data. Using the law of total probability, these can be estimated by integrating over parameter $\boldsymbol{\Theta}$ as follows:

$$f(L_k|y_{1:k}) = \int f(L_k|\boldsymbol{\Theta}, y_{1:k}) p(\boldsymbol{\Theta}|y_{1:k}) d\boldsymbol{\Theta} \tag{4.46}$$

$$F(L_k|y_{1:k}) = \int F(L_k|\boldsymbol{\Theta}, y_{1:k}) p(\boldsymbol{\Theta}|y_{1:k}) d\boldsymbol{\Theta} \tag{4.47}$$

where the $p(\boldsymbol{\Theta}|y_{1:k})$ is the posterior distribution of $\boldsymbol{\Theta}$ at time t_k as estimated earlier using Eq. 4.12. The expression for $f(L_k|\boldsymbol{\Theta}, y_{1:k})$ or $F(L_k|\boldsymbol{\Theta}, y_{1:k})$ can either be derived as a closed form solution (e.g., WP, GP) or can be estimated empirically. Once $F(L_k|\boldsymbol{\Theta}, y_{1:k})$ and $p(\boldsymbol{\Theta}|y_{1:k})$ are estimated, the CDF of L_k can be updated using Eq. 4.47. The updated distribution of RUL CDF can subsequently be used for reliability assessment and maintenance planning [196, 93]. Here, it is important to mention that the second phase parameters are used for future degradation level $y_t^\star$ prediction and RUL estimation. If a significant change point is not observed, then the second phase parameters are governed by the prior distribution obtained from historical data, which is the process followed in standard reliability theory.

The probability of failure calculated above will be utilized for maintenance planning of a monitored unit. For illustration purposes, a relatively simple age based replacement (ABR) policy can be employed (see Appendix C for derivations under ABR policy). Under ABR,

the system is replaced preventively after an interval of t_p with a preventive replacement cost of C_p. Moreover, a failure replacement is performed with a cost of C_f (assume $C_f > C_p$), whenever the degradation level exceeds a pre-defined threshold η_D in the time interval $[0, t_p]$. The expected cost rate (ECR) ([125]) for this model is then given by:

$$\begin{aligned} ECR(t_p) &= \frac{\text{Expected total replacement cost per cycle}}{\text{Expected cycle length}} \\ &= \frac{C_p[1 - F(t_p)] + C_f F(t_p)}{\int_0^{t_p}[1 - F(t)]dt} \end{aligned} \tag{4.48}$$

where, $F(t)$ is probability of failure at time t as estimated using Eq. 4.47. The optimum replacement time t_p is found by minimizing Eq. 4.48. The failure time distribution $F(t)$ is updated as condition monitoring data becomes available and the preventive replacement time t_p is calculated. The above maintenance step is the same for all the three models considered in this thesis, once the probability of failure $F(t)$ is known. In the following sections, the estimation of RUL and $F(t)$ are described for the models considered in this chapter.

4.4.1 Linear RV model

A simulation based approach is employed in this thesis to predict the future degradation level and the RUL distribution. The predictive distribution of future degradation level y_t^* of an unit at future time t, which is generated during the second phase of degradation, can be obtained by numerically evaluating the following integral:

$$p(y_t^*|\boldsymbol{y}) = \int\int p(y_t^*|\boldsymbol{y}, \boldsymbol{\beta}, \tau^2) p(\beta, \tau^2|\boldsymbol{y})\ d\boldsymbol{\beta}\ d\tau^2 \tag{4.49}$$

If ϵ^* is independent of ϵ, then $\boldsymbol{y}$ and y_t^* are independent, hence, $p(y_t^*|\boldsymbol{y}, \boldsymbol{\beta}, \tau^2) = p(y_t^*|\boldsymbol{\beta}, \tau^2)$, which can be written as,

$$p(y_t^*|\boldsymbol{\beta}, \tau^2) = \frac{1}{(2\Pi\tau^2)}\exp\left[-\frac{1}{2\tau^2}(y_t^* - \beta_1 - \beta_2 t^*)^2\right]. \tag{4.50}$$

The following procedure is used to draw the samples of y_t^* from Eq. 4.49 :

Step I: jointly draw $(\boldsymbol{\beta}^{(s)}, \tau^{2(s)})$ using MCMC;

Step II: draw y_t^* from $p(y_t^*|\boldsymbol{\beta}^{(s)}, \tau^{2(s)})$; and

Step III: repeat steps I and II for each draw using MCMC.

Once predicted y_t^* is known at different times t, the RUL and failure time distribution can be estimated. For example, the posterior cumulative distribution of the failure time T is given by,

$$F(t) = p(T < t|\boldsymbol{y}) = p(y_t^* > \eta_D|\boldsymbol{y}) \tag{4.51}$$

$$= \int_{\eta_D}^{\infty} p(y_t^*|\boldsymbol{y})d\boldsymbol{y} = \frac{1}{M}\sum_{s=1}^{M} I(y_t^{*(s)} > \eta_D) \tag{4.52}$$

where $y_t^{*(s)}$ is the predicted value of degradation signal at time t for s^{th} draw, $I(\cdot)$ is the indicator function. Other statistics of interest, such as the predictive mean of y_t^*, can be calculated using:

$$E[y_t^*|\boldsymbol{y}] = \int y_t^* p(y_t^*|\boldsymbol{y})dy_t^* = \frac{1}{M}\sum_{s=1}^{M} y_t^{*(s)} \tag{4.53}$$

The probability of failure calculated in Eq. 4.52 above will be utilized for maintenance planning.

4.4.2 GP model

Park et al. [164] derived a closed form expression for the PDF and CDF of the failure time distribution for a Gamma process. The CDF $F(t)$ estimated at time t is given by [164]:

$$F(t) = \frac{\Gamma(a_0 t, b_1(\eta_D - y_0))}{\Gamma(a_0 t)} \tag{4.54}$$

where, y_0 is the initial degradation, η_D is the failure threshold. The CDF can be updated with new measurements by marginalizing Eq. 4.54 with respect to parameter b_1, as given below:

$$F(t|\boldsymbol{y}) = \int_0^\infty \frac{\Gamma(a_0 t, b_1(\eta_D - y_0))}{\Gamma(a_0 t)} \times \frac{b_1^{\alpha_0'-1} e^{-(\beta_0 b_1)} {\beta_0'}^{\alpha_0'}}{\Gamma(\alpha_0')} db_1 \tag{4.55}$$

The update of failure CDF is a two-step procedure: first b_1 is updated using Eq. 4.41, following which marginalization with respect to b_1 using Eq. 4.55 is undertaken, resulting in the updated CDF. The distribution of RUL at time t_k given the degradation histories $y_1, y_2, \cdots y_k$, can be obtained by replacing $t = t - t_k$ and $\eta_D - y_0$ with $\eta_D - y_k$.

4.4.3 WP model

It is well known that the first hitting time (FHT) for the WP follows an Inverse Gaussian distribution [196]. The proof is given in Appendix B. The PDF and CDF of failure time

T are given by:

$$f_T(t|\boldsymbol{\Theta}, y_{1:k}) = \frac{\eta_D - y_k}{\sqrt{2\Pi(t-t_k)^3\sigma_2^2}} \exp\left(-\frac{(\eta_D - y_k - \nu_2(t-t_k))^2}{2\sigma_2^2(t-t_k)}\right) \tag{4.56}$$

$$F_T((t)|\boldsymbol{\Theta}, y_{1:k}) = 1 - \phi\left(\frac{\eta_D - y_k - \nu_2(t-t_k)}{\sigma_2\sqrt{(t-t_k)}}\right) + \exp\left(\frac{2\nu_2(\eta_D - y_k)}{\sigma_2^2}\right) + \phi\left(\frac{-(\eta_D - y_k) - \nu_2(t-t_k)}{\sigma_2\sqrt{(t-t_k)}}\right) \tag{4.57}$$

where ν_2 and σ_2 are the parameters of the second phase. The PDF and CDF of the RUL distribution at time t_k can be obtained by substituting $t - t_k = l_k$ in the above equations, and given by:

$$f_{L_k}(l_k|\boldsymbol{\Theta}, y_{1:k}) = \frac{\eta_D - y_k}{\sqrt{2\Pi l_k^3\sigma_2^2}} \exp\left(-\frac{(\eta_D - y_k - \nu_2 l_k)^2}{2\sigma_2^2 l_k}\right) \tag{4.58}$$

$$F_{L_k}(l_k|\boldsymbol{\Theta}, y_{1:k}) = 1 - \phi\left(\frac{\eta_D - y_k - \nu_2 l_k}{\sigma_2\sqrt{l_k}}\right) + \exp\left(\frac{2\nu_2(\eta_D - y_k)}{\sigma_2^2}\right)\phi\left(\frac{-(\eta_D - y_k) - \nu_2 l_k}{\sigma_2\sqrt{l_k}}\right) \tag{4.59}$$

It is interesting to note that only the last measurement y_k directly appears in the expression, while the degradation histories (i.e., $y_{1:k}$) are used in the estimation of model parameters $\boldsymbol{\Theta}$ (i.e., ν_1, σ_1, ν_2 and σ_2). It can be seen from Eq. 4.58 that the RUL PDF is degradation path dependent and depends upon the stochastic nature of $\boldsymbol{\Theta}$. In order to compute $f_{L_k}(l_k|y_{1:k})$ or $F_{L_k}(l_k|y_{1:k})$, the joint posterior density of $f_{L_k}(l_k|\boldsymbol{\Theta}, y_{1:k})$ or $F_{L_k}(l_k|\boldsymbol{\Theta}, y_{1:k})$ can be marginalized with respect to $\boldsymbol{\Theta}$ as follows:

$$f_{L_k}(l_k|y_{1:k}) = \int f_{L_k}(l_k|\boldsymbol{\Theta}, y_{1:k}) p(\boldsymbol{\Theta}|y_{1:k}) d\boldsymbol{\Theta} \tag{4.60}$$

$$F_{L_k}(l_k|y_{1:k}) = \int F_{L_k}(l_k|\boldsymbol{\Theta}, y_{1:k}) p(\boldsymbol{\Theta}|y_{1:k}) d\boldsymbol{\Theta} \tag{4.61}$$

where the $p(\boldsymbol{\Theta}|y_{1:k})$ is the posterior distribution of $\boldsymbol{\Theta}$ at time t_k as estimated earlier using Eq. 4.44.

Si et al. [197] kept the diffusion coefficient σ constant, which allowed them to estimate the RUL using a state space model. Assuming $y_{01} = 0$ in Eq. 4.8, they considered the following single phase WP model:

$$y_t = \nu t + \sigma W(t) \tag{4.62}$$

For a monitored unit at time t_i, with the obtained degradation measurement x_i, Eq. 4.62 can be re-written as:

$$\begin{aligned} y_t - y_{t_i} &= [\nu t + \sigma W(t)] - [\nu t_i + \sigma W(t_i)] \qquad (4.63) \\ &= \nu(t - t_i) + \sigma\,[W(t) - W(t_i)] \\ y_t &= y_{t_i} + \nu(t - t_i) + \sigma W(t - t_i) \qquad (4.64) \end{aligned}$$

Now, Eq. 4.64 can be reconstructed via a linear state-space model as,

$$\Lambda_{t_i} = \Lambda_{t_{i-1}} + \eta \tag{4.65}$$

$$y_{t_i} = y_{t_{i-1}} + \nu(t_i - t_{i-1}) + \sigma W(t_i - t_{i-1}) \tag{4.66}$$

where, $W(t_i - t_{i-1}) \sim N(0, t_i - t_{i-1})$. Note that in contrast to this method, both parameters ν and σ are considered as time-varying random variable in our approach and updated for RUL estimation. This is achieved because a flexible MCMC sampling based approach for posterior estimation is used.

4.5 Effect of correlation

For many degradation processes, the degradation rate in the second phase is correlated to the change point location. For example, based on experimental data from bearings, Chen et al. [31] concluded that when a change point occurs during the later stages of a bearing's life, the degradation rate in the second phase tends to be faster. This means that if a fault develops during the initial operational period, then the damage will progress slower, providing ample time for maintenance actions prior to complete failure. On the other hand, when a system or a component has already been in operation for a long period of time, then the RUL predictions and subsequent maintenance planning are critical due to the faster rate of degradation. Hence, it is important to consider this correlation between when the change point occurs and the degradation rate, for obtaining better estimates for the RUL.

Most previous studies [31, 17] assume that the location of change point does not have a significant effect on other degradation parameters, and independent priors for the change point λ and other model parameters (say, regression coefficients) are employed. For example, two separate multivariate normal priors for the two phases and a discrete uniform prior for λ, which is independent of the multivariate normal priors, were used by Chen et al. [31]. Similarly, an independent prior for each parameter was used by Carlin et al. [28]. However, including correlation through historical data can result in better failure time predictions.

Here, the method is illustrated for a random variable model; however, the proposed method is general and is applicable to other model types as well. The likelihood for a RV model has been given earlier in Eq. 4.16 and the joint prior of all the parameters

$(\theta_1, \theta_2, \beta_1, \beta_2, \sigma^2, \tau^2, \lambda)$ is given by:

$$\pi(\mathbf{\Theta}) = \pi(\theta_1, \theta_2, \beta_1, \beta_2, \sigma^2, \tau^2, \lambda) \tag{4.67}$$

The correlation structure between the degradation rate β_2 and the change point λ can be captured, say, using a bi-variate distribution (say, Gaussian). Let $\pi(\beta_2, \lambda)$ denote the joint prior distribution of (β_2, λ) and $\pi(\theta_1, \theta_2, \beta_1, \sigma^2, \tau^2 | \beta_2, \lambda)$ be the conditional distribution of other model parameters, given (β_2, λ). Now, the total probability theorem can be used to derive the joint prior distribution $\pi(\mathbf{\Theta})$ as follows:

$$\begin{aligned} \pi(\mathbf{\Theta}) &= \pi(\theta_1, \theta_2, \beta_1, \sigma^2, \tau^2, \beta_2, \lambda) \\ &= \pi(\theta_1, \theta_2, \beta_1, \sigma^2, \tau^2 | \beta_2, \lambda) \pi(\beta_2, \lambda) \end{aligned} \tag{4.68}$$

It is possible to perform Bayesian inference using the prior in Eq. 4.68. However, it will be computationally expensive and will require a large number of historical data sets for estimating the hyper-parameters. In the absence of such information, a simplified expression can be derived by assuming independence of parameters as given below:

$$\begin{aligned} \pi(\mathbf{\Theta}) &= \pi(\theta_1, \theta_2, \beta_1, \sigma^2, \tau^2 | \beta_2, \lambda) \pi(\beta_2, \lambda) \\ &= \pi(\theta_1 | \beta_2, \lambda) \pi(\theta_2 | \beta_2, \lambda) \pi(\beta_1 | \beta_2, \lambda) \pi(\sigma^2 | \beta_2, \lambda) \pi(\tau^2 | \beta_2, \lambda) \pi(\beta_2, \lambda) \\ &= \pi(\theta_1) \pi(\theta_2) \pi(\beta_1) \pi(\sigma^2) \pi(\tau^2) \pi(\beta_2, \lambda) \end{aligned} \tag{4.69}$$

Finally, the following prior distributions in terms of hyper-parameters $\boldsymbol{\xi} = (\mu_{\theta_1}, \sigma^2_{\theta_1}, \mu_{\theta_2}, \sigma^2_{\theta_2}, \mu_{\beta_1},$

$\sigma^2_{\beta_1}, a_{\sigma^2}, b_{\sigma^2}, a_{\tau^2}, b_{\tau^2}, \boldsymbol{\mu}, \boldsymbol{\Sigma}$) are considered:

$$\pi(\theta_1) \sim N(\mu_{\theta_1}, \sigma^2_{\theta_1}); \pi(\theta_2) \sim N(\mu_{\theta_2}, \sigma^2_{\theta_2}); \pi(\beta_1) \sim N(\mu_{\beta_1}, \sigma^2_{\beta_1})$$

$$\pi(\sigma^2) \sim IG(a_{\sigma^2}, b_{\sigma^2}); \pi(\tau^2 \sim IG(a_{\tau^2}, b_{\tau^2})$$

$$\pi \begin{pmatrix} \beta_2 \\ \\ \lambda \end{pmatrix} = BVN\left(\boldsymbol{\mu}, \boldsymbol{\Sigma}\right) = BVN\left(\begin{pmatrix} \mu_{\beta_2} \\ \\ \mu_\lambda \end{pmatrix} \begin{pmatrix} \sigma_{\beta_2^2} & \rho\sigma_\beta\sigma_\lambda \\ \\ \rho\sigma_\beta\sigma_\lambda & \sigma^2_\lambda \end{pmatrix}\right)$$

where N, IG and BVN denotes a normal, inverse Gaussian and bi-variate normal distribution, respectively. With this, the joint posterior distribution for $\boldsymbol{\Theta}$ is given by:

$$\begin{aligned} p(\boldsymbol{\Theta}|\boldsymbol{y}) \quad &= \pi(\theta_1)\pi(\theta_2)\pi(\beta_1)\pi(\sigma^2)\pi(\tau^2)\pi(\beta_2, \lambda) \times \tfrac{1}{(\sqrt{2\Pi\sigma^2})^\lambda} \exp\Big[-\textstyle\sum_{t=1}^{\lambda} (y_t - \theta_1 - \theta_2 t)^2/2\sigma^2\Big] \\ &\quad \tfrac{1}{(\sqrt{2\Pi\tau^2})^{(t-\lambda)}} \exp\big[-\textstyle\sum_{t=\lambda+1}^{t} (y_t - \beta_1 - \beta_2 t)^2/2\tau^2\big] \end{aligned} \tag{4.70}$$

The marginal posterior density functions are estimated by taking random samples from the joint posterior distribution using MCMC algorithm.

4.6 Significant change point

An important issue to address in the proposed degradation modeling approach is when multiple candidate change points are present in the signal. To explain this, consider the degradation paths shown in Fig. 4.7. These degardation paths will be used for the case study in the next chapter; the purpose here, however, is to illustrate how to ascertain a significant change point from multiple candidates if they exist in the degradation paths. The degradation paths in Fig. 4.7 show multiple change points which exist in each degradation path and do not appear to follow a clear two-phase behaviour in their degradation

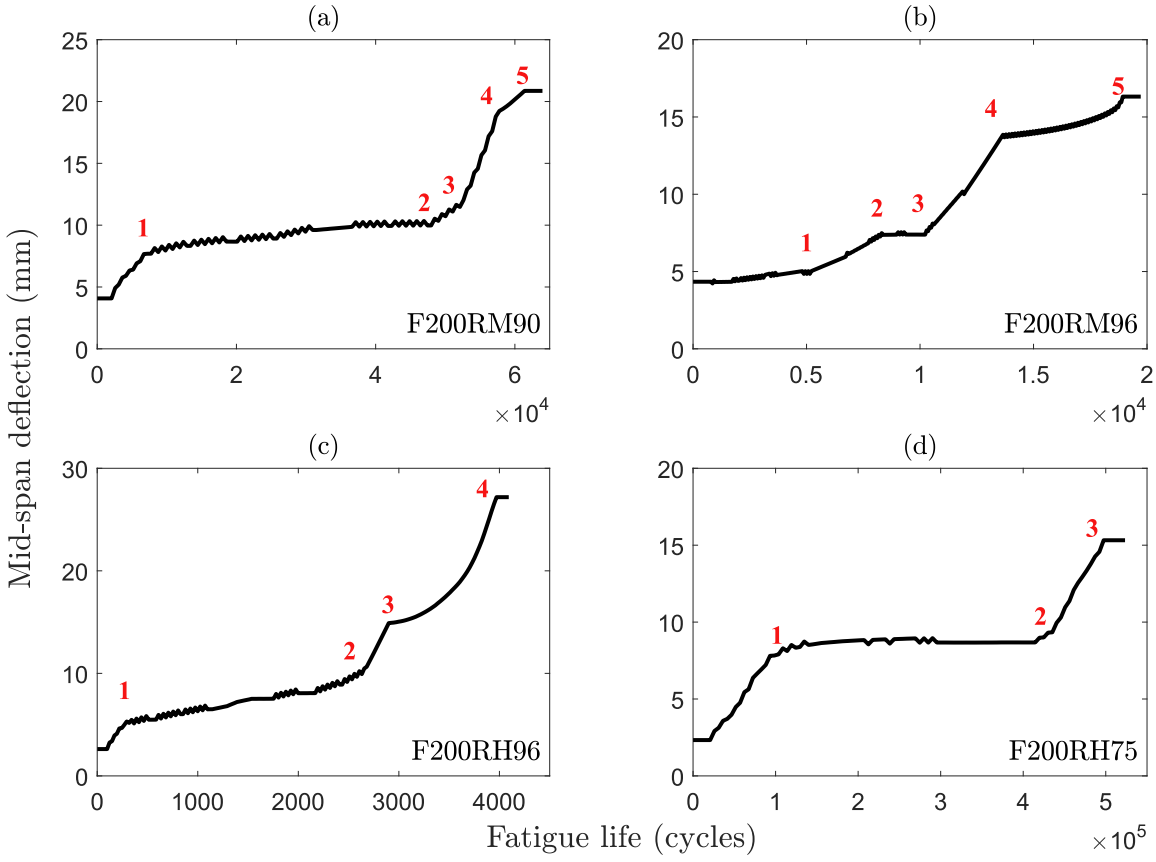

Figure 4.7: Significant change point

(the details are provided in the next chapter). For example, the degradation path in Fig. 4.7a contains five change point candidates and labeled in the figure.

Now, the question is which one of these change points is to be considered as the most significant change point for two-phase degradation modeling? Note that the problem is already constrained in that only one of the change points can be considered in the mathematical formulation. One approach is to select the most suitable change point based on practical constraints. For example, the change point location can be constrained to occur during a monitoring period only, which is typically during the later stages of its expected life and not during its initial operational life. This is applicable in those cases where the monitoring program only occurs during the most critical phase of a components' or a systems' life and not throughout the entire operational life. This is also consistent with the previous assumption that such monitoring is cost-effective for long-life components, where in most cases, only a limited monitoring program towards the expected end of life may be expected. The other constraint is that the estimated slope during the second phase is larger than during the first phase. This is also based on physical reasoning and assumes that a change point accelerates degradation. However, as seen subsequently, the latter constraint is automatically satisfied because a larger slope would naturally maximize the posterior density.

In using the Bayesian approach, the most significant change point is the one which maximizes the posterior density. For the degradation paths shown Fig. 4.7 posterior probability of a change point is shown in Fig. 4.8, along with the degradation path. Clearly, in each case, the most appropriate change point is associated with the maximum posterior density and is detected. For the detected change point, a two-phase model fit is also shown in the same figure. Alternatively, a ML approach can be used and change point with maximum likelihood value is selected. Table 4.1 presents the log-likelihood

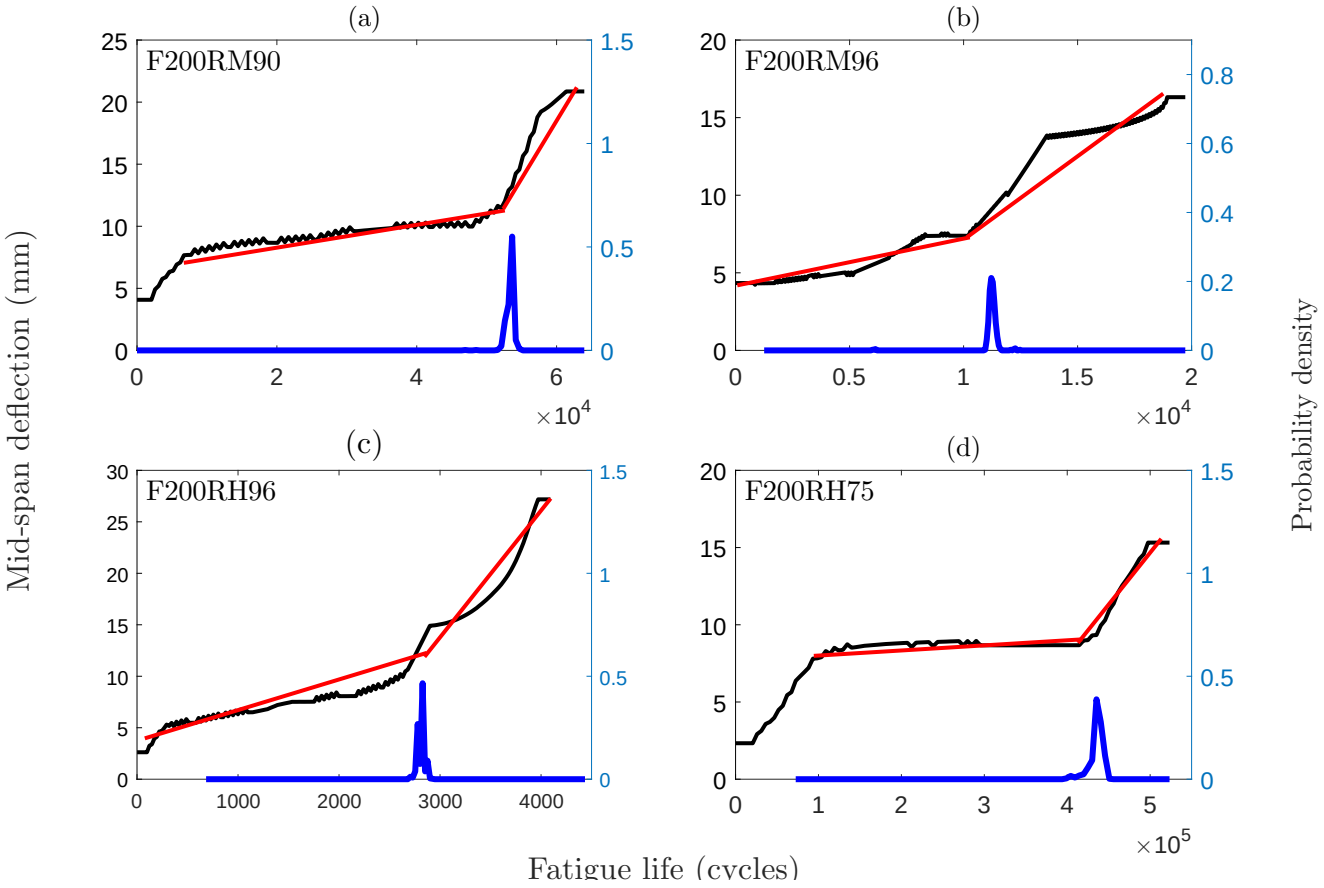

Figure 4.8: Posterior density of change point and two phase degradation model

Table 4.1: Log-likelihood for various change points

Beam	CP-1	CP-2	CP-3	CP-4	CP-5
F200RM90	-45	12	25	8	-10
F200RM96	-52	-48	21	7	-36
F200RH96	-50	22	14	-30	NA
F200RH75	-35	27	-47	NA	NA

values for different change point locations associated with the degradation signals. Based on maximum log-likelihood, the most probable change points are CP-3, CP-3, CP-2 and CP-2 for the four cases: F200RM90, F200RM96, F200RH96 and F200RH75, respectively. Clearly, both the Bayesian and ML approaches are in agreement. The results are explored in more detail in the next chapter when dealing with the case study for the civil engineering case.

4.7 Numerical example

Twenty five simulated degradation signals are generated according to Eq. 4.3. The relationship between the second phase degradation rate β_2 and the change point location λ is given by the following assumed relationship:

$$\beta_2 = 0.1(\frac{\lambda}{50})^2 \tag{4.71}$$

This equation assumes a quadratic relationship between the time of occurrence of the change point and the ensuing slope in the second phase. The change point location λ was varied from 50 to 100, in increments of 2. The parameters θ_1, θ_2, β_2, σ and τ are assumed to follow a normal distribution according to:

$$\theta_1 \sim N(1, 0.5^2), \theta_2 \sim N(0.01, 0.005^2), \quad \sigma \sim N(0, 0.2^2), \quad \tau \sim N(0, 0.3^2) \tag{4.72}$$

and the continuity constraint (i.e., $\theta_1 + \theta_2\lambda = \beta_1 + \beta_2\lambda$) is imposed at the junction of the two phases. Figure 4.9 shows the simulated degradation paths, where the y-axis is some measure of degradation y_t and the x-axis is the time. In Fig. 4.9 the relationship between

the degradation rate β_2 and the change point can easily observed. For this example, it is assumed that these degradation signals represent historical data from a population of units similar in characteristics to a monitored unit. These simulated paths will be used to generate prior specifications.

4.7.1 Prior specification

The four steps as discussed in subsection 4.3.1 are followed to develop the prior for use with the monitored information. Figure 4.10 shows the variation of log-likelihood with change point locations for all the units. The optimum change point location corresponding to the maximum log-likelihood is also shown in the same figure. The two phase model parameters and optimum change point locations for all the units are collected and distributions fit to the data (see Step-IV). The Q-Q plot for θ_1, θ_2 and β_1 are presented in Figure 4.11. As expected, most of the data points fall on to a straight line. The maximum likelihood principle is used to fit the distributions and the hyper-parameters for priors. The estimated prior distributions are given below:

$$\begin{aligned}
&\pi(\theta_1) \sim N(0.8, 0.5^2); \pi(\theta_2) \sim N(0.017, 0.004^2) \\
&\pi(\beta_1) \sim N(-16, 10^2); \pi(\sigma^2) \sim IG(4.3, \frac{1}{2}); \pi(\tau^2) \sim IG(15, \frac{1}{0.9}) \\
&\pi \begin{pmatrix} \lambda \\ \beta_2 \end{pmatrix} \sim BVN \left(\begin{pmatrix} 75.0 \\ 0.23 \end{pmatrix} \begin{pmatrix} 200 & 1.23 \\ 1.23 & 0.008 \end{pmatrix} \right)
\end{aligned} \tag{4.73}$$

Note that the parameters (β_2, λ) follow a bi-variate normal distribution. The joint probability densities for (β_2, λ) are shown in Figure 4.12, where the correlation between the degradation rate and the change point location is clearly observed. As expected, the prob-

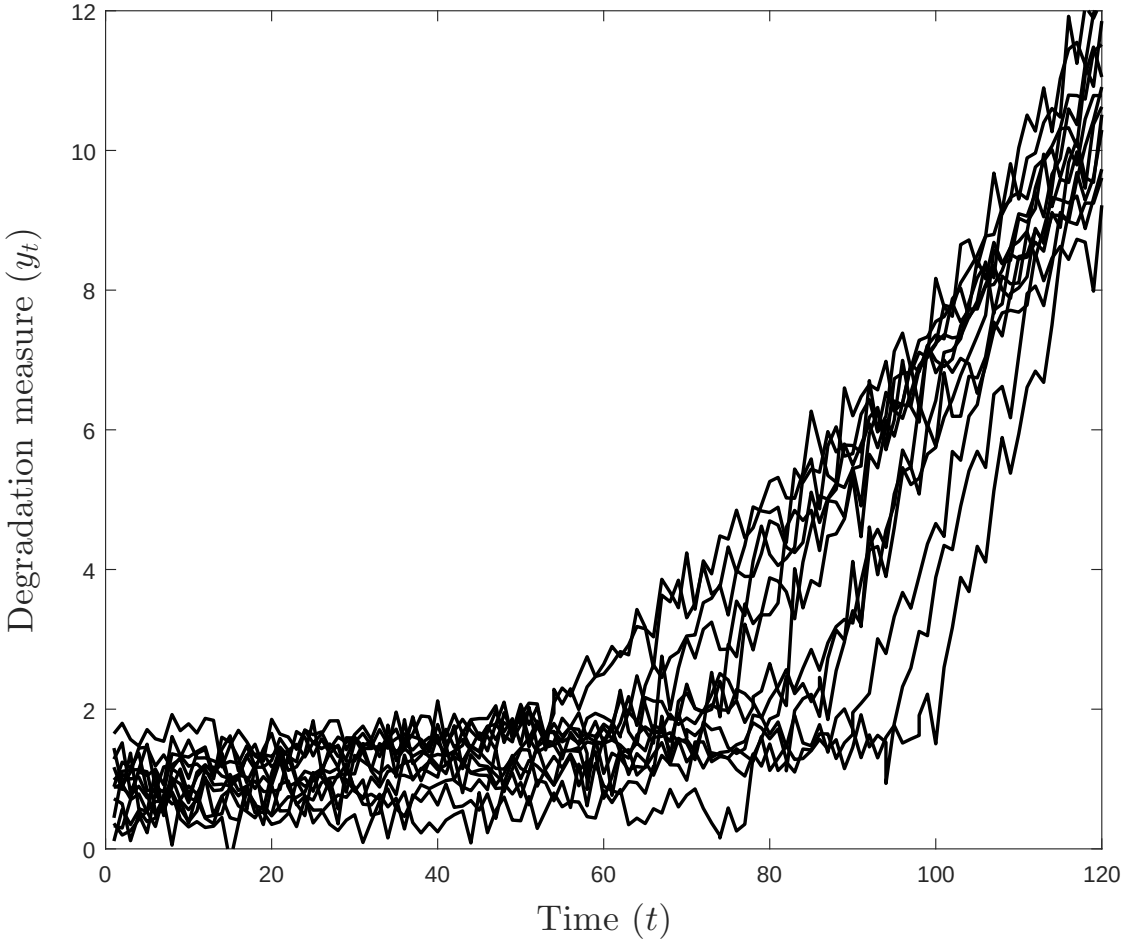

Figure 4.9: Simulated two-phase bearing degradation paths

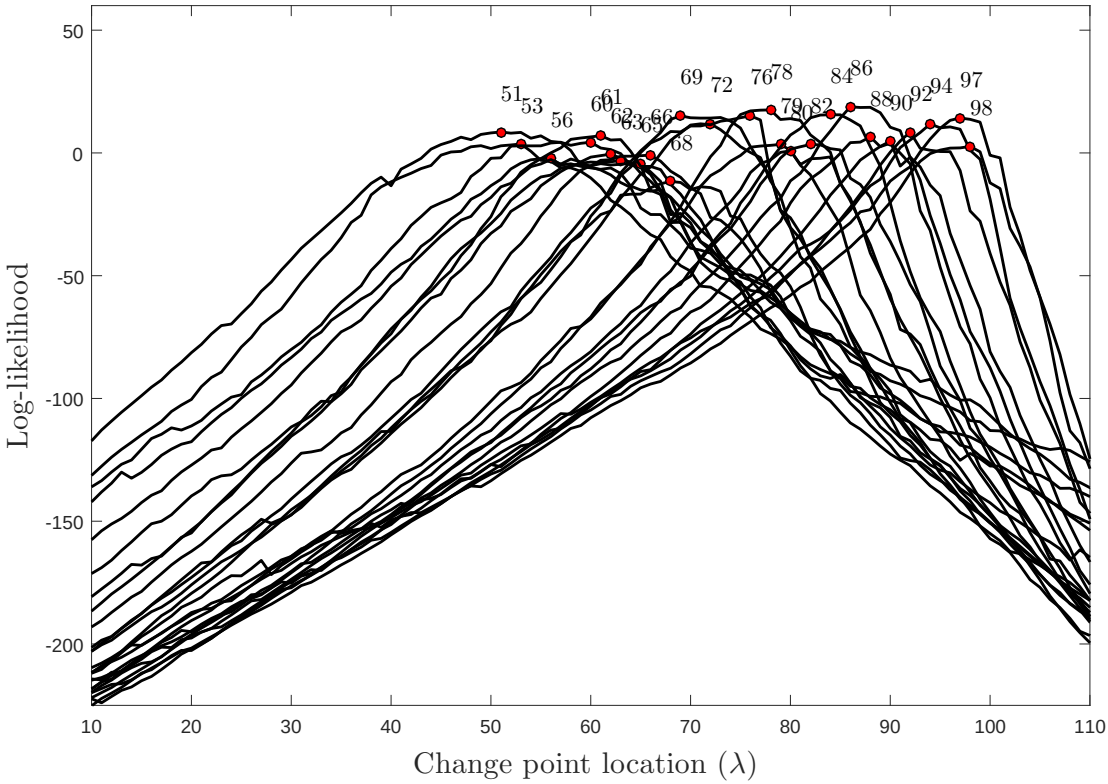

Figure 4.10: Variation of log-likelihood with change point location

ability increases along the diagonal, which means that with increasing λ, the degradation rate β_2 also increases.

4.7.2 Updating parameters

The prior distribution $\pi(\mathbf{\Theta})$ estimated from the historical units can now be integrated with the sensory data obtained from a monitored unit for model updating, RUL estimation and maintenance planning. To simulate a monitored unit, a degradation signal with the following parameters $\theta_1 = 1.5, \theta_2 = 0.02, \beta_2 = 0.15, \sigma_1 = 0.5, \sigma_2 = 0.8, \lambda = 50$ in Eq. 4.3 is

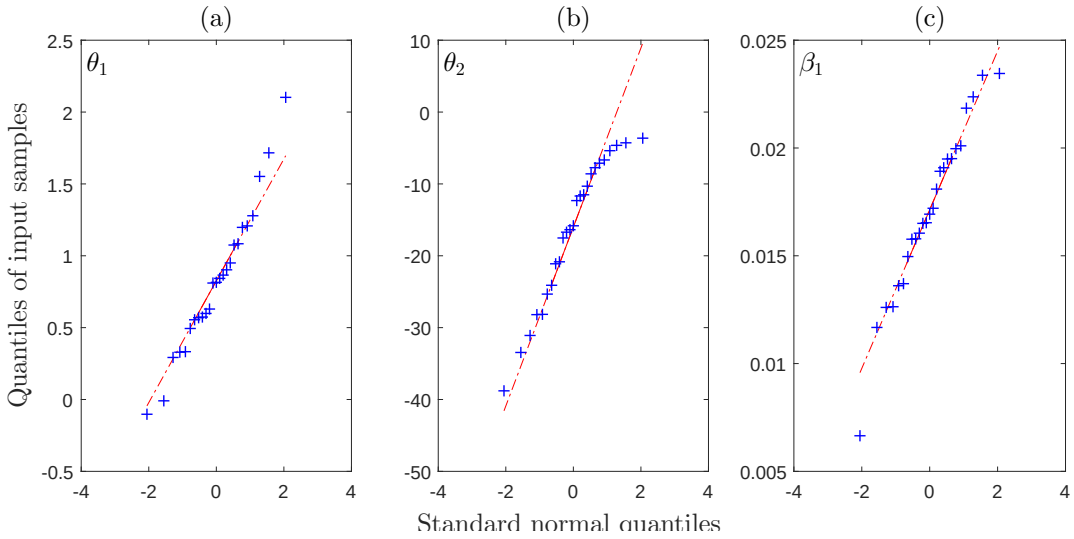

Figure 4.11: Q-Q plot for (a) θ_1 (b) θ_2 and (c) β_1

generated. The continuity constraint $\theta_1 + \theta_2\lambda = \beta_1 + \beta_2\lambda$ is imposed at the change point location.

The first step is the identification of the most probable change point location and the estimation of the two-phase model parameters using the degradation signal. In the proposed methodology these two (i.e., change point locations and model parameters) are estimated simultaneously using MCMC sampling. MCMC sampling is performed using the software package Winbug®. The sample size is calculated using the Raftery and Lewis diagnostics [178], which turns out to be approximately $15,000$ for reliable 95% highest posterior density (HPD) interval of parameters. The details of MCMC algorithm and Raftery and Lewis diagnostics can be found in Appendix D. A total of 20,000 samples are drawn from the joint posterior distribution $p(\boldsymbol{\Theta}|\boldsymbol{y})$ as given in Eq. 4.3. It is found that the simulated Markov chain converges to its stationary distribution after the first 5000 samples. Hence, the last 15,000 samples are retained to obtain the statistical estimates. Figure 4.13 shows the autocorrelation plot for a simulated degradation path of 15,000 samples. Clearly,

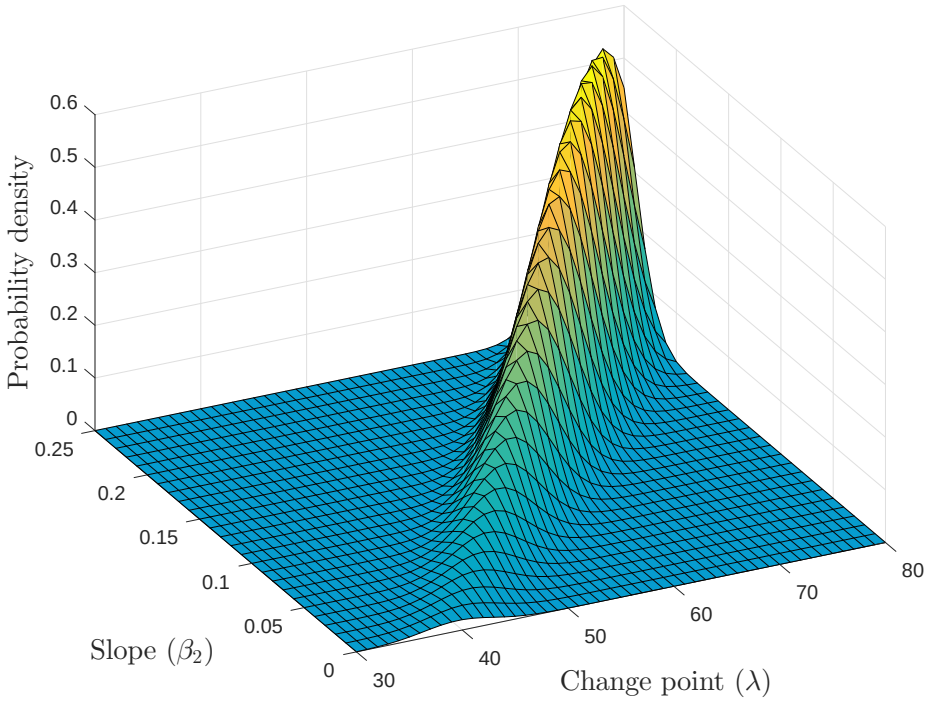

Figure 4.12: Correlation between change point location λ and degradation rate β_2

after three lags, the autocorrelation becomes almost insignificant, which means that that the distribution is stationary.

With this sample size, the posterior distribution of the change point location and the model parameters are updated at four time intervals namely, $t = 50, 60, 70$ and 80. Note that for this degradation path, the actual change point location is at $t = 50$. Figure 4.14 shows the degradation data available at different updating times and the corresponding marginal posterior density of the change point. In Fig. 4.14a, the model is updated when the degradation is still in its first phase. The corresponding posterior mean is approximately equal to 75, which is basically the same as the prior mean of λ as estimated using the historical data (see Eq. 4.73). In other words until $t = 50$ the posterior distribution is

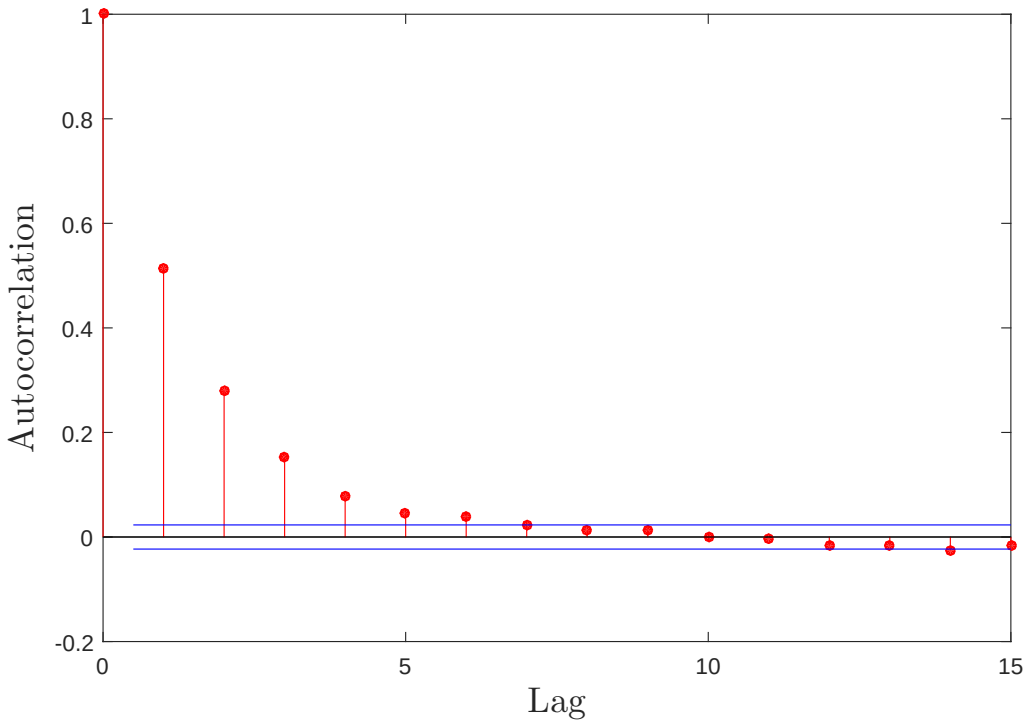

Figure 4.13: Autocorrelation plot for Monte Carlo sample size 15,000

governed by the prior obtained from the historical data, as no change point is detected. In Fig. 4.14b to Fig. 4.14d, the model is updated when the degradation has already entered into the second phase. The posterior distribution then concentrates around the actual change point. Figure 4.15 shows the estimated posterior distribution of degradation rates θ_2 and β_2. It is important to note that the posterior distribution of β_2 is initially diffused, and becomes narrower in the subsequent updates. This is because the posterior distribution of β_2 is governed by the prior in the initial stages of degradation. However, as more data becomes available from the second phase, estimates for β_2 improve and more accurately represents the degradation of a particular unit. In other words, mean of β_2 converges to its true value as more degradation data is utilized in the analysis (see 4.15b).

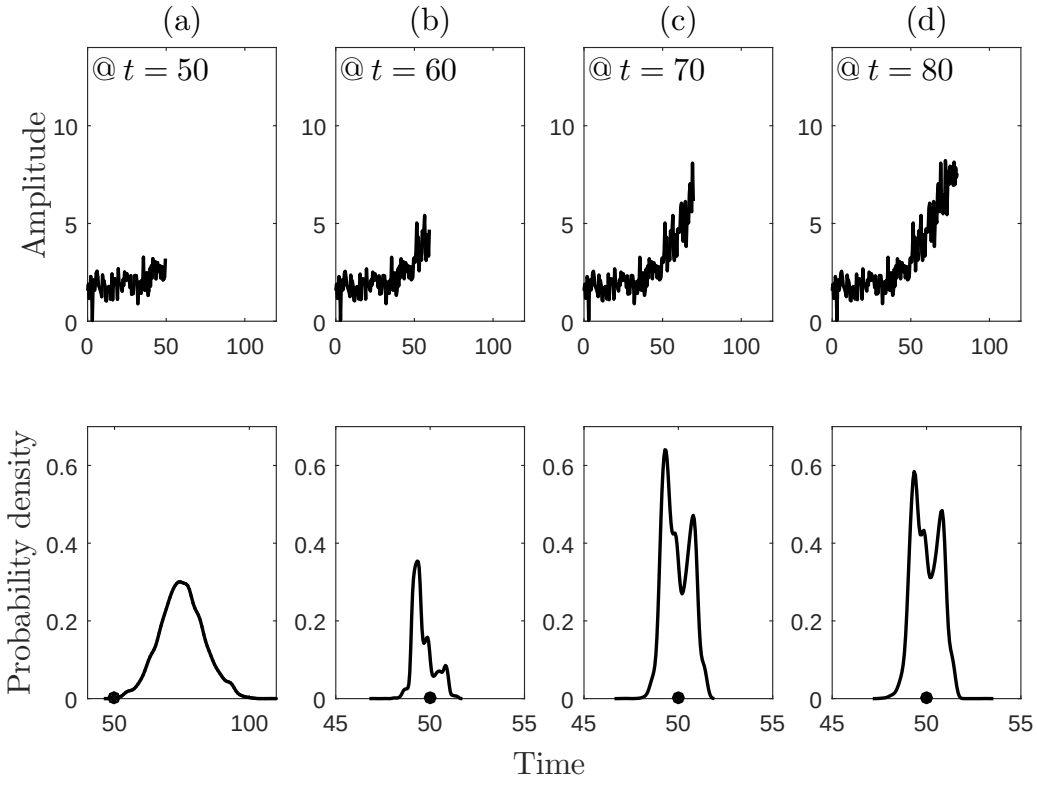

Figure 4.14: Posterior distribution of change point location at different times

In Bayesian statistics, uncertainty in parameter estimation, i.e., epistemic uncertainty, is generally quantified in terms of credible interval such as, highest posterior density (HPD). HPD intervals are the Bayesian analogue for classical confidence intervals and they summarize the distribution by specifying an interval which spans most of the distribution, say 90%, such that every point inside the interval has higher credibility than any point outside the interval. To estimate a HPD interval, first, samples are taken from posterior parameter distribution using MCMC, then, predicted samples are sorted from smallest to largest, and finally, various quantiles are estimated. Here, 5% quantile and 95% quantile are considered for 90% HPD interval estimation. It is worth to mention here that the similar steps are taken to estimate the credible interval of RUL prediction, with key difference that the

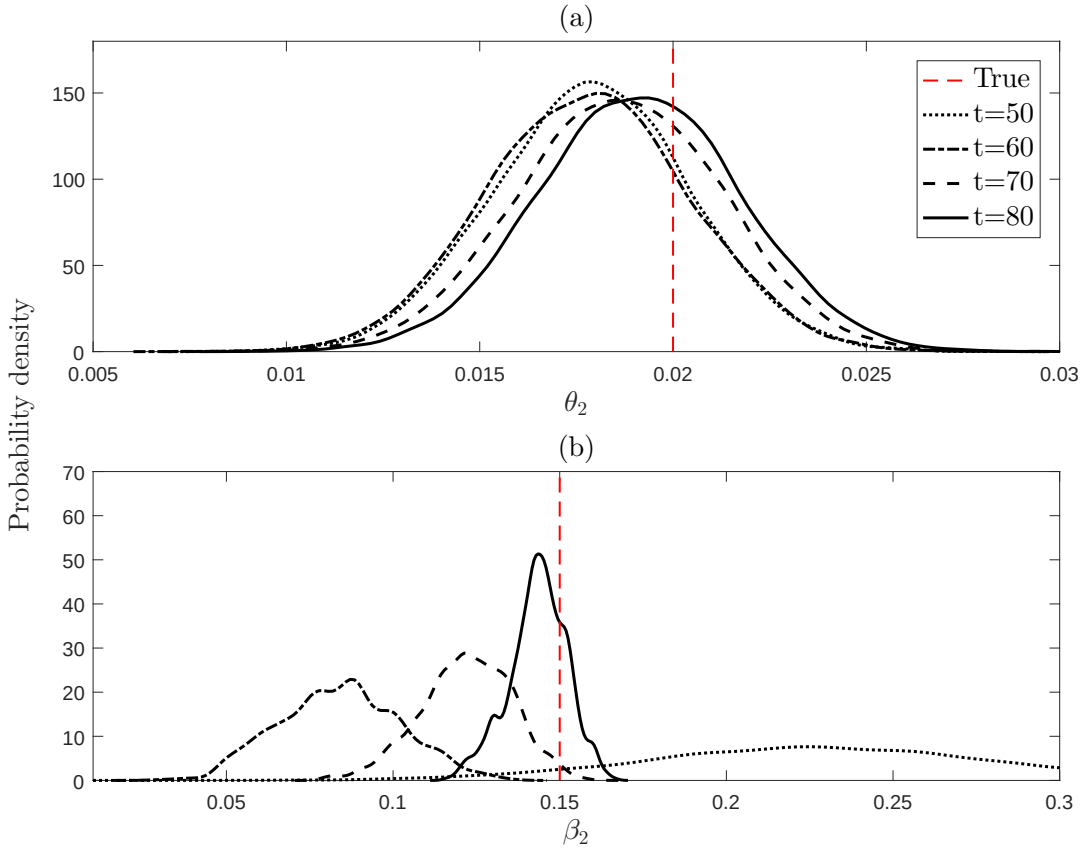

Figure 4.15: Posterior distribution of degradation rates at different times

MCMC samples are drawn from the predictive posterior distribution (see Eq. 4.49).

A summary of model parameters along with the various quantiles updated at time $t = 80$ is given in Table 4.2. It can be seen from the table that the posterior mean of model parameters (i.e., $\theta_1 = 1.55, \theta_2 = 0.02, \beta_2 = 0.14, \sigma_1 = 0.49, \sigma_2 = 0.66, \lambda = 50$) are very close to the true values (i.e., $\theta_1 = 1.5, \theta_2 = 0.02, \beta_2 = 0.15, \sigma_1 = 0.5, \sigma_2 = 0.8, \lambda = 50$) and true values lies within the 90% HPD interval.

Table 4.2: Posterior distribution summaries of model parameters estimated at $t = 80$

				Quantile				
Parameter	Mean	Std Dev	MC Error #	0.025	0.050	0.500	0.950	0.975
θ_1	1.55	0.08	6.6E-04	1.39	1.49	1.55	1.60	1.70
θ_2	0.02	0.00	2.5E-05	0.01	0.02	0.02	0.02	0.02
β_1	-3.79	0.57	7.8E-02	-4.85	-4.18	-3.82	-3.46	-2.52
β_2	0.14	0.01	1.2E-03	0.12	0.14	0.14	0.15	0.16
σ_1	0.49	0.03	2.9E-04	0.43	0.47	0.49	0.51	0.56
σ_2	0.66	0.05	1.1E-03	0.57	0.63	0.66	0.70	0.78
λ	50.00	0.72	1.4E-02	48.81	49.39	49.93	50.65	51.31

MC stands for Monte Carlo.

4.7.3 RUL prediction and maintenance planning

Once the degradation model of a monitored unit is updated using the available degradation data, Eq. 4.49 can be used to predict the degradation magnitude at any future time t. Here, it is important to mention that in this approach, the second phase model parameters are used for future predictions, which means that the RUL distribution is based upon the change point location. When a significant change point is not detected, predictions are influenced by priors. However, once the system enters into the second phase, the degradation data from the monitored unit governs the RUL distribution.

The updated RUL PDF corresponding to $t = 50, 60, 70$ and $t = 80$ are shown in Fig. 4.16 and a summary of the same is given in Table 4.3. Not surprisingly, the RUL PDF narrows over time. Moreover, one can see from Table 4.3 that the actual RUL is very close to the predicted mean RUL and lies within 90% HPD interval. Clearly, model predicts reasonably accurate RUL is both phases of degradation.

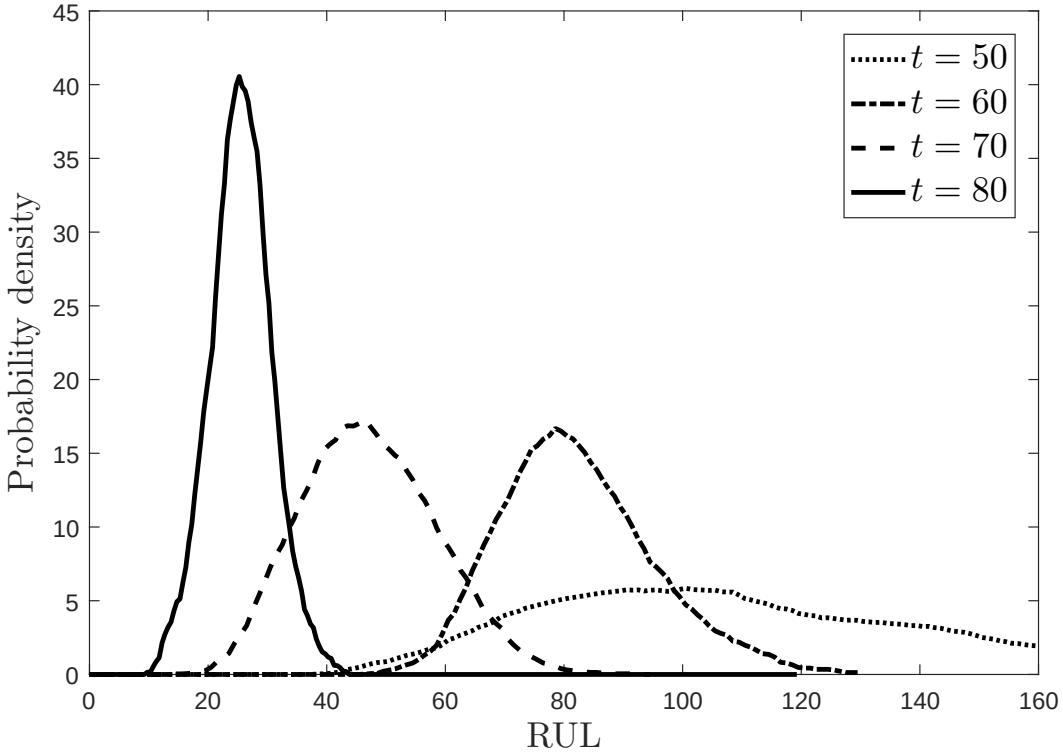

Figure 4.16: RUL update at different times

Table 4.3: A summary of RUL distribution estimated at different times

			Quantile				
	Mean	Std Dev	0.05	0.250	0.750	0.95	Actual
$t = 50$	83	60	10	34	66	104	70
$t = 60$	77	25	49	64	73	87	60
$t = 70$	38	10	22	34	54	62	50
$t = 80$	25	6	12	17	25	38	40

Finally, the model predictions can be used to estimate the optimum replacement time. The probability of failure at different times ($t = 50, 60, 70, 80$) is calculated using Eq. 4.52, which is subsequently used in Eq. 4.48 to optimize the expected cost rate. The following replacement cost $c_p = 1$ and $c_f = 5$ is assumed for this example. Figure 4.17 shows the variation of expected cost rate (ECR) with replacement time interval for different times. The optimum replacement times t_p updated at $t = 50, 60, 70, 80$ are $16, 30, 60$ and 66. The

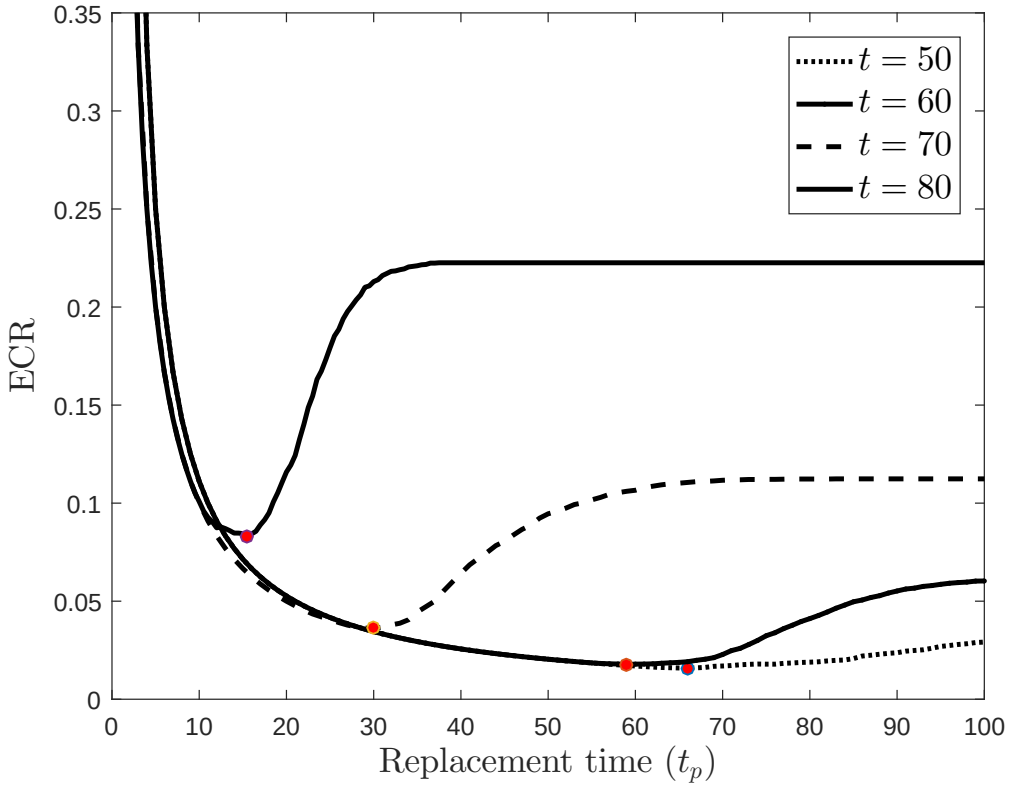

Figure 4.17: Optimal replacement time with increasing degradation

replacement time t_p is sensitive to the replacement cost c_p and c_f, so their values need to be estimated well by practitioners based on past failures and experience.

4.7.4 Effect of correlation on RUL

To illustrate the effect of correlation on RUL, additional 10 degradation paths are simulated according to the two-phase model in Eq. 4.3. These signals represents 10 in-situ units, which is monitored separately and will be used to evaluate the performance of the proposed methodology. The RUL for each path is estimated using Eq. 4.45, where the future degradation level $y_t^\star$ is simulated from the marginal posterior distribution given in Eq. 4.49. First, consider the scenario when the degradation is in the first phase say, $t = 50$. A total of 15,000 Monte Carlo samples are taken and a posterior summary of the RUL for the two approaches are calculated. Figure 4.18 shows the posterior mean, 5% quantile and 95 % quantile of the predicted RUL for the two cases (i.e., correlated and un-correlated). The actual RUL is also shown in the same figure. It is easy to observe that including correlation

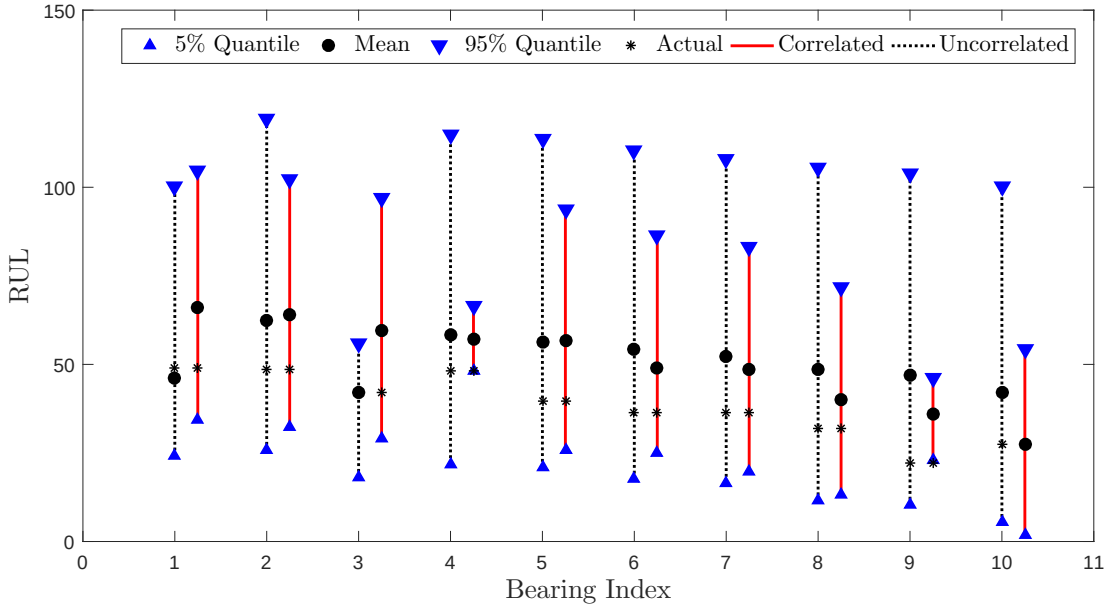

Figure 4.18: RUL prediction before the occurrence of the change point

results includes the actual RUL and results in a narrower prediction interval. Note that

the RUL predictions in the first phase are mostly governed by the prior knowledge. Next, the RUL for these signals are updated when the degradation is in the second phase, say $t = 80$. The previous steps are repeated and RUL is predicted. Figure 4.19 shows the posterior mean and 90% HPD interval of the predicted RUL. As expected, the 90% HPD interval for the correlated case is narrower than the independent case and the actual RUL is very close to the mean predicted RUL. Also, different bearings provide similar prediction intervals for this case. Note that the data from the second phase mostly governs the RUL predictions after a change point is detected. Moreover, if Fig. 4.18 is compared with Fig.

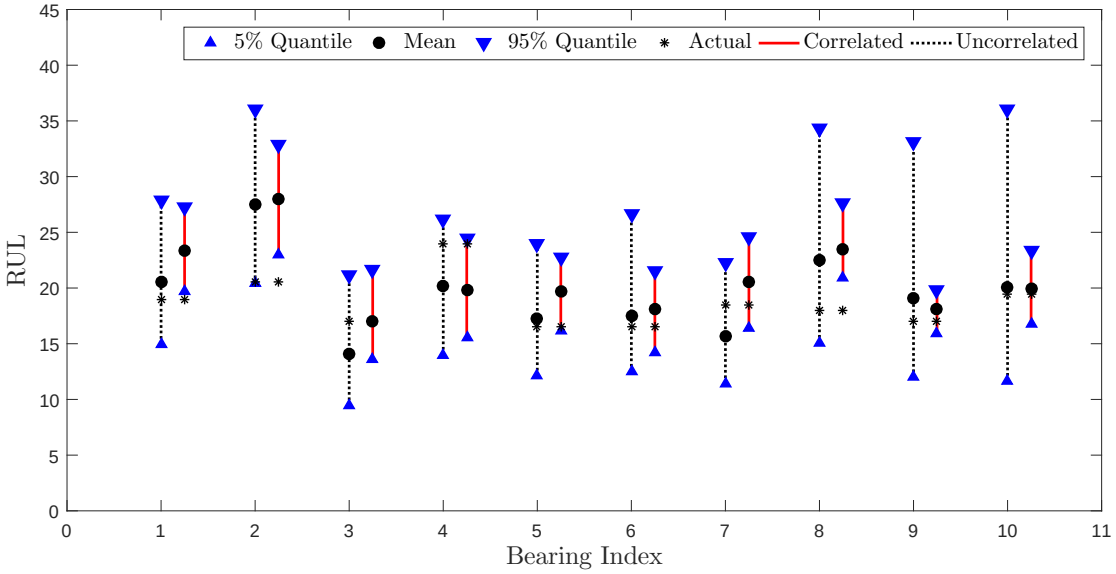

Figure 4.19: RUL prediction after change point

4.19, it is seen that the prediction interval for both cases (with and without correlation) is much smaller when the RUL is estimated after the change point.

4.8 Summary

In this chapter, an integrated approach for damage detection and prognosis incorporating measured condition information is presented. The proposed method is applicable to many civil and mechanical engineering infrastructure applications, whose degradation can be modeled as a two-phase process, where the transition from the first phase to the second phase can be viewed as an incipient fault. Three model types: random variable, Gamma process and Weiner process, are presented to model degradation. For these models, the procedure to estimate the model parameters and RUL using a Bayesian approach is described. The prior knowledge obtained from the historical degradation data is utilized to update the parameters and the RUL of a monitored unit. The proposed method also considers the correlation between degradation rate and change point location for better failure predictions. Finally, a simulated example was presented which demonstrates the effectiveness of this approach for damage detection and end of life predictions for components.

Chapter 5

Application case studies

5.1 Introduction

This chapter demonstrates the application of the methodology presented in Chapter 4 for damage detection and prognosis for civil and industrial applications. First, the proposed methodology is applied to the degradation of a concrete beam. In this case, the corrosion in embedded reinforcing bars causes a loss of bondage between concrete and the steel bar, while the corrosion itself is unobservable directly. In this case study, the slip in the reinforcing steel bar and the mid-span beam deflection are taken as surrogate measures. These measurements obtained from fatigue tests from the literature are modeled using a stochastic Gamma process and the end life characteristics of the beam are estimated. In a second case study, the degradation of rolling element bearings is considered. Vibration measurements (surrogates of degradation) obtained from run-to-failure bearing degradation test data are modeled using a two-phase random coefficient model and the RUL of a working unit is updated with monitored data. The main objective of this chapter is to demonstrate

the application of the proposed methodology to real-world case studies and to underscore both the advantages of the methodology being presented and its limitations.

5.2 Case study: corrosion in reinforced concrete beams

The fatigue strength and serviceability of a flexural reinforced concrete member depends upon the bond between steel and concrete, which is essential for the transfer of the load from concrete to the steel bars. In other words, bond is the mechanism by which stresses are transferred between the reinforcing steel bars and the concrete in a reinforced concrete member. The corrosion of steel reinforcement significantly reduces this bond strength. Corrosion produces corrosion rust products higher in volume than the original steel material, resulting in cracking of the concrete surrounding the bars. With increasing corrosion, the bond stresses between reinforcing steel and concrete decreases and the slip of the reinforcing bar relative to the concrete increases [6]. A typical example for such a condition is shown in Fig. 5.1 [2].

Another factor which contributes to the slip of steel bars is the repeated loading, causing fatigue. Repeated loading can initiate cracks in the concrete surrounding the steel bars, which propagate as the number of load cycles increases, leading to a destruction of the concrete-steel interface. This eventually results in the slip of the steel bars embedded within the concrete matrix. Often, such a loss of bond between concrete and steel results in a loss of composite action and is manifested as an increased overall deflection of the beam.

While the corrosion itself is not directly measurable, the slip of the reinforcing bars or the beam deflection are more readily observable using sensors and can be taken as an

Figure 5.1: Loss of bond between concrete and steel bars resulting in slip

indirect measure of bond strength between the reinforcing steel and concrete and used for degradation modeling. In the following section, the experimental steel-slip data obtained from near full-scale tests on reinforced concrete beams is utilized [5] for degradation modeling and RUL estimation, as described in the previous chapter.

5.2.1 Details of the experiments

The data-set analyzed here consists of slip versus load and beam mid-deflection versus load for eight corroded reinforced concrete beams repaired with carbon fiber-reinforced polymer (CFRP) sheets. All the beams were of the same size with a rectangular cross-section (254 x152 mm) and a length of 2000 mm (see Fig. 5.2 for longitudinal and cross sectional details). The beams were reinforced in the flexural zone with two external CFRP (each 100 mm wide x 1370 mm long trapezoidal in shape) sheets along both sides. The fatigue

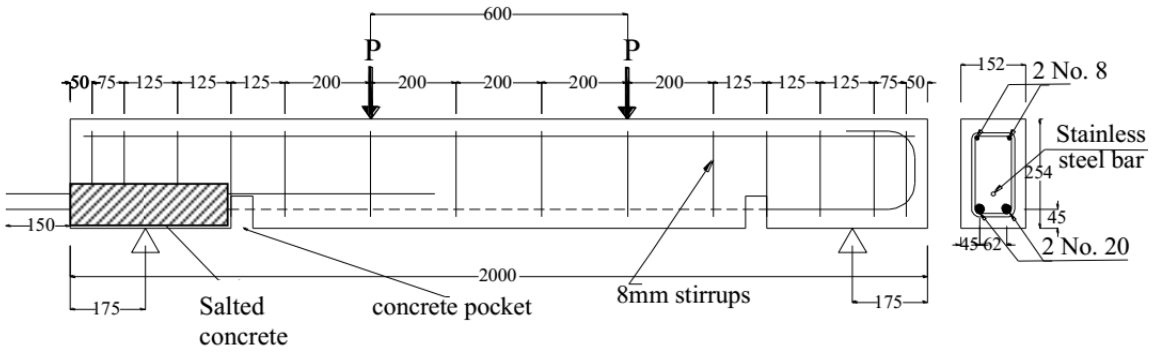

Figure 5.2: Schematic drawing for the experimental specimen [5]

tests under load control condition were performed in structural engineering laboratory at the university of Waterloo[5]. The test set-up is shown in Fig. 5.3. Beams were subjected to four point bending loads. A sine-wave load cycle was applied about the mean load using a MTS 407 controller at a frequency of 2 Hz. The minimum load was set at 10% of the maximum static load capacity of the control beam, so that the beam would not slip or bounce. The maximum load levels were varied to achieve fatigue lives between 10,000 and 1,000,000 cycles. As the number of cycles increased, a longitudinal crack initiated and propagated at the loaded end of the anchorage zone from the bottom of the beam. This crack continued to increase in length and width until the final failure of the beam.

Table 5.1 presents the maximum applied load, the fatigue lives of the specimens and the failure mode for the eight beam specimens. The nomenclature for the beam is given in Table 5.1, and is as follows: the first letter F signifies the fatigue loading, the number 200 is the anchorage length in mm, second letter R signifies that the beam is repaired by wrapping a CFRP sheets following corrosion, third letter M or H denotes the mild or high level of corrosion, respectively and the number in end is the range of applied load in KN. For example, the beam F200RH80 is tested under fatigue loading with an applied load range of 80 KN, which has an anchorage length of 200 mm and repaired using CFRP sheet

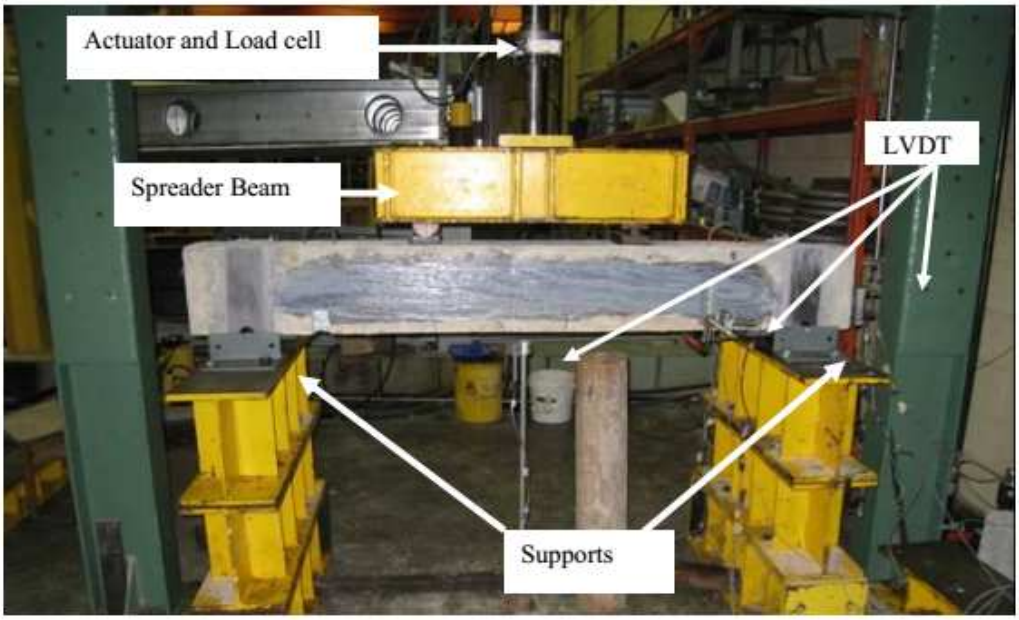

Figure 5.3: Test set-up for generating fatigue loads [5]

Table 5.1: Fatigue life for eight tested beams

Beam	Corrosion (mass loss in %)	Maximum load (KN)	Load range (KN)	Fatigue life (cycles)	Failure mode
F200RM72	6.18	82	72	301,163	Flexure
F200RM80	6.36	90	80	714,313	Flexure
F200RM90	6.18	100	90	63,961	Bond
F200RM96	7.28	106	96	19,723	Bond
F200RH75	13.33	85	75	523,369	Bond
F200RH80	13.92	90	80	634	Bond
F200RH88	10.58	98	88	70,369	Bond
F200RH96	13.80	106	96	4,093	Bond

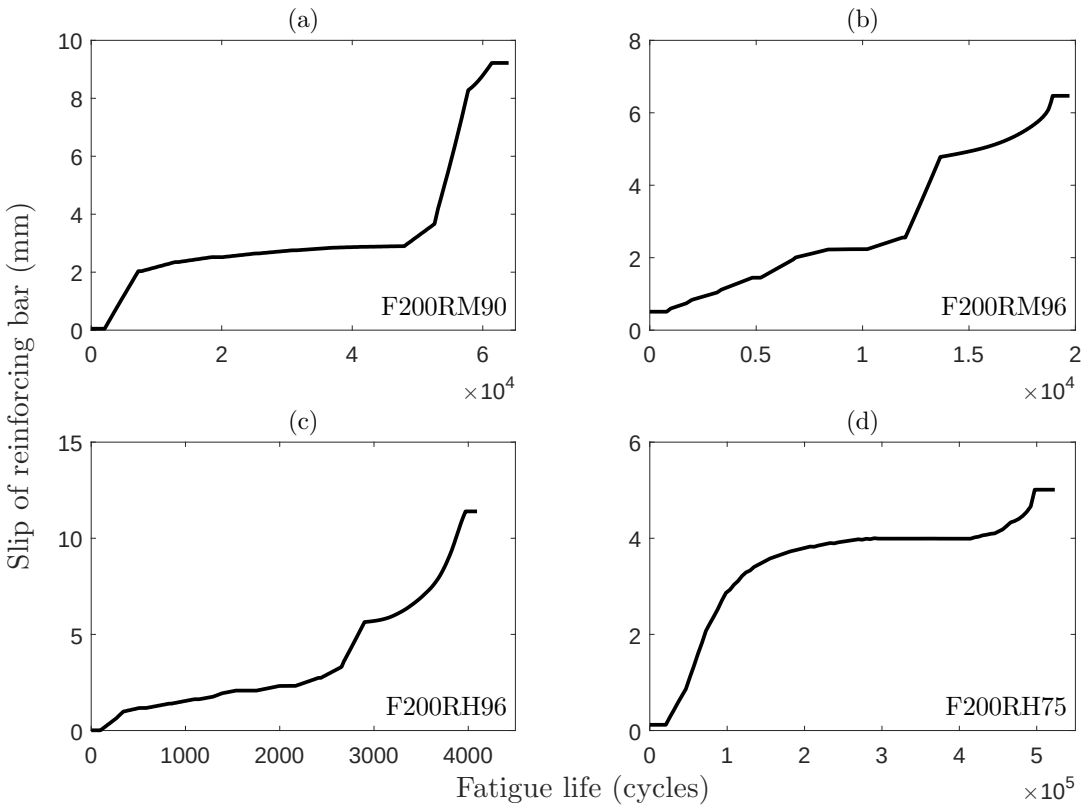

Figure 5.4: Slip length measured for the four beams

followed by a high corrosion level. Linear variable differential transducers (LVDTs) (range = 50 mm, accuracy = 0.01 mm) were used to measure the slip between concrete and steel bar at the free end of beam and the midspan beam deflection.

5.2.2 Details of the data-set

Fig. 5.4 and Fig. 5.5 show the relationship between the slip length and mid-span beam deflection measured for four of the beams, as a function of the number of cycles tested prior to failure. It is clear from Fig. 5.4 and Fig. 5.5 that the specimens show several phases in their fatigue characteristics: first, a gradual increase in the degradation measure

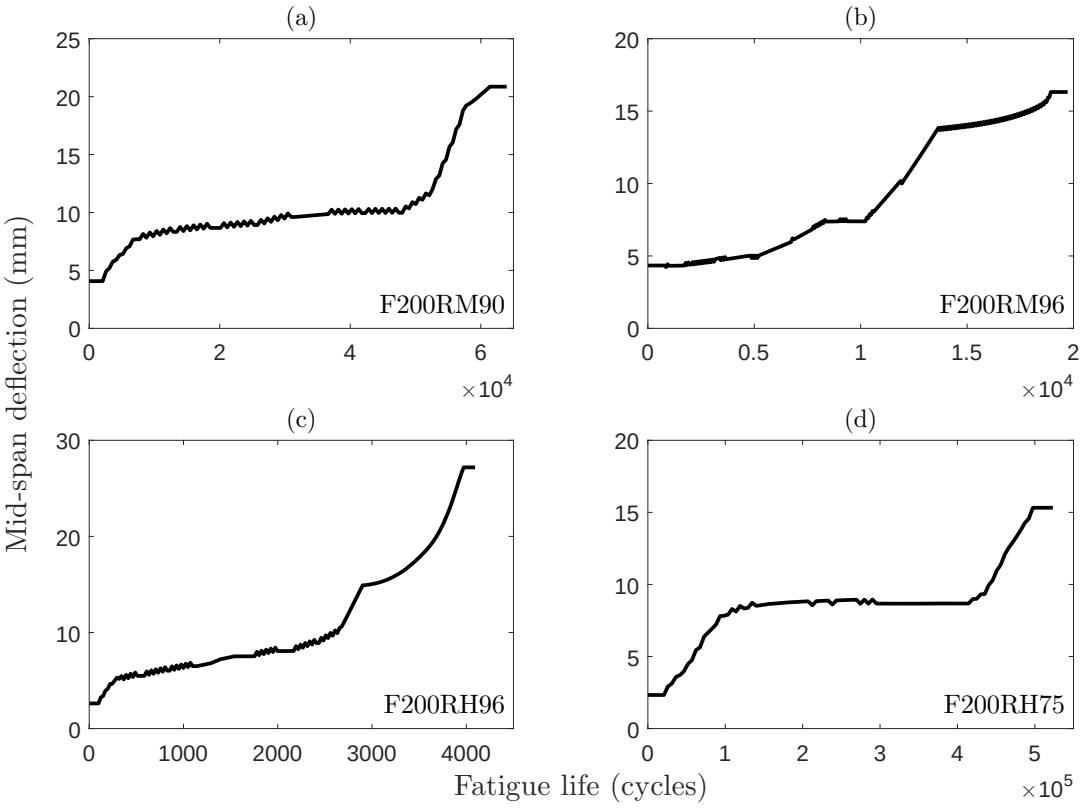

Figure 5.5: Mid-span beam deflection

during most of their life life, followed by a sharp increase in the slope during their final stages. This behaviour can be modeled using a two-phase degradation model described earlier, based on the constraint arguments and posterior probabilities computed at various change point locations. To elaborate the data presented, in Fig. 5.4a the slip reaches a value of 2.06 mm slip at 7200 cycles ($\approx$ 10% of its fatigue life), then the slip increases at a slower rate until it reaches a value of 2.9 mm at 48000 cycles ($\approx$ 80% of the fatigue life). This slip continues to increase to a value of 3.77 mm at 55000 ($\approx$ 90% of the fatigue life), after which it increases rapidly to 9.2 mm at 64000 (100% of the fatigue life). From a practical stand-point, if the 90% fatigue life point were to be estimated during

its operational life, then intervention should in theory be possible to avoid catastrophic failure. Hence, the main objectives of this case-study are two-fold: detect the change-point as it occurs from monitored information and subsequently estimate the RUL once this change-point is detected.

5.3 Results

As mentioned earlier, the increasing slip length of the steel bars and the mid-span beam deflection can be taken as surrogate measures for deterioration due to corrosion. Let y_{it} denote an appropriate surrogate measure of degradation of the i^{th} beam measured at time t. A stochastic Gamma process is selected to model the evolving degradation and subsequent RUL estimation of concrete beams. The GP is chosen because it can account for the temporal uncertainty associated with the degradation path, which could potentially better represent the characteristics of corrosion. Temporal uncertainty can also be modeled using other precesses (e.g., WP), but the GP has the monotonically increasing property, which makes it suitable to model the increasing slip and mid-span beam deflection (see Fig. 5.4 and 5.5). The validity of GP assumption is verified by plotting the slip measurements in a Q-Q plot. Fig. 5.6 shows that the measurements fall onto nearly a straight line confirming this assumption.

According to the definition of a Gamma process, the differential increment in the degradation measure $\triangle y_{ik} = y_{t_{ik}} - y_{t_{i(k-1)}}$ in time interval $\triangle t_{ik} = t_{ik} - t_{i(k-1)}$ follows a Gamma distribution $\Gamma(a_i \triangle t_{ik}, b_i)$ with shape parameter $a_i \triangle t_{ik}$ and scale parameter b_i. Let the measurements be taken at equal time intervals $\triangle t_{ik} = t_0$, then the probability density

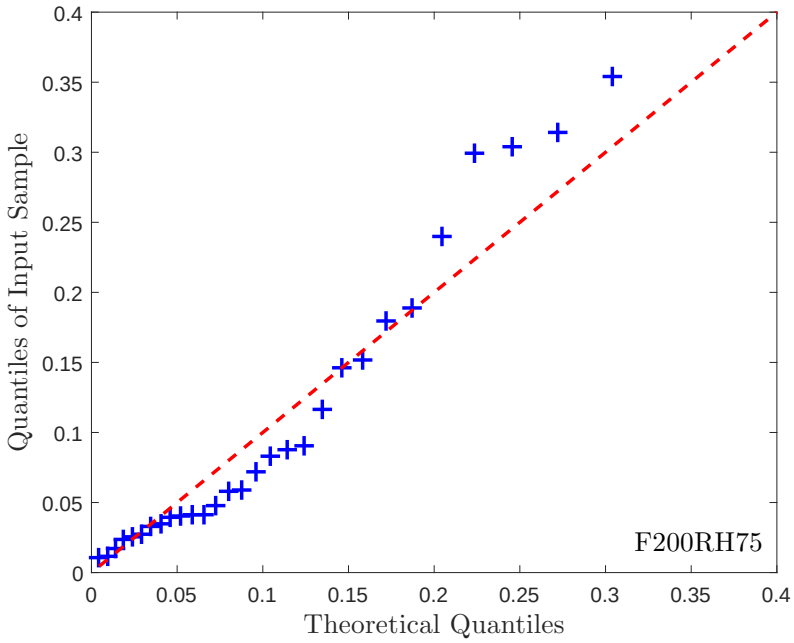

Figure 5.6: Q-Q plot for gamma distributed slip measurements for a beam

function for $\triangle y$ for the i^{th} beam is given by:

$$f_{(a_i t_0, b_i)}(\triangle y) = \frac{b_i^{a_i t_0} \triangle y^{a_i t_0 - 1} e^{-b_i \triangle y}}{\Gamma(a_i t_0)} \tag{5.1}$$

The likelihood function of the observed degradation increments $\triangle y_{ik}$ is a product of independent Gamma densities, and given by:

$$L(\triangle y_{i1}, \cdots \triangle y_{in} | a_i, b_i) = \prod_{k=1}^{n} \frac{b_i^{a_i t_0} \triangle y_{ik}^{a t_0 - 1} e^{-b \triangle y_{ik}}}{\Gamma(a_i t_0)} \qquad k = 1, 2, \cdots, n \tag{5.2}$$

where n is the number of observations.

The results of prior estimation and end life predictions using slip as well as mid-span beam deflection data are presented in the following sections. For comparison purposes,

both the two-phase and single phase models have been applied to this case-study.

5.3.1 Two-phase model

In this section, degradation data is modeled first using a two-phase model. The first step in the proposed methodology is change point detection and prior estimation.

Change detection and prior estimation

For prior specification, the slip data taken from seven of the beams (i.e., F200RM72, F200RM80, F200RM90, F200RH75, F200RH80, F200RH88 and F200RH96), and mid-span beam deflection data taken from five of the beams (i.e., F200RM90, F200RH75, F200RH80, F200RH88 and F200RH96) are considered. In both cases, data from one of the beams (say, F200RM96) is not included in the prior estimation and the test data from this beam will be treated as monitored data and will be used for posterior inference. Even though deflection measurements are taken for all of the eight beams, only six were considered in analysis because readings for the two beams (i.e., F200RM80 and F200RM72) were found to be defective.

For each beam considered above, first the change point location were identified (according to the procedure explained in Chapter 4 to identify the significant change point amongst all candidates). Figure 5.7 shows the posterior probability of change point location along with the deflection degradation path for four of the beams. It can be seen from the figure that the posterior density is localized to a small region and coincides with the actual change point location in the degradation path.

With the estimated change point, each degradation path was divided into two segments and Gamma degradation models were fitted to each segment, separately. Table 5.2 and

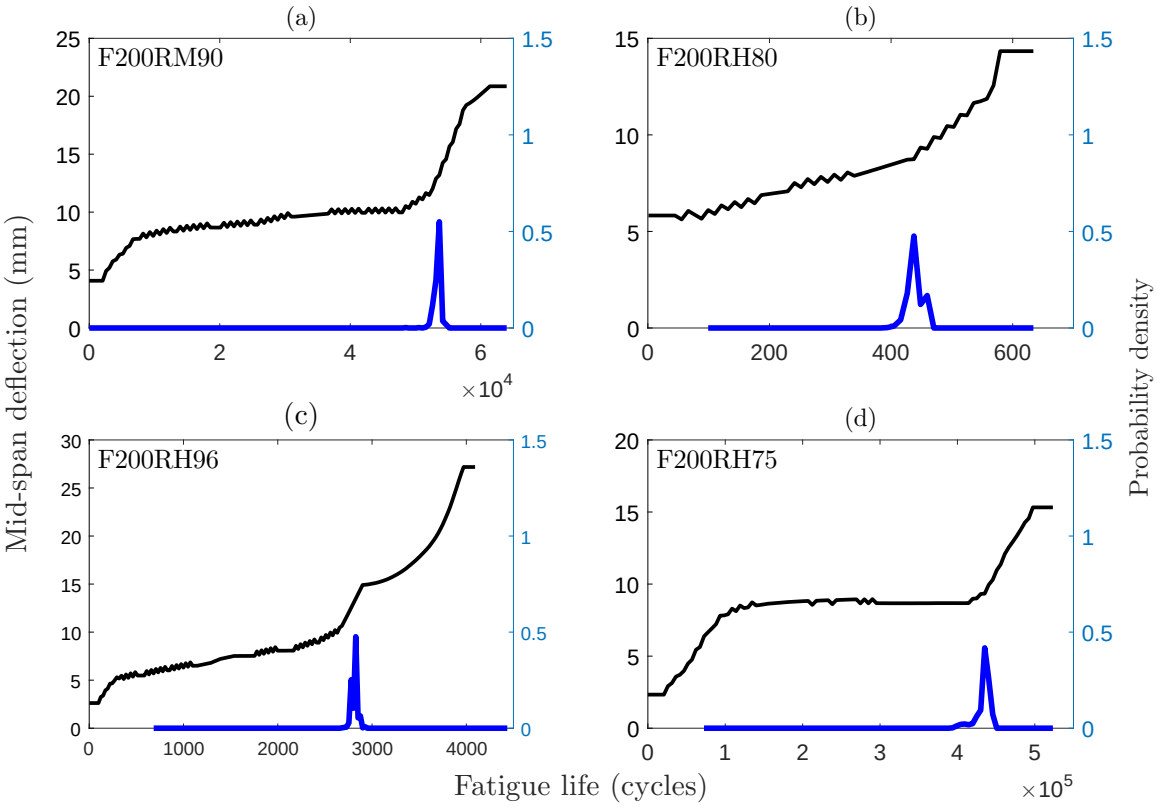

Figure 5.7: Degradation path and change point detection

Table 5.3 presents the estimated change point locations and the associated two-phase model parameters using slip and deflection data, respectively.

Table 5.2: Two-phase parameters and change point locations using slip data

	1^{st} phase		2^{nd} phase		change point
Beam	$\hat{a}_{1i}$	$\hat{b}_{1i}$	$\hat{a}_{2i}$	$\hat{b}_{2i}$	(cycles)
F200RM90	0.22	0.30	0.75	1.20	5.3×10^4
F200RH75	0.60	1.12	1.60	3.20	4.3×10^5
F200RH80	1.22	3.60	3.25	4.20	6.4×10^2
F200RH88	0.44	1.42	1.40	3.50	6.0×10^4
F200RH96	0.31	0.45	1.30	1.80	2.8×10^2
F200RM72	0.10	0.30	0.35	0.95	2.1×10^5
F200RM80	1.50	3.20	4.20	5.30	3.5×10^5

Table 5.3: Two-phase parameters and change point locations using deflection data

	1^{st} phase		2^{nd} phase		change point
Beam	$\hat{a}_{1i}$	$\hat{b}_{1i}$	$\hat{a}_{2i}$	$\hat{b}_{2i}$	(cycles)
F200RM90	0.31	0.15	1.2	0.72	5.2×10^4
F200RH75	0.42	0.32	1.80	1.40	4.3×10^5
F200RH80	1.92	2.66	3.25	4.20	6.4×10^2
F200RH88	0.67	1.95	2.46	3.50	6.0×10^4
F200RH96	0.35	0.24	1.55	1.20	2.8×10^2

Results show that the estimated change point locations are very similar using both the surrogates. This is not surprising since the slip and deflection curves as shown Fig. 5.4 and Fig. 5.5 exhibit similar characteristics.

Each estimate $(\hat{a}_{1i}, \hat{b}_{1i})$ and $(\hat{a}_{2i}, \hat{b}_{2i})$ is considered as a sample drawn from the prior distribution from the first and second phases, respectively. Hence, the prior distributions

are estimated using distribution fitting. Moreover, for Gamma distributed surrogate measurements, if the shape parameter a is kept fixed, then a conjugate prior exists for the unknown scale parameter b (see Eq. 4.38). Accordingly, the parameter a is fixed at its mean value a_0 and the hyper-parameters (α_0, β_0) for the scale parameter are estimated by distribution fitting. The estimated prior distributions for the two phases are :

$$\text{For slip:} \qquad a_{01} = 0.62, \qquad \pi(b_{01}) \sim Ga(\alpha_{01} = 1.28, \beta_{01} = 0.87) \tag{5.3}$$

$$a_{02} = 1.83, \qquad \pi(b_{02}) \sim Ga(\alpha_{02} = 3.16, \beta_{02} = 1.11) \tag{5.4}$$

$$\text{For deflection:} \qquad a_{01} = 0.73, \qquad \pi(b_{01}) \sim Ga(\alpha_{01} = 1.30, \beta_{01} = 1.96) \tag{5.5}$$

$$a_{02} = 2.05, \qquad \pi(b_{02}) \sim Ga(\alpha_{02} = 2.48, \beta_{02} = 1.12) \tag{5.6}$$

where $Ga(\cdot)$ denotes the Gamma distribution.

Parameter and end of life updates for the monitored specimen

The prior information obtained from the seven specimens are then used to update the model parameters and the end of life of the monitored unit. As mentioned previously, one of the specimens, F200RM96, is assumed to be the monitored unit, whose parameters and end of life are to be updated with measurement data. For this beam, a change point is detected at 70% of degradation ($\approx 1.4 \times 10^4$ cycles). The degradation model parameters of this beam are updated at six time intervals, in which three intervals are taken from the first phase (i.e., before the change detection) and three intervals from the second phase. Note that, for the update in the second-phase of degradation, data taken only after the change point detection are utilized.

Fig. 5.8 and Fig. 5.9 show the updated posterior distributions of b using slip and

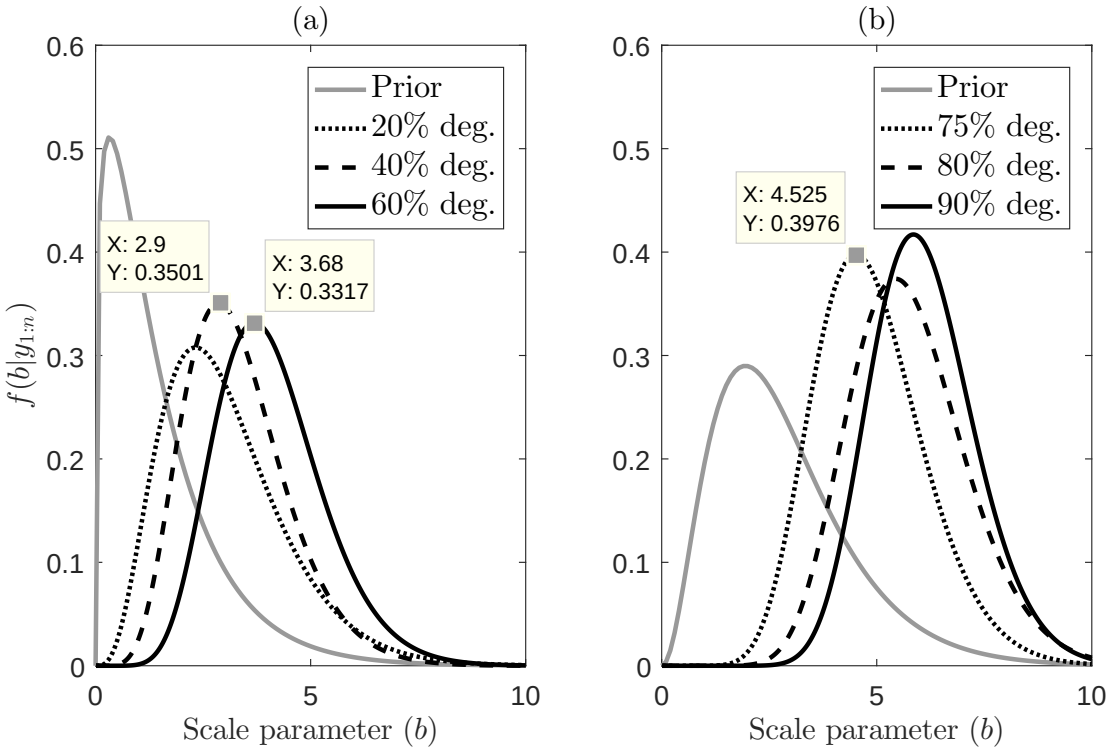

Figure 5.8: Update of b using slip data (a) before and (b) after change detection

deflection data, respectively. Note from these plots the shift in the posterior mode before and after the change detection for both of the surrogates. For example, in case of slip, the shift occurs from $b = 3.7$ to $b = 4.5$ for 60% to 75% degradation data, respectively. This is to be expected, as the process parameter has changed once a damage is initiated at 70% degradation. Another thing that can be observed from Fig. 5.8 and Fig. 5.9 is that at a higher degradation magnitude (between 80 to 100 percent), the posterior distribution narrows and better aligns with the true value of b with a smaller HPD interval (HPD interval is the Bayesian analog of the classical confidence interval).

The next step is to predict and update the end life for the beam specimen F200RM96 using monitored data. As described earlier, if the shape parameter is fixed, then a closed

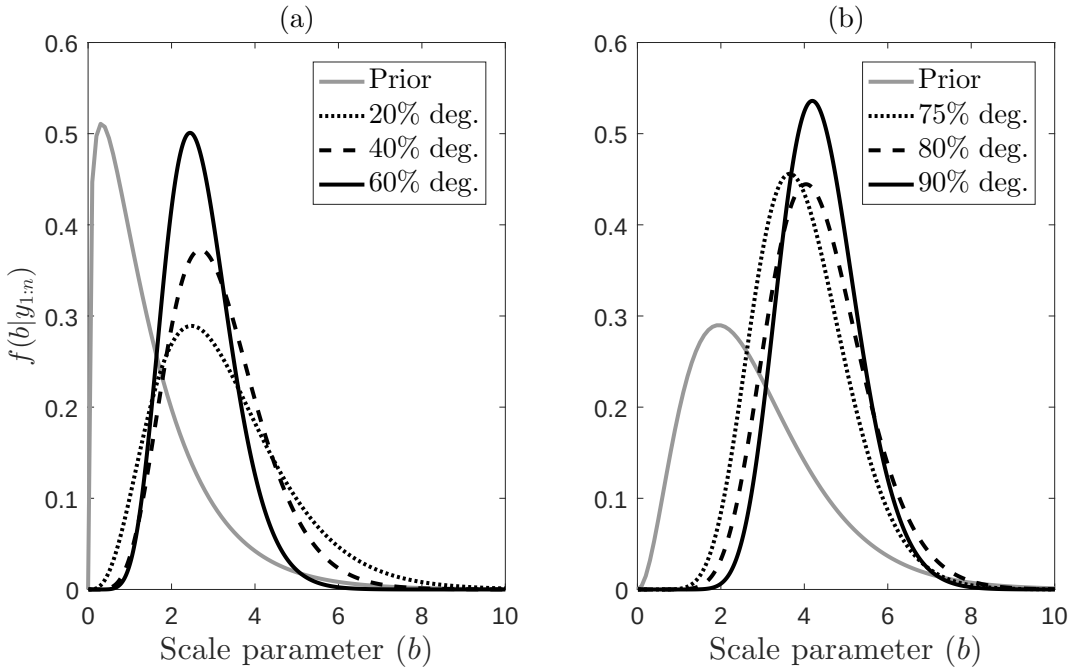

Figure 5.9: Update of b using deflection data (a) before and (b) after change detection

form expression for the probability of failure at any time t in the future can be derived. The failure CDF is obtained using Eq. 4.55, where the failure threshold η_D is assumed to be 6 mm over the slip length and 15 mm over the mid-span deflection. This choice is made arbitrarily and is based upon the visual inspection of the degradation path for this beam. In other words, the beam is considered to have failed if the slip length or mid-span deflection is greater than 6 mm or 15 mm, respectively.

Fig. 5.10 and Fig. 5.11 show the updated end of life using slip and deflection measurements, respectively. The failure times are updated at 20, 40, 60, 75, 80 and 90 percent of degradation, respectively. Note that for this beam, a change point is detected at 70 percent degradation. In other words, three time intervals before the change point detection and three intervals after the change detection are considered for failure time updating. From Fig. 5.10 and Fig. 5.11, it can be seen that both surrogates (i.e., slip

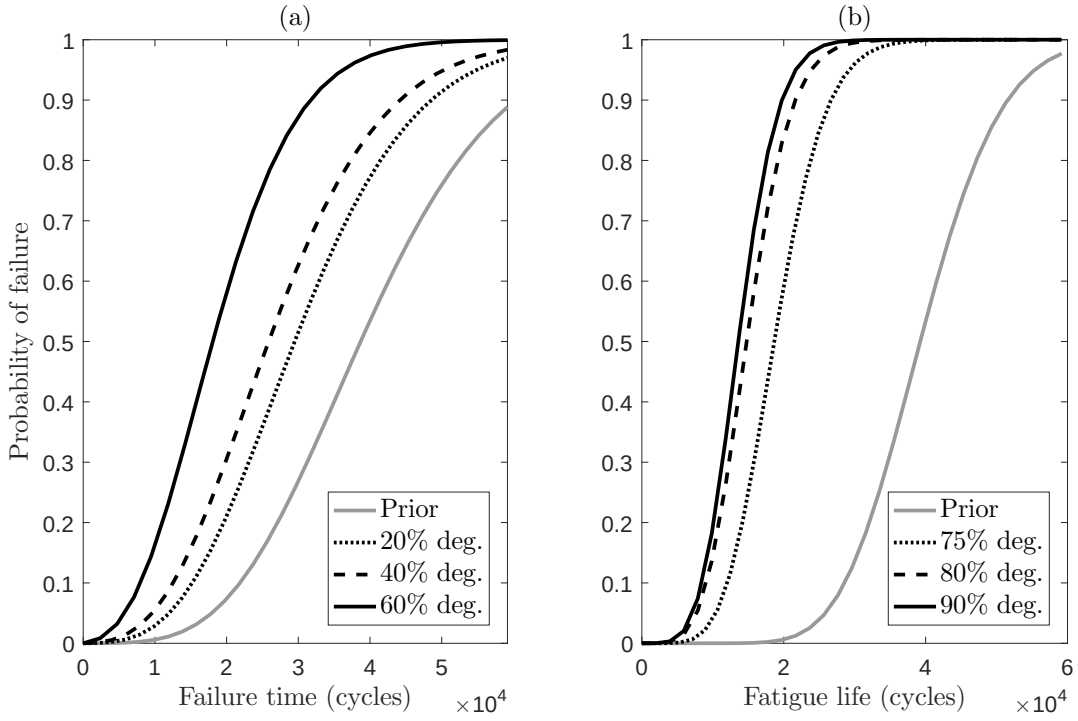

Figure 5.10: Updated end life predictions using slip measurements: (a) before and (b) after, change detection

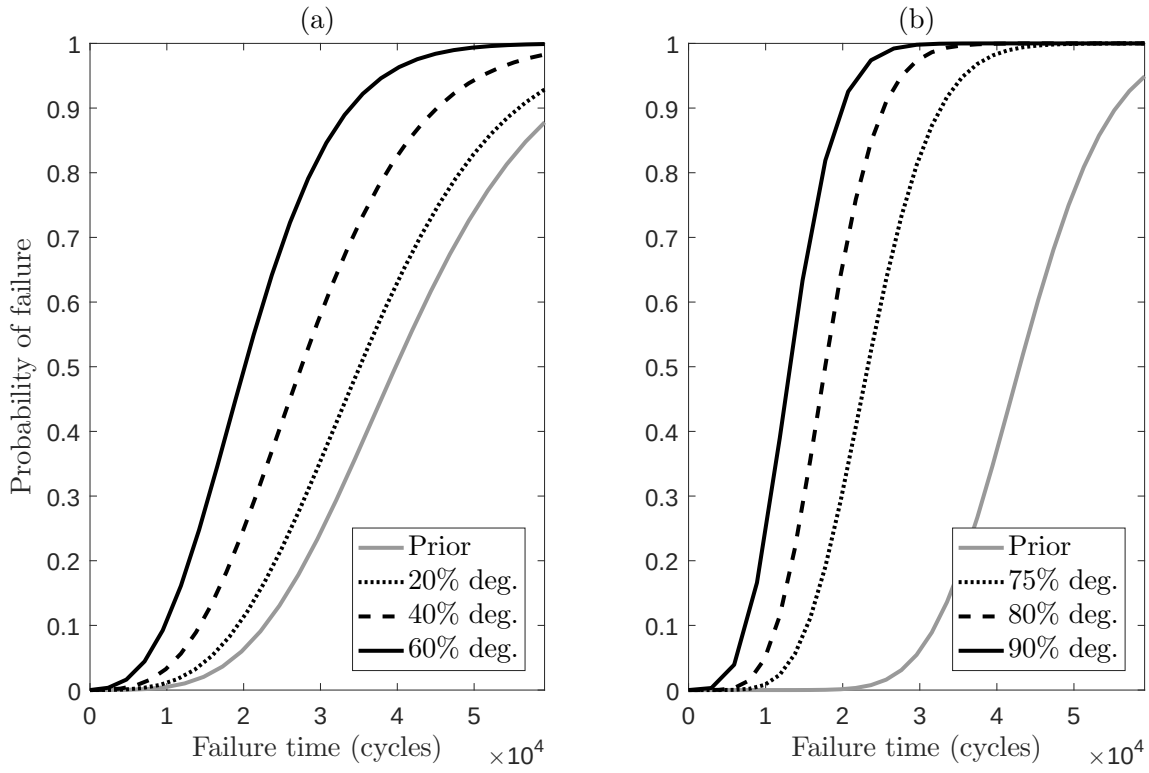

Figure 5.11: Updated end life predictions using deflection measurements: (a) before and (b) after, change detection

Table 5.4: End life predictions and error in prediction

	based on slip length		based on mid-span deflection	
% Deg.	95% End life ($\times 10^4$ cycles)	Prediction error ($\times 10^4$ cycles)	95% End life ($\times 10^4$ cycles)	Prediction error ($\times 10^4$ cycles)
0	6.12	4.15	6.50	4.53
20	5.32	3.35	6.02	4.05
40	5.02	3.05	5.15	3.18
60	3.60	1.63	4.02	2.05
75	2.95	0.98	3.61	1.64
80	2.36	0.39	2.81	0.84
90	2.17	0.20	2.35	0.38

and deflection) predict very similar end of life values. However, the predicted failure time before change detection is relatively large compared to the failure time predicted after the change detection. For example, when 60% of slip data is utilized, the 95 percent CDF of failure time is 3.8×10^4 cycles; this changes to 2.7×10^4 cycles when predicted using 75% monitored data. Moreover, different failure curves before change point detection are well separated and have lower slopes relative to the curves after change detection. In other words, predictions made after change point detection are relatively precise.

Based on Fig. 5.10 and Fig. 5.11, the performance of the two surrogate measures i.e., slip and mid-span deflection for end life predictions can be compared. Table 5.4 presents the predicted end of life and error in the prediction calculated at various degradation level for the two cases. A closer look at the results in Table 5.4 reveals that the prediction error is low when slip is used for degradation modeling compared to deflection, which is not surprising. However, it is often impractical to measure the slip length for an in-situ component, where deflection can be measured easier. Based on the analysis described above, the two phase degradation model either using slip of reinforcing bars or the mid-

span beam deflection can be used for monitoring and for the prediction of beam structural failure. For comparison purposes, in the following section, the proposed methodology is illustrated using a single phase model.

5.3.2 Single-phase model

In this section, results using a single phase degradation model fit to the degradation data are presented, assuming that the degradation path does not contain a change point. As with the two-phase model, results were obtained using both slip and deflection as surrogates. For this model, all the steps remain same as described above, excluding the change point detection step.

Prior estimation

For prior specification, Gamma degradation models were fit for each specimen separately, and the model parameters estimated. Table 5.5 summarizes the estimated parameters using slip and deflection measurements. Each estimate (a_i, b_i) is considered as a sample drawn from the prior distribution and the prior distributions are estimated using distribution fitting. As in the previous section, the parameter, a is fixed at its mean value a_0 and the hyper-parameters (α_0, β_0) were estimated by fitting a Gamma distribution to b_i's. The validity of the assumption that the scale parameters $\hat{b}_i$'s indeed follow a Gamma distribution is checked using a q-q plot. For example, Fig. 5.12 shows the q-q plot for slip measurements. Clearly, the points fall approximately on to a straight line, confirming that $\hat{b}_i$ follows a Gamma distribution. The estimated priors for the single phase models are:

Table 5.5: Single phase parameters using slip and deflection

	Using slip		Using deflection	
Beam	Shape ($\hat{a}_i$)	Scale ($\hat{b}_i$)	Shape ($\hat{a}_i$)	Scale ($\hat{b}_i$)
F200RM90	0.49	0.58	0.61	0.37
F200RH75	1.08	2.24	0.56	0.50
F200RH80	2.45	4.65	2.63	2.95
F200RH88	0.83	2.37	1.16	2.13
F200RH96	0.61	0.50	0.63	0.24
F200RM72	0.11	0.40	NA	NA
F200RM80	2.69	3.97	NA	NA

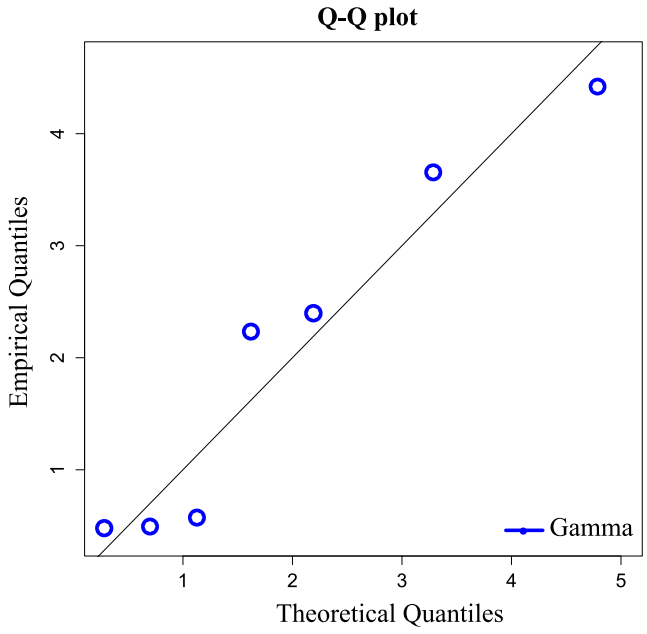

Figure 5.12: Q-Q plot of scale parameters for slip

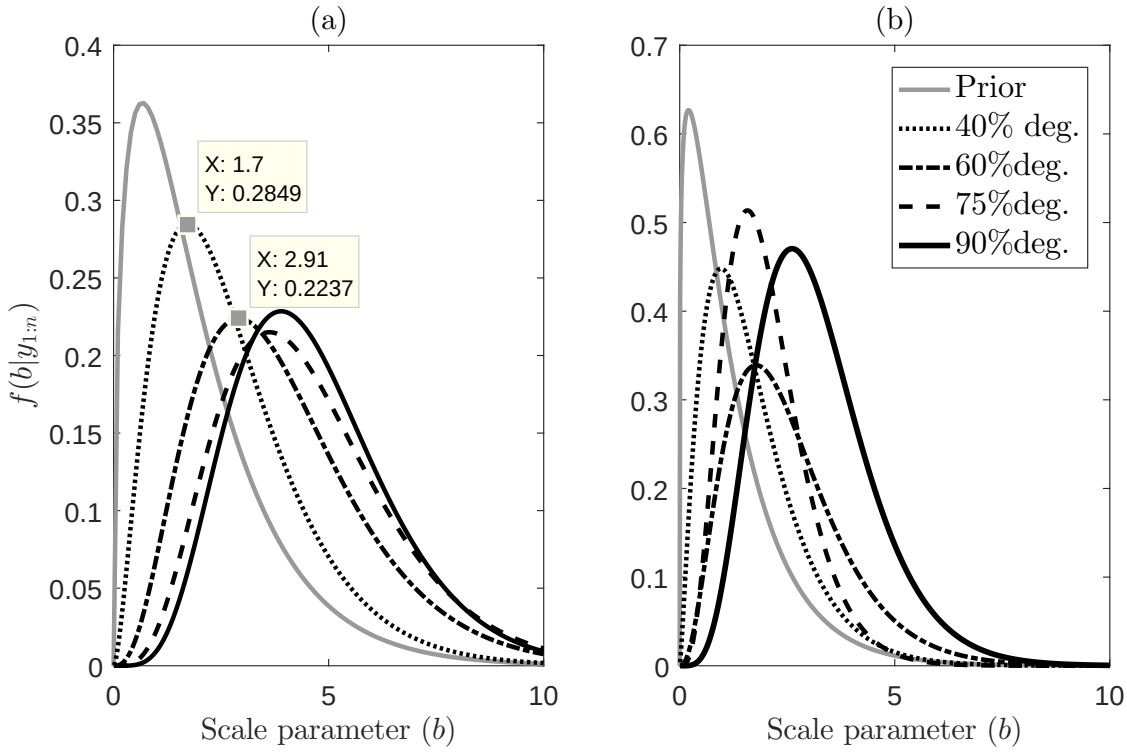

Figure 5.13: Model parameter update using monitored (a) slip and (b) deflection measurements

$$\text{For slip:} \qquad a_0 = 1.18, \qquad \pi(b_0) \sim Ga(\alpha_0 = 1.41, \beta_0 = 0.67) \tag{5.7}$$

$$\text{For deflection:} \qquad a_0 = 1.12, \qquad \pi(b_0) \sim Ga(\alpha_0 = 1.20, \beta_0 = 0.97) \tag{5.8}$$

Parameter and end of life updates for the monitored specimen

The prior information given previously is used to update the model parameters and the end of life for the monitored specimen, F200RM96. The posterior distribution of b is obtained using Eq. 4.41. Fig. 5.13 shows the updated value of b for this beam, when 40, 60, 75 and 90 percent of degradation data are utilized. It is clear from the results that as more data instances are utilized, the posterior mode of b increases for both slip as well as deflection

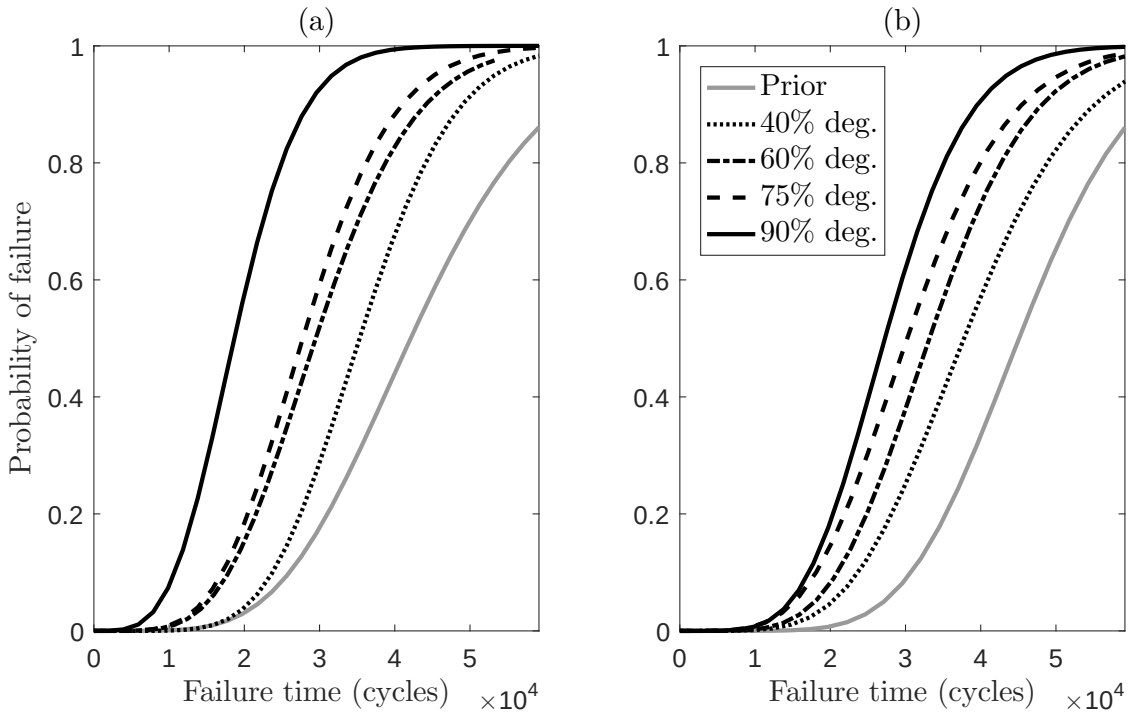

Figure 5.14: Updated RUL distribution using (a) slip (b) mid-span beam deflection

measurements. For example, the posterior mode of $\hat{b}$ corresponding to 40, 60, 75 and 90 percent of degradation are 1.7, 2.9, 3.6 and 3.9, respectively. This gradual increase in the parameter estimates is expected for increasing degradation. It is worth mentioning here that the posterior mode, which is the MAP estimate for a parameter, is often taken as the point estimate (analogous to the ML estimate) in Bayesian statistics. Another point to notice in Fig. 5.13 is that there is no sudden shift in the posterior mode as observed earlier in the two-phase model.

Next, the end of life for this beam is updated with the monitored data. Figure 5.14, shows the predicted failure time for 40, 60, 75 and 90 percent of degradation. It can be seen from Fig. 5.14 that the mid-span deflection gives longer predictions for the end of life compared to using slip as the surrogate. This behaviour is also observed for the two-

Table 5.6: End life predictions using slip measurements for two models

	Two-phase model		Single phase model	
% Deg.	95% End life ($\times 10^4$ cycles)	Prediction error ($\times 10^4$ cycles)	95% End life ($\times 10^4$ cycles)	Prediction error ($\times 10^4$ cycles)
0	6.12	4.15	6.83	4.86
40	5.02	3.05	5.35	3.38
60	3.60	1.63	4.81	2.84
75	2.95	0.98	4.53	2.56
90	2.17	0.20	3.15	1.18

phase model earlier. Moreover, for both of the surrogates, the failure curve is relatively flat during the initial stages of degradation, which results in unrealistic long fatigue life for the beam. For example, when only the 40 percent of slip data is utilized, the 95% failure CDF corresponds to 5.32×10^4 cycles, which is much greater than the actual fatigue life of 1.97×10^4 cycles. However, as more data points are utilized in the estimation, the failure curve becomes steeper and the end of life predictions improve. But the results are never better than obtained using the two-phase model. To compare the performance of the two models, the predicted failure times and the respective errors are presented in Table 5.6. It can be seen from the results that the prediction error for the two-phase model is relatively less, for nearly all degradation magnitudes. In summary, the two-phase model is a better choice (based on the results obtained from the experimental study) compared to the single phase model for health monitoring and RUL estimation of concrete beams. In the following section, another application of the two-phase degradation model is presented.

Limitations for practical implementation

One of the main limitations of this methodology for practical implementation (e.g., on bridges) is that both load variations and actual degradations could result in change points. Of course, the change points from structural changes are of interest, not from load variations. This issue was avoided in this study by utilizing data from load-controlled tests. One way address this limitation in practical applications is to either employ this methodology under controlled conditions, that is by loading the bridge with known weights (e.g., trucks), or to isolate the portion of the data into that caused by the load alone from the one caused due to changes in the member properties. This topic needs to be further explored and addressed adequately before this method can be directly implemented in practice.

5.4 Case study: application to rolling element bearings

In this section, the proposed methodology is applied to rolling element bearing degradation data. Generally, defects in a bearing occur on the inner race, outer race or in the rolling elements (see Appendix A). Once a fault develops on any one of the components, it grows over time due to fatigue, i.e., the balls impacting the fault periodically. Each time a ball passes over the fault an impulse is generated. Vibration measurements are ideal surrogates to detect such faults as these periodic impulses become more prominent with increasing fault size [54].

5.4.1 Bearing data-set

The data utilized in this thesis is from from the publicly available Prognostics Center of Excellence (PCoE) through the prognostic data repository contributed by the Intelligent Maintenance System (IMS), University of Cincinnati [104]. The schematic diagram of the experimental test rig is shown in Fig. 5.15, which comprises of four bearings installed on a shaft. The rotation speed was kept constant at 2000 RPM by an AC motor coupled to the shaft through rubber belts. A radial load of 6000 lbs is applied to the shaft on two bearings (bearing 2 and bearing 3) through a spring mechanism. High sensitivity quartz ICP accelerometers (PCB 353B33) were installed on the bearing housing as shown in Fig. 5.15. Data collection was facilitated by NI DAQ card 6062E at a sampling rate of 20 kHz

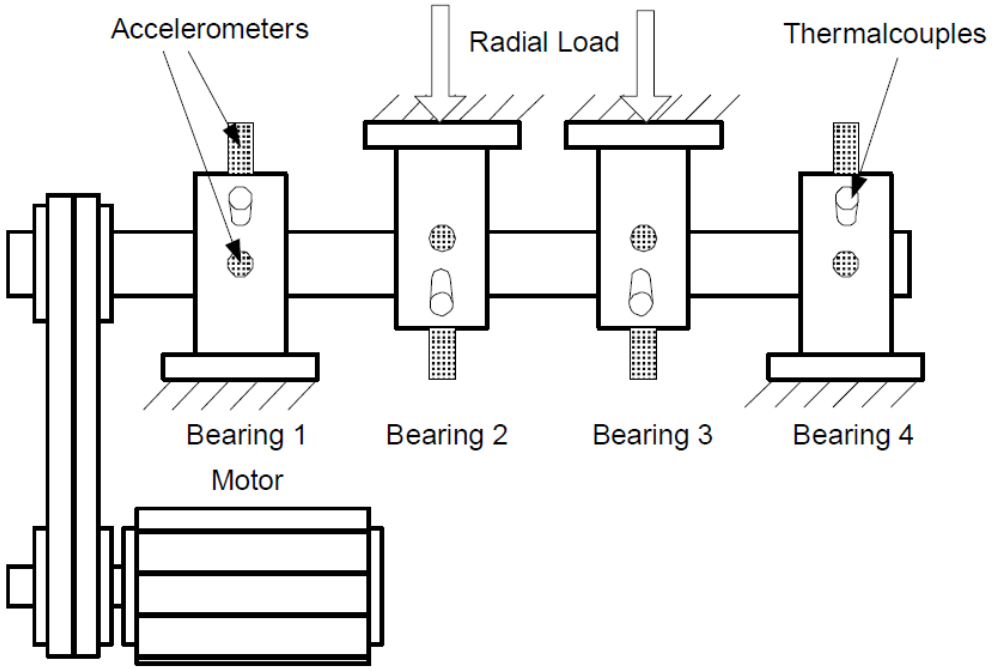

Figure 5.15: Schematic of the bearing test rig and sensor placement ([175, 116])

for one second, in intervals of ten minutes until bearing failure. Three sets of experiments

Table 5.7: Bearing test-to-failure result

	Bearing-1	Bearing-2	Bearing-3	Bearing-4
Set-1	ND	ND	IRD	RED
Set-2	ORD	ND	ND	ND
Set-3	ND	ND	ORD	ND

were performed, each consisting of four bearings. The results from experiments are given in Table 5.7, where IRD, ORD, RED, ND denotes the inner race, outer race, rolling element and no defect, respectively. The inspection pictures taken at the end of the test showing various faults are presented in Figure 5.16.

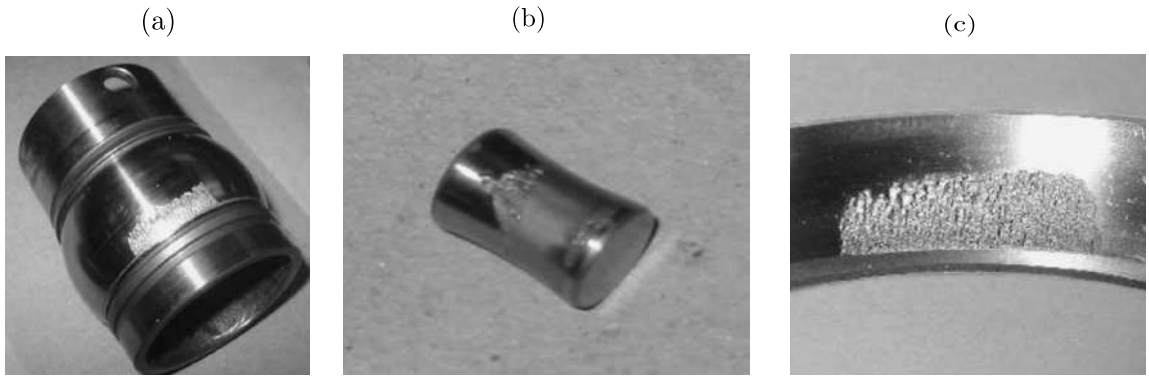

Figure 5.16: (a) Inner race fault (b)Rolling element fault (c) Outer race fault [175]

It is well known that faults that occur in bearings result in impulses during contact. These impulses excite the fundamental frequencies of the structure supporting the bearing and manifest themselves in the spacing of the impulses, rather than in the overall frequency content [54]. Hence, the main challenge in quantifying bearing degradation lies in our ability to isolate the aforesaid impulses, from the resulting vibration measurements which are convolved with the transmission path. The impulsivity of the signal become more pronounced and easier to detect using signal processing techniques once the flaws reach some critical size (unknown). Hence, the physics that govern the underlying degra-

dation phenomenon described here is naturally suited to be modeled using the two-phase model described in this study. First, an auto-regressive minimum entropy deconvolution (MED) filter is described, which is utilized to de-noise the raw signal and accentuate the impulsiveness of the signal. This forms the backbone of the method in that this is used as the degradation signal.

Background on AR-MED filter

Suppose that the bearing impulses are labeled x, then the output of a FIR filter, with h representing the propagation as well as the transducer impulse response characteristics, is given by:

$$z(k) = \sum_{l=1}^{L} h(l)x(k-l) \tag{5.9}$$

where, L is the filter order. Ideally, if the impulses $x(k)$ were to be recovered from $z(k)$, then it is possible to quantify the extent of degradation using the extent of impulsiveness of x. At best, however, what we can hope to achieve is to recover an estimate of x since we have access only to the noise corrupted measurements z and the transmission path characteristics are unknown. In this seminal work ([248]), this problem of *blind deconvolution* was solved by estimating the inverse filter coefficients, g, which produces estimates of x, according to:

$$y(k) = \sum_{l=1}^{L} g(l)z(k-l) \tag{5.10}$$

such that $y(k) = \beta x(k-\delta)$, where β is an arbitrary scaling constant and δ is an arbitrary constant time delay.

Wiggins' minimum entropy deconvolution (MED) algorithm poses the estimation of the deconvolution filter coefficients g as an optimization problem, where the objective is

to maximize the sum of normalized squares of the variances :

$$V = \frac{\sum_k y_k^4}{\left(\sum_k y_k^2\right)^2}; \qquad i = 1 \cdots N_s \tag{5.11}$$

This objective measure maximizes the numbers of the large, nonzero spikes compared with the small ones, or in other words, it has the effect of simplifying the appearance of a signal. Solving this optimization problem, results in the following matrix equation:

$$\frac{\sum_k y^2(k)}{\sum_k y^4(k)} \sum_k y^3(k) z(k-l) = \sum_l g(l) \sum_k z(i-l) z(i-k). \tag{5.12}$$

The left hand side of this equation contains the cross-correlation of the filter outputs cubed with the inputs and the right hand side contains the autocorrelation of the inputs and the filter coefficients. The nonlinear nature of this equation requires an iterative numerical solution procedure to solve for the deconvolution filter coefficients, and this procedure, called the objective function method (OFM), is described in these references ([105, 190, 248]).

Measurements typically contain both deterministic (e.g., gear meshing, shaft rotation) as well as impulsive parts, convolved through the transmission path characteristics, according to:

$$z(n) = (w(n) + d(n)) \odot h(n) + e(n) \tag{5.13}$$

where $\odot$ represents convolution and $e(n)$ represents uncorrelated additive noise in the measurements. As proposed here ([190]), the deterministic part can be removed from the measurements by retaining just the residual of the AR model $\epsilon(n)$ for MED processing.

Such a model is given by:

$$z(n) = -\sum_{i=1}^{p} \psi(n) z(n-i) + \epsilon(n) \tag{5.14}$$

where, ψ_i are the AR coefficients and ϵ is the residual. The model order p is selected by a suitable measure such as AIC, or in this case by maximizing the kurtosis of the residual signal since this is a natural measure for impulsiveness of the signal [190]. If the

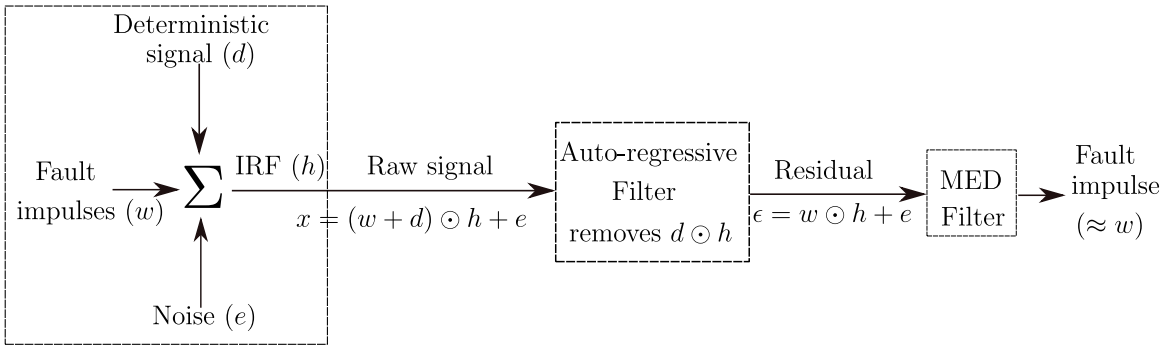

Figure 5.17: Signal enhancement using AR-MED filter

measurement noise is assumed to be uncorrelated to both inputs and outputs, it is easy to see from Eq. 5.12, that this will not affect the results of the OFM algorithm. The residual so obtained will retain the impulsive parts of the signal, provided p is so selected that it is less than the spacing between two consecutive impulses, as this ensures that the model does not treat these impacts as being deterministic. Next, this method is applied to pre-process the run-to-failure bearing signal.

Signal processing

First, the raw vibration measurements in ten minute intervals (for one second window length) are enhanced using the AR-MED filter and the kurtosis value is calculated. For

illustration purposes, Fig. 5.18 shows the signal enhancement for bearing-1 of set-2, which was identified as having with a severe outer race fault at the end of experiment. The raw vibration signal, 3 hours prior to failure is also shown in Fig. 5.18(a), which shows a kurtosis value of 3.2 (nearly Gaussian), and this does not indicate an impending failure of the bearing. However, when this signal is filtered using an AR(20) filter, the kurtosis

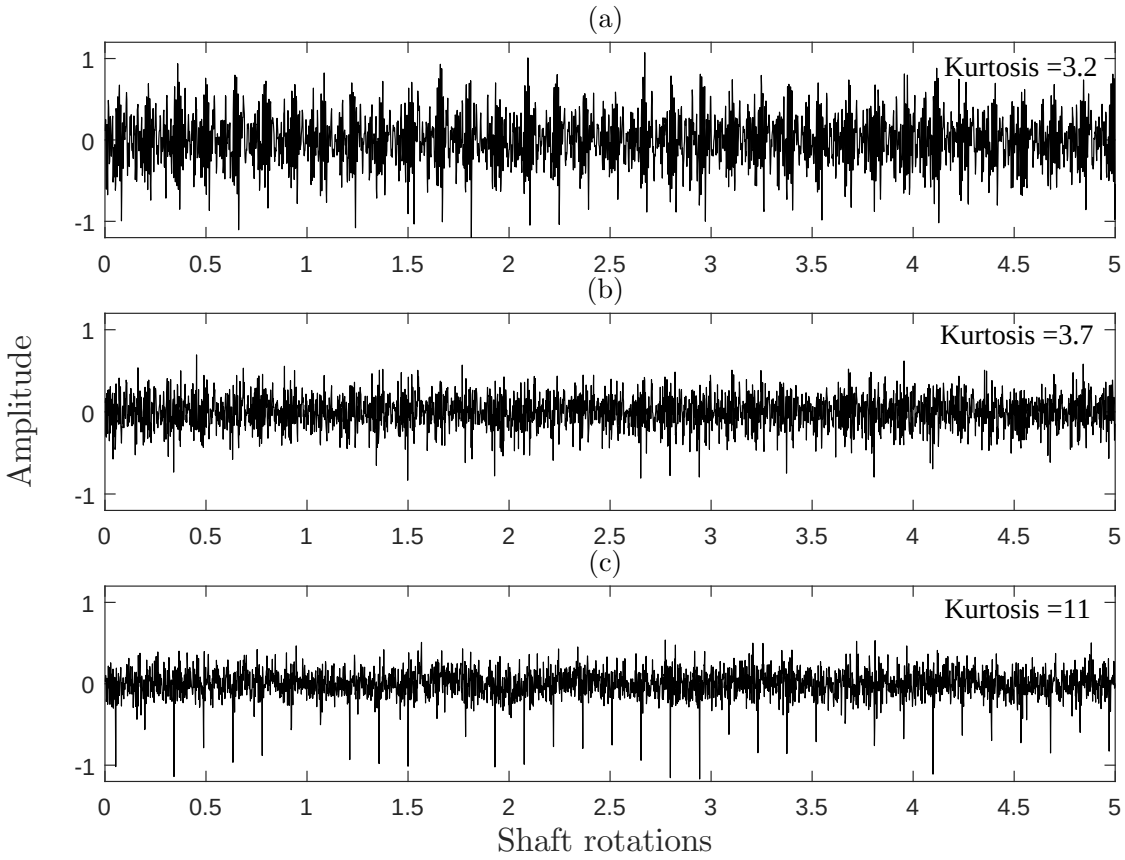

Figure 5.18: (a) Bearing-1 signal 3 hours prior to failure; (b) residual of the AR filter; (c) signal enhancement using AR-MED filter

increases to 3.7; while slightly higher than the raw signal, but still relatively low to be characterized as faulty. Moreover, when the MED filter is applied to the AR residual (as in Fig. 5.18b), the kurtosis value increases to 11 and the bearing fault impulses are clearly

visible, as evident in Fig. 5.18c.

The first step is the prior specification. Since, failure data for the population of similar bearings is unavailable, failure data from four bearings of the same test are used for prior specification. For this purpose the historical data obtained from four failed bearings as given in Table 5.7 is considered. These bearings are Bearing-4 (set-1), Bearing-3 (set-1), Bearing- 3, (set-3) and Bearing-1 (set-2), and represented by B-1, B-2, B-3 and B-4 respectively in the ensuing discussion. These bearings were selected because a defect (either in the outer race, inner race or the rolling element) was identified during tests. First, the run-to-failure vibration signals for these bearings was de-noised by applying the AR-MED filter. For this purpose, the vibration signal of each bearing at an interval of 10 minutes was used to calculate kurtosis. To generate the degradation paths, kurtosis values were further transformed to the logarithmic scale, as the degradation phenomenon is assumed to grow exponentially , and their transformation fits the linear model.

In Figure 5.19 the degradation paths for bearings B-1, B-2, B-3 and B-4 are shown, where the y-axis is the logarithm of the kurtosis and x-axis is the time. In the same figure, the posterior density of the change point location is also overlaid for clarity. It is interesting to note that the posterior density is very narrow and can be assumed to be concentrated at a point. In other words, $t = 260, 110, 338, 116$ (see Fig. 5.19) are considered as the change locations for bearing B-1, B-2, B-3 and B-4, respectively and the parameters are estimated using the maximum likelihood principle. Table 5.8 summarizes the estimated two-phase model parameters for these bearings.

Despite the rather limited sample size, this information can still be used to obtain a

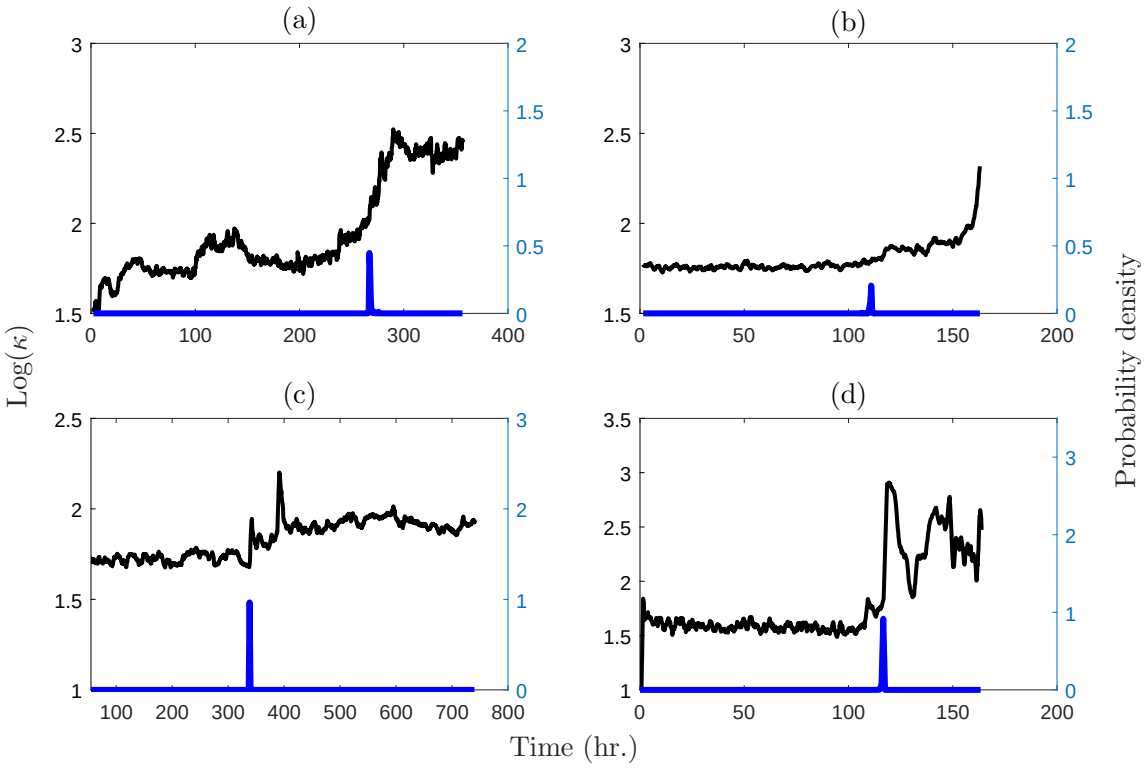

Figure 5.19: Degradation path for four failed bearings (a) B-1 (b) B-2 (c) B-3 (d) B-4

rough prior distribution, which is given below:

$$\begin{aligned}
&\pi(\theta_1) \sim N(1.6, 0.07^2); \pi(\theta_2) \sim N(0.0005, 0.0004^2) \\
&\pi(\beta_1) \sim N(1.9, 0.9^2); \pi(\sigma^2) \sim IG(140, \frac{1}{.6}); \pi(\tau^2) \sim IG(125, \frac{1}{0.9}) \\
&\pi \begin{pmatrix} \lambda \\ \beta_2 \end{pmatrix} \sim BVN \left(\begin{pmatrix} 206.0 \\ 0.0030 \end{pmatrix} \begin{pmatrix} 12500 & 0.15 \\ 0.15 & 1.12 \times 10^{-6} \end{pmatrix} \right)
\end{aligned} \tag{5.15}$$

Once the prior is specified, parameter updating and RUL predictions of a monitored unit are performed next. For this, it is assumed that the Bearing B-1 is monitored in real time and its degradation model and RUL needs to be updated with available data.

Table 5.8: Two-phase parameters for four run-to-failure bearing

Bearing	θ_1	$\theta_2(\times 10^{-2})$	σ	β_1	$\beta_2(\times 10^{-2})$	τ	λ
B-1	1.67	0.09	0.10	1.40	0.31	0.10	258
B-2	1.70	0.08	0.11	1.33	0.21	0.15	110
B-3	1.74	0.01	0.10	1.85	0.45	0.05	338
B-4	1.57	0.03	0.11	2.33	0.23	0.28	116

Consider three updates, corresponding to the three stages of degradation—first, when the degradation is in the initial phase (say, $t = 150$); second, when the state transitions from the first phase to the second phase (say, $t = 250$) and finally, when the bearing is in the second phase of degradation (say, $t = 300$).

The posterior distribution of the change point corresponding to these times are estimated using MCMC sampling. Figure 5.20 shows the trace and density plots of the change point updated at $t = 150, 250$ and $t = 300$, respectively. From Fig. 5.20 it can be seen that the 90% HPD interval of change point is approximately confined between 185 to 225, when estimated at $t = 150$. Clearly, at the earlier stages of degradation the change point estimate is influenced by the prior distribution obtained from the historical data (see Eq. 5.15). However, as more data is utilized, the estimates represent the observed change point location of B-1. For instance, when updated at time $t = 250$ the posterior shifts, and is confined between 250 to 260, which includes the actual change point (actual value is 258). Finally, the posterior distribution becomes very narrow and concentrates around $t = 255$ when estimated at $t = 300$.

The other model parameters (i.e., degradation rates, intercepts and error variances of the two phases) and RUL are also updated with the available degradation data. Figure 5.21 presents the posterior distribution of first and second phase model parameters updated at $t = 150, 250$ and 300, respectively. Note the slight shift in the mean values of the

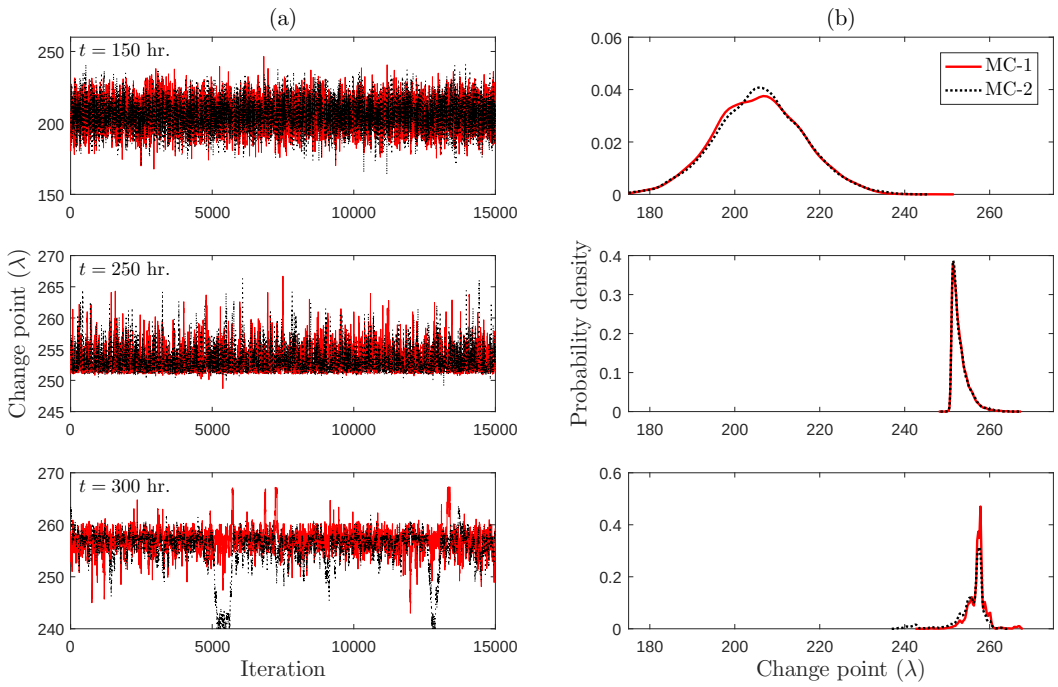

Figure 5.20: Change point detection for bearing B-1 at different times: (a) trace plot; (b) posterior density

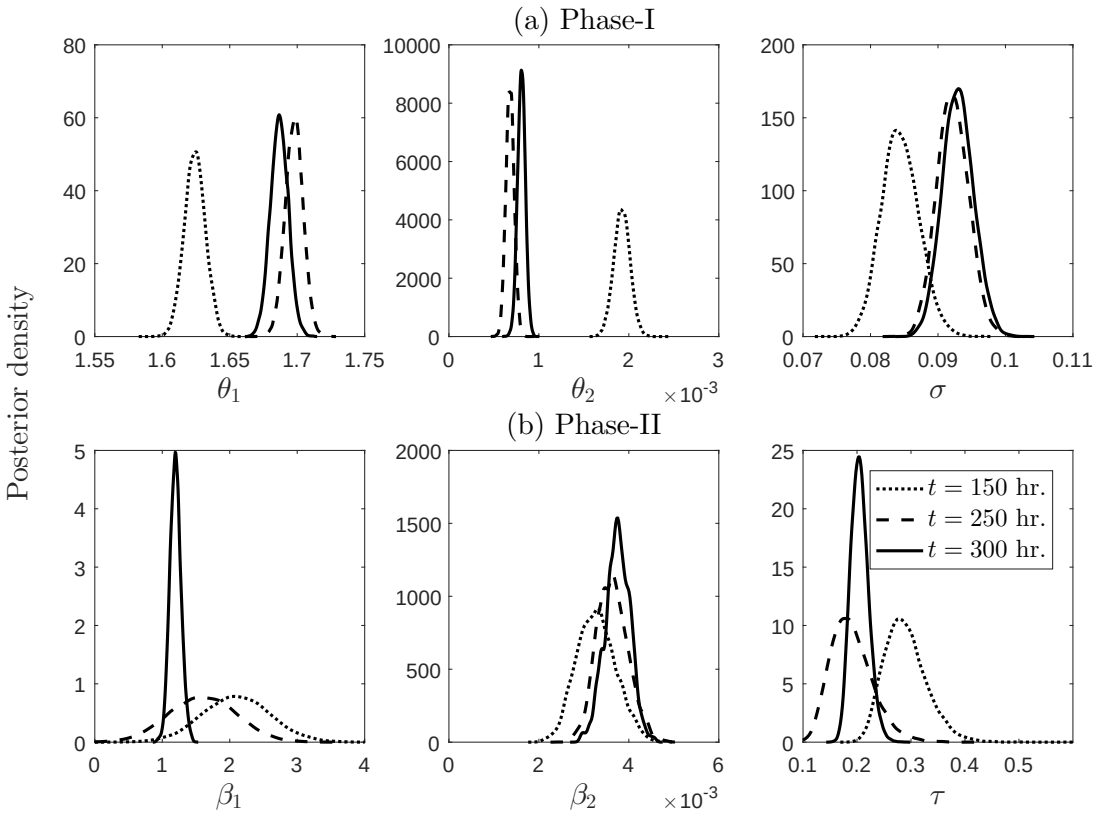

Figure 5.21: Model parameters update at different times (a) Phase-I (b) Phase-II

distribution, which is a result of the number of samples of the degradation data used in the posteriori calculations. This aspect was discussed earlier with reference to a single-phase model in Chapter 3 (see Section 3.4). Similar shift is also observed in the two-phase model resulting from MCMC simulations. The posterior summaries including the mean value and the 90% HPD interval of the same are given in Table 5.9. From Table 5.9 (or from Fig. 5.21) it is clear that the mean value of the degradation rate θ_2 changes significantly from $t = 150$ to $t = 250$, which stabilizes after $t > 250$. This happens because, as more data is utilized in updating the first phase parameters improve, however once a change point is detected, the same set of data is used to estimate the first phase parameters. However,

Table 5.9: Posterior distribution summaries for two phase model parameters

	$t = 150$ hr.		$t = 250$ hr.		$t = 300$ hr.	
Parameter	Mean	$(Q_{0.05} - Q_{0.95})$	Mean	$(Q_{0.05} - Q_{0.95})$	Mean	$(Q_{0.05} - Q_{0.95})$
θ_1	1.62	(1.61 - 1.64)	1.70	(1.69 - 1.71)	1.69	(1.68 - 1.70)
$\theta_2(\times 10^{-2})$	0.19	(0.18 - 0.21)	0.07	(0.06 - 0.08)	0.08	(0.07 - 0.09)
$\sigma(\times 10^{-1})$	0.84	(0.80 - 0.89)	0.92	(0.88 - 0.96)	0.93	(0.89 - 0.97)
β_1	1.60	(0.79 - 2.44)	1.60	(0.78 - 2.43)	1.20	(1.06 - 1.34)
$\beta_2(\times 10^{-2})$	0.33	(0.26 - 0.4)	0.38	(0.33 - 0.45)	0.37	(0.33 - 0.42)
τ	0.29	(0.23 - 0.36)	0.29	(0.23 - 0.36)	0.21	(0.18 - 0.23)

Table 5.10: A summary of RUL distribution estimated at different times

		Quantile						
	Mean	Std Dev	0.05	0.250	.50	0.750	0.95	Actual
$t = 150$	145	25	13	60	140	205	260	210
$t = 250$	96	16	10	42	92	123	155	110
$t = 300$	43	11	6	33	45	65	103	60

the second phase degradation rate has a relatively large value, even at $t = 150$, when the degradation is still in its initial stages, since the prior information obtained from the historical units influences the posterior distribution of the second phase parameters. For bearing B-1 the estimated RUL PDF is shown in Figure 5.22, which shows that the RUL PDF sharpens as more data is utilized in the predictions. The summary of predicted RUL estimates along with various quantiles and the actual RUL are summarized in Table 5.10. Clearly, for all the three times considered, the 90% HPD interval contains the actual RUL. Moreover, the predicted mean RUL is very close to the actual RUL. This shows that the method proposed in this thesis produces reasonably good estimates even when the bearing is in its initial stages of degradation. The effect of correlation between β_2 and λ on RUL is

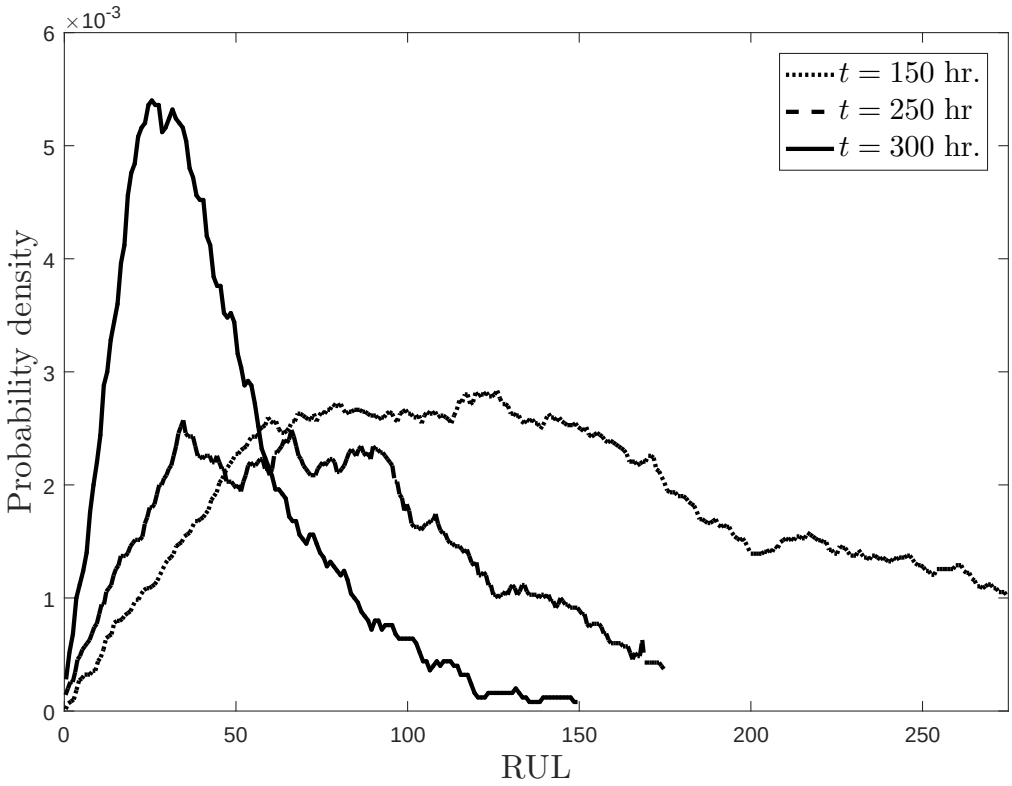

Figure 5.22: Estimated RUL PDF at different times

investigated and the results are presented in Fig. 5.23. One can observe from the results that considering correlation results in a smaller RUL interval and hence is important to consider this relationship in prognosis of bearings.

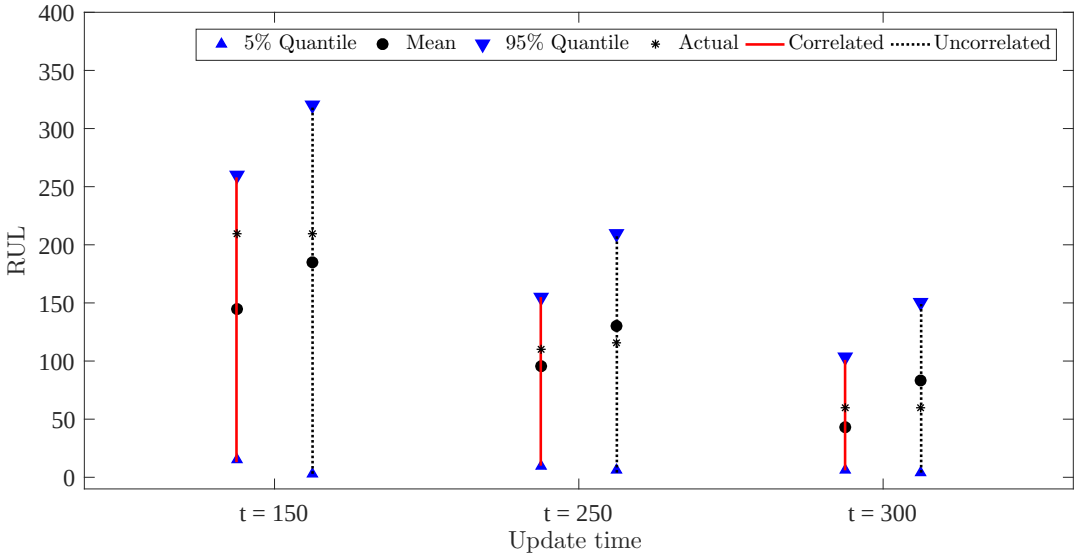

Figure 5.23: Effect of correlation on RUL

5.5 Summary

In this chapter, the proposed degradation modeling framework is applied to both civil and industrial engineering components. The two degradation processes investigated are: the deterioration of reinforced concrete structure and the degradation of rolling element bearings. The degradation of reinforced concrete is modeled using a stochastic gamma process, while the degradation of rolling element bearings is undertaken using random variable model. The main objective of this chapter is to demonstrate the application of various steps described in the previous chapter to real-life examples. Results shows that

the model parameters and end life predictions of a working unit in both cases improves as more condition data becomes available. Moreover, the integration of historical data to construct priors results in reasonably good RUL estimates even during the initial stages of degradation. It is found that the slip length of reinforcing concrete bar or mid-span beam deflection is a good surrogate measure for concrete degradation modeling. For rolling element bearing, the surrogates are obtained through more sophisticated signal processing techniques. It was also shown that the resulting RUL intervals are narrower when the correlation between the degradation rate and change point location is considered in the formulation.

Chapter 6

Conclusions and recommendations

The thesis presents an integrated approach for effective maintenance planning using measured condition information for civil and industrial infrastructure applications. The two aspects of CBM—damage detection and prognosis—are undertaken in a single Bayesian framework, where the prior knowledge obtained from historical data is integrated with monitored information and used for RUL estimation and maintenance planning of the monitored unit. This study has resulted in a holistic approach to utilize indirect measurements for degradation of critical components and subsequently to predict the RUL and to plan maintenance actions in cases where degradation is not directly observable. Most importantly, the feasibility in such cases has been demonstrated. This chapter highlights the significant contributions, key conclusions, and recommendations for future work.

6.1 Significant contributions

The significant contributions resulting from this work is as follows:

1. An integrated framework for damage detection, RUL estimation and maintenance planning for components where direct degradation is unobservable has been developed and shown to be feasible. Within the proposed framework of a two-phase degradation modeling approach, damage is detected by identifying the change point in the degradation path, while RUL estimation and maintenance planning are undertaken using the estimated model parameters.

2. A Bayesian approach has been developed to integrate the degradation information obtained from the historical units for effective maintenance planning of a monitored unit. The advantage of this approach is that it results in reasonably good RUL predictions, even when the system or component is in the initial stages of degradation.

3. The methodology developed in this dissertation is general and has been successfully applied to three types of degradation models: random variable, Gamma and Weiner process models. For these processes, algorithms for change-point detection, parameter updating and RUL prediction are developed in detail. Through this methodology, the proposed framework can be applied to a wide verity of degradation processes and applications.

4. An attempt to incorporate the correlation structure amongst various model parameters has been made in the current thesis. In particular, the degradation rate and change point location, which are often found to be correlated for bearing degradation, has been explicitly accounted for in the formulation.

5. The proposed method has been successfully applied to bearing degradation and the deterioration of reinforced concrete beams under fatigue loading. For both applications, the parameters of the degradation model are estimated using experimental

data, and the RUL distribution of a monitored unit is updated with monitored condition data.

6. Several peer-reviewed journal and conference articles (see Appendix E) have resulted from this work.

6.2 Conclusions

Having highlighted the significant contributions of this dissertation, the central conclusions are summarized as follows:

1. The examples and case studies demonstrate that integrating prior knowledge from the historical units with the degradation data of a working unit results in more cost effective maintenance decisions.

2. It was found that as more degradation data is utilized from the monitoring unit, the progressing fault is detected in a timely manner and result in better model parameter estimates. Moreover, the reasonable accurate estimates of RUL can be achieved even during the initial stages of degradation.

3. From the comparison study using numerical as well as experimental bearing degradation data, it was found that including correlation between the degradation rate and the change point in the model results in a narrower RUL distribution.

4. The case study demonstrated that the proposed degradation modeling framework can successfully be applied to various real-life applications such as bearing degradation and deterioration of reinforced concrete structure. However, developing an

appropriate surrogate measure is critical and may not be an easy task. For instance, developing an appropriate surrogate measure for bearing deterioration involves extensive signal pre-processing and this has to be taken into account while trying to implement this methodology.

6.3 Recommendations for future work

There are several possible extensions of the current research in the context of effective condition based maintenance of critical civil and mechanical infrastructure using condition monitoring data. A few such extensions are outlined as follows:

1. The proposed algorithm assumes that the degradation can be modeled in two-phases. However, several processes show multi-phase degradation. Future studies could extend the two-phase degradation model to a more general multi-phase model, where the optimum number of phases can be chosen by applying model selection principle such as Akaike information criterion (AIC), Bayesian information criterion (BIC) or on Bayes factor.

2. The current study is limited to a model that has the same functional form in both the phases of degradation. A model with different functional forms in the two phases such as, linear-exponential, Weiner-Gamma, linear-Weiner could be investigated to expand the scope of what was proposed here.

3. Degradation signals are often compounded and contaminated by measurement errors, making change detection and degradation modeling a difficult task. Therefore, a two-phase model with measurement noise can be investigated. Moreover, the degradation

rate in any given phase is not constant. The use of time-scale transformation can be investigated to make it approximately constant.

4. For degradation modeling of rolling element bearings, more sophisticated features from the signal processing literature could be used and the relative performance compared with the current feature types.

5. The experimental data for the case of structural engineering application was limited to just 8 specimens. The applicability of this method using a more elaborate data set and application examples would likely enhance our understanding of the performance of the proposed method, including effective features to use for damage detection and prognosis, in the civil engineering domain.

References

[1] https://www.dreamstime.com/royalty-free-stock-photo-ball-bearing-image23239975. (last accessed on 25 Sept. 2017). xv, 3

[2] http://www.learnandearnd5.blogspot.ca/2017/06/corrosion-of-concrete-mechanism-of.html. (last accessed on 25 Sept. 2017). xv, 4, 114

[3] M. Abdel-Hameed. Inspection and maintenance policies of devices subject to deterioration. *Advances in Applied Probability*, pages 917–931, 1987. 42

[4] R. Ahmad and S. Kamaruddin. An overview of time-based and condition-based maintenance in industrial application. *Computers & Industrial Engineering*, 63(1):135–149, 2012. 41

[5] R. Al-Hammoud. Bond behaviour of corroded and cfrp repaired rc beams subjected to monotonic and repeated loading. 2012. xvii, 115, 116, 117

[6] R. Al-Hammoud, K. Soudki, and T. H. Topper. Bond analysis of corroded reinforced concrete beams under monotonic and fatigue loads. *Cement and Concrete Composites*, 32(3):194–203, 2010. 114

[7] A. Al-Hussein and A. Haldar. Structural damage prognosis of three-dimensional large structural systems. *Structure and Infrastructure Engineering*, pages 1–13, 2017. 18

[8] S. Alaswad and Y. Xiang. A review on condition-based maintenance optimization models for stochastically deteriorating system. *Reliability Engineering & System Safety*, 157:54–63, 2017. 42

[9] J. B. Ali, B. Chebel-Morello, L. Saidi, S. Malinowski, and F. Fnaiech. Accurate bearing remaining useful life prediction based on weibull distribution and artificial neural network. *Mechanical Systems and Signal Processing*, 56:150–172, may 2015. 30

[10] J. Altmann and J. Mathew. Multiple band-pass autoregressive demodulation for rolling-element bearing fault diagnosis. *Mechanical systems and signal processing*, 15(5):963–977, 2001. 24

[11] S. V. Amari and L. McLaughlin. Optimal design of a condition-based maintenance model. In *Reliability and Maintainability, 2004 Annual Symposium-RAMS*, pages 528–533. IEEE, 2004. 42

[12] M. Amarnath, R. Shrinidhi, A. Ramachandra, and S. Kandagal. Prediction of defects in antifriction bearings using vibration signal analysis. *Journal of the Institution of Engineers(India), Part MC, Mechanical Engineering Division*, 85:88, 2004. 195

[13] W. an Yan, B. wei Song, G. lin Duan, and Y. min Shi. Real-time reliability evaluation of two-phase Wiener degradation process. *Communications in Statistics - Theory and Methods*, 46(1):176–188, feb 2016. 33, 40

[14] J. Antoni. The spectral kurtosis: a useful tool for characterising non-stationary signals. *Mechanical Systems and Signal Processing*, 20(2):282–307, 2006. xv, 23, 25, 26, 27

[15] J. Antoni. Fast computation of the kurtogram for the detection of transient faults. *Mechanical Systems and Signal Processing*, 21(1):108–124, 2007. 26

[16] S. J. Bae and P. H. Kvam. A nonlinear random-coefficients model for degradation testing. *Technometrics*, 46(4):460–469, 2004. 35

[17] S. J. Bae, T. Yuan, S. Ning, and W. Kuo. A bayesian approach to modeling two-phase degradation using change-point regression. *Reliability Engineering & System Safety*, 134:66–74, 2015. 32, 40, 92

[18] R. Barlow and L. Hunter. Optimum preventive maintenance policies. *Operations Research*, 8(1):90–100, 1960. 41, 207

[19] T. Barszcz and R. B. Randall. Application of spectral kurtosis for detection of a tooth crack in the planetary gear of a wind turbine. *Mechanical Systems and Signal Processing*, 23(4):1352–1365, 2009. 26

[20] P. Baruah and R. B. Chinnam. HMMs for diagnostics and prognostics in machining processes. *International Journal of Production Research*, 43(6):1275–1293, 2005. 33

[21] E. Bechhoefer and M. Kingsley. A review of time synchronous average algorithms. In *Annual Conference of the Prognostics and Health Management Society, San Diego, CA, Sept*, pages 24–33, 2009. 195

[22] E. Bechhoefer, P. Menon, and M. Kingsley. Bearing envelope analysis window selection using spectral kurtosis techniques. In *Prognostics and Health Management (PHM), 2011 IEEE Conference on*, pages 1–6. IEEE, 2011. 27

[23] Z. Benyamini and U. Yechiali. Optimality of control limit maintenance policies under nonstationary deterioration. *Probability in the Engineering and Informational Sciences*, 13(01):55–70, 1999. 41

[24] L. Bornn, C. R. Farrar, G. Park, and K. Farinholt. Structural health monitoring with autoregressive support vector machines. *Journal of Vibration and Acoustics*, 131(2):021004, 2009. 16, 17

[25] S. Braun and B. Datner. Analysis of roller/ball bearing vibrations. *Journal of Mechanical Design*, 101(1):118–125, 1979. 194

[26] J. M. Brownjohn, A. De Stefano, Y.-L. Xu, H. Wenzel, and A. E. Aktan. Vibration-based monitoring of civil infrastructure: challenges and successes. *Journal of Civil Structural Health Monitoring*, 1(3-4):79–95, 2011. 16

[27] J. M. W. Brownjohn. Structural health monitoring of civil infrastructure. *Philosophical Transactions of the Royal Society A: Mathematical, Physical and Engineering Sciences*, 365(1851):589–622, feb 2007. 30

[28] B. P. Carlin, A. E. Gelfand, and A. F. Smith. Hierarchical bayesian analysis of changepoint problems. *Applied statistics*, pages 389–405, 1992. 92

[29] B. Castanier, C. Bérenguer, and A. Grall. A sequential condition-based repair/replacement policy with non-periodic inspections for a system subject to continuous wear. *Applied stochastic models in business and industry*, 19(4):327–347, 2003. 42

[30] chao shih Liu. *Fault detection of rolling element bearings*. PhD thesis, University of Washington, 2005. 22

[31] N. Chen and K. L. Tsui. Condition monitoring and remaining useful life prediction using degradation signals: revisited. *IIE Transactions*, 45(9):939–952, sep 2013. 32, 39, 79, 92

[32] N. Chen, Z.-S. Ye, Y. Xiang, and L. Zhang. Condition-based maintenance using the inverse Gaussian degradation model. *European Journal of Operational Research*, 243(1):190–199, 2015. 32

[33] Z. Chen and S. Zheng. Lifetime distribution based degradation analysis. *Reliability, IEEE Transactions on*, 54(1):3–10, 2005. 35

[34] T. Cheng, M. D. Pandey, and J. A. van der Weide. The probability distribution of maintenance cost of a system affected by the gamma process of degradation: Finite time solution. *Reliability Engineering & System Safety*, 108:65–76, 2012. 32, 37

[35] E. Cinlar, Z. P. Bazant, and E. M. Osman. Stochastic process for extrapolating concrete creep. *Journal of Engineering Mechanics*, 103(ASCE 13447 Proceeding), 1977. 32, 37

[36] G. Comanducci, F. Magalhães, F. Ubertini, and Á. Cunha. On vibration-based damage detection by multivariate statistical techniques: Application to a long-span arch bridge. *Structural Health Monitoring*, page 1475921716650630, 2016. 17

[37] F. Combet and L. Gelman. Optimal filtering of gear signals for early damage detection based on the spectral kurtosis. *Mechanical Systems and Signal Processing*, 23(3):652–668, 2009. 26

[38] X. Deng and Q. Wang. Crack detection using spatial measurements and wavelet analysis. *International Journal of Fracture*, 91(2):L23–L28, 1998. 25

[39] X. Deng, Q. Wang, and V. Giurgiutiu. Structural health monitoring using active sensors and wavelet transforms. In *Proceedings of SPIE*, volume 3668, pages 363–370, 1999. 25

[40] A. Djebala, N. Ouelaa, and N. Hamzaoui. Detection of rolling bearing defects using discrete wavelet analysis. *Meccanica*, 43(3):339–348, 2008. 22

[41] S. W. Doebling, C. R. Farrar, M. B. Prime, et al. A summary review of vibration-based damage identification methods. *Shock and vibration digest*, 30(2):91–105, 1998. 16

[42] K. A. Doksum and A. Hbyland. Models for variable-stress accelerated life testing experiments based on wener processes and the inverse gaussian distribution. *Technometrics*, 34(1):74–82, 1992. 35

[43] K. a. Doksum and a. Hoyland. Models for Variable-Stress Accelerated Life Testing Experiments Based on Wiener Processes and the Inverse Gaussian Distribution. *Theory of Probability & Its Applications*, 37(1):137–139, 1993. 33

[44] M. Dong and D. He. Hidden semi-Markov model-based methodology for multi-sensor equipment health diagnosis and prognosis. *European Journal of Operational Research*, 178(3):858–878, 2007. 33

[45] M. Dong and D. He. Hidden semi-markov model-based methodology for multi-sensor equipment health diagnosis and prognosis. *European Journal of Operational Research*, 178(3):858–878, 2007. 42

[46] M. Dong, D. He, P. Banerjee, and J. Keller. Equipment health diagnosis and prognosis using hidden semi-Markov models. *International Journal of Advanced Manufacturing Technology*, 30(7-8):738–749, 2006. 33

[47] D. Draper. Assessment and propagation of model uncertainty. *Journal of the Royal Statistical Society. Series B (Methodological)*, pages 45–97, 1995. 50

[48] R. Dwyer. Detection of non-gaussian signals by frequency domain kurtosis estimation. In *Acoustics, Speech, and Signal Processing, IEEE International Conference on ICASSP'83.*, volume 8, pages 607–610. IEEE, 1983. 25

[49] D. Dyer and R. Stewart. Detection of rolling element bearing damage by statistical vibration analysis. *Journal of mechanical design*, 100(2):229–235, 1978. 26

[50] S. Ebersbach, Z. Peng, and N. Kessissoglou. The investigation of the condition and faults of a spur gearbox using vibration and wear debris analysis techniques. *Wear*, 260(1):16–24, 2006. 20

[51] R. Edirisinghe, S. Setunge, and G. Zhang. Application of gamma process for building deterioration prediction. *Journal of Performance of Constructed Facilities*, 27(6):763–773, 2013. 32, 37

[52] A. H. Elwany and N. Z. Gebraeel. Sensor-driven prognostic models for equipment replacement and spare parts inventory. *IIE Transactions*, 40(7):629–639, 2008. 30, 34, 41

[53] A. H. Elwany, N. Z. Gebraeel, and L. M. Maillart. Structured replacement policies for components with complex degradation processes and dedicated sensors. *Operations Research*, 59(3):684–695, jun 2011. 42

[54] H. Endo and R. Randall. Enhancement of autoregressive model based gear tooth fault detection technique by the use of minimum entropy deconvolution filter. *Mechanical Systems and Signal Processing*, 21(2):906–919, 2007. 136, 138

[55] M. P. Enright and D. M. Frangopol. Probabilistic analysis of resistance degradation of reinforced concrete bridge beams under corrosion. *Engineering structures*, 20(11):960–971, 1998. 19

[56] R. L. Eshleman. *Condition monitoring of machinery*. McGraw Hill Professional, 2009. 22

[57] W. Fan and P. Qiao. Vibration-based damage identification methods: a review and comparative study. *Structural Health Monitoring*, 10(1):83–111, 2011. 16

[58] X. Fan and M. J. Zuo. Machine fault feature extraction based on intrinsic mode functions. *Measurement Science and Technology*, 19(4):045105, 2008. 29

[59] X. Fang, H. Luo, and J. Tang. Structural damage detection using neural network with learning rate improvement. *Computers & structures*, 83(25):2150–2161, 2005. 16

[60] C. R. Farrar and K. Worden. *Structural health monitoring: a machine learning perspective*. John Wiley & Sons, 2012. 15

[61] J. Feng, Q. Sun, and T. Jin. Storage life prediction for a high-performance capacitor using multi-phase Wiener degradation model. *Communications in Statistics - Simulation and Computation*, 41(8):1317–1335, sep 2012. xv, 8

[62] J. Feng, Q. Sun, and T. Jin. Storage life prediction for a high-performance capacitor using multi-phase Wiener degradation model. *Communications in Statistics - Simulation and Computation*, 41(8):1317–1335, sep 2012. 33, 40

[63] E. Figueiredo, G. Park, C. R. Farrar, K. Worden, and J. Figueiras. Machine learning algorithms for damage detection under operational and environmental variability. *Structural Health Monitoring*, 10(6):559–572, 2011. 16

[64] D. M. Frangopol, J. S. Kong, and E. S. Gharaibeh. Reliability-based life-cycle management of highway bridges. *Journal of computing in civil engineering*, 15(1):27–34, 2001. 19

[65] D. M. Frangopol, K.-Y. Lin, and A. C. Estes. Life-cycle cost design of deteriorating structures. *Journal of Structural Engineering*, 123(10):1390–1401, 1997. 19

[66] D. M. Frangopol, A. Strauss, and S. Kim. Bridge reliability assessment based on monitoring. *Journal of Bridge Engineering*, 13(3):258–270, 2008. 19, 42

[67] M. A. Freitas, M. L. G. de Toledo, E. A. Colosimo, and M. C. Pires. Using degradation data to assess reliability: a case study on train wheel degradation. *Quality and Reliability Engineering International*, 25(5):607–629, 2009. 31

[68] M. A. Freitas, T. R. dos Santos, M. C. Pires, and E. A. Colosimo. A closer look at degradation models: classical and bayesian approaches. In *Advances in Degradation Modeling*, pages 157–180. Springer, 2010. 31

[69] S. Gamse and M. Oberguggenberger. Assessment of long-term coordinate time series using hydrostatic-season-time model for rock-fill embankment dam. *Structural Control and Health Monitoring*, 24(1), 2016. 30

[70] S. Gamse, W.-H. Zhou, F. Tan, K.-V. Yuen, and M. Oberguggenberger. Hydrostatic-season-time model updating using bayesian model class selection. *Reliability Engineering & System Safety*, 2017. 30

[71] N. Gebraeel. Sensory-updated residual life distributions for components with exponential degradation patterns. *Automation Science and Engineering, IEEE Transactions on*, 3(4):382–393, 2006. 31, 34, 39

[72] N. Gebraeel, A. Elwany, and J. Pan. Residual life predictions in the absence of prior degradation knowledge. *Reliability, IEEE Transactions on*, 58(1):106–117, 2009. 31, 34, 54

[73] N. Gebraeel and J. Pan. Prognostic degradation models for computing and updating residual life distributions in a time-varying environment. *Reliability, IEEE Transactions on*, 57(4):539–550, 2008. 39

[74] N. Z. Gebraeel, M. A. Lawley, R. Li, and J. K. Ryan. Residual-life distributions from component degradation signals: A bayesian approach. *IiE Transactions*, 37(6):543–557, 2005. xv, 8

[75] N. Z. Gebraeel, M. A. Lawley, R. Li, and J. K. Ryan. Residual-life distributions from component degradation signals: A bayesian approach. *IIE Transactions*, 37(6):543–557, 2005. 30, 31, 34, 38, 39

[76] Z. Geng and L. Qu. Vibrational diagnosis of machine parts using the wavelet packet technique. *British Journal of Non-Destructive Testing*, 36(1):11–15, 1994. 24

[77] N. Gorjian, L. Ma, M. Mittinty, P. Yarlagadda, and Y. Sun. A review on degradation models in reliability analysis. In *Engineering Asset Lifecycle Management*, pages 369–384. Springer, 2010. 30

[78] A. Grall, C. Bérenguer, and L. Dieulle. A condition-based maintenance policy for stochastically deteriorating systems. *Reliability Engineering & System Safety*, 76(2):167–180, 2002. 32, 37, 41, 42

[79] A. Gupta and J. W. Baker. Estimating spatially varying event rates with a change point using bayesian statistics: Application to induced seismicity. *Structural Safety*, 65:1–11, 2017. 32, 40

[80] A. Gupta and J. W. Baker. Estimating spatially varying event rates with a change point using Bayesian statistics: Application to induced seismicity. *Structural Safety*, 65:1–11, 2017. 32

[81] M. Hamada. Using Degradation Data to Assess Reliability. *Quality Engineering*, 17(4):615–620, 2005. 31

[82] M. S. Hamada, A. Wilson, C. S. Reese, and H. Martz. *Bayesian reliability*. Springer Science & Business Media, 2008. 34

[83] T. Harvey, R. Wood, and H. Powrie. Electrostatic wear monitoring of rolling element bearings. *Wear*, 263(7):1492–1501, 2007. 20

[84] R. Heng and M. Nor. Statistical analysis of sound and vibration signals for monitoring rolling element bearing condition. *Applied Acoustics*, 53(1):211–226, 1998. 20

[85] D. Ho and R. Randall. Optimisation of bearing diagnostic techniques using simulated and actual bearing fault signals. *Mechanical systems and signal processing*, 14(5):763–788, 2000. 200

[86] N. E. Huang, Z. Shen, S. R. Long, M. C. Wu, H. H. Shih, Q. Zheng, N.-C. Yen, C. C. Tung, and H. H. Liu. The empirical mode decomposition and the hilbert spectrum for nonlinear and non-stationary time series analysis. In *Proceedings of the Royal Society of London A: mathematical, physical and engineering sciences*, volume 454, pages 903–995. The Royal Society, 1998. 28

[87] X. Huang and J. Chen. Time-dependent reliability model of deteriorating structures based on stochastic processes and bayesian inference methods. *Journal of Engineering Mechanics*, 141(3):04014123, 2014. 32, 37

[88] X. Huang and J. Chen. Time-dependent reliability model of deteriorating structures based on stochastic processes and Bayesian inference methods. *Journal of Engineering Mechanics*, 141(3):1–11, 2014. 32

[89] I. Iervolino, M. Giorgio, and E. Chioccarelli. Gamma degradation models for earthquake-resistant structures. *Structural Safety*, 45:48–58, 2013. 32

[90] C. James Li and J. Ma. Wavelet decomposition of vibrations for detection of bearing-localized defects. *Ndt & E International*, 30(3):143–149, 1997. 24

[91] A. K. Jardine, D. Lin, and D. Banjevic. A review on machinery diagnostics and prognostics implementing condition-based maintenance. *Mechanical systems and signal processing*, 20(7):1483–1510, 2006. 41

[92] A. K. Jardine, D. Lin, and D. Banjevic. A review on machinery diagnostics and prognostics implementing condition-based maintenance. *Mechanical systems and signal processing*, 20(7):1483–1510, 2006. 42

[93] A. K. Jardine and A. H. Tsang. *Maintenance, replacement, and reliability: theory and applications*. CRC press, 2013. 86

[94] R. Jiang and A. K. S. Jardine. Health state evaluation of an item: A general framework and graphical representation. *Reliability Engineering and System Safety*, 93(1):89–99, 2008. 31

[95] C. Junsheng, Y. Dejie, and Y. Yu. The application of energy operator demodulation approach based on emd in machinery fault diagnosis. *Mechanical systems and signal processing*, 21(2):668–677, 2007. 29

[96] M. J. Kallen and J. M. V. Noortwijk. Statistical inference for Markov deterioration models of bridge conditions in the Netherlands. *Third International Conference on Bridge Maintenance, Safety and Management (IABMAS)*, pages 16–19, 2006. 33

[97] S. Karlin and H. M. Taylor. A first course in stochastic processes. *Academic, San Diego*, 1975. 35

[98] X. Ke, Z. Xu, S. K. L. of Industrial Control Technology, C. of Control Science, and Engineering. Amodel for degradation prediction with change point based on wiener process. IEEE, 4673. 39

[99] D. Kong, N. Balakrishnan, and L. Cui. Two-Phase Degradation Process Model With Abrupt Jump at Change Point Governed by Wiener Process. pages 1–16, 2017. 33

[100] J. Lawless and M. Crowder. Covariates and random effects in a gamma process model with application to degradation and failure. *Lifetime Data Analysis*, 10(3):213–227, 2004. 32, 37

[101] K. Le Son, M. Fouladirad, A. Barros, E. Levrat, and B. Iung. Remaining useful life estimation based on stochastic deterioration models: A comparative study. *Reliability Engineering & System Safety*, 112:165–175, 2013. 85

[102] M. S. Lebold, K. M. Reichard, D. Ferullo, and D. Boylan. Open system architecture for condition-based maintenance: overview and training material, 2003. 43

[103] D. Leducq. Hydraulic noise diagnostic using wavelet analysis. In *INTER-NOISE and NOISE-CON Congress and Conference Proceedings*, volume 1990, pages 997–1000. Institute of Noise Control Engineering, 1990. 24

[104] J. Lee, H. Qiu, G. Yu, and J. Lin. *Rexnord Technical Services: Bearing Data Set*. Moffett Field, CA: IMS, Univ. Cincinnati. NASA Ames Prognostics Data Repository (http://ti.arc.nasa.gov/project/prognostic-data-repository), NASA Ames, 2007. (accessed February 3, 2017). 137

[105] J.-Y. Lee and A. Nandi. Extraction of impacting signals using blind deconvolution. *Journal of Sound and Vibration*, 232(5):945–962, 2000. 140

[106] Y. Lei, Z. He, and Y. Zi. Application of the eemd method to rotor fault diagnosis of rotating machinery. *Mechanical Systems and Signal Processing*, 23(4):1327–1338, 2009. 29

[107] Y. Lei, J. Lin, Z. He, and M. J. Zuo. A review on empirical mode decomposition in fault diagnosis of rotating machinery. *Mechanical Systems and Signal Processing*, 35(1):108–126, 2013. 23

[108] H. Li, Y. Zhang, and H. Zheng. Hilbert-huang transform and marginal spectrum for detection and diagnosis of localized defects in roller bearings. *Journal of mechanical science and technology*, 23(2):291–301, 2009. 29

[109] H. Li, Y. Zhang, and H. Zheng. Bearing fault detection and diagnosis based on order tracking and teager-huang transform. *Journal of Mechanical Science and Technology*, 24(3):811–822, 2010. 29

[110] H. Li and H. Zheng. Bearing fault detection using envelope spectrum based on emd and tkeo. In *Fuzzy Systems and Knowledge Discovery, 2008. FSKD'08. Fifth International Conference on*, volume 3, pages 142–146. IEEE, 2008. 29

[111] H. Li, H. Zheng, and L. Tang. Wigner-ville distribution based on emd for faults diagnosis of bearing. *Fuzzy Systems and Knowledge Discovery*, pages 803–812, 2006. 29

[112] J. Li, Z. Wang, Y. Zhang, H. Fu, C. Liu, and S. Krishnaswamy. Degradation data analysis based on a generalized Wiener process subject to measurement error. *Mechanical Systems and Signal Processing*, 94:57–72, 2017. 32

[113] Z. Li and Y. Zhang. Extreme value theory-based structural health prognosis method using reduced sensor data. *Structure and Infrastructure Engineering*, 10(8):988–997, 2014. 18

[114] Z. Li, Y. Zhang, and C. Wang. A sensor-driven structural health prognosis procedure considering sensor performance degradation. *Structure and Infrastructure Engineering*, 9(8):764–776, 2013. 19

[115] H. Liao, E. A. Elsayed, and L.-Y. Chan. Maintenance of continuously monitored degrading systems. *European Journal of Operational Research*, 175(2):821–835, 2006. 32, 37

[116] H. Liao, W. Zhao, and H. Guo. Predicting remaining useful life of an individual unit using proportional hazards model and logistic regression model. In *Reliability and Maintainability Symposium, 2006. RAMS'06. Annual*, pages 127–132. IEEE, 2006. xviii, 137

[117] J. Lin. Feature extraction of machine sound using wavelet and its application in fault diagnosis. *NDT & e International*, 34(1):25–30, 2001. 24, 25

[118] J. Lin, M. Asplunda, and A. Paridaa. Reliability analysis for degradation of locomotive wheels using parametric bayesian approach. *Quality and Reliability Engineering International*, 30(5):657–667, 2014. 31

[119] J. Lin and L. Qu. Feature extraction based on morlet wavelet and its application for mechanical fault diagnosis. *Journal of sound and vibration*, 234(1):135–148, 2000. 23

[120] C.-S. Liu. *Fault detection of rolling element bearings*. PhD thesis, University of Washington, 2005. 200

[121] K. Loparo. Bearings vibration data set, case western reserve university, 2003. 197

[122] C. J. Lu and W. O. Meeker. Using degradation measures to estimate a time-to-failure distribution. *Technometrics*, 35(2):161–174, 1993. 30, 31, 33, 34, 85

[123] D. Lu, M. D. Pandey, and W.-C. Xie. An efficient method for the estimation of parameters of stochastic gamma process from noisy degradation measurements. *Proceedings of the Institution of Mechanical Engineers, Part O: Journal of Risk and Reliability*, 227(4):425–433, 2013. 32

[124] G. Manson, K. Worden, K. Holford, and R. Pullin. Visualisation and dimension reduction of acoustic emission data for damage detection. *Journal of Intelligent Material Systems and Structures*, 12(8):529–536, 2001. 16

[125] R. Manzini, A. Regattieri, H. Pham, and E. Ferrari. Basic models and methods for maintenance of production systems. *Maintenance for Industrial Systems*, pages 313–395, 2010. 87

[126] S. Masri, M. Nakamura, A. Chassiakos, and T. Caughey. Neural network approach to detection of changes in structural parameters. *Journal of engineering mechanics*, 122(4):350–360, 1996. 16

[127] J. Mata. Interpretation of concrete dam behaviour with artificial neural network and multiple linear regression models. *Engineering Structures*, 33(3):903–910, 2011. 30

[128] P. McFadden and J. Smith. Model for the vibration produced by a single point defect in a rolling element bearing. *Journal of Sound and Vibration*, 96(1):69–82, 1984. 194

[129] P. McFadden and J. Smith. Vibration monitoring of rolling element bearings by the high-frequency resonance technique—a review. *Tribology international*, 17(1):3–10, 1984. 22, 200

[130] P. McFadden and M. Toozhy. Application of synchronous averaging to vibration monitoring of rolling element bearings. *Mechanical Systems and Signal Processing*, 14(6):891–906, 2000. 22

[131] S. A. McInerny and Y. Dai. Basic vibration signal processing for bearing fault detection. *Education, IEEE Transactions on*, 46(1):149–156, 2003. 193

[132] Q. Miao, D. Wang, and M. Pecht. Rolling element bearing fault feature extraction using emd-based independent component analysis. In *Prognostics and Health Management (PHM), 2011 IEEE Conference on*, pages 1–6. IEEE, 2011. 29

[133] T. Miyachi and K. Seki. An investigation of the early detection of defects in ball bearings using vibration monitoring-practical limit of detectability and growth speed of defects. In *Proceedings of the International Conference on Rotordynamics, JSMEIFToMM, Tokyo*, pages 14–17, 1986. 21

[134] M. Mollineaux and R. Rajagopal. Structural health monitoring of progressive damage. *Earthquake Engineering & Structural Dynamics*, 44(4):583–600, 2015. 17

[135] D. C. Montgomery. *Introduction to statistical quality control*. John Wiley & Sons, 2007. 17

[136] G. Morcous. Performance Prediction of Bridge Deck Systems Using Markov Chains. *Journal of Performance of Constructed Facilities*, 20(2):146–155, 2006. 33

[137] G. Morcous, Z. Lounis, and M. Mirza. Identification of environmental categories for Markovian deterioration models of bridge decks. *Journal of Bridge Engineering*, 8(6):353–361, 2003. 33

[138] L. Mujica, J. Rodellar, A. Fernandez, and A. Guemes. Q-statistic and t2-statistic pca-based measures for damage assessment in structures. *Structural Health Monitoring*, page 1475921710388972, 2010. 16, 17

[139] L. E. Mujica, J. Vehi, M. Ruiz, M. Verleysen, W. Staszewski, and K. Worden. Multivariate statistics process control for dimensionality reduction in structural assessment. *Mechanical Systems and Signal Processing*, 22(1):155–171, 2008. 16

[140] N. K. Mutlib, S. B. Baharom, A. El-Shafie, and M. Z. Nuawi. Ultrasonic health monitoring in structural engineering: buildings and bridges. *Structural Control and Health Monitoring*, 23(3):409–422, 2016. 15

[141] K. K. Nair and A. S. Kiremidjian. Time series based structural damage detection algorithm using gaussian mixtures modeling. *Journal of dynamic systems, measurement, and control*, 129(3):285–293, 2007. 17

[142] K. K. Nair, A. S. Kiremidjian, and K. H. Law. Time series-based damage detection and localization algorithm with application to the asce benchmark structure. *Journal of Sound and Vibration*, 291(1):349–368, 2006. 16, 17

[143] W. B. Nelson. *Accelerated testing: statistical models, test plans, and data analysis*, volume 344. John Wiley & Sons, 2009. 30

[144] S. K. Ng and F. Moses. Bridge deterioration modeling using semi-Markov theory, 1998. 33

[145] M. B. Nigro, S. N. Pakzad, and S. Dorvash. Localized structural damage detection: A change point analysis. *Computer-Aided Civil and Infrastructure Engineering*, 29(6):416–432, 2014. 33

[146] N. Nikolaou and I. Antoniadis. Rolling element bearing fault diagnosis using wavelet packets. *Ndt & E International*, 35(3):197–205, 2002. 23

[147] M. Nikulin, N. Limnios, N. Balakrishnan, W. Kahle, and C. Huber-Carol. Advances in degradation modeling. *Applications to Reliability, Survival Analysis, and Finance*, 2010. 30, 35

[148] T. NISBET. Rolling bearings in service: By t. nisbet & gw mullett., 1978. 194

[149] G. Niu, B.-S. Yang, and M. Pecht. Development of an optimized condition-based maintenance system by data fusion and reliability-centered maintenance. *Reliability Engineering & System Safety*, 95(7):786–796, 2010. 43

[150] H. Noh, R. Rajagopal, and A. Kiremidjian. Sequential structural damage diagnosis algorithm using a change point detection method. *Journal of Sound and Vibration*, 332(24):6419–6433, 2013. 40

[151] H. Noh, R. Rajagopal, and A. S. Kiremidjian. Sequential structural damage diagnosis algorithm using a change point detection method. *Journal of Sound and Vibration*, 332(24):6419–6433, 2013. 32

[152] I. Ntzoufras. *Bayesian modeling using WinBUGS*, volume 698. John Wiley & Sons, 2011. 52

[153] H. Ocak and K. A. Loparo. Hmm-based fault detection and diagnosis scheme for rolling element bearings. *Journal of Vibration and Acoustics*, 127(4):299–306, 2005. 33

[154] P. Omenzetter and J. M. W. Brownjohn. Application of time series analysis for bridge monitoring. *Smart Materials and Structures*, 15(1):129, 2006. 16

[155] S. Osman and W. Wang. A normalized hilbert-huang transform technique for bearing fault detection. *Journal of Vibration and Control*, 22(11):2771–2787, 2016. 22

[156] C. Pachaud, R. Salvetat, and C. Fray. Crest factor and kurtosis contributions to identify defects inducing periodical impulsive forces. *Mechanical Systems and Signal Processing*, 11(6):903–916, 1997. 21

[157] Z. Pan and N. Balakrishnan. Reliability modeling of degradation of products with multiple performance characteristics based on gamma processes. *Reliability Engineering and System Safety*, 96(8):949–957, 2011. 32

[158] Z. Pan and N. Balakrishnan. Reliability modeling of degradation of products with multiple performance characteristics based on gamma processes. *Reliability Engineering & System Safety*, 96(8):949–957, 2011. 37

[159] A. Pandey, M. Biswas, and M. Samman. Damage detection from changes in curvature mode shapes. *Journal of sound and vibration*, 145(2):321–332, 1991. 16

[160] M. Pandey, D. Lu, and D. Komljenovic. The impact of probabilistic modelling on predicting the remaining life of pipes in nuclear plants. In *17th International Conference on Nuclear Engineering*, pages 503–511. American Society of Mechanical Engineers, 2009. 19, 30

[161] M. Pandey, X. Yuan, and J. Van Noortwijk. Gamma process model for reliability analysis and replacement of aging structural components. *Proceedings ICOSSAR, Rome, Italy, Paper*, (311), 2005. 35

[162] M. D. Pandey. Probabilistic models for condition assessment of oil and gas pipelines. *Ndt & E International*, 31(5):349–358, 1998. 19, 30

[163] M. D. Pandey, X. X. Yuan, and J. M. van Noortwijk. Gamma process model for reliability analysis and replacement of aging structural components. *Nineth International Conference on Structural Safety and Reliability*, pages 2439–2444, 2005. 32

[164] C. Park and W. Padgett. Accelerated degradation models for failure based on geometric brownian motion and gamma processes. *Lifetime Data Analysis*, 11(4):511–527, 2005. 89

[165] M. Patil, J. Mathew, and P. RajendraKumar. Bearing signature analysis as a medium for fault detection: A review. *Journal of Tribology*, 130(1):014001, 2008. 195

[166] N. Patrick, G. Rafael, M. Kamal, et al. Pronostia.. an experimental platform for bearings accelerated life test. In *IEEE International Conference on Prognostics and Health Management, Denver, CO*, 2012. xvi, 38

[167] W. Peng, Y.-F. Li, Y.-J. Yang, H.-Z. Huang, and M. J. Zuo. Inverse Gaussian process models for degradation analysis: A Bayesian perspective. *Reliability Engineering & System Safety*, 130:175–189, 2014. 32

[168] Y. Peng and M. Dong. A prognosis method using age-dependent hidden semi-Markov model for equipment health prediction. *Mechanical Systems and Signal Processing*, 25(1):237–252, 2011. 33

[169] Z. Peng, W. T. Peter, and F. Chu. A comparison study of improved hilbert–huang transform and wavelet transform: application to fault diagnosis for rolling bearing. *Mechanical systems and signal processing*, 19(5):974–988, 2005. 22

[170] W. T. Peter, Y. Peng, and R. Yam. Wavelet analysis and envelope detection for rolling element bearing fault diagnosis—their effectiveness and flexibilities. *Journal of Vibration and Acoustics*, 123(3):303–310, 2001. 23

[171] G. Prakash, A. Sadhu, S. Narasimhan, and J.-M. Brehe. Initial service life data towards structural health monitoring of a concrete arch dam. *Structural Control and Health Monitoring*. 30

[172] V. Purushotham, S. Narayanan, and S. A. Prasad. Multi-fault diagnosis of rolling bearing elements using wavelet analysis and hidden markov model based fault recognition. *Ndt & E International*, 38(8):654–664, dec 2005. 23, 33

[173] S. Qian. *Introduction to time-frequency and wavelet transforms*. Prentice Hall, 2002. 24

[174] H. Qin, S. Zhang, and W. Zhou. Inverse Gaussian process-based corrosion growth modeling and its application in the reliability analysis for energy pipelines. *Frontiers of Structural and Civil Engineering*, 7(3):276–287, 2013. 32

[175] H. Qiu, J. Lee, J. Lin, and G. Yu. Wavelet filter-based weak signature detection method and its application on rolling element bearing prognostics. *Journal of sound and vibration*, 289(4):1066–1090, 2006. xviii, 137, 138

[176] S.-T. Quek, Q. Wang, L. Zhang, and K.-K. Ang. Sensitivity analysis of crack detection in beams by wavelet technique. *International journal of mechanical sciences*, 43(12):2899–2910, 2001. 25

[177] A. E. Raftery and V. Akman. Bayesian analysis of a poisson process with a change-point. *Biometrika*, pages 85–89, 1986. xv, 8

[178] A. E. Raftery and S. Lewis. How many iterations in the gibbs sampler? Technical report, Washington university seattle, Department of statistics, 1991. 102, 214

[179] V. Rai and A. Mohanty. Bearing fault diagnosis using fft of intrinsic mode functions in hilbert–huang transform. *Mechanical Systems and Signal Processing*, 21(6):2607–2615, 2007. 29

[180] R. B. Randall. *Frequency analysis*. Brül & Kjor, 1987. 22

[181] R. B. Randall. *Vibration-based condition monitoring: industrial, aerospace and automotive applications*. John Wiley & Sons, 2011. 20

[182] R. B. Randall and J. Antoni. Rolling element bearing diagnostics—a tutorial. *Mechanical systems and signal processing*, 25(2):485–520, 2011. 20, 26

[183] R. B. Randall, J. Antoni, and S. Chobsaard. The relationship between spectral correlation and envelope analysis in the diagnostics of bearing faults and other cyclostationary machine signals. *Mechanical systems and signal processing*, 15(5):945–962, 2001. 22

[184] A. Rastegari and M. Bengtsson. Implementation of condition based maintenance in manufacturing industry-a pilot case study. In *Prognostics and Health Management (PHM), 2014 IEEE Conference on*, pages 1–8. IEEE, 2014. 42

[185] R. Rubini and U. Meneghetti. Application of the envelope and wavelet transform analyses for the diagnosis of incipient faults in ball bearings. *Mechanical systems and signal processing*, 15(2):287–302, 2001. 23

[186] A. Sadhu, G. Prakash, and S. Narasimhan. A hybrid hidden markov model towards fault detection of rotating components. *Journal of Vibration and Control*, page 1077546315627934, 2016. 22

[187] N. Sawalhi. *Diagnostics, prognostics and fault simulation for rolling element bearings*. PhD thesis, The University of New South Wales Australia, 2007. 27

[188] N. Sawalhi and R. Randall. Simulating gear and bearing interactions in the presence of faults: Part i. the combined gear bearing dynamic model and the simulation of localised bearing faults. *Mechanical Systems and Signal Processing*, 22(8):1924–1951, 2008. 26

[189] N. Sawalhi and R. Randall. Simulating gear and bearing interactions in the presence of faults: Part ii: Simulation of the vibrations produced by extended bearing faults. *Mechanical Systems and Signal Processing*, 22(8):1952–1966, 2008. 26

[190] N. Sawalhi, R. Randall, and H. Endo. The enhancement of fault detection and diagnosis in rolling element bearings using minimum entropy deconvolution combined with spectral kurtosis. *Mechanical Systems and Signal Processing*, 21(6):2616–2633, 2007. 21, 25, 26, 27, 140, 141

[191] C. Sbarufatti, A. Manes, and M. Giglio. Application of sensor technologies for local and distributed structural health monitoring. *Structural Control and Health Monitoring*, 21(7):1057–1083, 2014. STC-13-0033.R2. 15

[192] R. R. Schoen, T. G. Habetler, F. Kamran, and R. Bartfield. Motor bearing damage detection using stator current monitoring. *Industry Applications, IEEE Transactions on*, 31(6):1274–1279, 1995. 20

[193] G. A. Seber and A. J. Lee. *Linear regression analysis*, volume 936. John Wiley & Sons, 2012. 78

[194] Z. Shi, S. Law, and L. Zhang. Structural damage detection from modal strain energy change. *Journal of engineering mechanics*, 126(12):1216–1223, 2000. 16

[195] J.-H. Shin and H.-B. Jun. On condition based maintenance policy. *Journal of Computational Design and Engineering*, 2(2):119–127, 2015. 42

[196] X.-S. Si, W. Wang, M.-Y. Chen, C.-H. Hu, and D.-H. Zhou. A degradation path-dependent approach for remaining useful life estimation with an exact and closed-form solution. *European Journal of Operational Research*, 226(1):53–66, 2013. 85, 86, 89

[197] X.-S. Si, W. Wang, C.-H. Hu, M.-Y. Chen, and D.-H. Zhou. A wiener-process-based degradation model with a recursive filter algorithm for remaining useful life estimation. *Mechanical Systems and Signal Processing*, 35(1):219–237, 2013. 32, 36, 91

[198] X.-S. Si, W. Wang, C.-H. Hu, and D.-H. Zhou. Remaining useful life estimation – a review on the statistical data driven approaches. *European Journal of Operational Research*, 213(1):1–14, aug 2011. 84, 85, 86

[199] R. Singh, J. H. Park, and S. N. Atluri. Growth of multiple cracks and their linkup in a fuselage lap joint. *AIAA journal*, 32(11):2260–2268, 1994. 18

[200] N. Singpurwalla. Gamma processes and their generalizations: an overview. In *Engineering probabilistic design and maintenance for flood protection*, pages 67–75. Springer, 1997. 70

[201] D. M. Siringoringo and Y. Fujino. System identification of suspension bridge from ambient vibration response. *Engineering Structures*, 30(2):462–477, 2008. 15

[202] M. Snchez-Silva. *Reliability and life-cycle analysis of deteriorating systems*. Springer, 2015. 33

[203] H. Sohn, J. A. Czarnecki, and C. R. Farrar. Structural health monitoring using statistical process control. *Journal of Structural Engineering*, 126(11):1356–1363, 2000. 16, 17

[204] H. Sohn and C. R. Farrar. Damage diagnosis using time series analysis of vibration signals. *Smart materials and structures*, 10(3):446, 2001. 16

[205] W. Staszewski. Structural and mechanical damage detection using wavelets. *The Shock and Vibration Digest*, 30(6):457–472, 1998. 25

[206] W. Staszewski. Wavelet based compression and feature selection for vibration analysis. *Journal of sound and vibration*, 211(5):735–760, 1998. 24

[207] A. Strauss, R. Wan-Wendner, A. Vidovic, I. Zambon, Q. Yu, D. M. Frangopol, and K. Bergmeister. Gamma prediction models for long-term creep deformations of prestressed concrete bridges. *Journal of Civil Engineering and Management*, 23(6):681–698, 2017. 32

[208] C. Su, J.-C. Lu, D. Chen, and J. M. Hughes-Oliver. A random coefficient degradation model with ramdom sample size. *Lifetime Data Analysis*, 5(2):173–183, 1999. 35

[209] W.-S. Su, F.-T. Wang, Z.-X. Zhang, Z.-G. Guo, and H.-K. Li. Application of emd denoising and spectral kurtosis in early fault diagnosis of rolling element bearings. *Zhendong yu Chongji(Journal of Vibration and Shock)*, 29(3):18–21, 2010. 27

[210] W. Sui, S. Osman, and W. Wang. An adaptive envelope spectrum technique for bearing fault detection. *Measurement Science and Technology*, 25(9):095004, 2014. 23

[211] J. Sun, L. Li, and L. Xi. Modified two-stage degradation model for dynamic maintenance threshold calculation considering uncertainty. *IEEE Transactions on Automation Science and Engineering*, 9(1):209–212, 2012. 31

[212] Y. Sun, S. Liu, R. Li, Z. Ye, Y. Kang, and S. Chen. A new magnetic flux leakage sensor based on open magnetizing method and its on-line automated structural health monitoring methodology. *Structural Health Monitoring*, page 1475921715604387, 2015. 15

[213] J. Tian, Z. Li, and X. Su. Crack detection in beams by wavelet analysis of transient flexural waves. *Journal of Sound and Vibration*, 261(4):715–727, 2003. 25

[214] Z. Tian, T. Jin, B. Wu, and F. Ding. Condition based maintenance optimization for wind power generation systems under continuous monitoring. *Renewable Energy*, 36(5):1502–1509, 2011. 42

[215] D.-A. Tibaduiza, M.-A. Torres-Arredondo, L. Mujica, J. Rodellar, and C.-P. Fritzen. A study of two unsupervised data driven statistical methodologies for detecting and classifying damages in structural health monitoring. *Mechanical Systems and Signal Processing*, 41(1):467–484, 2013. 16

[216] D. Tobon-Mejia, K. Medjaher, N. Zerhouni, and G. Tripot. Hidden markov models for failure diagnostic and prognostic. In *Prognostics and System Health Management Conference (PHM-Shenzhen), 2011*, pages 1–8. IEEE, 2011. 33

[217] D. A. Tobon-Mejia, K. Medjaher, N. Zerhouni, and G. Tripot. A data-driven failure prognostics method based on mixture of Gaussian hidden Markov models. *IEEE Transactions on Reliability*, 61(2):491–503, 2012. 33

[218] C. C. Tsai, S. T. Tseng, and N. Balakrishnan. Optimal design for degradation tests based on gamma processes with random effects. *IEEE Transactions on Reliability*, 61(2):604–613, 2012. 32

[219] R. S. Tsay. *Analysis of financial time series*, volume 543. John Wiley & Sons, 2005. 72

[220] F. Ubertini, G. Comanducci, and N. Cavalagli. Vibration-based structural health monitoring of a historic bell-tower using output-only measurements and multivariate statistical analysis. *Structural Health Monitoring*, page 1475921716643948, 2016. 17

[221] J. Van Noortwijk. A survey of the application of gamma processes in maintenance. *Reliability Engineering & System Safety*, 94(1):2–21, 2009. 30, 32, 37, 71

[222] J. Van Noortwijk, M. Kallen, and M. Pandey. Gamma processes for time-dependent reliability of structures. *Advances in safety and reliability, proceedings of ESREL*, pages 1457–1464, 2005. 37

[223] J. Van Noortwijk and M. D. Pandey. A stochastic deterioration process for time-dependent reliability analysis. *Proceedings of the Eleventh IFIP WG 7.5 Working Conference on Reliability and Optimization of Structural Systems*, (November 2003):259–265, 2003. 32

[224] O. A. Vanli. A Failure Time Prediction Method for Condition-Based Maintenance. *Quality Engineering*, 26(3):335–349, 2014. 32

[225] O. A. Vanli. A failure time prediction method for condition-based maintenance. *Quality Engineering*, 26(3):335–349, 2014. 30, 40

[226] P. Večeř, M. Kreidl, and R. Šmíd. Condition indicators for gearbox condition monitoring systems. *Acta Polytechnica*, 45(6), 2005. 21, 30

[227] V. Vrabie, P. Granjon, C. Servière, et al. Spectral kurtosis: from definition to application. In *Proceedings of the 6th IEEE International Workshop on Nonlinear Signal and Image Processing*, 2003. 26

[228] D. Wang and K.-L. Tsui. Two novel mixed effects models for prognostics of rolling element bearings. *Mechanical Systems and Signal Processing*, 99:1–13, 2018. 39

[229] H. Wang. A survey of maintenance policies of deteriorating systems. *European journal of operational research*, 139(3):469–489, 2002. 41, 42

[230] H. Wang, T. Xu, and J. Yang. Lifetime prediction based on degradation data analysis with a change point. In *Proceedings of the First Symposium on Aviation Maintenance and Management-Volume II*, pages 527–534. Springer, 2014. 71

[231] Q. Wang and X. Deng. Damage detection with spatial wavelets. *International journal of solids and structures*, 36(23):3443–3468, 1999. 25

[232] V. Z. Wang, T. Pease, and S. Robinson. Statistical damage prognosis for in-service civil structures against hazards: Formulations and applications. *Journal of Engineering Mechanics*, 142(3):04015090, 2015. 18

[233] W. Wang and H. Lee. An energy kurtosis demodulation technique for signal denoising and bearing fault detection. *Measurement Science and Technology*, 24(2):025601, 2013. 25

[234] W. Wang and P. McFadden. Application of wavelets to gearbox vibration signals for fault detection. *Journal of sound and vibration*, 192(5):927–939, 1996. 24

[235] W.-b. Wang. A model to determine the optimal critical level and the monitoring intervals in condition-based maintenance. *International Journal of Production Research*, 38(6):1425–1436, 2000. 42

[236] W. Q. Wang, F. Ismail, and M. F. Golnaraghi. Assessment of gear damage monitoring techniques using vibration measurements. *Mechanical Systems and Signal Processing*, 15(5):905–922, 2001. 20

[237] X. Wang. Wiener processes with random effects for degradation data. *Journal of Multivariate Analysis*, 101(2):340–351, 2010. 32, 36

[238] X. Wang, P. Jiang, B. Guo, and Z. Cheng. Real-time reliability evaluation with a general Wiener process-based degradation model. *Quality and Reliability Engineering International*, 30(2):205–220, jan 2013. xv, 8

[239] X. Wang, P. Jiang, B. Guo, and Z. Cheng. Real-time Reliability Evaluation for an Individual Product Based on Change-point Gamma and Wiener Process. *Quality and Reliability Engineering International*, 30(4):513–525, 2014. 32

[240] X. Wang, P. Jiang, B. Guo, and Z. Cheng. Real-time reliability evaluation for an individual product based on change-point gamma and wiener process. *Quality and Reliability Engineering International*, 30(4):513–525, 2014. 40

[241] X. Wang, P. Jiang, B. Guo, and Z. Cheng. Real-time reliability evaluation with a general Wiener process-based degradation model. *Quality and Reliability Engineering International*, 30(2):205–220, 2014. 32

[242] X. Wang and D. Xu. An Inverse Gaussian Process Model for Degradation Data. *Technometrics*, 52(2):188–197, 2010. 32

[243] Z. Wang and K. Ong. Autoregressive coefficients based hotelling's t2 control chart for structural health monitoring. *Computers & Structures*, 86(19-20):1918–1935, oct 2008. 16, 17

[244] Z. Wang and K. Ong. Multivariate statistical approach to structural damage detection. *Journal of engineering mechanics*, 136(1):12–22, 2009. 16, 17

[245] Z. Wang and K. Ong. Structural damage detection using autoregressive-model-incorporating multivariate exponentially weighted moving average control chart. *Engineering structures*, 31(5):1265–1275, 2009. 16, 17

[246] G. Whitmore and F. Schenkelberg. Modelling accelerated degradation data using wiener diffusion with a time scale transformation. *Lifetime data analysis*, 3(1):27–45, 1997. 32, 36

[247] G. a. Whitmore, M. J. Crowder, and J. F. Lawless. Failure inference from a marker process based on a bivariate Wiener model. *Lifetime data analysis*, 4(3):229–251, 1998. 32

[248] R. A. Wiggins. Minimum entropy deconvolution. *Geoexploration*, 16(1-2):21–35, 1978. 139, 140

[249] T. Williams, X. Ribadeneira, S. Billington, and T. Kurfess. Rolling element bearing diagnostics in run-to-failure lifetime testing. *Mechanical Systems and Signal Processing*, 15(5):979–993, 2001. 21

[250] K. Worden and A. Lane. Damage identification using support vector machines. *Smart Materials and Structures*, 10(3):540, 2001. 16

[251] D. Xu, Y. Xu, X. Chen, W. Zha, and X. Li. Life cycle vibration analysis based on emd of rolling element bearing under alt by constant stress. In *Reliability, Maintainability and Safety, 2009. ICRMS 2009. 8th International Conference on*, pages 1177–1182. IEEE, 2009. 29

[252] R. Yan and R. X. Gao. Hilbert–huang transform-based vibration signal analysis for machine health monitoring. *IEEE Transactions on Instrumentation and measurement*, 55(6):2320–2329, 2006. 29

[253] H.-T. Yang and C.-C. Liao. A de-noising scheme for enhancing wavelet-based power quality monitoring system. *IEEE Transactions on Power Delivery*, 16(3):353–360, 2001. 24

[254] R. Yao and S. N. Pakzad. Autoregressive statistical pattern recognition algorithms for damage detection in civil structures. *Mechanical Systems and Signal Processing*, 31:355–368, 2012. 17

[255] Z. Ye and N. Chen. The inverse Gaussian process as a degradation model. *Technometrics*, 56(August):1–28, 2013. 32

[256] Z.-S. Ye, Y. Wang, K.-L. Tsui, and M. Pecht. Degradation data analysis using wiener processes with measurement errors. *Reliability, IEEE Transactions on*, 62(4):772–780, 2013. 32, 36

[257] X.-X. Yuan and M. Pandey. A nonlinear mixed-effects model for degradation data obtained from in-service inspections. *Reliability Engineering & System Safety*, 94(2):509–519, 2009. 31

[258] X.-X. Yuan, M. Pandey, and G. Bickel. A probabilistic model of wall thinning in candu feeders due to flow-accelerated corrosion. *Nuclear Engineering and Design*, 238(1):16–24, 2008. 19, 30

[259] X. X. Yuan, M. D. Pandey, and G. A. Bickel. A probabilistic model of wall thinning in CANDU feeders due to flow-accelerated corrosion. *Nuclear Engineering and Design*, 238(1):16–24, 2008. 32

[260] B. Zhang, L. Zhang, and J. Xu. Degradation feature selection for remaining useful life prediction of rolling element bearings. *Quality and Reliability Engineering International*, 32(2):547–554, 2016. 30

[261] X. Zhang, R. Xu, C. Kwan, S. Y. Liang, Q. Xie, and L. Haynes. An integrated approach to bearing fault diagnostics and prognostics. In *2005 American Control Conference ThB15.2 June 8-10, 2005. Portland, OR, USA*, pages 2750–2755. IEEE, 2005. 33

[262] Y. Zhang and R. Randall. Rolling element bearing fault diagnosis based on the combination of genetic algorithms and fast kurtogram. *Mechanical Systems and Signal Processing*, 23(5):1509–1517, 2009. 26

[263] H.-J. Zimmermann. An application-oriented view of modeling uncertainty. *European Journal of operational research*, 122(2):190–198, 2000. 50

[264] J. Zou, J. Chen, Y. Pu, and P. Zhong. On the wavelet time-frequency analysis algorithm in identification of a cracked rotor. *The Journal of Strain Analysis for Engineering Design*, 37(3):239–246, 2002. 25

[265] M. J. Zuo, J. Renyan, and R. C. M. Yam. Approaches for reliability modeling of continuous-state devices. *IEEE Transactions on Reliability*, 48(1):9–18, 1999. 31

APPENDICES

Appendix A

Bearing faults and vibration condition indicators

A.1 Bearing vibration signatures

The main components of a bearing are: inner race, outer race, ball and cage, as shown in Figure A.1. The inner race remains fixed to the shaft and rotates with the shaft-speed. The outer race is fixed to a housing and remains stationary during operation. The rolling balls are placed between the inner and outer races and transfer the load over a very small surface (ideally point contact) on the raceways. The cage separates the rolling elements, preventing contact between them during operation [131]. Loads and their distribution resulting from the shaft are transferred to other components through the balls as shown in Figure A.1.

There are many mechanisms that can lead to bearing failure, including mechanical damage, crack damage, misalignment, overload, faulty installation, brinelling, fatigue, contam-

ination, loss of lubrication and corrosion. Generally, defects occur in the outer race, inner race, rolling element or in the cage. A detailed review on the causes of bearing failures can be found in [148]. Once a defect occurs in the bearing, its vibrational behaviour changes with respect to a healthy bearing, which is key to vibration based bearing monitoring.

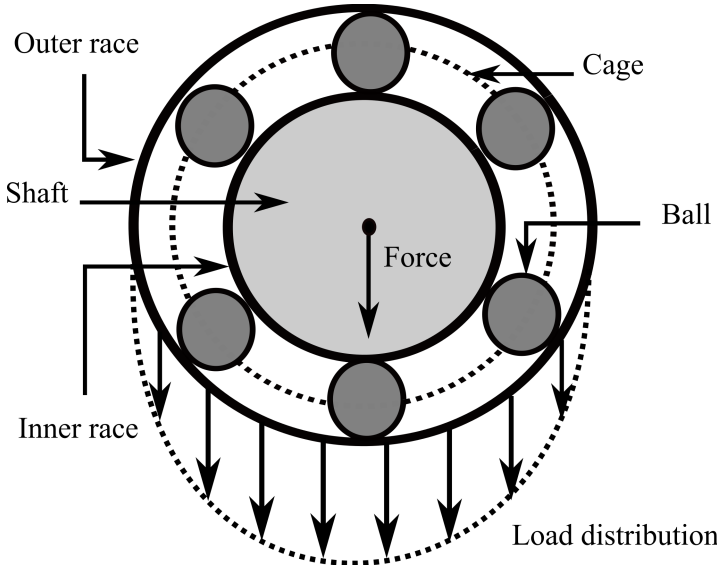

Figure A.1: Rolling element bearing components and load distribution

The vibration characteristics generated by various bearing defects are explained in [25, 128]. When a defect in a bearing component contacts another surface, periodic impulses are generated, causing the bearing to vibrate. The bearing responds by "ringing" at its natural frequency, a response that decays quickly because of damping. The excitation and response occur each time one of the balls rolls over the flaw, so that the fundamental frequency of the response waveforms is the rate at which the elements roll over the flaw. It is this fundamental frequency that is of interest in the detection of bearing faults, not the resonance frequency at which the bearing rings, and it can be predicted from the bearing geometry and the speeds at which the bearing shaft rotates. It can be calculated using the

following formulae [165, 12]:

$$\text{Ball pass frequency, outer race :} \quad BPFO = \frac{nf_r}{2}(1 - \frac{d}{D}cos\phi) \tag{A.1}$$

$$\text{Ball pass frequency, inner race :} \quad BPFI = \frac{nf_r}{2}(1 + \frac{d}{D}cos\phi) \tag{A.2}$$

$$\text{Fundamental train frequency (cage speed) :} \quad FTF = \frac{f_r}{2}(1 - \frac{d}{D}cos\phi) \tag{A.3}$$

$$\text{Ball (roller) spin frequency} \quad BSF = \frac{D}{2d}(1 - (\frac{d}{D}cos\phi)^2) \tag{A.4}$$

where, f_r is the shaft speed, d is the mean diameter of the rolling element, D is the pitch diameter of the bearing, n is the number of rolling elements, and ϕ is the angle of the load from the radial plane.

A.2 Condition indicators

Time domain condition indicators [21] are widely used in the literature for fault diagnosis of rolling element bearings and gear-boxes. These condition indicators are simple to calculate and can be implemented in real time. Table A.2 presents some of these condition indicators with their mathematical expressions, where s is a window of vibration signal containing N measurements and s_i is the i^{th} measurement point.

Table A.1: Condition indicators

Condition indicators	Expression
Mean value	$\overline{s} = \frac{\sum_{i=1}^{N} s_i}{N}$
Root-mean-square value (RMS)	$s_{rms} = \sqrt{\frac{1}{N}\sum_{i=1}^{N}({s_i}^2)}$
Skewness	$g = \frac{\frac{1}{N}\sum_{i=1}^{N}(s_i-\overline{s})^3}{[\frac{1}{N}\sum_{i=1}^{N}(s_i-\overline{s})^2]^{3/2}}$
Kurtosis	$\kappa = \frac{N\sum_{i=1}^{N}(s_i-\overline{s})^4}{[\sum_{i=1}^{N}(s_i-\overline{s})^2]^2}$
Shape factor	$s_{shape} = \frac{s_{rms}}{\overline{s}}$
Crest factor	$\mathrm{CF} = \frac{s_{max}-s_{min}}{s_{rms}}$

A.3 Fast Fourier transform

The Fourier transform of a signal $x(t)$ in terms of the cyclic frequency f can be written as

$$X(f) = \mathcal{F}[x(t)] = \int_{-\infty}^{+\infty} x(t)e^{-j2\pi ft}dt \tag{A.5}$$

and its inverse Fourier transform is given by

$$X(t) = \mathcal{F}^{-1}[X(f)] = \int_{-\infty}^{+\infty} X(f)e^{j2\pi ft}df \tag{A.6}$$

FFT is an algorithm that numerically approximates the Fourier transform. An example FFT for an inner race fault is shown in Figure A.2, where the characteristic frequency (BPFI = 160 Hz) and its harmonics can be seen. Note that the sidebands corresponding to the 7^{th} harmonic in Figure A.2 is separated by 30 Hz, which is the rotating frequency. Ideally, such sidebands should be visible in all the harmonics, but due to noise present in

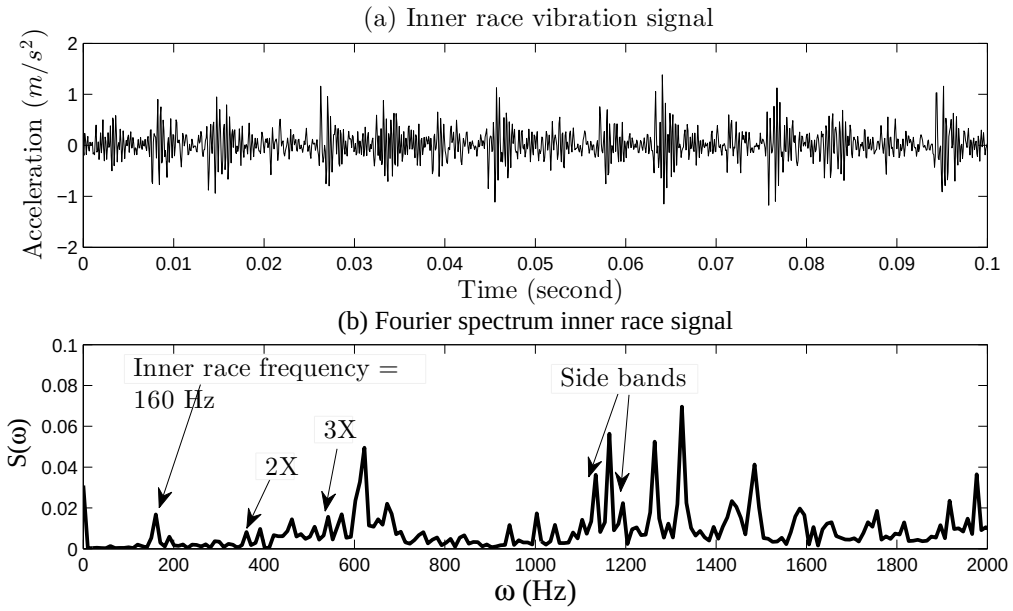

Figure A.2: Inner race fault (7 mils diameter)

the signal it is clearly visible only in some of the harmonics.

Another application of the frequency spectrum is to quantify the severity of faults. As an example, Figure A.3 shows the time history and frequency spectrum for a normal and defective bearing. For the defective case, fault diameters are 7, 14 and 21 millinches, respectively. Clearly, defective bearings generate a boarder spectrum spread than their corresponding normal bearing [121]. The main vibration components of a normal bearing are concentrated in the lower frequency region (below 1 kHz) and its overall power spectrum energy is significantly lower than that of the defective bearing. The spectrum of the defective bearings spread from the low to high frequency ranges with several frequency regions. Moreover, as the defect size increases, changes in the energy in the higher frequency region is more sensitive to bearing defects than the frequency components in the lower frequency region.

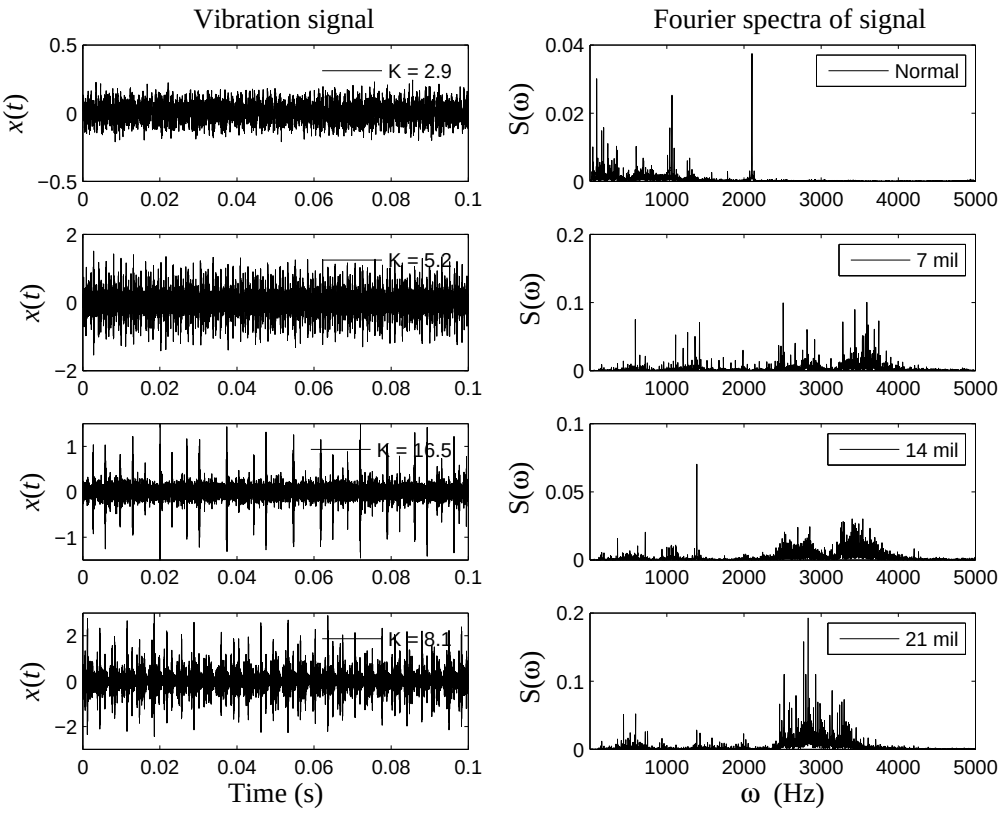

Figure A.3: Time history and spectrum of normal and increasing inner race defect

A.4 Amplitude modulation

Identification of critical fault frequencies allows us to monitor the progression of a bearing fault. However, amplitude modulations in the vibration signal could make this task difficult. Amplitude modulation is caused when the load on a bearing varies, typically with rotational speed. For example, consider a bearing which is mounted horizontally. Due to the gravitational forces or vertical load coming onto the shaft, the pressure between the element and the bearing surfaces may be greater at the bottom of the bearing than the top. If there is a defect on one of the rolling elements, then the impact from this may be stronger when the element is at the bottom of the bearing than when it is at the top. If the defect occurs in the outer race, the amplitude modulation subjected to load variations will not be as prominent in the vibration signal. Figure A.4 shows an amplitude modulated bearing signal, where the defect signal is assumed to be sinusoidal with a frequency of 100 Hz and modulated by by another sinusoid of frequency 10 Hz.

The amplitude modulation, caused by the multiplication of the higher frequency signal (f_H) and the lower frequency modulation signal (f_L), results in a signal, $a(t)$ which can be given as:

$$\begin{aligned} a(t) &= \sin(2\pi f_H t)(1 + \sin(2\pi f_L t)) \\ a(t) &= \sin(2\pi f_H t) + \frac{\cos(2\pi(f_H - f_L)t)}{2} + \frac{\cos(2\pi(f_H + f_L)t)}{2} \end{aligned} \tag{A.7}$$

That is, the resultant frequency spectrum will contain peaks at frequencies f_H, $f_H - f_L$ and $f_H + f_L$. For the faulty bearing signal, the components $f_H - f_L$ and $f_H + f_L$ are the side bands and f_H is characteristic fault frequency. Figure A.5 shows the frequency spectrum for the simulated amplitude modulated signal. Clearly, two side-bands and bearing fault

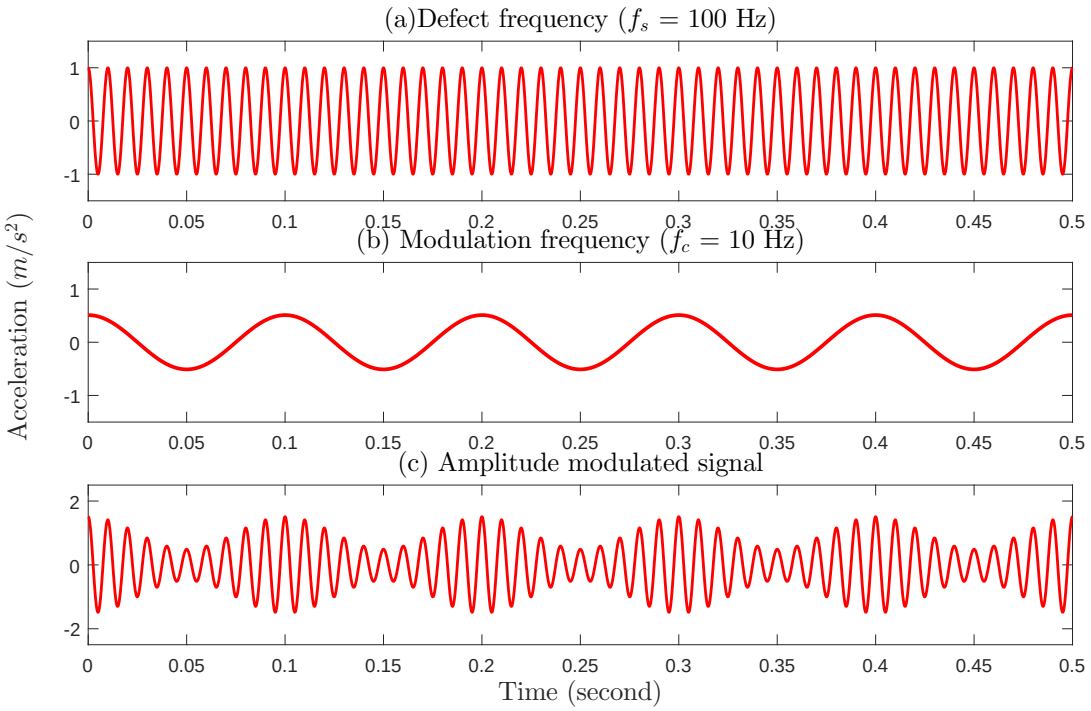

Figure A.4: A simulated signal showing amplitude modulation

frequencies are visible in the spectrum.

A.5 Envelope analysis

Envelope analysis [85, 120], also known as high frequency resonance technique, is frequently used for extracting the impulsive characteristics from a vibration signal in the presence of high background noise. As its name suggests, envelope analysis attempts to determine the overall extremities of a signal. This technique is widely used by the maintenance industry for early gear and bearing fault detection [129]. Impacts produced due to rolling element faults modulate a signal at the associated bearing pass frequencies, such as: BPFO, BPFI and BSF as described in the previous section. Envelope analysis is based on the

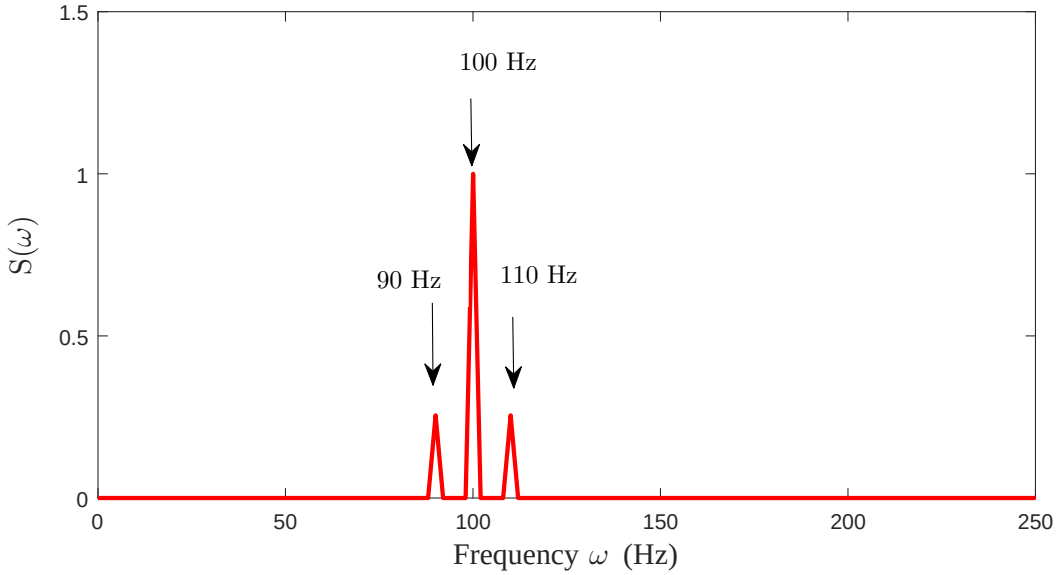

Figure A.5: FFT of simulated signal showing defect frequency and side-bands

demodulation of high frequency resonance associated with bearing element impacts. The process of recovering the modulating signal from the amplitude modulated signal is called demodulation and it is accomplished by a detector circuit. A detector circuit performs the following two functions: i) it rectifies the modulated wave i.e. negative half of the modulated wave is eliminated and ii) it separates the modulating signal from the carrier. This is achieved by a low pass filter, which removes the carrier frequency. The vibration signal obtained after demodulation contains only the fault information. The power of this method comes from the fact that it can detect faulty conditions even in the case of low SNR.

To illustrate the process of envelope analysis a series of impulses are simulated as shown in Figure A.6. The impulse repeats at a frequency of 100 Hz and the modulation frequency is 10 Hz. The envelope spectrum of the simulated pulse train is shown in Figure A.7. One can see that the 10 Hz modulating frequency (which is the rotational speed) and defect

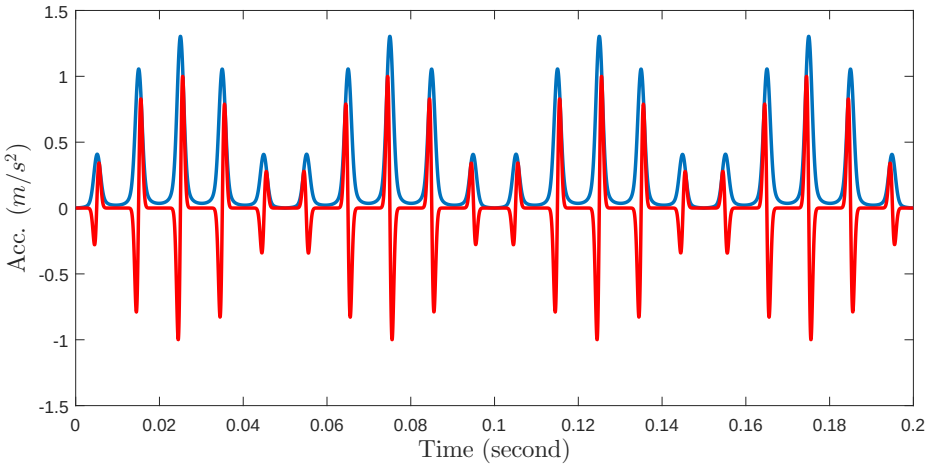

Figure A.6: Amplitude modulated simulated impulse train and envelope

frequency 100 Hz and its harmonics with the side-bands. The side-bands are separated by 10 Hz from each of the defect harmonics.

Finally, Gaussian noise was added to the simulated amplitude modulated impulse trains as shown in Figure A.8. Frequency spectrum of this signal is shown in Figure A.9, where the defect frequency with its harmonics and side-bands separated by the rotating speed is clearly visible.

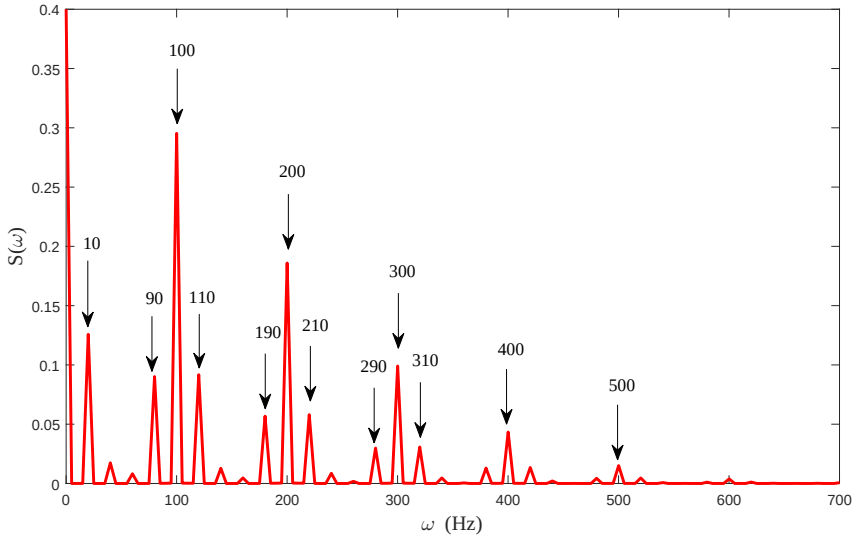

Figure A.7: Envelope spectrum of modulated impulse train

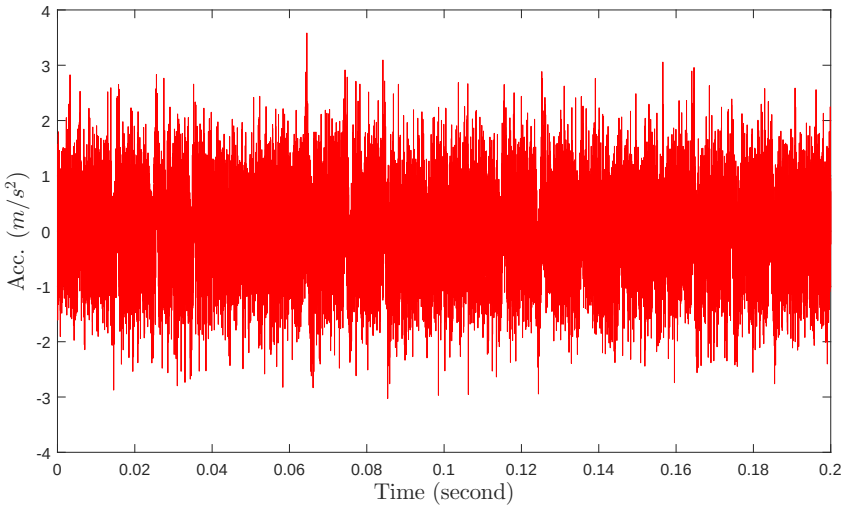

Figure A.8: Simulated modulated impulse train with added noise

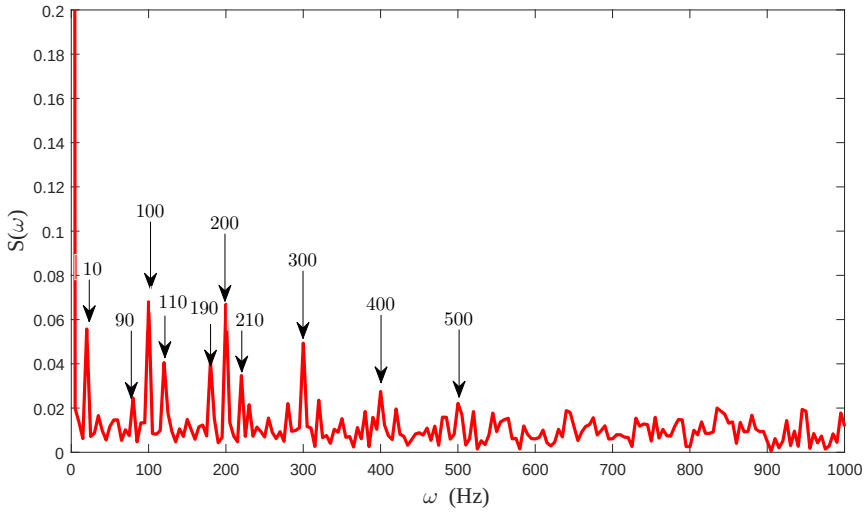

Figure A.9: Envelope spectrum for the simulated impulse train with added noise

Appendix B

First hitting time for Weiner process

Let W_t be a standard Weiner process. Let $b > 0$ and define T_b as the first time that $W_t = b$. That is:

$$T_b = \min \{t \geq 0 : W_t = b\} \tag{B.1}$$

Here, the objective is to compute the distribution of T_b. Define $\hat{W}_t = W_{T_b+t} - W_{T_b}$ to be the future value of W_t after time T_b. Note that T_b is random, so $\hat{W}_t$ is random as well. Here, it is possible to verify all the conditions of Lévy's Theorem and conclude that $\hat{W}_t$ is again a Weiner process. This is because W_t is a strong Markov process, which means the Markov property of W_t will hold when applied at random times, e.g., T_b. Thus, the future of W_t after T_b is independent of its history up to T_b.

From this, the following relationship can be written:

$$P(W_t > b | T_b < t) = P(\hat{W}_{t-T_b} > 0) = 1/2 \tag{B.2}$$

since $P(\hat{W}_s > 0) = 1/2$ for any time s by symmetry. However, the LHS of Eq. B.2 can also be written as:

$$P(W_t > b | T_b < t) = \frac{P(W_t > b, T_b < t)}{P(T_b < t)} = \frac{P(W_t > b)}{P(T_b < t)} \tag{B.3}$$

since the only way that W_t is above b is if the hitting time of b has already occurred. From Eq. B.2 and Eq. B.3:

$$\frac{P(W_t > b)}{P(T_b < t)} = \frac{1}{2} \tag{B.4}$$

$$P(T_b < t) = 2P(W_t > b) \tag{B.5}$$

$$= 2\int_{b/\sqrt{t}}^{\infty} \frac{1}{\sqrt{2\pi}} e^{-x^2/2} dx \tag{B.6}$$

It can be observed from Eq. B.6 that, as $t \to \infty$ then the integral $2\int_{b/\sqrt{t}}^{\infty} \frac{1}{\sqrt{2\pi}} e^{-x^2/2} dx = 1$, which means $P(T_b) = 1$, irrespective of the value of b. Therefore, the Weiner process hits any level b with probability 1.

Furthermore, PDF of T_b can be found by differentiating Eq. B.6 with respect to t:

$$f(T_b) = \frac{dP(T_b < t)}{dt} = \frac{|b| e^{-b^2/2t}}{\sqrt{2\pi t^3}} \tag{B.7}$$

which is basically an inverse-gamma distribution. This proves that the first hitting time for a Weiner process follows an inverse-gamma distribution.

Appendix C

Maintenance policies

A deteriorating system can either be replaced at a constant time interval (called preventive replacement) or at failure (called failure replacement). Generally, failure replacement cost is greater than the preventive replacement cost. This is because failure could lead to indirect consequences resulting from the delay related to the maintenance action. A balance is required between the amount spent on preventive replacement and its resulting benefits and failure replacements. The two replacement policies, age based and constant replacement policy as proposed by Barlow and Hunter [18], are widely employed in the industry. In the following section, a brief background on age based replacement policy is presented. These two polices are illustrated in Fig. C.1.

C.1 Age based replacement

Let C_f be the unit cost due to replacement after failure and C_p be the unit cost due to preventive replacement (assume $C_f > C_p$). A schematic diagram of age based preventive

replacement is shown is Figure C.1. Whenever a failure occurs, failure replacement is performed and the time is reset to zero and then the system runs for a time t_p, after which preventive replacement is performed. The expected cost rate (ECR) can be expressed as:

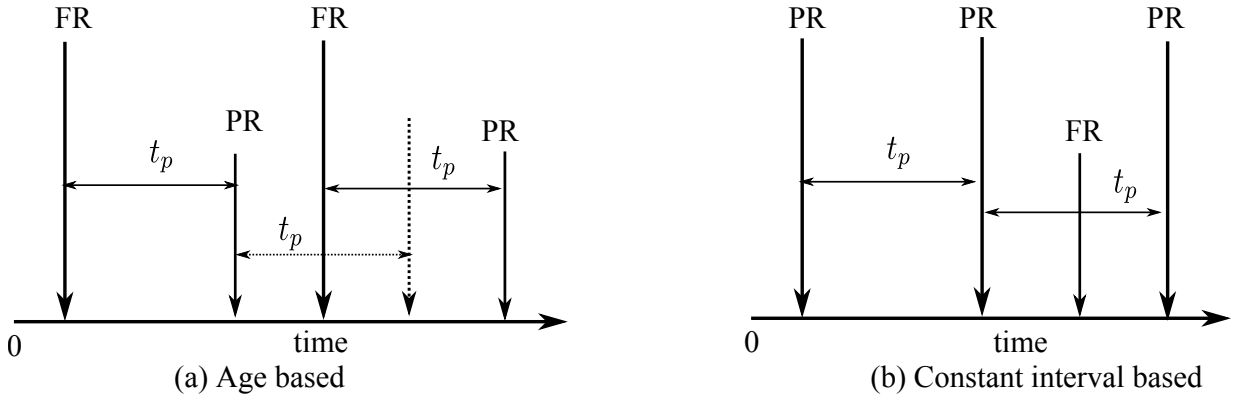

Figure C.1: Preventive replacement policies (a) Age based (b) Constant interval based

$$\begin{aligned} ECR(t_p) &= \frac{\text{Expected total replacement cost per cycle}}{\text{Expected cycle length}} \\ &= \frac{C_p R(t_p) + C_f[1 - R(t_p)]}{t_p R(t_p) + m(t_p)[1 - R(t_p)]} \\ &= \frac{C_p R(t_p) + C_f[1 - R(t_p)]}{t_p R(t_p) + \int_0^{t_p} t f(t) dt} \end{aligned} \tag{C.1}$$

where,

$$m(t_p) = \frac{\int_{-\infty}^{t_p} t f(t) dt}{1 - R(t_p)} \tag{C.2}$$

$f(t)$ = probability function of the life time of the system

$R(t)$ = survival or the reliability probability function

where t_p is the age of system and $m(t_p)$ is the mean time of failure (MTTF). The optimization problem is to minimize the expected cost rate (i.e., the cost per unit of operation time). It is easy to check that $t_p \to \infty$, $R(t_p) \to 0$ and correspondingly ECR $\to \frac{C_f}{m(t_p)}$. By

using integration by parts, the denominator of Equation C.1, $t_p R(t_p) + \int_0^{t_p} t f(t) dt$ can be simplified to $\int_0^{t_p} R(t) dt$ and Equation C.1 can be written as:

$$ECR(t_p) = \frac{C_p R(t_p) + C_f[1 - R(t_p)]}{\int_0^{t_p} R(t) dt} \tag{C.3}$$

The optimal replacement time can be found by minimizing ECR(t_p) i.e., setting the derivative equal to zero i.e.,

$$\frac{dECR(t_p)}{dt_p} = 0 \tag{C.4}$$

For this case, a closed form solution also exists and is given by Equation C.5

$$\lambda(t)G(t) = \frac{c}{c-1} - R(t) \tag{C.5}$$

where,

$$c = \frac{C_f}{C_p} > 1, \quad G(t) = \int_0^t R(t) dt, \qquad \lambda(t) = \frac{f(t)}{1 - F(t)};$$

It is important to note that the cost rate depends upon the type of distribution. For example, if the lifetime follows a Weibull distribution, the reliability is given by Equation C.6:

$$R(t) = \ e^{-(\frac{t}{\alpha})^{\beta}} \tag{C.6}$$

and Equation C.1 can be written as:

$$ECR(t_p) = \frac{C_p e^{-(\frac{t_p}{\alpha})^\beta} + C_f[1 - e^{-(\frac{t_p}{\alpha})^\beta})]}{\int_0^{t_p} e^{-(\frac{t}{\alpha})^\beta} dt} \tag{C.7}$$

The corresponding optimal replacement time is given by Equation C.5, where the hazard rate,

$$\lambda(t) = \frac{\beta}{\alpha}(\frac{t}{\alpha})^{\beta-1} \tag{C.8}$$

$$G(t) = \frac{\alpha}{\beta}\int_0^z z^{\frac{1}{\beta}-1}e^{-z}dz = \frac{\alpha}{\beta}\Gamma(\frac{1}{\beta}, z);\ \text{where, } z = (\frac{t}{\alpha})^\beta \tag{C.9}$$

where, β is the shape parameter and α is the scale parameter of the Weibull distribution and

$$\Gamma(k, z) = \int_0^z x^{k-1}e^{-x}dx \tag{C.10}$$

where, $\Gamma(k, z)$ is the lower incomplete gamma function.

Appendix D

Metropolis-Hastings algorithm

The posterior distribution $p(\theta|y)$ of parameter θ given the data y can be obtained using Baye's rule:

$$p(\theta|y) = \frac{\pi(\theta)L(y|\theta)}{\int p(\theta)L(y|\theta)d\theta} \tag{D.1}$$

where $\pi(\theta)$ is the prior, $L(\theta|y)$ is the likelihood of data and $\int p(\theta)L(y|\theta)d\theta$ is the normalizing constant. It is not always possible to calculate the normalizing constant, which makes estimation of posterior distribution almost impossible in many cases. However, a sampling based approach can be taken to evaluate the posterior distribution. One of the well known sampling techniques is the Markov chain Monte Carlo (MCMC) procedure, which uses Metropolis-Hastings (MH) algorithm for random draws. The key idea of MH algorithm is to construct and sample from a Markov chain whose stationary distribution is the target distribution $g(\theta|y)$. The posterior distribution and target distribution are related as:

$$p(\theta|y) = \frac{\pi(\theta)L(y|\theta)}{\int p(\theta)L(y|\theta)d\theta} \propto \pi(\theta)L(y|\theta) = g(\theta|y) \tag{D.2}$$

Let us say that the objective is to sample from a posterior distribution $p(\theta|y)$. Instead of sampling directly from the posterior distribution (which is not possible since the normalizing constant is unknown), samples are drawn from an alternative proposal distribution $q(\theta|y)$. The MH algorithm consists of choosing an initial value θ^0, and iteratively accepting or rejecting the candidate samples drawn from the proposal distribution $q(\theta|y)$. The algorithm proceeds according to the following four steps:

1. Select an initial value θ_0.
2. Given θ_{i-1}, draw a candidate value θ^* from the proposal distribution $q(\theta^*|\theta_{i-1})$.
3. Compute the acceptance ratio, α

$$\alpha = \frac{g(\theta^*)/q(\theta^*|\theta_{i-1})}{g(\theta_{i-1})/q(\theta_{i-1}|\theta^*)} \tag{D.3}$$

$$= \frac{g(\theta^*)q(\theta_{i-1}|\theta^*)}{g(\theta_{i-1})q(\theta^*|\theta_{i-1})} \tag{D.4}$$

4. If $\alpha \geq 1$, then set $\theta_i = \theta^*$ and if $\alpha < 1$ then set $\theta_i = \theta^*$ with probability α or $\theta_i = \theta_{i-1}$ with probability $1 - \alpha$.

Note that, both the target distribution $g(\theta)$ and the proposal distribution $q(\theta)$ are used to calculate the acceptance ratio (see Eq. D.4) in step-3. Basically, step-3 and step-4 work as a correction mechanism, since the proposal distribution is not the target distribution.

Based on the choice of proposal distribution $q(\theta)$, various MH algorithms can be constructed. In general, a proposal distribution may or may not depend upon the previous iteration's value of θ. If it does not depend upon the previous iteration value i.e.,

$$q(\theta^*|\theta_{i-1}) = q(\theta^*) \tag{D.5}$$

then the resulting algorithm is called an *independence* chain. In other words, in this case candidate samples are always drawn from the same distribution $q(\theta^*)$. On the other hand, if the proposal distribution depends upon the previous iteration then it is named as Random-Walk Metropolis-Hastings. A typical random walk MH algorithm can be expressed as:

$$q(\theta^*|\theta_{i-1}) = h(\theta^* - \theta_{i-1}) \tag{D.6}$$

where h is a symmetric density function about the origin. For example, $h(\cdot)$ can be a normal density function. If $h(\cdot)$ is normal then the candidate samples are drawn from a normal distribution with mean θ_{i-1} and a constant variance. For such a case, the calculation of acceptance ratio α (see Eq. D.4) becomes simple. Since, the normal distribution is symmetric, the following relation holds,

$$q(\theta^*|\theta_{i-1}) = q(\theta_{i-1}|\theta^*) \tag{D.7}$$

and the acceptance ratio (α) is simply equal to $g(\theta^*)/g(\theta_{i-1})$.

It is clear from the step-4 of the MH algorithm that not all the candidates are accepted. There are two things that needs to be considered to decide *how often a candidate is accepted?* First, it is required that the proposal density $q(\theta|y)$ should approximate the target distribution $g(\theta|y)$, which suggests a high acceptance rate. Second, the ratio $g(\theta|y)/q(\theta|y)$ should be bounded, which means a lower acceptance rate. This is because, to bound $g(\theta|y)/q(\theta|y)$, particularly in the tail portion of the posterior distribution, a relatively diffuse posterior distribution is required. Clearly, a balance is needed between the two for the selection of an optimum acceptance rate. For example, in the case of a Random-Walk MH sampler, if the acceptance rate is high, then the random walk will take very small

steps and will take a very long time to converge to the posterior distribution. On the other hand, if the acceptance rate is low, then the random walk takes too large a step and many of the candidate samples will be discarded due to low acceptance rate. For random walk chains with normal proposal densities, a acceptance rate between 25% to 45% has been suggested in the literature.

Another important question in MCMC sampling is "how many samples needs to taken so that the posterior distribution is fully explored ?" This is often done by performing *Raftery and Lewis diagnostics* test[178]. This test checks during sampling to providea a bound for the accuracy of the estimated quantiles of the variables of interest.

Let it be desired to measure some posterior quantile of interest Q. If some acceptable tolerance r for Q and a probability s of being within that tolerance is defined, then the Raftery and Lewis diagnostic will calculate the number of iterations N and the number of burn-ins M necessary to satisfy the specified conditions. In other words, $\Theta = \{M, N\}$ is chosen such that,

$$P(\Theta < Q \pm r) < s \tag{D.8}$$

The number of iterations and burn-in needed is first approximated by running and testing a shorter pilot chain. The minimum length of pilot Markov chain can be calculated using the following formula:

$$n_{min} = \left[\phi^{-1} \left(\frac{s+1}{2} \right) \frac{\sqrt{q(1-q)}}{r} \right]^2 \tag{D.9}$$

where ϕ^{-1} is the inverse of normal CDF.

Appendix E

List of publications

Articles in refereed journals:

1. Prakash, G., & Narasimhan, S. (2017). Bayesian two-phase Gamma process model for damage detection and prognosis. *Journal of Engineeing Mechanics*, 144(2).

2. Prakash, G., Narasimhan, S., & Pandey, M. D. (2017), Condition based maintenance of low speed rolling element bearings using hidden Markov model, *International Journal of Prognostics and Health Management*, 8(5), 16pp. <https://www.phmsociety.org/node/2183>

3. Prakash, G., Narasimhan, S., & Pandey, M. D. (2017), A probabilistic approach to remaining useful life prediction of rolling element bearings, *Journal of Structural health monitoring* (Accepted)